

**Development and customization of new 3D generation tracheal prosthesis  
with different biological activities regarding to their functional side**

**Joan Gilabert Porres**

<http://hdl.handle.net/10803/402441>

**ADVERTIMENT.** L'accés als continguts d'aquesta tesi doctoral i la seva utilització ha de respectar els drets de la persona autora. Pot ser utilitzada per a consulta o estudi personal, així com en activitats o materials d'investigació i docència en els termes establerts a l'art. 32 del Text Refós de la Llei de Propietat Intel·lectual (RDL 1/1996). Per altres utilitzacions es requereix l'autorització prèvia i expressa de la persona autora. En qualsevol cas, en la utilització dels seus continguts caldrà indicar de forma clara el nom i cognoms de la persona autora i el títol de la tesi doctoral. No s'autoritza la seva reproducció o altres formes d'explotació efectuades amb finalitats de lucre ni la seva comunicació pública des d'un lloc aliè al servei TDX. Tampoc s'autoritza la presentació del seu contingut en una finestra o marc aliè a TDX (framing). Aquesta reserva de drets afecta tant als continguts de la tesi com als seus resums i índexs.

**ADVERTENCIA.** El acceso a los contenidos de esta tesis doctoral y su utilización debe respetar los derechos de la persona autora. Puede ser utilizada para consulta o estudio personal, así como en actividades o materiales de investigación y docencia en los términos establecidos en el art. 32 del Texto Refundido de la Ley de Propiedad Intelectual (RDL 1/1996). Para otros usos se requiere la autorización previa y expresa de la persona autora. En cualquier caso, en la utilización de sus contenidos se deberá indicar de forma clara el nombre y apellidos de la persona autora y el título de la tesis doctoral. No se autoriza su reproducción u otras formas de explotación efectuadas con fines lucrativos ni su comunicación pública desde un sitio ajeno al servicio TDR. Tampoco se autoriza la presentación de su contenido en una ventana o marco ajeno a TDR (framing). Esta reserva de derechos afecta tanto al contenido de la tesis como a sus resúmenes e índices.

**WARNING.** The access to the contents of this doctoral thesis and its use must respect the rights of the author. It can be used for reference or private study, as well as research and learning activities or materials in the terms established by the 32nd article of the Spanish Consolidated Copyright Act (RDL 1/1996). Express and

## DOCTORAL THESIS

Title	Development and customization of new 3D generation tracheal prosthesis with different biological activities regarding to their functional side
Presented by	Joan Gilabert Porres
Centre	IQS School of Engineering
Department	Bioengineering
Directed by	Dr. Salvador Borrós Gómez & Dr. Victor Ramos Pérez

*This page left blank intentionally*

*To my family,*



*This page left blank intentionally*

*“Failure is simply the opportunity to begin again, this time more intelligently”*

*Henry Ford*

*This page left blank intentionally*

# Acknowledgments

La dificultat que presenta escriure aquestes línies no té res que envejar al moment d'escriure un treball científic.

Voldria començar agraint al Salvador tot el que ha fet per mi. Gràcies per brindar-me aquesta oportunitat de creixement acadèmic i personal. Gràcies per fer possible la realització d'aquest treball i pel suport incondicional en tots els moments, en els bons i en els no tan bons (encara recordo el moment en que algú va decidir no renovar-me la beca del Grup i tu hi vas intercedir de diverses maneres per resoldre el problema). Sempre has estat allí tot i sabent que de vegades m'equivocava. Moltes gràcies per ajudar-me a veure les coses positives on jo no les veia i pels moments de teràpia per tirar endavant.

També voldria agrair el Víctor per la seva paciència i suport. Gràcies per la teva ajuda en el dia a dia, en les discussions acadèmiques, planificació d'experiments i per fer-me tocar de peus a terra quan m'imaginava idees molt boges.

Moltes gràcies també a la gent de l'Hospital de Bellvitge, en especial a l'Antoni Rosell, per haver-nos fet partícips d'aquesta necessitat clínica i haver confiat en nosaltres. Per suposat, a la Dra. Sara Matí i la Dra. Josefina Liñares per involucrar-nos en el projecte, pels experiments microbiològics i el suport en la planificació i preparativa de les mostres. També vull agrair a la Dra. Noelia i la Rosa M<sup>a</sup> per la seva ajuda i suport en la preparativa de textos i presentacions sobre la part més clínica del treball. Finalment, voldria agrair a la Dra. Ana Montes, pel seu suport, ajuda i hores de treball per planificar els experiments cel·lulars i poder extreure informació rellevant. Ens hem passat moltes hores barallant-nos amb les nanopartícules i les cèl·lules.

Gracies també a la Dra. Montse Agut i l'Oscar per la seva ajuda i per deixar-nos utilitzar el seu laboratori per realitzar les proves microbiologies. En alguns moments semblava que envaïa el laboratori de microbiologia per a realitzar els experiments. ;-)

També vull agrair, com jo dic, a la família GEMAT@s (us llistaria a tots però sabeu que no acabaríem) que sempre han estat al meu costat ajudant-me, donant-me suport, fent cafès (per aguantar les immenses tardes de laboratori), discutint sobre resultats i el que no eren resultats, treballant al límit per complir *deadlines* i per suposat, per les estones de bauxa que hem gaudit durant aquests anys. En particular, voldria agrair al Robert i a l'Anna, el nou *triumvirat* o la p\*\*\* màfia, com diu el Salvador, per totes les hores que ens hem passat al laboratori fent que la feina i els resultats sortissin. Hem discutit sobre ciència, religió, taxa de natalitat... i ens hem ajudat en tot moment per a que aquesta i les vostres tesis tirin endavant. Moltes gràcies per tot! Sabeu que em teniu per al que faci falta.

Finalment, voldria agrair el suport de Lola, Gabi, Núria, Ivo x2 i Rosita, per haver-me acollit com un més i fer-me sentir especial cada dia. Moltes gràcies per haver-me ajudat en tots els aspectes del dia

a dia. Per suposat a Núria, fas que cada dia sigui especial i que valgui la pena tirar endavant, inclús quan jo no ho veig ;-)

Finalment, gràcies als de casa, als meus pares, germà, tiet, Pep i padrí, per l'esforç que heu fet i per haver confiat sempre amb mi. Sé que les coses no han estat fàcils, però tot i així, heu tirat endavant i heu cregut en mi, costés el que costés.

***Moltes gràcies a tots i cadascú de vosaltres per formar part de tot el viscut.***

---

Aquesta tesi ha estat possible gràcies a la Secretaria d'Universitats i Recerca del Departament d'Economia i Coneixement de la Generalitat de Catalunya i als Fons Socials Europeus per l'ajut de contractació de personal investigador novell FI-DGR (2014 FI\_B 00622, 2015 FI\_B1 00107 i 2016 FI\_B2 00056).

## Abstract

Stents are expandable tubes made of different materials that are used to open a conduct that has been obstructed. Specifically, in the field of tracheal stents, there has been a need for improvement due to post-implantation problems, such as bacterial colonization, granulation tissue formation, migration and acute pain. Bacterial colonization by potentially pathogenic microorganisms (PPMs) reduces the quality of life of patients inducing infection or even sepsis, which can lead to patient death, if appropriate measures are not taken. Moreover, re-stenosis of post-inflammatory scars, as well as the growth of inflammatory granulation tissue, can be a life-threatening complication. However, both complications could be resolved by pharmacologically activating the stents with antiproliferative drugs. To avoid these problems, it is reasonable to propose the local use of antiproliferative drugs, such as paclitaxel (PCTXL), with a controlled release to reduce the recurrence of the stenosis, resulting in tissue healing and reduced stent implantation time. Finally, tracheal stents suffer from poor adaptability to the implantation area. This lack of fitting leads to migration of the stent along the trachea, causing pain and threatening critical parts like the vocal cords. In addition, this migration or displacement of the stent causes the formation of granuloma tissue at the edges of the stents due to mechanical stress and rubbing. However, both problems, stent migration and granuloma tissue formation, can be avoided by re-designing the stent using 3D printing technology to increase the adaptability creating a suitable stent for the desired implantation zone.

The above-mentioned complications are urging physicians and patients to demand a new generation of stents with different properties that can allow the treatment of several pathologies, such as re-stenosis, and avoid associated problems, such as infection, migration and bleeding.

This work develops an innovative coating technology using plasma treatments to create an antibacterial coating. The resulting materials were capable to reduce bacterial colonization and avoid biofilm formation. Surface treatments have been adapted to create micro- and nanostructured surfaces using silver as antibacterial agent. The developed metallic silver coating showed hydrophobic behaviour and antibacterial activity against Gram-positive and Gram-negative strains. In addition, an adaptation of this coating was used in combination with an adaptation of a previously developed drug delivery platform, such as nanoparticles, to encapsulate paclitaxel and allow sustained release from the surface of the material. Pegylated polyester nanoparticles were fabricated using a synthesized amine-terminal polymer and showed paclitaxel encapsulation properties with a controlled release. The developed drug release system was effective against different types of cells, such as patient-extracted stenotic cells.

Finally, in order to provide a solution to the low adaptability that causes stent migration and granulation tissue, this work explores the use of the additive manufacturing technologies to fabricate a customized anatomical device with the aim of revolutionizing the current stent technology and offering an innovative solution to uncovered clinical needs. The developed work represents a proof of concept of a protocol to fabricate anatomical objects using patient information and additive manufacturing technology. As a result of the manufacturing protocol, an anatomical silicone-based stent was

successfully fabricated using patients scan, 3D software and different additive manufacturing technologies.

## Resum

Els *stents* són tubs expansibles fets de diferents materials que s'utilitzen per obrir conductes que han estat obstruïts. Específicament, en el camp dels *stents* traqueals, existeix una necessitat de millora per evitar els problemes post-implantació, tals com la colonització bacteriana, la formació de teixit de granulació, la migració del dispositiu i el dolor agut. La colonització bacteriana per microorganismes potencialment patògens (PPM, sigles en anglès) redueix la qualitat de vida dels pacients, indueix infecció o fins i tot sèpsia, i pot conduir a la mort del pacient si no es prenen les mesures adequades. A més, la re-estenosis de les cicatrius postinflamatòries, així com el creixement del teixit inflamatori de granulació, poden ser complicacions potencialment mortals. No obstant això, ambdues complicacions podrien resoldre's activant farmacològicament els *stents* mitjançant fàrmacs antiproliferatius. Per evitar aquesta problemàtica, és raonable proposar l'ús local de fàrmacs antiproliferatius, com per exemple el paclitaxel (PCTXL), que redueix la recurrència de la estenosis mitjançant un alliberament controlat, donant com resultat la cicatrització del teixit i la reducció del temps d'implantació del *stent*. Així mateix, els *stents* traqueals sofreixen d'una mala adaptabilitat a l'àrea d'implantació. Aquesta falta d'ajust condueix a la migració del *stent* al llarg de la tràquea, causant dolor crític i greus problemes en zones delicades com les cordes vocals. A més, aquesta migració o desplaçament del *stent* provoca la formació de teixit de granulació en els extrems, a causa de l'estrès mecànic i el fregament. No obstant això, tots dos problemes, la migració i la formació de teixit de granulació, es poden evitar redissenyant el *stent*, mitjançant tecnologia d'impressió 3D per augmentar l'adaptabilitat creant un dispositiu completament anatòmic.

Aquestes complicacions fan que els metges i els pacients sol·licitin una nova generació de *stents* amb diferents propietats que permetin el tractament de diverses patologies, com la re-estenosis, i que evitin problemes associats, com la infecció, la migració i el sagnat.

Aquest treball desenvolupa una tecnologia innovadora de recobriments, utilitzant tractaments per plasma per crear un recobriment antibacterià. Els materials resultants han estat capaços de reduir la colonització bacteriana i evitar la formació de biofilm. Els tractaments de superfície s'han adaptat per crear superfícies micro- i nanoestructurades, utilitzant plata com a agent antibacterià. El recobriment de plata metàl·lica desenvolupat, va mostrar un comportament hidrofòbic i una activitat antibacteriana contra soques Gram-positives i Gram-negatives. A més, es va utilitzar una modificació d'aquest recobriment en combinació amb una plataforma d'alliberament controlat de fàrmacs mitjançant nanopartícules, per encapsular paclitaxel i permetre l'alliberament controlat des de la superfície del material. Les nanopartícules de polièster-PEG es van fabricar utilitzant un polímer sintètic amb amines terminals i va presentar propietats d'encapsulació de paclitaxel i un alliberament controlat del mateix. Així, el sistema d'alliberament de fàrmac desenvolupat va ser eficaç contra diferents tipus de cèl·lules com les cèl·lules estenòtiques extrems del pacient.

Per tant, i amb la finalitat de proporcionar una solució a la baixa adaptabilitat que provoca la migració del *stent* i el teixit de granulació, aquest treball presenta com a solució l'ús de les tecnologies de



fabricació additiva per obtenir un dispositiu anatòmic personalitzat i millorar així l'adaptabilitat. Aquesta tesi ha desenvolupat un protocol com a prova de concepte, per crear objectes anatòmics, utilitzant la informació dels pacients i la tecnologia de fabricació d'additiva. Com a resultat, el *stent* de silicona anatòmic es va fabricar amb èxit mitjançant diferents tecnologies de fabricació additiva, i es van proporcionar propietats antibacterianes mitjançant els recobriments desenvolupats prèviament.

## Resumen

Los *stents* son tubos expandibles hechos de diferentes materiales que se utilizan para abrir conductos que han sido obstruidos. Específicamente, en el campo de los *stents* traqueales, existe una necesidad de mejora para evitar los problemas post-implantación, tales como la colonización bacteriana, la formación de tejido de granulación, la migración del dispositivo y el dolor agudo. La colonización bacteriana por microorganismos potencialmente patógenos (PPM, siglas en inglés) reduce la calidad de vida de los pacientes, induce infección o incluso sepsis y puede conducir a la muerte del paciente, si no se toman las medidas adecuadas. Además, la re-estenosis de las cicatrices post-inflamatorias, así como el crecimiento del tejido inflamatorio de granulación, pueden ser complicaciones potencialmente mortales. Sin embargo, ambas complicaciones podrían resolverse activando farmacológicamente los *stents* mediante fármacos antiproliferativos. Para evitar esta problemática, es razonable proponer el uso local de fármacos antiproliferativos, como por ejemplo el paclitaxel (PCTXL), que reduce la recurrencia de la estenosis mediante una liberación controlada, dando como resultado la cicatrización del tejido y la reducción del tiempo de implantación del *stent*. Así mismo, los *stents* traqueales sufren de una mala adaptabilidad en el área de implantación. Esta falta de ajuste conduce a la migración del *stent* a lo largo de la tráquea, causando dolor crítico y graves problemas en zonas delicadas como las cuerdas vocales. Además, esta migración o desplazamiento del *stent* provoca la formación de tejido de granulación en los bordes de los *stents*, debido al estrés mecánico y al frotamiento. Sin embargo, ambos problemas, la migración del *stent* y la formación de tejido de granulación, se pueden evitar rediseñando el *stent*, usando tecnología de impresión 3D para aumentar la adaptabilidad creando un dispositivo completamente anatómico.

Estas complicaciones hacen que los médicos y los pacientes soliciten una nueva generación de *stents* con diferentes propiedades que permitan el tratamiento de varias patologías, como la re-estenosis, y que eviten problemas asociados, como la infección, la migración y el sangrado.

Este trabajo desarrolla una tecnología innovadora de recubrimientos, utilizando tratamientos por plasma para crear un recubrimiento antibacteriano. Los materiales resultantes han sido capaces de reducir la colonización bacteriana y evitar la formación de *biofilm*. Los tratamientos de superficie se han adaptado para crear superficies micro- y nano-estructuradas, utilizando plata como agente antibacteriano. El recubrimiento de plata metálica desarrollado, mostró un comportamiento hidrófobo y una actividad antibacteriana contra cepas Gram-positivas y Gram-negativas. Además, se utilizó una modificación de este recubrimiento en combinación con una plataforma de liberación controlada de fármacos mediante nanopartículas, para encapsular paclitaxel y permitir la liberación controlada desde la superficie del material. Las nanopartículas de poliéster-PEG se fabricaron utilizando un polímero sintético con aminas terminales y presentó propiedades de encapsulación de paclitaxel y una liberación controlada del mismo. Así, el sistema de liberación de fármaco desarrollado fue eficaz contra diferentes tipos de células como las células estenóticas extraídas del paciente.

Por consiguiente, y con el fin de proporcionar una solución a la baja adaptabilidad que provoca la migración del *stent* y el tejido de granulación, este trabajo presenta como solución el uso de las tecnologías de fabricación aditivas para obtener un dispositivo anatómico personalizado y mejorar así la adaptabilidad. Esta tesis ha desarrollado un protocolo como prueba de concepto, para crear objetos anatómicos, utilizando la información de los pacientes y la tecnología de fabricación de aditiva. Como resultado, el *stent* de silicona anatómico se fabricó con éxito mediante diferentes tecnologías de fabricación aditivas, y se proporcionaron propiedades antibacterianas mediante los recubrimientos desarrollados previamente.

# Table of Contents

ACKNOWLEDGMENTS .....	VII
ABSTRACT.....	IX
TABLE OF CONTENTS.....	XV
LIST OF FIGURES.....	XVII
LIST OF TABLES .....	XIX
LIST OF EQUATIONS .....	XIX
LIST OF SCHEMES.....	XIX
LIST OF ABBREVIATIONS.....	XXI
LIST OF PUBLICATIONS.....	XXIII
LIST OF PATENTS.....	XXIII
ORAL PRESENTATIONS.....	XXIV
LIST OF POSTERS.....	XXIV
<b>CHAPTER I. INTRODUCTION .....</b>	<b>1</b>
1.1 INTRODUCTION.....	3
1.2 REFERENCES.....	12
<b>CHAPTER II. ANTIBACTERIAL SURFACES.....</b>	<b>21</b>
2.1 INTRODUCTION.....	23
2.2 MATERIALS AND METHODS.....	30
2.2.1 <i>Materials</i> .....	30
2.2.2 <i>Preparation of substrates</i> .....	30
2.2.3 <i>Plasma Reactor</i> .....	30
2.2.3.1.1 Reactor 1: Horizontal Plasma Reactor (HPR).....	30
2.2.3.1.2 Reactor 2: Stainless Steel Vertical Plasma Reactor (SSVPR).....	31
2.2.4 <i>Plasma Polymerization</i> .....	32
2.2.5 <i>Plasma Grafting and Activation</i> .....	33
2.2.6 <i>Surface Selectivity, Patterning and Structuration</i> .....	33
2.2.6.1.1 Surface Selectivity.....	33
2.2.6.1.2 Surface Patterning, Micro-Patterning and $\mu$ Contact Printing ( $\mu$ CP).....	33
2.2.7 <i>Modified Surface Characterization</i> .....	35
2.2.8 <i>Silver Deposition</i> .....	35
2.2.9 <i>Silver Release and Total Silver Amount</i> .....	36
2.2.10 <i>Bacterial in vitro Assay</i> .....	36
2.2.11 <i>Animal Cell in vitro Assay</i> .....	36
2.3 RESULTS AND DISCUSSION.....	38
2.3.1 <i>Grafting modification on nylon and PTFE plates</i> .....	38
2.3.2 <i>Microstructuring of grafted PTFE plates</i> .....	39
2.3.3 <i>Silver Deposition on grafted PTFE plates</i> .....	40
2.3.4 <i>PECVD modification on PTFE plates</i> .....	42
2.3.5 <i>Silver Deposition on PTFE plates</i> .....	44
2.3.6 <i>PECVD Modification and Structuration of PDMS Plates</i> .....	45
2.3.7 <i>Silver modification onto PDMS plates by PECVD</i> .....	47
2.3.7.1.1 ToF-SIMS Analysis of Modified Surfaces.....	48
2.3.7.1.2 Surface Structuration of Silver Coated PDMS Samples.....	50
2.3.7.1.3 Behavior of Silver Coated 3D Structures.....	53
2.3.7.1.4 Silver Release of Coated PDMS Samples.....	54
2.3.7.1.5 Bacteria Cultures onto Silver Coated Surfaces.....	57
2.3.7.1.6 In Vitro Cytotoxicity of Silver Coated Samples.....	58
2.4 CONCLUDING REMARKS.....	60
2.5 REFERENCES.....	61
<b>CHAPTER III. DRUG DELIVERY SYSTEM WITH IMMOBILIZED NANOPARTICLES.....</b>	<b>69</b>

3.1	INTRODUCTION .....	71
3.2	MATERIALS AND METHODS.....	75
3.2.1	<i>Materials</i> .....	75
3.2.2	<i>Preparation of substrates</i> .....	75
3.2.3	<i>Surface modification by plasma techniques</i> .....	75
3.2.4	<i>Polymer Synthesis</i> .....	76
3.2.4.1.1	Microwave Polycondensation Polymer (PAm).....	76
3.2.4.1.2	Polymerization via acid chloride (PAmN).....	76
3.2.5	<i>Nanoparticles Synthesis</i> .....	76
3.2.6	<i>Nanoparticles Characterization</i> .....	77
3.2.6.1.1	Determination of Nanoparticles Size, Polydispersity and Surface Charge and Morphology	77
3.2.6.1.2	Drug Incorporation Efficiency and Immobilized Drug Quantification.....	78
3.2.6.1.3	In vitro Drug Release Analysis.....	78
3.2.7	<i>Nanoparticles Immobilization</i> .....	79
3.2.7.1.1	FBS coating of silicones .....	79
3.2.7.1.2	Collagen coating of silicones .....	79
3.2.8	<i>Determination of in vitro cytotoxicity of drug-loaded nanoparticles</i> .....	79
3.2.8.1.1	Cytotoxicity of Drug Loaded Nanoparticles.....	80
3.2.8.1.2	Viability of Drug Loaded Nanoparticles Immobilized onto PDMS plates .....	81
3.2.8.1.3	Live & Dead Staining .....	81
3.2.8.1.4	Dapi/Phalloidin Staining .....	81
3.3	RESULTS AND DISCUSSION .....	83
3.3.1	<i>Synthesis and Characterization of Block Co-polymers PAmX</i> .....	83
3.3.2	<i>Preparation and Characterization of Nanoparticles</i> .....	89
3.3.2.1.1	Size Distribution and Zeta Potential.....	90
3.3.2.1.2	Drug incorporation Efficiency.....	91
3.3.2.1.3	In vitro Drug Release from Loaded Nanoparticles .....	92
3.3.3	<i>Nanoparticles Immobilization</i> .....	94
3.3.4	<i>In vitro Assessment of Developed Nanoparticles</i> .....	95
3.3.4.1.1	In vitro Antiproliferative Efficiency of Suspended NPs.....	95
3.3.4.1.2	In vitro Antiproliferative Efficiency of Immobilized NPs.....	98
3.4	CONCLUDING REMARKS .....	101
3.5	REFERENCES .....	103
<b>CHAPTER IV.</b>	<b>DESIGN OF A 3D PRINTED TRACHEAL DEVICE .....</b>	<b>107</b>
4.1	INTRODUCTION .....	109
4.2	MATERIALS AND METHODS.....	114
4.2.1	<i>Materials</i> .....	114
4.2.2	<i>3D model generation</i> .....	114
4.2.2.1.1	Data acquisition .....	114
4.2.2.1.2	Software.....	114
4.2.3	<i>3D Printer</i> .....	115
4.2.4	<i>Prosthesis unmoulding</i> .....	115
4.2.1	<i>Surface modification and Silver Deposition.</i> .....	115
4.3	RESULTS .....	117
4.3.1	<i>Data Extraction and Analysis</i> .....	117
4.3.1.1.1	Data import .....	117
4.3.1.1.2	Region of Interest (ROI).....	117
4.3.1.1.3	Thresholding and Assessment of Tracheal Tissue .....	118
4.3.2	<i>Treatment and modelling of the STL file</i> .....	125
4.3.3	<i>3D Printing of extracted model</i> .....	127
4.3.4	<i>Mould design of anatomical silicone tracheal stent</i> .....	129
4.3.5	<i>3D Printing of Designed Mould and PDMS injection</i> .....	132
4.3.6	<i>Silver deposition onto 3D anatomical stent</i> .....	133
4.4	CONCLUDING REMARKS .....	135
4.5	REFERENCES .....	137
<b>CHAPTER V.</b>	<b>CONCLUSIONS.....</b>	<b>141</b>

## List of Figures

Figure I-1. Granulation tissue at the edges of the tracheal stent.....	6
Figure I-2. Trachea reconstruction from a Computed Tomography (CT) Scan.....	7
Figure I-3. Different immobilization methods.....	8
Figure I-4. Chemical structure of pentafluorophenyl methacrylate.....	9
Figure II-1. Piece metal removal of a metal stent.....	23
Figure II-2. Different tracheal tubes.....	24
Figure II-3. Pulsed plasma polymerization process.....	26
Figure II-4. Scheme of different plasma treatment techniques.....	28
Figure II-5. Horizontal Plasma Reactor (HPR).....	31
Figure II-6. Stainless Steel Vertical Plasma Reactor (SSVPR).....	32
Figure II-7. Schematic representation of the used masks.....	34
Figure II-8. Master stamp.....	34
Figure II-9. Folded nylon membrane after the grafting treatment.....	38
Figure II-10. Water contact angles (WCA) of modified samples.....	39
Figure II-11. $\mu$ Structured samples using $\mu$ contact printing technique.....	40
Figure II-12. Schematic representation of antibacterial coating.....	41
Figure II-13. PTFE sample coated with silver in a three-step process.....	41
Figure II-14. WCA measurements of different studied samples.....	43
Figure II-15. Wettability behaviour of modified PTFE sample.....	44
Figure II-16. PTFE sample coated with metallic silver.....	44
Figure II-17. SEM images of the PDMS samples.....	46
Figure II-18. Fluorescent micro-structured PFM coated PDMS.....	46
Figure II-19. Bi-side modification of PDMS samples.....	47
Figure II-20. WCA, $\sigma$ (deg), of silicon wafer samples.....	48
Figure II-21. Surface microscopy of structured silver surfaces.....	50
Figure II-22. Surface characterization of samples: SEM images of silver modified samples.....	51
Figure II-23. Surface morphology of silver-coated PDMS samples after immersion with different liquids.....	52
Figure II-24. WCA of silicone and silver modified silicone with water and mucine.....	53
Figure II-25. Surface behaviour of 3D modified samples.....	54
Figure II-26. Silver release.....	55
Figure II-27. Concentration of silver in solutions incubated with oxic and anoxic conditions.....	56
Figure II-28. Scheme of silver ion release.....	56
Figure II-29. Bacterial viability on coated and noncoated samples.....	58
Figure II-30. Cell viability of silver modified samples on COS-7.....	59
Figure III-1. FTIR spectra of the synthesized polymers.....	84
Figure III-2. $^1\text{H-NMR}$ of the PAm polymer.....	85

Figure III-3. <sup>1</sup> H-NMR of the PAmN polymer.....	86
Figure III-4. <sup>1</sup> H-NMR stack of PEG bis amine (green) and PAmN polymer (red).....	87
Figure III-5. GPC elution profiles of synthesized polymers. ....	88
Figure III-6. GPC elution profiles of PAmX and its nanoparticles.....	89
Figure III-7. Zeta potential and size characterization of the synthesized nanoparticles. ....	91
Figure III-8. NPs Characterization .....	92
Figure III-9. In vitro release kinetics of PCTXL loaded nanoparticles.....	93
Figure III-10. Scheme of the amine bearing nanoparticles behaviour under different pH conditions. ...	94
Figure III-11. Immobilization of PCTXL loaded nanoparticles .....	95
Figure III-12. Cell viability of different in vitro cell lines with synthesized NPs .....	96
Figure III-13. Cell viability of different ex vivo cell lines with synthesized NPs.....	97
Figure III-14. Cell viability of human fibroblast with non-treated and treated PDMS with O <sub>2</sub> plasma. ...	98
Figure III-15. Cell viability of Normal Human Dermal Fibroblasts (NHDFs) on coated and noncoated samples.....	99
Figure IV-1. Workflow to manufacture anatomical personalized medical device. ....	111
Figure IV-2. AM classification technologies according to the raw material. ....	112
Figure IV-3. Scheme of different 3D printers used in this work. ....	115
Figure IV-4. Different views of axial, coronal and sagittal planes of thorax after file imported. ....	118
Figure IV-5. Visualization of different mask selection with threshold and 3D reconstruction. ....	120
Figure IV-6. Overview of the generated mask by different methods. ....	122
Figure IV-7. 3D reconstruction of masks obtained by different methods.....	124
Figure IV-8. Different 3D models generated.....	124
Figure IV-9. Overview of the branched airway. ....	126
Figure IV-10. Oversized trachea with 1.5 mm offset. ....	127
Figure IV-11. 3D-printed trachea model using FDM technology (Fortus 400mc®). ....	128
Figure IV-12. Printing process of the trachea model using the Stalactite printer. ....	129
Figure IV-13. Mould cavity creation from the trachea airway. ....	130
Figure IV-14. Injection mould with different channels for injection and air release. ....	131
Figure IV-15. Final design of the tracheal stent mould to inject silicone. ....	131
Figure IV-16. Image of the mold's printing process with a stereolithography printer.....	132
Figure IV-17. Anatomical silicone stents manufactured using 3D printing technology.....	133
Figure IV-18. Patient's anatomical stent with antibacterial properties.....	134

## List of Tables

<i>Table II-1. Structure of Characteristic Peaks of pp-PFM.</i> .....	49
<i>Table III-1. Characterization of different synthesized nanoparticles by GPC.</i> .....	88
<i>Table III-2. Characterization of different synthesized nanoparticles by GPC.</i> .....	89
<i>Table IV-1. Commands for Data import into 3D Slicer and Mimics®.</i> .....	117
<i>Table IV-2. Commands of selected ROI for 3D Slicer and Mimics®.</i> .....	118
<i>Table IV-3. Commands to create new masks for segmentation.</i> .....	119
<i>Table IV-4. Selection of most used commands to edit mask pixels.</i> .....	121
<i>Table IV-5. Selection of the most used commands to edit mask pixels.</i> .....	122
<i>Table IV-6. Most used commands to crop the STL file in 3-matic®.</i> .....	126

## List of Equations

<i>Equation II-1</i> .....	26
<i>Equation II-2</i> .....	26
<i>Equation III-1. Nanoparticles Recovery.</i> .....	77
<i>Equation III-2. Drug Content (D.C. %).</i> .....	78
<i>Equation III-3. Encapsulation Efficiency (E.E. %).</i> .....	78
<i>Equation III-4. Drug immobilization content (D.I.C. ng/mm<sup>2</sup>).</i> .....	78
<i>Equation III-5. Cell Viability.</i> .....	81

## List of Schemes

<i>Scheme II-1. Silver Mirror Process.</i> .....	36
<i>Scheme III-1. Synthesis of block co-polymer PAmX by polycondensation.</i> .....	83



*This page left blank intentionally*

## List of Abbreviations

<b>3DP</b>	3D printing
<b>A549</b>	A549 ATCC® CCL-185TM; Bronchial-alveolar epithelial human cells
<b>AM</b>	Additive manufacturing
<b>CAD</b>	Computer-aided design
<b>CAT</b>	Computerised-axial tomography
<b>COS-7</b>	<i>Cercopithecus aethiops</i> kidney fibroblast SV40 transformed ATCC® CRL-1651™)
<b>CT</b>	Computed Tomography
<b>Da</b>	Daltons
<b>DAPI</b>	4',6-diamidino-2-phenylindole
<b>DC</b>	Drug content
<b>DEMEM</b>	Dulbecco's modified eagle's medium
<b>DICOM</b>	Digital imaging and communication in medicine
<b>DMD</b>	Direct metal deposition
<b>DNA</b>	Deoxyribonucleic acid
<b>EB</b>	Ethidium bromide
<b>EBM</b>	Electron beam melting
<b>ECM</b>	Extracellular matrix
<b>EE</b>	Encapsulation efficiency
<b>EMEM</b>	Eagle's minimal essential medium
<b>F-12K</b>	Kaighn's modification of ham's F-12 medium
<b>FBS</b>	Fetal bovine serum
<b>FDA</b>	Fluorescein diacetate
<b>FDM</b>	Fused deposition modelling
<b>FRESH</b>	Freeform reversible embedding of suspended hydrogels
<b>FTIR</b>	Fourier transform infrared spectroscopy
<b>GPC</b>	Gel permeation chromatography
<b>h</b>	Hours
<b>H<sup>1</sup>-NMR</b>	Proton nuclear magnetic resonance
<b>HEPES</b>	4-(2-hydroxyethyl)-1-piperazineethanesulfonic acid
<b>HU</b>	Hounsfield unit
<b>IEP</b>	Isoelectric point
<b>IMR-90</b>	IMR-90, ATCC® CCL-186™; Human lung normal fibroblasts
<b>IR</b>	Infrared spectrum
<b>ITS</b>	Insulin human transferrin and sodium selenite
<b>LENS</b>	Laminated engineered net shaping
<b>LMD</b>	Laser metal deposition
<b>LOM</b>	Laminated object manufacturing
<b>Milli-Q</b>	Ultrapure water (Millipore®)
<b>min</b>	Minutes
<b>Mn</b>	Number average molecular weight

<b>Mp</b>	Molecular weight of the highest peak
<b>MRI</b>	Magnetic resonance imaging
<b>MW</b>	Molecular weight
<b>Mw</b>	Weight average molecular weight
<b>Mz</b>	Higher average molecular weights , n=2
<b>NHDFs</b>	Normal human dermal fibroblasts
<b>NMR</b>	Nuclear magnetic resonance
<b>NP</b>	Nanoparticle
<b>PAm</b>	Synthesized polymers through microwave
<b>PAmN</b>	Synthesized polymers through acid chloride
<b>PAmX</b>	Synthesized polymers
<b>PBS</b>	Phosphate-buffered saline
<b>PCTXL</b>	Paclitaxel
<b>PDMS</b>	Polydimethyl siloxane
<b>PEG</b>	Polyethylene glycol
<b>PFA</b>	Paraformaldehyd
<b>PFM</b>	Pentafluorophenyl methacrylate
<b>pp-PFM</b>	Plasma polymerized PFM
<b>PTFE</b>	Polytetrafluoroethylene
<b>Q</b>	Polydispersivity
<b>ROI</b>	Region of interest
<b>SL</b>	Stereolithography
<b>SLM</b>	Selective laser melting
<b>SLS</b>	Selective laser sintering
<b>STL</b>	Stereolithography file format
<b>T-01 MVV</b>	Primary respiratory human fibroblast cells
<b>TFF</b>	Tangential flow filtration
<b>TSB</b>	Tryptic soy broth
<b><math>\alpha</math>-SMA</b>	$\alpha$ -Smooth muscle actin

## List of Publications

(1) Gilabert-Porres, J.; Martí, S.; Calatayud, L.; Ramos, V.; Rosell, A.; Borrós, S. Design of a Nanostructured Active Surface against Gram-Positive and Gram-Negative Bacteria through Plasma Activation and in Situ Silver Reduction. *ACS Appl. Mater. Interfaces* **2016**, *8* (1), 64–73 DOI: 10.1021/acsami.5b07115.

(2) Montes-Worboys, A.; Gilabert-Porres, J.; Lopez-Lisbona, R.; Cubero-Frutos, N.; Borros, S.; Rosell, A. Effect of paclitaxel delivered nanoparticles to treat tracheal stenosis. *Eur. Respir. J.* **2015**, *46* (suppl 59), PA4870 DOI: 10.1183/13993003.congress-2015.PA4870.

(3) Díez-Ferrer, M.; Martí, S.; Calatayud, L.; Gilabert, J.; Ardanuy, C.; Borros, S.; López-Lisbona, R.; Cubero, N.; Linares, J.; Dorca, J.; et al. In vitro evaluation of silver-coated silicone tracheobronchial stents on growth and attachment of clinical isolates. *Eur. Respir. J.* **2014**, *44* (Suppl 58), P700.

(4) Martí, S.; Calatayud, L.; Gilabert, J.; Díez-Ferrer, M.; Puig, C.; Cubero, N.; López-Lisbona, R. M.; Borrós, S.; Ardanuy, C.; Liñares, J.; et al. Colonization of central airways after tracheobronchial stenting: could silver-coated silicone stents be a solution? *Under Revis. Plos One*.

(5) Gilabert-Porres, J.; Montes-Worboys, A.; Borros, S.; Rosell, A. Design of an immobilized drug delivery platform with paclitaxel-loaded nanoparticles to treat stenotic tissue. *In Preparation*.

## List of Patents

(1) López García, L.; Ramírez Gutiérrez, O. H.; Francesch de Castro, L.; Borrós Gómez, S.; Agulló Chaler, N.; Gilabert Porres, J.; Vilar Abril, L. Ink Composition for Inkjet Printing. *WO 2014/188029 A1* **2014**.

(2) Borrós, S.; Gilabert, J.; Martí, S.; Molina, M.; Montes, A.; Ramos, V.; Rosell, A. Process for Manufacturing a Customizable Medical Device and Device Obtained by Said Process. *WO 2016/023980* **2014**.

## Oral Presentations

(1) Gilabert-Porres, J.; López-Lisbona, R. M.; Cubero de Frutos, N.; Borrós, S.; Rosell-Gratacos, A.; Montes-Worboys, A. Effect of paclitaxel delivered nanoparticles to treat tracheal stenosis. *3rd Eur. Congr. Bronchol. Interv. Pulmonol.* **2015**.

## List of Posters

(1) Montero, L.; Estrada, O.; Gilabert, J.; Ramos-Pérez, V.; Villa, R.; Borrós, S. Following the mechanism of biofilm formation tailoring surface modification on impedance sensors. *Eur. Cells Mater.* **2011**, 21 (SUPPL.2), 62.

(2) Gilabert, J.; Estrada, O.; Soler, G.; Ramos, V.; Borrós, S. Bioactive Prosthesis Enhancing Healing Process for Orthodontics. *Restor. Work.* **2012**.

(3) Martí, S.; Calatayud, L.; Gilabert, J.; Ardanuy, C.; Borrós, S.; López-Lisbona, R. M.; Cubero, N.; Rosell, A.; Linares, J. In vitro evaluation of silver-coated silicone on growth and attachment of clinical isolates from patients with tracheobronchial stents. *Eurobiofilms Third Eur. Congr. Microb. Biofilms-Basic Clin. Asp.* **2013**.

(4) Gilabert, J.; Bardají, S.; Ramos, V.; Borrós, S. Novel thixotropic paste containing prp to enhance maxillofacial bone recovery. *25th Eur. Conf. Biomater.* **2013**.

(5) Díez-Ferrer, M.; Martí, S.; Calatayud, L.; Gilabert, J.; Ardanuy, C.; Borrós, S.; López-Lisbona, R. M.; Cubero, N.; Linares, J.; Dorca, J.; et al. Avaluació in vitro del creixement i adherència d'aïllaments microbiològics en pròtesis traqueobronquials de silicona amb revestiment de plata. *XXXII Diada Pneumològica (Poster)* **2014**.

(6) Gilabert, J.; Borrós, S. New Selectively Bioactive Surfaces Fabricated by PECVD. *Mater. Sci. Eng. Young Res. meet Prof.* **2014**.

(7) Díez-Ferrer, M.; Martí, S.; Calatayud, L.; Gilabert, J.; Ardanuy, C.; Borrós, S.; López-Lisbona, R. M.; Cubero, N.; Linares, J.; Rosell, A. Evaluación in vitro del crecimiento y adherencia de aislamientos microbiológicos en prótesis traqueobronquiales de silicona con revestimiento de plata. *XX Congr. Nac. Asoc. Española Endosc. Respir. y Neumol. Interv.* **2014**.

(8) Díez-Ferrer, M.; Martí, S.; Calatayud, L.; Gilabert, J.; Ardanuy, C.; Borrós, S.; López-Lisbona, R.; Cubero, N.; Linares, J.; Dorca, J.; et al. In vitro evaluation of silver-coated silicone tracheobronchial stents on growth and attachment of clinical isolates. *Eur. Respir. J.* **2014**, 44 (Suppl 58).

(9) Díez-Ferrer, M.; Martí, S.; Calatayud, L.; Gilabert, J.; Ardanuy, C.; Borrós, S.; López-Lisbona, R. M.; Cubero, N.; Linares, J.; Rosell, A. In vitro evaluation of silver-coated silicone tracheobronchial stents of growth and attachment of clinical isolates. 18th WCBIP/WCBE **2014**.

(10) Montes-Worboys, A.; Gilabert-Porres, J.; Lopez-Lisbona, R.; Cubero-Frutos, N.; Borros, S.; Rosell, A. Effect of paclitaxel delivered nanoparticles to treat tracheal stenosis. Eur. Respir. J. **2015**, 46 (suppl 59) DOI: 10.1183/13993003.congress-2015.PA4870.

*This page left blank intentionally*

## **Chapter I. Introduction**



*This page left blank intentionally*

## 1.1 Introduction

In 1900, human life expectancy never exceeded the progressive decrease in quality of tissues, therefore there was no need for tissue replacement. For centuries, when a tissue became diseased or damaged, people could treat or remove that specific part with limited resources. However, during the last century, the situation changed thanks to medical advances, such as the development of antibiotics like penicillin, chemical treatments and more important, hygiene, which increased the human survival.<sup>1</sup> In the last few years, there has been an explosive growth of transplantations and implantations of medical devices to replace damaged tissues and increase the life expectancy.<sup>2,3</sup>

During the last few decades, many efforts of biomedical engineers have been centered on the replacement of body tissues, structures or organs with living tissues, known as **transplants**. However, the limitations involving transplants include ethical or immunological concerns, availability of tissues, second-site morbidity, tendency to resorption, compromise in biomechanical properties and the use of immunosuppressant drugs. These limitations urge the need to develop alternatives with ameliorated fully synthetic materials or modified natural materials, such as **implants** or prosthesis.<sup>4</sup>

Implants are being used for different reasons, such as the replacement of tissues that have either been damaged or destroyed through pathological processes, to treat congenital defects and corrective trauma or cosmetic surgery. For example, metallic prostheses are used in orthopedic surgery to replace bone tissue that has been fractured or damage due to aging. In the treatment of wounds the application of biomaterials may be in the form of suture materials, artificial ligaments and bone fixators.<sup>5</sup> However, biomaterials were not only used as prosthesis, coatings for sensors<sup>6,7</sup>, pacemakers and drug delivery systems within the body, among others<sup>8,9</sup>, are other examples of applications that requires biomaterials.

Biomaterials have generated much interest to develop devices, organs or tissues to be in contact with body fluids and body parts acting as a native part of the body without the previous limitations and, ideally, without causing major unwanted responses.<sup>10</sup> Biomaterials have evolved during the years and nowadays three different generations are clearly differentiated: **bioinert materials** (first generation), **bioactive and biodegradable materials** (second generation) and **materials designed to stimulate specific cellular responses at the molecular level** (third generation).<sup>11</sup>

The main limitation of the inert biomaterials is that these materials are adopted from other areas of science and technology without substantial redesign for medical use. However, the human body consists of a highly corrosive environment and a broad variety of textures and mechanical properties and such requirements are imposed to select the best materials for each device. Second generation of biomaterials present the ability to interact with the biological environment to enhance the biological response. Additionally, this kind of biomaterials has the ability to undergo a progressive degradation while new tissue regenerates and heals. Despite all the progress that has been made, the structure of the tailor-made biomaterials is relatively simple in comparison to that of the complex cellular structure of the tissues being replaced.<sup>5</sup> Finally, the third generation of biomaterials are able to stimulate specific

cellular responses at the molecular level through their 3D environment. These materials combine the bioactivity and biodegradability together with 3D porous structures that stimulate cellular homing, attachment and proliferation and functionalized surfaces with proteins to mimic the extracellular matrix (ECM).<sup>11</sup>

Although first generation materials helped in the development of new medical treatments, there are still some complications that bioengineers have to take into account when designing a new implant or prosthesis regarding to **Biocompatibility** and **Biofunctionality**, such as chemical signaling (receptor-ligand recognition, intracellular signals cascade, cellular response), interfacial stability with host tissues, biomechanical mismatch of elastic moduli, matrix deformation, cell deformation, micro or nanostructure, matrix stiffness, controlled degradation, generation of wear debris, maintenance of a stable blood supply, lack of ability to self-repair, the ability to modify their structure and properties in response to environmental factors, such as mechanical load or blood flow and their limited lifetimes.<sup>4,12</sup> Regarding the non-specific response from biological systems upon implantation, this phenomenon can be caused because the biomaterial does not mimic the environment. In order to obtain a suitable biomaterial, it is important that the material fulfils the requirements of biocompatibility and biofunctionality for each specific application. Because of that, a common approach is to fabricate medical devices with the biomaterial having the adequate bulk properties and additionally adding a surface treatment to enhance its surface properties.<sup>13</sup>

In the present days, implants such as jaw bone<sup>14</sup>, heart valves<sup>15</sup>, pacemaker<sup>8,16</sup> and vascular<sup>8,17</sup> and non-vascular<sup>18-21</sup> stents have to be in close contact with tissues of different nature.<sup>22</sup> In this context, it is important to use smart engineered biomaterials<sup>23,24</sup> in order to keep the biocompatibility and the biofunctionality between the surfaces of the devices and the surrounding tissues. These smart materials shall present the bulk material properties to match the mechanical and structural behavior and, additionally, present specific features to elicit the desired response on each tissue depending on its surface. However, the performance of this devices that are designed to be implanted at the interface of surfaces with drastically different properties is challenging and consequently, this new generation of materials needs multifunctional surfaces that should be designed to specifically interact with the different tissues and applications. This is especially relevant for devices whose surfaces are directly in contact with tissues and fluids, such as the case of a stent.

In the present days, tracheal implants are a clear example of medical devices that require the engineering of biomaterials with multifunctional surfaces. Tracheal stents are hollow tubes used to treat laryngotracheal stenosis, which causes the reduction of the trachea wall, by restoring the airway passage to the lungs. This reduction in the trachea wall caused by tracheal stenosis or cancer<sup>25</sup> leads to a considerable reduction in the quality of life of the patients with problems of breathing, speaking and swallowing.<sup>26</sup> In order to restore airway passage, different debulking methods can be endoscopically used to recover lumen patency, and once reopened, stents are implanted to avoid restenosis.<sup>27-29</sup> The only property of current stents consists on mechanical expansion to maintain the passage open. However, different complications related to stent implantation<sup>30,31</sup>, such as stent migration, obstruction

by secretions and granulomas<sup>32,33</sup>, persistent bacteria colonization<sup>34</sup> and recurrence<sup>35</sup>, are threatening the life of patients and often the initial pathology remains unhealed.

Considering the previous listed problems that affects tracheal stents, this work pretends to develop a customizable solution for each of them by grouping all the post-implantation problems into three different blocks, such as avoid bacteria colonization, design a drug delivery platform to treat stenotic tissue and recurrence, and re-design the stent with an anatomical geometry to increase the adaptability and avoid migration and the formation granulation tissue.

As mentioned before, one of the most common complications related to stent implantation is bacterial colonization.<sup>36-38</sup> Bacterial colonization can reduce quality of life, induce infection or even sepsis that can cause death of the patient, if appropriate care is not taken.<sup>33,39</sup> Bacterial colonization and biofilm formation onto the implanted medical devices are a serious problem accounting for over 80% of intrahospital microbial infections.<sup>40</sup> Although antibiotics can treat the great majority of them, they are not completely effective in the case of a contaminated device, can generate resistance, increase the cost<sup>41</sup> and produce adverse effects on patients.<sup>40,42</sup> Silver presents high toxicity against microorganisms, wide spectrum of action, non-bacterial resistance and is not toxic to human tissues.<sup>43</sup> Because of that, prevention by avoiding biofilm formation by means of covering catheters and tubs with different antimicrobial agents like silver can be more convenient.<sup>44,45</sup>

The second main problem consists in a recurrence of tracheobronchial stenosis after stent removal and granulation tissue formation, Figure I-1. Tracheal resection surgery is the gold standard treatment with excellent results in the 90% of the cases, but it is not always a definitive treatment.<sup>30,46-48</sup> The recurrence rate can reach, up to 10%<sup>35</sup>, present a rate of major complications of 8-12%<sup>30,31</sup> and a mortality rate of 5%<sup>46,49</sup>. In addition, there are other treatments like the endoscopic treatment, combined with different techniques, such as laser thermal ablation or electrocautery, the resection and mechanical dilatation with rigid bronchoscopy, the mechanical balloon dilatations and the silicone stent implantation.<sup>28,29</sup> However, the effectivity of long term multimodal endoscopic treatment is not exempt from recurrence and presents a great variability accounting nearly half of the patients (55-90%).<sup>50,51</sup>

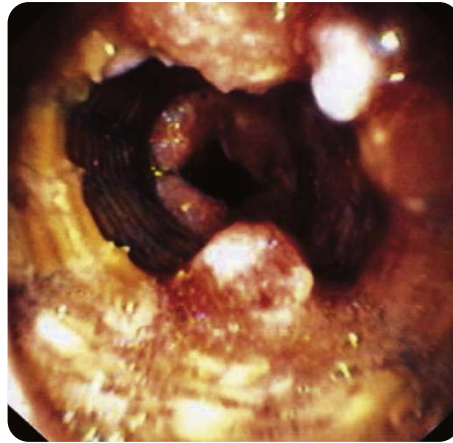


**Figure I-1.** Granulation tissue at the edges of the tracheal stent. This type of tissue is caused by the rubbing and movement of the stent over the tracheal airway.<sup>33</sup>

In the recent years, some clinical experiences using topical drugs to treat subglottic stenosis have been published. Pharmacological treatment in combination with the endoscopy, is based in the intralesional injection of corticoids or, more recently, topical use of mitomycin-C.<sup>52,53</sup> Both have shown mixed results in small series of patients. Now, none of these treatments are definitive, but some animal models with dogs have shown that after weekly repeated topical treatments of mitomycin in metallic prosthesis, the stents did not induce the formation of granulation tissue.<sup>54</sup>

In other applications, e.g. cardiology, antiproliferative drug eluting stents have become a great advance to avoid re-stenosis.<sup>55,56</sup> Similarly, in tracheal stenosis, researchers observed in animal studies that auto-expandable metallic silicone prostheses previously soaked with paclitaxel (PCTXL) avoided granulation tissue formation in 100%, 96%, 76% and 65% of cases at 1, 4, 8 and 12 weeks respectively, in contrast of the non-drug eluting stents, which were occluded at first week.<sup>57</sup> Recently, other antiproliferative drugs, such as Pirfenidone and Rapamycin, used as treatment for other pulmonary pathologies, such as idiopathic pulmonary fibrosis, are being used as possible future treatments for benign and malignant tracheal stenosis applied from a prosthesis.<sup>58</sup>

Finally, the last main problem related with post-implantation disadvantages consisted on the low adaptability of the current stents to the trachea airway. As human trachea is not a perfect circular transversal profile (Figure I-2), but an elliptical, D-Shaped, U-Shaped or triangular contour depending on sex and age, the current stents present poor adaptability in the implantation area.<sup>59,60</sup> This lack of fitting leads to migration of the stent along the trachea causing severe pain and threatening critical parts of the airway, such as the vocal cords.<sup>61</sup> Besides, this migration or movement of the stent causes granuloma tissue at the edges of the stents as a consequence of mechanical stress and rubbing.<sup>32,62</sup> In addition, this inflammatory tissue can be a life threatening complication, if not treated with glucocorticoids or endoscopic thermal ablation.<sup>63-65</sup> Some designs have tried to mimic de tracheal geometry such as Natural Stent (TNO Company, Seoul – Korea),<sup>66</sup> but despite all possibilities several complications, such as migration, formation of granulation tissue around the stent and retained secretions, are threaten the stent implantation.<sup>67</sup> However, these problems can be avoided with

increasing the adaptability and designing a suitable stent for the desired implantation zone with an anatomical redesign of the stent.<sup>68</sup>

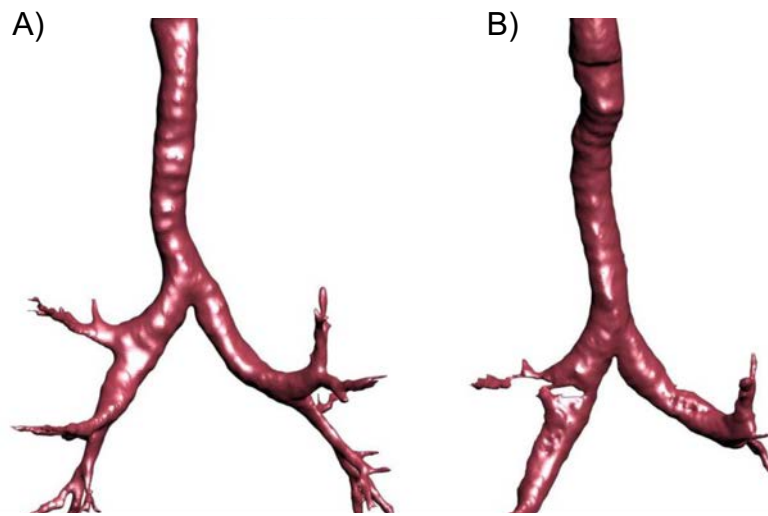


**Figure I-2.** Trachea reconstruction from a Computed Tomography (CT) Scan. **A)** Inspiration reconstruction and **B)** Expiration reconstruction.<sup>69</sup>

Taking all of these into account, the problems related with the tracheal stent implantation are caused by a low biocompatibility and low biofunctionality of the stent. Since biocompatibility and biofunctionality are determined by the interaction between the surface of the material and the surrounding tissues, in order to overcome the drawbacks of the tracheal stent, it is imperative to control the influencing factors that determine the behavior of the cells (or even bacterial colonization), such as the chemical structure and composition of the surface, hydrophilicity, hydrophobicity, morphology, the structure of a multi-component system (crystalline and amorphous domains), stiffness and the topography.<sup>5</sup> Therefore, the modification and control of the free-surface of the medical devices is critical to provide surface-cell interaction resulting in a higher biocompatibility.<sup>13</sup>

For instance, surface modifications can encourage the immobilization of biomolecules, such as proteins or other chemical motifs to enhance cell recognition.<sup>70</sup> Surface modification techniques allow to modify the surface of the materials, changing their surface properties without changing the bulk properties of the material.<sup>70</sup> The most interesting advantage of surface modification is that it can modify almost all types of materials.<sup>71</sup> Additionally, not only the chemical structure of the surface is important for the cellular recognition and biocompatibility, but also the structuration of the surface provides important information for cell adhesion and spreading.<sup>72,73</sup>

The immobilization of a bioactive compound onto a polymeric surface can be done by adsorption via electrostatic interactions, ligand-receptor pairing or covalent attachment. However, one of the most interesting methods is the covalent bond because it provides a more stable bond between the compound and the functionalized surface. This stability increases the half-life of the biomolecule onto



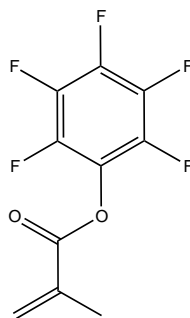


**Figure I-4.** Chemical structure of pentafluorophenyl methacrylate.

PFM coated surfaces present high reactivity against primary amines in aqueous solutions, that can be used to covalently bind proteins, such as bovine serum albumin (BSA) and fibrinogen, chemical moieties and nanoparticles to the surface.<sup>79</sup>

Therefore, plasma techniques can be used to develop reactive surfaces in order to provide different functionalities or bioactivities to the medical device. In addition, the advantage of the plasma process to occurs in vapor/gas phase, allows complex geometries to be easily modified. Thus, the surfaces of anatomical structures, such as prosthesis or *stents*, can be modified to increase the biocompatibility and the implanted device interaction, with the surrounding tissue.

Finally, in addition to the development of a bioactive coatings to provide antibacterial properties and a drug release system, there is a need to increase the adaptability of the device to the anatomical area where it is implanted. However, anatomical geometries cannot be fabricated by conventional manufacturing processes because of the limitations of the technology. In this context, over the past few decades, printing technology has advanced from two-dimensional (2D) printing to an additive process in which successive layers of material are distributed to form three-dimensional (3D) shapes, leading to complex geometries for a wide range of applications, eliminating parts, materials, waste and reducing the need for tooling.<sup>81-83</sup> This technology allows to create complex structures and can be applied to enable rapid prototyping and manufacturing in industry to produce customized products, such as bicycle parts, jewelry and electrical components. In addition, 3D printing is transforming other fields like science, education and specially medicine with an undeniable impact of 3D printing technology for our society.<sup>84</sup>

Nowadays, there is a close relationship between the 3D printing field and regenerative medicine to the point that 3D printing technology has completely changed the paradigm of personalized medicine. 3D printing creates a new approach that can be applied in nearly all issues that personalized medicine tries to overcome. For instance, reconstructive surgery<sup>85,86</sup>, scaffolds for aortic valve replacement<sup>87</sup> and trachea prostheses for stenosis treatment<sup>88</sup> are only few cases where 3D printing technologies is showing a critical impact by redesigning the devices and the treatments to provide a more personalized treatment (geometry of the scaffold or prosthesis) to treat the individual pathology which a specific patient is suffering.



Actually, 3D printing technology aims to go much further seeking to reproduce any part of the human body<sup>89</sup>, such as the research in the development of materials to simulate complex tissues such as cartilage<sup>90-93</sup>, the fabrication of bioactive scaffolds<sup>94</sup> or directly the printing of living tissue<sup>95</sup>. In addition, 3D printing technologies show a great potential to develop personalized geometries, even personalized organs, due to its ability to recreate complex parts of the human body with high precision, its versatility that can be useful to fabricate new prostheses and, to produce custom products at relatively low prices using new materials.

Despite all the progress made with different tracheal stent designs, the post-implantations problems remain still unsolved, threatening the life of the patients and shortening the life quality of the patients.

In the first place, the new developments regarding to antibacterial agents such as silver nanoparticles or antibacterial drugs, anchored on the surface of the medical devices could be a very promising solution to avoid the bacterial colonization of the device and to enhance the performance implant.<sup>96</sup>

Secondly, the research and clinical trials performed with antiproliferative drugs (topically administered) show a great potential to reduce the recurrence rate of the stenotic or tumor tissue and reduce the formation of the granulation tissue. Therefore, the tracheal stent or other medical device could be used as a controlled drug deliver platform to locally release different types of drugs (such as PCTXL or mitomycin) to treat abnormal proliferation or other types of pathologies. In this case, the surface plasma techniques show a great potential for the immobilization of chemical molecules, such as small drugs, or even high structures, such as proteins, antibodies<sup>97</sup> and nanoparticles.

Finally, in order to overcome the drawbacks and problems caused by the low adaptability of the current stent geometries, 3D printing technologies and computer-aided design (CAD) can facilitate the design and manufacture of new complex geometries of scaffolds, which fit more naturally and adapt to the patient geometries. As a result, the new scaffolds should present less migration rate, avoid the formation of the granulation tissue at the edges of the patient and increase the performance of the prosthesis, reducing the chronic pain.

Taking into account the above-mentioned limitations of the current treatments for tracheal diseases, the main objective of this thesis is the development of new personalized prostheses (tracheal stent or similar) with different bioactivity, such as antibacterial and antiproliferative (regarding to its surfaces, internal and external) and with a customized geometry based on the patient anatomy.

Therefore, in order to accomplish the main objective of this work, this thesis have been separated into the following goals:

- Development, optimization and characterization of a covalent surface modification of different substrates in order to create reactive surfaces to be personalized with different bioactive agents (Chapter II).

- Design and characterization of flexible antibacterial surfaces functionalized with silver coating to be used in the internal or external tracheal stents surfaces (Chapter II).
- Development and characterization of flexible antiproliferative surfaces functionalized with degradable drug loaded nanoparticles to be used in the external tracheal stent surfaces (Chapter III).
- Design a protocol to extract, optimize and model different images from a CT scan (using different CAD software) to design injection molds to be printed with 3D printing technologies. This injection molds will be used to inject silicone and obtain a personalized and fully adaptable tracheal stent to the patient anatomy (Chapter IV).

## 1.2 References

- (1) Hench, L. L. Biomaterials: a forecast for the future. *Biomaterials* **1998**, *19* (16), 1419–1423 DOI: 10.1016/S0142-9612(98)00133-1.
- (2) Castner, D. G.; Ratner, B. D. Biomedical surface science: Foundations to frontiers. *Surf. Sci.* **2002**, *500* (1–3), 28–60 DOI: 10.1016/S0039-6028(01)01587-4.
- (3) Bronzino, J. D. *The Biomedical Engineering HandBook. Volume I*, Second.; CRC Press LLC & Springer-Verlag GmbH & Co.KG: Boca Raton, 2000.
- (4) Pal, S. *Design of Artificial Human Joints & Organs*; Springer US: Boston, MA, 2014.
- (5) Klee, D.; Höcker, H. Polymers for biomedical applications: Improvement of the interface compatibility. *Adv. Polym. Sci.* **1999**, *149*, 1–57 DOI: 10.1007/3-540-48838-3\_1.
- (6) Dai, L.; StJohn, H. A. W.; Bi, J.; Zientek, P.; Chatelier, R. C.; Griesser, H. J. Biomedical coatings by the covalent immobilization of polysaccharides onto gas-plasma-activated polymer surfaces. *Surf. Interface Anal.* **2000**, *29* (1), 46–55 DOI: 10.1002/(SICI)1096-9918(200001)29:1<46::AID-SIA692>3.0.CO;2-6.
- (7) Favia, P.; D'Agostino, R. Plasma treatments and plasma deposition of polymers for biomedical applications. *Surf. Coatings Technol.* **1998**, *98* (1–3), 1102–1106 DOI: 10.1016/S0257-8972(97)00285-5.
- (8) Mani, G.; Feldman, M. D.; Patel, D.; Agrawal, C. M. Coronary stents: A materials perspective. *Biomaterials* **2007**, *28* (9), 1689–1710 DOI: 10.1016/j.biomaterials.2006.11.042.
- (9) Finkelstein, A.; McClean, D.; Kar, S.; Takizawa, K.; Varghese, K.; Baek, N.; Park, K.; Fishbein, M. C.; Makkar, R.; Litvack, F.; et al. Local drug delivery via a coronary stent with programmable release pharmacokinetics. *Circulation* **2003**, *107* (5), 777–784 DOI: 10.1161/01.CIR.0000050367.65079.71.
- (10) Williams, D. F. On the mechanisms of biocompatibility. *Biomaterials* **2008**, *29* (20), 2941–2953 DOI: 10.1016/j.biomaterials.2008.04.023.
- (11) Navarro, M.; Michiardi, A.; Castaño, O.; Planell, J. a. Biomaterials in orthopaedics. *J. R. Soc. Interface* **2008**, *5* (27), 1137–1158 DOI: 10.1098/rsif.2008.0151.
- (12) Langer, R.; Tirrell, D. a. Designing materials for biology and medicine. *Nature* **2004**, *428* (6982), 487–492 DOI: 10.1038/nature02388.
- (13) Chu, P. K.; Chena, J. .; Wang, L. P.; Huangb, N. Plasma-surface modification of biomaterials. *Mater. Sci. Eng. R Reports* **2002**, *36* (5–6), 143–206 DOI: 10.1016/S0927-796X(02)00004-9.

- 
- (14) Fortin, Y.; Sullivan, R. M.; Rangert, B. R. The Marius Implant Bridge: Surgical and Prosthetic Rehabilitation for the Completely Edentulous Upper Jaw with Moderate to Severe Resorption: A 5-Year Retrospective Clinical Study. *Clin. Implant Dent. Relat. Res.* **2002**, *4* (2), 69–77 DOI: 10.1111/j.1708-8208.2002.tb00155.x.
- (15) Jiang, H.; Manolache, S.; Wong, A. C. L.; Denes, F. S. Plasma-enhanced deposition of silver nanoparticles onto polymer and metal surfaces for the generation of antimicrobial characteristics. *J. Appl. Polym. Sci.* **2004**, *93* (3), 1411–1422 DOI: 10.1002/app.20561.
- (16) Esposito, M.; Kennergren, C.; Holmström, N.; Nilsson, S.; Eckerdal, J.; Thomsen, P. Morphologic and immunohistochemical observations of tissues surrounding retrieved transvenous pacemaker leads. *J. Biomed. Mater. Res.* **2002**, *63* (5), 548–558 DOI: 10.1002/jbm.10306.
- (17) O'Brien, B.; Carroll, W. The evolution of cardiovascular stent materials and surfaces in response to clinical drivers: A review. *Acta Biomater.* **2009**, *5* (4), 945–958 DOI: 10.1016/j.actbio.2008.11.012.
- (18) Ernst, A.; Majid, A.; Feller-Kopman, D.; Guerrero, J.; Boiselle, P.; Loring, S. H.; O'Donnell, C.; Decamp, M.; Herth, F. J. F. F.; Gangadharan, S.; et al. Airway stabilization with silicone stents for treating adult tracheobronchomalacia: a prospective observational study. *Chest* **2007**, *132* (2), 609–616 DOI: 10.1378/chest.06-2708.
- (19) Loring, S. H.; O'Donnell, C. R.; Feller-Kopman, D. J.; Ernst, A. Central Airway Mechanics and Flow Limitation in Acquired Tracheobronchomalacia. *Chest* **2007**, *131* (4), 1118–1124 DOI: 10.1378/chest.06-2556.
- (20) Han, X. W.; Wu, G.; Li, Y. D.; Zhang, Q. X.; Guan, S.; Ma, N.; Ma, J. Overcoming the Delivery Limitation: Results of an Approach to Implanting an Integrated Self-expanding Y-shaped Metallic Stent in the Carina. *J. Vasc. Interv. Radiol.* **2008**, *19* (5), 742–747 DOI: 10.1016/j.jvir.2008.01.022.
- (21) Ng, A. H. C.; Ng, N. S. P.; Zhu, G. H.; Lim, L. H. Y.; Venkatraman, S. S. A fully degradable tracheal stent: In vitro and in vivo characterization of material degradation. *J. Biomed. Mater. Res. - Part B Appl. Biomater.* **2012**, *100 B* (3), 693–699 DOI: 10.1002/jbm.b.32501.
- (22) Ratner, B. D. The engineering of biomaterials exhibiting recognition and specificity. *J. Mol. Recognit.* **1996**, *9* (July 1995), 617–625 DOI: 10.1002/(sici)1099-1352(199634/12)9:5/6<617::aid-jmr310>3.0.co;2-d.
- (23) Balint, R.; Cassidy, N. J.; Cartmell, S. H. Conductive polymers: towards a smart biomaterial for tissue engineering. *Acta Biomater.* **2014**, *10* (6), 2341–2353 DOI: 10.1016/j.actbio.2014.02.015.

- (24) Kopeček, J. Smart and genetically engineered biomaterials and drug delivery systems. *Eur. J. Pharm. Sci.* **2003**, *20* (1), 1–16 DOI: 10.1016/S0928-0987(03)00164-7.
- (25) Chin, C. S.; Litle, V.; Yun, J.; Weiser, T.; Swanson, S. J. Airway Stents. *Ann. Thorac. Surg.* **2008**, *85* (2), S792–S796 DOI: 10.1016/j.athoracsur.2007.11.051.
- (26) Baiguera, S.; Jungebluth, P.; Burns, A.; Mavilia, C.; Haag, J.; De Coppi, P.; Macchiarini, P. Tissue engineered human tracheas for in vivo implantation. *Biomaterials* **2010**, *31* (34), 8931–8938 DOI: 10.1016/j.biomaterials.2010.08.005.
- (27) Melkane, A. E.; Matar, N. E.; Haddad, A. C.; Nassar, M. N.; Almoutran, H. G.; Rohayem, Z.; Daher, M.; Chalouhy, G.; Dabar, G. Management of postintubation tracheal stenosis: Appropriate indications make outcome differences. *Respiration* **2010**, *79* (5), 395–401 DOI: 10.1159/000279225.
- (28) Galluccio, G.; Lucantoni, G.; Battistoni, P.; Paone, G.; Batzella, S.; Lucifora, V.; Iacono, R. Dello. Interventional endoscopy in the management of benign tracheal stenoses: definitive treatment at long-term follow-up. *Eur. J. Cardio-thoracic Surg.* **2009**, *35* (3), 429–433 DOI: 10.1016/j.ejcts.2008.10.041.
- (29) Brichet, A.; Verkindre, C.; Dupont, J.; Carlier, M. L.; Darras, J.; Wurtz, A.; Ramon, P.; Marquette, C. H. Multidisciplinary approach to management of postintubation tracheal stenoses. *Eur. Respir. J.* **1999**, *13* (4), 888–893 DOI: 10.1034/j.1399-3003.1999.13d32.x.
- (30) Rea, F.; Callegaro, D.; Loy, M.; Zuin, A.; Narne, S.; Gobbi, T.; Grapeggia, M.; Sartori, F. Benign tracheal and laryngotracheal stenosis: Surgical treatment and results. *Eur. J. Cardio-thoracic Surg.* **2002**, *22* (3), 352–356 DOI: 10.1016/S1010-7940(02)00342-1.
- (31) Marulli, G.; Rizzardi, G.; Bortolotti, L.; Loy, M.; Breda, C.; Hamad, A.-M.; Sartori, F.; Rea, F. Single-staged laryngotracheal resection and reconstruction for benign strictures in adults. *Interact. Cardiovasc. Thorac. Surg.* **2008**, *7* (2), 227–230 DOI: 10.1510/icvts.2007.168054.
- (32) Pérez del Palomar, A.; Trabelsi, O.; Mena, A.; López-Villalobos, J. L.; Ginel, A.; Doblaré, M. Patient-specific models of human trachea to predict mechanical consequences of endoprosthesis implantation. *Philos. Trans. A. Math. Phys. Eng. Sci.* **2010**, *368* (1921), 2881–2896 DOI: 10.1098/rsta.2010.0092.
- (33) Charokopos, N.; Foroulis, C. N.; Rouska, E.; Sileli, M. N.; Papadopoulos, N.; Papakonstantinou, C. The management of post-intubation tracheal stenoses with self-expandable stents: early and long-term results in 11 cases. *Eur. J. Cardio-Thoracic Surg.* **2011**, *40* (4), 919–924 DOI: 10.1016/j.ejcts.2010.12.042.
- (34) Martínez-Ballarín, J. I.; Díaz-Jiménez, J. P.; Castro, M. J.; Moya, J. a. Silicone stents in the

- management of benign tracheobronchial stenoses: Tolerance and early results in 63 patients. *Chest* **1996**, *109* (3), 626–629 DOI: 10.1378/chest.109.3.626.
- (35) Abbasidezfouli, A.; Akbarian, E.; Shadmehr, M. B.; Arab, M.; Javaherzadeh, M.; Pejhan, S.; Abbasi-Dezfouli, G.; Farzanegan, R. The etiological factors of recurrence after tracheal resection and reconstruction in post-intubation stenosis. *Interact. Cardiovasc. Thorac. Surg.* **2009**, *9* (3), 446–449 DOI: 10.1510/icvts.2009.202978.
- (36) Casal, R. F. Update in airway stents. *Curr. Opin. Pulm. Med.* **2010**, *16* (4), 321–328 DOI: 10.1097/MCP.0b013e32833a2601.
- (37) Lund, M. E.; Garland, R.; Ernst, A. Airway stenting: Applications and Practice management considerations. *Chest* **2007**, *131* (2), 579–587 DOI: 10.1378/chest.06-0766.
- (38) Noppen, M.; Piérard, D.; Meysman, M.; Claes, I.; Vincken, W. Bacterial Colonization of Central Airways after Stenting. *Am. J. Respir. Crit. Care Med.* **1999**, *160* (2), 672–677 DOI: 10.1164/ajrccm.160.2.9812081.
- (39) Zakaluzny, S. Complications of tracheobronchial airway stents. *Otolaryngol. - Head Neck Surg.* **2003**, *128* (4), 478–488 DOI: 10.1016/S0194-5998(03)00002-0.
- (40) Davies, D. Understanding biofilm resistance to antibacterial agents. *Nat. Rev. Drug Discov.* **2003**, *2* (2), 114–122 DOI: 10.1038/nrd1008.
- (41) Rupp, M. E.; Fitzgerald, T.; Marion, N.; Helget, V.; Puumala, S.; Anderson, J. R.; Fey, P. D. Effect of silver-coated urinary catheters: Efficacy, cost-effectiveness, and antimicrobial resistance. *Am. J. Infect. Control* **2004**, *32* (8), 445–450 DOI: 10.1016/j.ajic.2004.05.002.
- (42) Chen, W.; Liu, Y.; Courtney, H. S.; Bettenga, M.; Agrawal, C. M.; Bumgardner, J. D.; Ong, J. L. In vitro anti-bacterial and biological properties of magnetron co-sputtered silver-containing hydroxyapatite coating. *Biomaterials* **2006**, *27* (32), 5512–5517 DOI: 10.1016/j.biomaterials.2006.07.003.
- (43) Zhao, L.; Wang, H.; Huo, K.; Cui, L.; Zhang, W.; Ni, H.; Zhang, Y.; Wu, Z.; Chu, P. K. Antibacterial nano-structured titania coating incorporated with silver nanoparticles. *Biomaterials* **2011**, *32* (24), 5706–5716 DOI: 10.1016/j.biomaterials.2011.04.040.
- (44) Knetsch, M. L. W.; Koole, L. H. New Strategies in the Development of Antimicrobial Coatings: The Example of Increasing Usage of Silver and Silver Nanoparticles. *Polymers (Basel)*. **2011**, *3* (4), 340–366 DOI: 10.3390/polym3010340.
- (45) Greulich, C.; Braun, D.; Peetsch, A.; Diendorf, J.; Siebers, B.; Epple, M.; Köller, M. The toxic effect of silver ions and silver nanoparticles towards bacteria and human cells occurs in the same concentration range. *RSC Adv.* **2012**, *2* (17), 6981 DOI: 10.1039/c2ra20684f.

- (46) Lorenz, R. R. Adult laryngotracheal stenosis: etiology and surgical management. *Curr. Opin. Otolaryngol. Head Neck Surg.* **2003**, *11* (6), 467–472 DOI: 10.1097/00020840-200312000-00011.
- (47) Ashiku, S. K.; Kuzucu, A.; Grillo, H. C.; Wright, C. D.; Wain, J. C.; Lo, B.; Mathisen, D. J.; Pearson, F. G.; Wood, D. E. Idiopathic laryngotracheal stenosis: Effective definitive treatment with laryngotracheal resection. *J. Thorac. Cardiovasc. Surg.* **2004**, *127* (1), 99–107 DOI: 10.1016/j.jtcvs.2002.11.001.
- (48) París, F.; Borro, J. M.; Tarrazona, V.; Casillas, M.; Galan, G.; Caffarena, J. M.; Segui, J. Management of non-tumoral tracheal stenosis in 112 patients. *Eur. J. Cardiothorac. Surg.* **1990**, *4* (5), 265-268-269 DOI: 10.1016/1010-7940(90)90250-4.
- (49) Grillo, H. C.; Donahue, D. M.; Mathisen, D. J.; Wain, J. C.; Wright, C. D. Postintubation tracheal stenosis: Treatment and results. *J. Thorac. Cardiovasc. Surg.* **1995**, *109* (3), 486–493 DOI: 10.1016/S0022-5223(95)70279-2.
- (50) Martínez-Ballarín, J. I.; Díaz-Jiménez, J. P.; Castro, M. J.; Moya, J. A. Silicone Stents in the Management of Benign Tracheobronchial Stenoses. *Chest* **1996**, *109* (3), 626–629 DOI: 10.1378/chest.109.3.626.
- (51) Maldonado, F.; Loiselle, A.; Depew, Z. S.; Edell, E. S.; Ekbohm, D. C.; Malinchoc, M.; Hagen, C. E.; Alon, E.; Kasperbauer, J. L. Idiopathic subglottic stenosis: An evolving therapeutic algorithm. *Laryngoscope* **2014**, *124* (2), 498–503 DOI: 10.1002/lary.24287.
- (52) Iñiguez-Cuadra, R.; San Martín Prieto, J.; Iñiguez-Cuadra, M.; Zúñiga Erranz, S.; Jofré Pavez, D.; González Bombardiere, S.; Guilemany Toste, J. M.; Iñiguez-Sasso, R. Effect of mitomycin in the surgical treatment of tracheal stenosis. *Arch. Otolaryngol. Head Neck Surg.* **2008**, *134* (7), 709–714 DOI: 10.1001/archotol.134.7.709.
- (53) Warner, D.; Brietzke, S. E. Mitomycin C and airway surgery: How well does it work? *Otolaryngol. - Head Neck Surg.* **2008**, *138* (6), 700–709 DOI: 10.1016/j.otohns.2008.02.011.
- (54) Choong, C. K.; Haddad, F. J.; Gee, E. Y.; Cooper, J. D. Feasibility and safety of airway bypass stent placement and influence of topical mitomycin C on stent patency. *J. Thorac. Cardiovasc. Surg.* **2005**, *129* (3), 632–638 DOI: 10.1016/j.jtcvs.2004.07.062.
- (55) Fattori, R.; Piva, T. Drug-eluting stents in vascular intervention. *Lancet (London, England)* **2003**, *361* (9353), 247–249 DOI: 10.1016/S0140-6736(03)12275-1.
- (56) Vogt, F.; Stein, A.; Rettemeier, G.; Krott, N.; Hoffmann, R.; Dahl, J. Vom; Bosserhoff, A. K.; Michaeli, W.; Hanrath, P.; Weber, C.; et al. Long-term assessment of a novel biodegradable paclitaxel-eluting coronary poly lactide stent. *Eur. Heart J.* **2004**, *25* (15), 1330–1340 DOI:

- 10.1016/j.ehj.2004.06.010.
- (57) Choong, C. K.; Phan, L.; Massetti, P.; Haddad, F. J.; Martinez, C.; Roschak, E.; Cooper, J. D. Prolongation of patency of airway bypass stents with use of drug-eluting stents. *J. Thorac. Cardiovasc. Surg.* **2006**, *131* (1), 60–64 DOI: 10.1016/j.jtcvs.2005.07.057.
- (58) Walter, R. F. H.; Zarogoulidis, P.; Mairinger, F. D.; Werner, R.; Darwiche, K.; Zarogoulidis, K.; Freitag, L. Cell viability of fibroblasts to pifenidone and sirolimus. *Int. J. Pharm.* **2014**, *466* (1–2), 38–43 DOI: 10.1016/j.ijpharm.2014.03.003.
- (59) MacKenzie, C. F.; McAslan, T. C.; Shin, B.; Schellinger, D.; Helrich, M. The shape of the human adult trachea. *Anesthesiology* **1978**, *49* (1), 48–50.
- (60) Mehta, S.; Myat, H. M. The cross-sectional shape and circumference of the human trachea. *Ann. R. Coll. Surg. Engl.* **1984**, *66* (5), 356–358.
- (61) Dumon, J. F. A dedicated tracheobronchial stent. *Chest* **1990**, *97* (2), 328–332 DOI: 10.1378/chest.97.2.328.
- (62) Stone, P. H.; Coskun, A. U.; Kinlay, S.; Clark, M. E.; Sonka, M.; Wahle, A.; Ilegbusi, O. J.; Yeghiazarians, Y.; Popma, J. J.; Orav, J.; et al. Effect of endothelial shear stress on the progression of coronary artery disease, vascular remodeling, and in-stent restenosis in humans: in vivo 6-month follow-up study. *Circulation* **2003**, *108* (4), 438–444 DOI: 10.1161/01.CIR.0000080882.35274.AD.
- (63) Rhen, T.; Cidlowski, J. a. Antiinflammatory Action of Glucocorticoids — New Mechanisms for Old Drugs. *N. Engl. J. Med.* **2005**, *353* (16), 1711–1723 DOI: 10.1056/NEJMra050541.
- (64) Schleimer, R. P. Glucocorticoids Suppress Inflammation but Spare Innate Immune Responses in Airway Epithelium. *Proc. Am. Thorac. Soc.* **2004**, *1* (3), 222–230 DOI: 10.1513/pats.200402-018MS.
- (65) Takahashi, K.; Inoue, H.; Sadamatsu, H.; Umeguchi, H.; Sueoka-Aragane, N.; Kimura, S. A Case of Relapsing Polychondritis Successfully Treated with Combination of a Glucocorticoid and Cyclosporine. *Int. J. Clin. Med.* **2015**, *6* (7), 439–443 DOI: 10.4236/ijcm.2015.67057.
- (66) RYU, Y. J.; KIM, H.; YU, C.-M.; CHOI, J. C.; KWON, Y. S.; KIM, J.; SUH, S. W. Comparison of Natural and Dumon airway stents for the management of benign tracheobronchial stenoses. *Respirology* **2006**, *11* (6), 748–754 DOI: 10.1111/j.1440-1843.2006.00955.x.
- (67) PARK, H. Y.; KIM, H.; KOH, W.-J.; SUH, G. Y.; CHUNG, M. P.; KWON, O. J. Natural stent in the management of post-intubation tracheal stenosis. *Respirology* **2009**, *14* (4), 583–588 DOI: 10.1111/j.1440-1843.2009.01498.x.



- (68) Saito, Y.; Imamura, H. Airway Stenting. *Surg. Today* **2005**, *35* (4), 265–270 DOI: 10.1007/s00595-004-2942-y.
- (69) Tam, M. D.; Laycock, S. D.; Jayne, D.; Babar, J.; Noble, B. 3-D printouts of the tracheobronchial tree generated from CT images as an aid to management in a case of tracheobronchial chondromalacia caused by relapsing polychondritis. *J. Radiol. Case Rep.* **2013**, *7* (8), 34–43 DOI: 10.3941/jrcr.v7i8.1390.
- (70) Alves, C. M.; Yang, Y.; Carnes, D. L.; Ong, J. L.; Sylvia, V. L.; Dean, D. D.; Agrawal, C. M.; Reis, R. L. Modulating bone cells response onto starch-based biomaterials by surface plasma treatment and protein adsorption. *Biomaterials* **2007**, *28* (2), 307–315 DOI: 10.1016/j.biomaterials.2006.09.010.
- (71) Tirrell, M.; Kokkoli, E.; Biesalski, M. The role of surface science in bioengineered materials. *Surf. Sci.* **2002**, *500* (1–3), 61–83 DOI: 10.1016/S0039-6028(01)01548-5.
- (72) Sardella, E.; Gristina, R.; Senesi, G. S.; D'Agostino, R.; Favia, P. Homogeneous and micro-patterned plasma-deposited PEO-like coatings for biomedical surfaces. *Plasma Process. Polym.* **2004**, *1* (1), 63–72 DOI: 10.1002/ppap.200400013.
- (73) Csucs, G.; Michel, R.; Lussi, J. W.; Textor, M.; Danuser, G. Microcontact printing of novel copolymers in combination with proteins for cell-biological applications. *Biomaterials* **2003**, *24* (10), 1713–1720 DOI: 10.1016/S0142-9612(02)00568-9.
- (74) Goddard, J. M.; Hotchkiss, J. H. Polymer surface modification for the attachment of bioactive compounds. *Prog. Polym. Sci.* **2007**, *32* (7), 698–725 DOI: 10.1016/j.progpolymsci.2007.04.002.
- (75) Desmet, T.; Morent, R.; De Geyter, N.; Leys, C.; Schacht, E.; Dubruel, P. Nonthermal plasma technology as a versatile strategy for polymeric biomaterials surface modification: A review. *Biomacromolecules* **2009**, *10* (9), 2351–2378 DOI: 10.1021/bm900186s.
- (76) Francesch de Castro, L. Surface modification of Polymers by plasma polymerization techniques for tissue engineering, Universitat Ramon Llull, 2008.
- (77) Uyama, Y.; Kato, K.; Ikada, Y. Surface Modification of Polymers by Grafting. In *Grafting/Characterization Techniques/Kinetic Modeling*; Galina, H., Ikada, Y., Kato, K., Kitamaru, R., Lechowicz, J., Uyama, Y., Wu, C., Eds.; Advances in Polymer Science; Springer Berlin Heidelberg: Berlin, Heidelberg, 1998; Vol. 137, pp 1–39.
- (78) Francesch, L.; Borros, S.; Knoll, W.; Förch, R. Surface reactivity of pulsed-plasma polymerized pentafluorophenyl methacrylate (PFM) toward amines and proteins in solution. *Langmuir* **2007**, *23* (7), 3927–3931 DOI: 10.1021/la062422d.
- (79) Duque, L.; Menges, B.; Borros, S.; Förch, R. Immobilization of biomolecules to plasma

- polymerized pentafluorophenyl methacrylate. *Biomacromolecules* **2010**, *11* (10), 2818–2823 DOI: 10.1021/bm100910q.
- (80) Francesch, L.; Garreta, E.; Balcells, M.; Edelman, E. R.; Borrós, S. Fabrication of bioactive surfaces by plasma polymerization techniques using a novel acrylate-derived monomer. *Plasma Process. Polym.* **2005**, *2* (8), 605–611 DOI: 10.1002/ppap.200500042.
- (81) Vaezi, M.; Seitz, H.; Yang, S. A review on 3D micro-additive manufacturing technologies. *Int. J. Adv. Manuf. Technol.* **2013**, *67* (5–8), 1721–1754 DOI: 10.1007/s00170-012-4605-2.
- (82) Berman, B. 3-D printing: The new industrial revolution. *Bus. Horiz.* **2012**, *55* (2), 155–162 DOI: 10.1016/j.bushor.2011.11.003.
- (83) Huang, Y.; Leu, M. C.; Mazumder, J.; Donmez, A. Additive Manufacturing: Current State, Future Potential, Gaps and Needs, and Recommendations. *J. Manuf. Sci. Eng.* **2015**, *137* (1), 14001 DOI: 10.1115/1.4028725.
- (84) Gross, B. C.; Erkal, J. L.; Lockwood, S. Y.; Chen, C.; Spence, D. M. Evaluation of 3D printing and its potential impact on biotechnology and the chemical sciences. *Anal. Chem.* **2014**, *86* (7), 3240–3253 DOI: 10.1021/ac403397r.
- (85) Hernández-Alfaro, F.; Guijarro-Martínez, R. New protocol for three-dimensional surgical planning and CAD/CAM splint generation in orthognathic surgery: an in vitro and in vivo study. *Int. J. Oral Maxillofac. Surg.* **2013**, *42* (12), 1547–1556 DOI: 10.1016/j.ijom.2013.03.025.
- (86) Hernández-Alfaro, F.; Ruiz-Magaz, V.; Chatakun, P.; Guijarro-Martínez, R. Mandibular reconstruction with tissue engineering in multiple recurrent ameloblastoma. *Int. J. Periodontics Restorative Dent.* **2012**, *32* (3), e82–6 DOI: 10.11607/prd.00.1060.
- (87) Hockaday, L. a; Kang, K. H.; Colangelo, N. W.; Cheung, P. Y. C.; Duan, B.; Malone, E.; Wu, J.; Girardi, L. N.; Bonassar, L. J.; Lipson, H.; et al. Rapid 3D printing of anatomically accurate and mechanically heterogeneous aortic valve hydrogel scaffolds. *Biofabrication* **2012**, *4* (3), 35005 DOI: 10.1088/1758-5082/4/3/035005.
- (88) Zopf, D. A.; Hollister, S. J.; Nelson, M. E.; Ohye, R. G.; Green, G. E. Bioresorbable Airway Splint Created with a Three-Dimensional Printer. *N. Engl. J. Med.* **2013**, *368* (21), 2043–2045 DOI: 10.1056/NEJMc1206319.
- (89) Mironov, V.; Kasyanov, V.; Drake, C.; Markwald, R. R. Organ printing: promises and challenges. *Regen. Med.* **2008**, *3* (1), 93–103 DOI: 10.2217/17460751.3.1.93.
- (90) Brinkman, W. T.; Nagapudi, K.; Thomas, B. S.; Chaikof, E. L. Photo-cross-linking of type I collagen gels in the presence of smooth muscle cells: Mechanical properties, cell viability, and function. *Biomacromolecules* **2003**, *4*, 890–895 DOI: 10.1021/bm0257412.

- (91) Geckil, H.; Xu, F.; Zhang, X.; Moon, S.; Demirci, U. Engineering hydrogels as extracellular matrix mimics. *Nanomedicine (Lond)*. **2010**, 5 (3), 469–484 DOI: 10.2217/nnm.10.12.
- (92) Park, J. Y.; Choi, J.-C.; Shim, J.-H.; Lee, J.-S.; Park, H.; Kim, S. W.; Doh, J.; Cho, D.-W. A comparative study on collagen type I and hyaluronic acid dependent cell behavior for osteochondral tissue bioprinting. *Biofabrication* **2014**, 6 (3), 35004 DOI: 10.1088/1758-5082/6/3/035004.
- (93) Suri, S.; Schmidt, C. E. Photopatterned collagen-hyaluronic acid interpenetrating polymer network hydrogels. *Acta Biomater.* **2009**, 5 (7), 2385–2397 DOI: 10.1016/j.actbio.2009.05.004.
- (94) Khalil, S.; Nam, J.; Sun, W. Multi-nozzle deposition for construction of 3D biopolymer tissue scaffolds. *Rapid Prototyp. J.* **2005**, 11, 9–17 DOI: 10.1108/13552540510573347.
- (95) Murphy, S. V; Atala, A. 3D bioprinting of tissues and organs. *Nat. Biotechnol.* **2014**, 32, 773–785 DOI: 10.1038/nbt.2958.
- (96) Jamuna-Thevi, K.; Bakar, S. A.; Ibrahim, S.; Shahab, N.; Toff, M. R. M. Quantification of silver ion release, in vitro cytotoxicity and antibacterial properties of nanostructured Ag doped TiO<sub>2</sub> coatings on stainless steel deposited by RF magnetron sputtering. *Vacuum* **2011**, 86 (3), 235–241 DOI: 10.1016/j.vacuum.2011.06.011.
- (97) Hu, C.-C.; Chiou, A.-H.; Hsu, C.-Y. Effects of NH<sub>3</sub> PECVD treatment time on the performance of multiwall carbon nanotubes for antibody immobilization. *J. Biomed. Mater. Res. Part B Appl. Biomater.* **2015**, No. July, 1–9 DOI: 10.1002/jbm.b.33477.

## **Chapter II. Antibacterial Surfaces**

*This page left blank intentionally*

## 2.1 Introduction

As mentioned in the previous chapter, bacterial colonization and biofilm formation on implanted medical devices, i.e. tracheal stents, are a serious problem accounting for over 80% of microbial infections in the body.<sup>1</sup> Moreover, in recent years, the incidence of laryngotracheal stenosis in the adult population has been rising due to the increasing number of patients suffering from post-intubation injury, approximately 1 in 200,000 adults per year.<sup>2</sup> Prolonged ischemia by inappropriate pressure of the cuffed endotracheal tube, together with concomitant infection, can cause necrosis of the tracheal wall. This damage results in the formation of granulation tissue first and abnormal scarring tissue afterward.<sup>3</sup> Depending on the decrease of the tracheal-free section lumen, or stenosis, this injury can induce dyspnea at exertion, if it is mild, or even the death by asphyxia, if it is severe.

This pathology requires restoration of the free airway to the lungs that can be accomplished by complicated resective surgery techniques or through insertion of a silicon trachea prosthesis (stent).<sup>4</sup> A variety of silicone or metallic stents are currently used to restore the stenosed airway. Metallic stents may seem a good solution, but they can cause damage of tissue by penetration, fracture of the stent, bronchial or tracheal wall perforations or release of metallic ions.<sup>5,6</sup>



**Figure II-1.** Piece metal removal of a metal stent.<sup>7</sup>

The use of silicone stents was first evaluated in 1965, when Montgomery reported the use of the silicone T-Tube tracheal stent. In 1990, Dumon designed the currently most widely used stent.<sup>3,8,9</sup> Some of the reason why silicone stents are a safe solution is because they avoid all the problems with the breakage of the stent, the diffusion of metallic ions and perforations or tissue damage.<sup>10,11</sup> Additionally, silicone has been found to be a relatively non-irritating substance, which makes it a suitable material for a structural prosthesis.<sup>12</sup> However, they present the disadvantage of interfering with mucociliary function, avoiding the clearance of bronchial secretion and are potentially life-threatening due to the risk of displacement<sup>13,14</sup>.

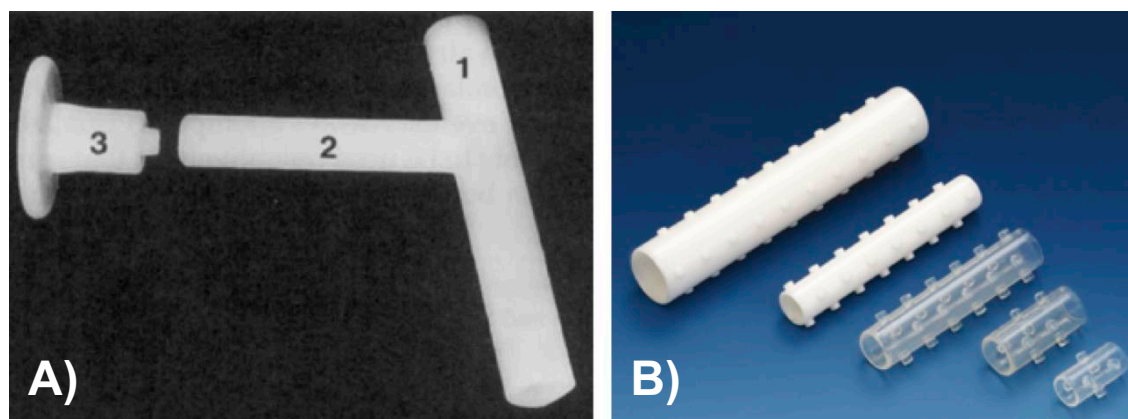


**Figure II-2.** Different tracheal tubes. **A)** Montgomery silicone tracheal T-tube stent<sup>15</sup> and **B)** Dumon stent.<sup>16</sup>

One of the major complications of stent implantation is bacterial colonization with potentially pathogenic microorganisms, such as *Pseudomonas aeruginosa*, *Staphylococcus aureus*, and many others,<sup>17</sup> that may threaten the viability of the prosthesis or even cause the death of the patient, if appropriate care is not taken. Bacterial colonization is mainly associated with poor quality of life in terms of daily symptoms, such as coughing, sputum, or halitosis. In addition, in some patients it can threaten their lives by obstruction of the stent by thickened mucous plugs and even cause severe infection, sepsis, and deaths.

The reason why there is bacterial colonization on the stent is not fully understood. It has been hypothesized that bacterial colonization may be related to microscopic irregularities on the macroscopically smooth internal surface of the stent.<sup>18</sup> However, it has been demonstrated that the use of antibiotic-impregnated stents showed interesting results reducing the colonization during the initial implantation days.<sup>17</sup>

Since the discovery of penicillin, antiseptics and other antibacterial agents such as gentamicin, titanium dioxide, or chitosan coatings are used to treat a broad range of bacterial infections increasing human survival.<sup>19</sup> Despite the success of narrow and broad spectrum antibiotics, not all bacterial infections can be resolved; in addition, bacteria can generate resistance to those antibacterial agents.<sup>20</sup> Therefore, the use of hypochlorite<sup>21</sup>, copper salts<sup>22,23</sup> or chlorhexidine<sup>24,25</sup> should be an attractive strategy to avoid the development of resistant strains and reduce bacterial infection. Silver is an excellent agent to fight bacterial infections as it has been corroborated since ancient times. Hippocrates used silver as an antibacterial agent to treat the Greeks,<sup>26</sup> and recently the use of silver as an antibacterial has risen again to treat bacterial infections due to its high toxicity against microorganisms, wide spectrum of action, reduced bacterial resistance, and low toxicity to animal cells.<sup>27</sup> Due to its broad spectrum of antibacterial activity, silver has been used in multiple applications, such as topical bandages for burn wounds<sup>28,29</sup>, topical creams for burns<sup>30,31</sup>, additives in food<sup>32</sup>, chronic wounds<sup>33</sup>, urinary catheters<sup>34</sup> or dialysis catheters<sup>35</sup>, with excellent results reducing and avoiding bacterial colonization and infection.

The mechanism of action of silver ions is not clearly defined, but there is some evidence of silver ions interacting with thiol (sulfhydryl) groups of the proteins and enzymes, losing essential activities, such as replication and respiration. Silver ions are deposited in the cell wall as granules damaging the cell wall, and consequently, the cytoplasmic membrane, cytoplasmic contents, and outer cell layers exhibit structural abnormalities.<sup>36</sup> Finally, silver-coated surfaces of medical implant can avoid bacterial infections and biofilm formation.<sup>37</sup> At this point, it is fundamental to control the surface of the biomaterial because this is where the interactions between tissue body, bacteria, and medical devices are produced. Therefore, it is necessary to use surface modification technology to create covalently attached silver-coatings.

As it has been previously introduced in the introduction chapter of this work, plasma treatment techniques are interesting methods to modify material surfaces. These techniques can be used to enable chemical surface modifications, fabricate thin films, and can be applied to flexible and complex shaped scaffolds without cracking. These modifications can be easily tailored concerning type and density of functional groups without changing the intrinsic bulk properties of the substrate.<sup>38-40</sup> Furthermore, surface functionalization can be achieved by avoiding the use of hazardous solvents because these kinds of techniques are solvent-free.<sup>41</sup> Additionally, plasma allows the production of different topologies on surfaces, presents the ability to model the macroscopic and microscopic surface morphology, and carries out chemical patterning.<sup>41</sup>

Plasma-based techniques are effective methods for the modification of medical implants because they can change chemical properties<sup>42</sup>, improve the adhesion strength<sup>43</sup>, surface and coating properties<sup>20,44,45</sup> and biocompatibility<sup>38,46-48</sup>. In addition, plasma processes provide reproducible modifications and reactors or processes can be scaled up to industrial dimensions.<sup>42</sup> Another advantage of plasma is its ability to allow protein<sup>47,49</sup> or other biomolecules immobilization or polymer coatings deposition with final sterile surfaces.<sup>46</sup>

*Plasma Polymerization (PP)* also called **PECVD** (*Plasma Enhanced Chemical Vapour Deposition*) or plasma deposition is referred to a deposition of polymeric thin films on the surface of the substrate without changing the bulk properties of the material.<sup>46</sup> PECVD has been described previously as an excellent technique to obtain thin films that are biocompatible<sup>50,51</sup>, adherent<sup>52</sup>, and flexible enough to minimize static forces on the surrounding tissue<sup>53</sup> and endure the flexibility of the material. However, the functionalization or the chemical structures of the resulting polymer is controlled by experimental conditions, and the chemical structures can range from highly functional polymers networks of low cross-link densities to polymer networks of low functional groups, but high cross-link densities.<sup>54,55</sup>

Despite a wide variety of different functional monomers used in plasma polymerization such as allylamine<sup>56</sup>, acrylic acid<sup>57</sup> or allyl alcohol/1,7-octadiene<sup>58</sup>, in the last few years our lab GEMAT has been working to obtain highly functional groups on the surface by using the polymerization of a monomer with a terminal reactive group. Pentafluorophenyl methacrylate (PFM) is one of such monomers that offers a highly reactive ester group (that efficiently reacts with amino groups) and a vinyl structure that can be easily polymerized by PECVD technique.<sup>54</sup> The resulting reactive polymeric thin



films were covalently attached to the surfaces. These plasma polymerized PFM (pp-PFM) surfaces are capable of being adapted to the flexibility of elastic materials such as PDMS, can be micro- and nanostructured, and can react preferably with amine bearing molecules to obtain biocompatible and bioactive surfaces with antibacterial properties.<sup>40,59,60</sup>

The optimization of working parameters shows a great impact in the final properties of the polymer layer. Previous works on the plasma-polymerized PFM (*pp-PFM*) have proved that the deposition under pulsed plasma conditions controlled by the duty cycle (*DC*), Equation II-1, is crucial for the correct formation of the active polymer film.<sup>54</sup> The *DC* is defined as the relation between the time in which plasma is on ( $t_{on}$ ) and the total duration of the pulse ( $t_{on} + t_{off}$ ).

$$DC = \frac{t_{on}}{t_{on} + t_{off}} \quad \text{Equation II-1}$$

Pulsed plasma is characterized for being carried out at higher power  $P_{peak}$  (working power), Equation II-2, maintaining the same equivalent power ( $P_{eq}$ ) as the continuous plasma. This can be possible because the  $P_{eq}$  (that is actually reaching the sample) is dependent on the pulse due to the relation with the *DC* and the  $P_{peak}$ .<sup>61</sup>

$$P_{eq} = P_{peak} \cdot DC \quad \text{Equation II-2}$$

The tuning properties of the duty cycle and the different processes that takes place during a pulsed plasma polymerization can be observed in Figure II-3 and can be directly compared to the treatment that the surface is receiving, when continuous plasma is applied.

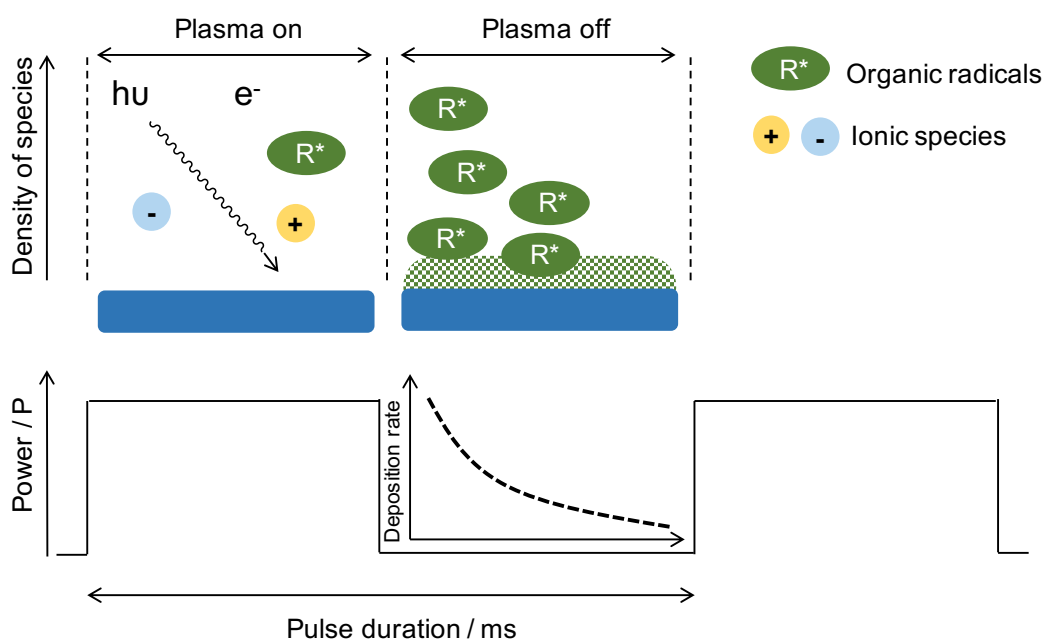


Figure II-3. Pulsed plasma polymerization process.

Initially, during the activation ( $t_{on}$ ), the dissociation of the monomer and the gas present in the chamber yields different ions, radicals and electrons. Additionally, UV radiation is generated due to the relaxation process of the electronically excited species. The material surface is then exposed to an excited and high reactive atmosphere resulting in the surface modification, deposition, and ablation process. However, during the relaxation process ( $t_{off}$ ), ions and electrons disappears due to their limited lifetime and high reactivity. In contrast, the organic radicals formed during the activation process have a longer lifetime than these other species and they remain on the chamber sufficient time to continue the radical polymerization on the surface. As a result, the monomer is activated and reacts producing the polymer chain onto the surface of the material with soft conditions, avoiding secondary reactions, and retaining a higher reactive functionality.<sup>54,61</sup>

During the plasma polymerization, there is a fragmentation and a deposition of organic monomers into a thin film on the surface of a substrate under vacuum. The building blocks of the coating are generated in the plasma by the fragmentation of the gas feed (the monomer).<sup>42</sup> This activated monomer, monofunctional or difunctional free radicals, can react with themselves to form a polymer chain. Either this growing polymer chain or the activated monomer, can react with the activated surface. Finally, the reaction between radical species ends the growing of the polymer chain as in a free radical polymerization.<sup>62,63</sup>

**Plasma treatment**, uses O<sub>2</sub>, N<sub>2</sub>, H<sub>2</sub>, NH<sub>3</sub>, CO<sub>2</sub>, CF<sub>4</sub> or inert gases such as Ar or He. The plasma of these gases generates charged particles that interact with the surface, usually via free radicals' chemistry, generating a functionalization. This process leads to covalent bonds suitable for the attachment of other coatings, to cross-link the topmost surface layer and finally a surface ablation, which can be used for surface cleaning, activation and plasma grafting.<sup>42,64–66</sup>

Additionally, the treatment can be used as an ablation process (plasma etching). The ablation can be produced by reactions with active species, generated in the plasma, with the surface, in order to form volatile products.<sup>65,67</sup> In this kind of process, the atoms of the gas (Ar, O<sub>2</sub>) are excited ions that collide with atoms on the surface and these surface's atoms dislodges from the crystalline structure transferring its energy to a neighboring atom. This energy transfer continues until one of the atoms is knocked out into the vapor phase.<sup>46,67</sup> As a result of this knocking out, the surface contains active sites that can be used for the immobilization of molecules. Normally, this technique is used to obtain clean surfaces by removing dust or remaining coatings or as a pre-treatment, to activate the surface, before a plasma deposition or direct immobilization of chemical molecules.

During a plasma treatment, it is possible to obtain a mixture of processes, such as functionalization with a monomer or with hydrophilic groups if oxygen is used, Figure II-4. Similar to pulsed plasma polymerization, the grafting process avoids the monomer exposure to harsh conditions in order to preserve its chemical integrity when polymerized. Thus, the surfaces are coated with a low density of organic molecules by depositing a monomer, such as pentafluorophenyl methacrylate molecule. In addition, hydroxyl groups can be obtained when the activated surfaces, that has not been reacted with the organic monomer, come in contact with the atmosphere (oxygen and nitrogen). This type of surface

functionalization can be interesting to enhance the interaction between the soluble bioactive molecules with the reactive surface coated with PFM in order to provide a covalent bond.

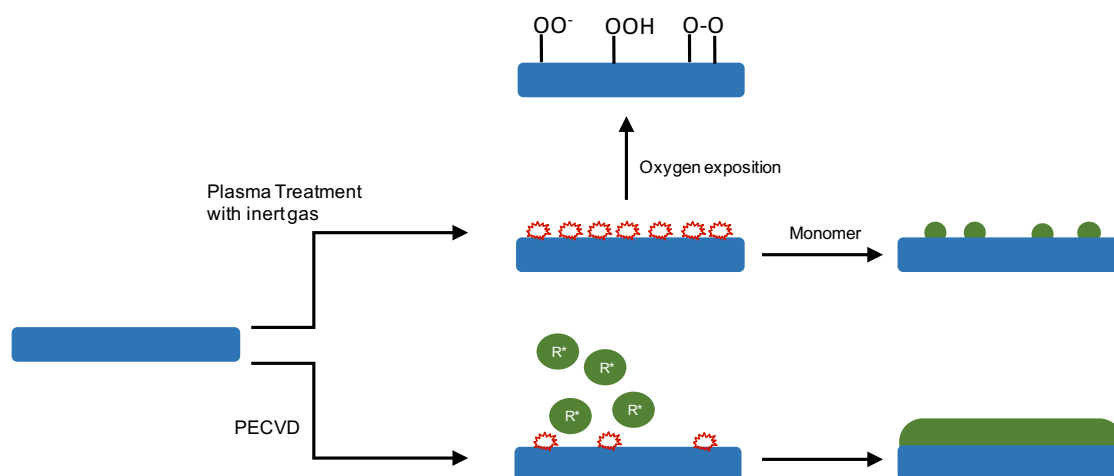


**Figure II-4.** Scheme of different plasma treatment techniques.

In a previous work carried out at GEMAT group, a comparison between the two plasma techniques for immobilization, plasma grafting and plasma polymerization (PECVD) was evaluated. Results showed that plasma polymerization with PFM resulted in a thick coating film with high density of reactive PFM groups and a high roughness, while in plasma grafting the conditions were smoother and a low density of reactive groups and homogeneous surface with less roughness of PFM was obtained. This homogeneity and low roughness of PFM on the surface were suitable for enzyme and protein immobilization, because biomolecules could be spaced out, avoiding the agglomeration, which could difficult the accessibility of the substrate for the active site. Furthermore, this work proved that plasma-grafting modification allowed the retention of the native structure of biomolecules upon immobilization, whereas immobilization via PECVD resulted in a mixture of conformations.<sup>68</sup>

Therefore, as mentioned before, there is an increasing need to create antibacterial surfaces for medical devices capable to avoid bacterial colonization and biofilm formation in combination with high biocompatibility. Considering the previous developed work to create bioreactive surfaces onto different materials using plasma treatments, this chapter goes beyond surface modification to describes a methodology for immobilizing bioactive molecules on different materials, such as silicone, to obtain functionalized surfaces capable of interacting with human tissues.

Finally, this chapter describes a micro- and nanostructured silver coatings onto flexible PDMS surfaces for sustained release of silver ions, resulting in antibacterial and hydrophobic surfaces that avoid biofilm formation surfaces, which have potential applicability on implanted medical devices. PDMS substrate (used as control for medical grade silicone) are coated with PFM using PECVD technique in order to obtain a flexible thin coating that is incubated with amine sugar (glucosamine). Because of the sugar aldehyde thin film, silver ions are reduced on the surface to obtain a nanostructured silver coating on a highly flexible PDMS surface. In addition, this work develops a new

customizing modification method capable of selectively functionalizing different sides of a (polymeric) substrate. The resulting material presents different bioactivity for each side, with the potential of micro- and nano-structuration of the surface. This approach opens the possibility to design medical devices with high personalizing potential, able to include in the same material different functionalities, such as antibacterial properties on one side, and a drug delivery system on the other.

## 2.2 Materials and Methods.

### 2.2.1 Materials.

Argon 5.0 and oxygen 5.0 were purchased from Abelló Linde S.A. (Barcelona, Spain). PFM was purchased from Apollo Scientific LTD (Stockport, UK). D-(+)-Glucosamine hydrochloride, sodium dodecyl sulphate (SDS), Hellmanex, nitric acid, fluorescein-5-thiosemicarbazide and silver nitrate were purchased from Sigma-Aldrich (Madrid, Spain). Ethanol were purchased from Scharlab (Barcelona, Spain), a Sylgard 184 kit was purchased from Ellsworth Adhesives (Madrid, Spain) and Si-wafers were purchased from Wafer World (West Palm Beach, FL, USA). Alexa Fluor<sup>®</sup> 350 and Alexa Fluor<sup>®</sup> 488 (AF350 and AF488 respectively) were purchased from Invitrogen (Carlsbad, CA, USA). Ultrapure water (Milli-Q) was obtained using a Synergy UV<sup>®</sup> system from Merck Millipore (Billerica, MA, USA).

### 2.2.2 Preparation of substrates.

The substrates used were Si-wafers and PDMS samples. In order to fabricate the PDMS plates, the Sylgard kit (10:1) was spread by a paint applicator to obtain films of 500  $\mu\text{m}$  thickness. Additionally, cylindrical PDMS tubes (10 mm of internal diameter, 45 mm of length) were obtained by spreading the kit (10:1) into PTFE (polytetrafluoroethylene) cylinders with PTFE concentric tubes. Both films and tubes were incubated overnight at 70°C. The PDMS films were cut in circular shapes of 21 and 10 mm. It is important to denote that due to the high hydrophobicity and electrostatic charge of PDMS, samples need an accurate washing treatment. PDMS samples were washed with 5% SDS solution, rinsed with Milli-Q water, washed with 2% Hellmanex solution, rinsed again with Milli-Q water and finally with ethanol. Si-wafers were washed with the same protocol as PDMS samples. Finally, samples were dried in a stream of nitrogen and stored.

### 2.2.3 Plasma Reactor.

#### 2.2.3.1.1 Reactor 1: Horizontal Plasma Reactor (HPR).

The surface modifications carried out in this work were performed using a horizontal plasma reactor designed and developed at GEMAT as it can be observed in Figure II-5. This reactor is a home-built 70 cm long and 4 cm cylindrical Pyrex reactor. The cylindrical tube contains the glass sample holder to introduce the samples for modification. Plasma were performed using an excitation frequency of 13.56 MHz. Gases and monomers were feed to the system using a needle valve. At the opposite extreme of the reactor there is a CO<sub>2</sub> / acetone cooled trap to collect the excess of the non-reacted monomer before reaching the pump (RV12 903 Edwards, UK). At the centre of the reactor there is an active Pirani gauge type vacuum meter (PN D02182000 Edwards, UK) to monitor the reaction pressure. In a home built system, the pulse generator controlled the pulsing of the radio frequency signal, which is amplified by a 150 W amplifier and passed via an analogue wattmeter and a matching box to a 10 cm long spiral located around the exterior of the reactor. The typical base pressure to all experiments was 0.02-0.03 mbar and gases and the PFM monomer vapour were introduced at a constant pressure of

0.7 and 0.15 mbar, respectively. The reactor's inner volume is approximately 3 L, while the effective plasma volume is about 1.7 L.

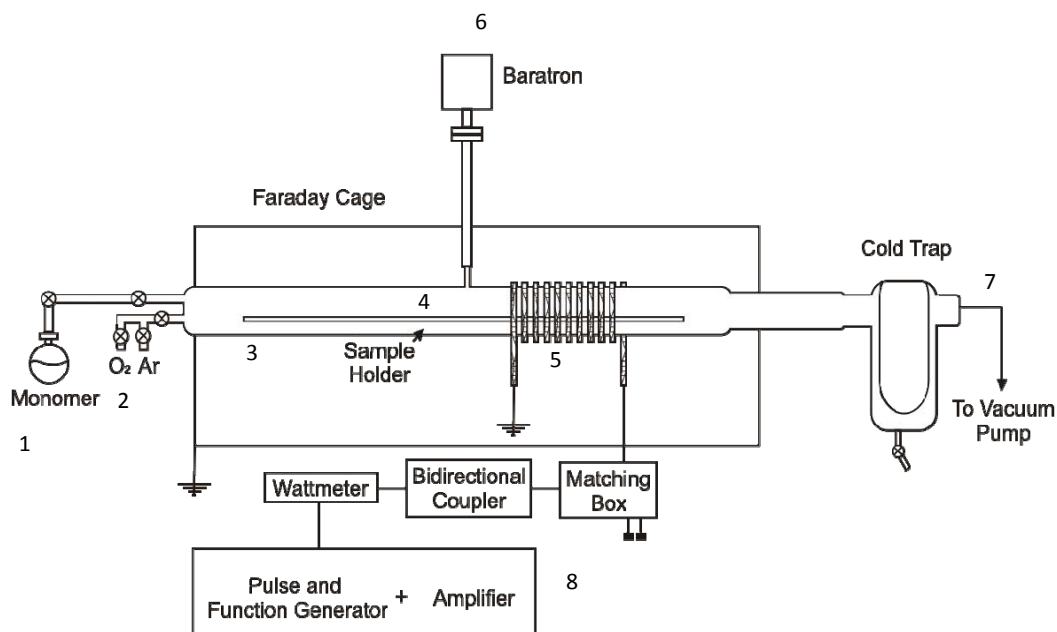


**Figure II-5.** Horizontal Plasma Reactor (HPR). Schematic diagram of horizontal plasma reactor and its electrical components: (1) Monomer, (2) Gases, (3) Glass tube, (4) Sample holder, (5) coil, (6) Pirani gauge, (7) Cold trap, and (8) Wattmeter and matching box.

### 2.2.3.1.2 Reactor 2: Stainless Steel Vertical Plasma Reactor (SSVPR).

The surface modifications carried out in this work were performed using a stainless steel vertical plasma reactor. This reactor consists of a stainless steel chamber (diameter, 25.5 cm; length, 41.6 cm) vertical plate reactor, Figure II-6. The ground electrode is the reactor chamber, and the radio frequency (RF) electrode is an aluminium plate, which is used to hold the samples for polymerization. Additionally, the RF electrode is connected to a RF pulse generator (13.56 MHz) via a matching box. Gases and monomers were supplied via a standard manifold with gas fluxes adjusted with a tree of needle valves. The system pressure is monitored using a vacuum gauge controller (MKS PDR900, Andover, MA, USA) connected with a cold cathode/micropirani vacuum transducer (MKS 972 DualMag) positioned at the centre of the reactor. The system has a nitrogen cold trap and a chemical trap filled with active carbon connected to avoid nonreacted monomer from reaching the pump (Trivac D 16BCS/PFPE Leybold, Cologne, Germany).

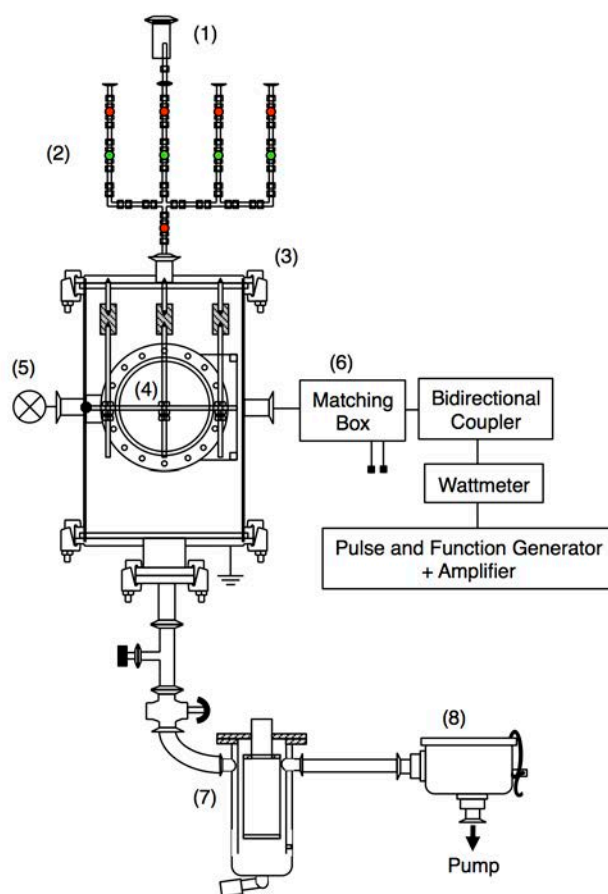


**Figure II-6.** Stainless Steel Vertical Plasma Reactor (SSVPR). Schematic diagram of stainless steel vertical plasma reactor and its electrical components: (1) monomer feed, (2) gases feed, (3) cylindrical chamber, (4) holder sample, (5) pirani gauge, (6) matching box and electrical system, (7) cold trap, and (8) chemical trap.

#### 2.2.4 Plasma Polymerization.

Plasma polymerizations were carried as described in previous work.<sup>40,55</sup> Before introduction of the substrate, the chamber was cleaned in continuous wave  $O_2/Ar$  (1:1) plasma for approximately 1 h at a power of 150 W. Samples were placed on the centre of the coil in the HPR or at the centre of an aluminium plate in the SSVPR reactor. Vacuum was started until the base pressure of 0.02 mbar for HPR or 0.001-0.003 mbar for SSVPR was reached, respectively. Then, PFM was regulated through the needle valve and introduced to the reactor chamber in a vapour phase (heated at 75 °C) until 0.15 mbar for HPR and 0.02-0.03 mbar for SSVPR, respectively. The continuous radio frequency power was fixed at 15 W (working power) and pulsed plasma polymerization duty cycle (DC) of 10/20 [DC =  $t_{on}/(t_{on}+t_{off})$ ]<sup>61</sup> was carried out for 3-10 min. Plasma discharge was then turned off, and the PFM vapour flow rinsed was kept constant for additional 15 min. After the polymerization process, plasma-polymerized PFM (pp-PFM) samples were carefully removed from the reaction chamber and stored until further use under argon atmosphere.

## 2.2.5 Plasma Grafting and Activation

The grafting started with an activation of the surface with O<sub>2</sub> or a mixture of gases, Ar and O<sub>2</sub>. After the plasma treatment, samples were brought into contact with the PFM from the gas phase or immersed into liquid PFM. Samples were introduced into the reactor chamber and vacuum was started until the base pressure. Secondly, needle valves that regulate gases were opened to introduce Ar, O<sub>2</sub> or a mixture of gases 50% (Ar:O<sub>2</sub>) until they reached a work pressure of 0.7-0.75 mbar for HPR and 0.14 mbar for SSVPR, respectively. Thirdly, the frequency generator was switched on and set up individually for each experiment to the working power (10-120 W) and the treatment time (1-60 min). After the plasma activation treatment, the needle valves of the gases were closed.

In order to perform a plasma grafting of PFM, the monomer was regulated through the needle valve and introduced to the reactor chamber in a vapour phase (heated at 75 °C) until 0.15 mbar for the desired experimental time (1-40 min).

In order to perform a hydrophilic activation, instead of PFM, oxygen gas was fed until reach a working pressure of 0.7 mbar for HPR and 0.14 mbar for SSVPR, respectively, for the desired experimental time (1-40 min).

After the treatment, the monomer or gases valves were closed, vacuum was cut off, and samples were removed from the reactor and stored with argon atmosphere until further use.

## 2.2.6 Surface Selectivity, Patterning and Structuration.

### 2.2.6.1.1 Surface Selectivity

In order to selectively modify both sides of a sample, each side of the sample was modified with a micro-patterned pp-PFM layer (protecting the opposite side with aluminium foil) and subsequently reacted with the desired amine-bearing molecule such as either AF350 or AF488 fluorescent dye in Milli-Q water (blue and green respectively). After functionalization with the first molecule, samples were rinsed with Milli-Q water and dried under argon stream. Then, in order to obtain the second side modified, PFM were plasma-polymerized onto the non-modified surface (protecting the previous functionalized side) and reacted with a different molecule.

### 2.2.6.1.2 Surface Patterning, Micro-Patterning and $\mu$ Contact Printing ( $\mu$ CP).

The patterning and micro-patterning process were carried out by the modification of the substrate with a mask or with a cooper grid (G50P, Gilder Grids, Grantham, U.K.). The mask was stacked on the top of the substrates, by applying pressure, before the plasma treatments. The cooper grid was carefully placed on the desired part of the substrate guaranteeing full contact between the surface and the grid. Samples were then treated with plasma treatments. When the modification process was over, the mask or grid was carefully retired taking care not to scratch the modification.



As it can be seen in Figure II-7, the experiments detailed on this work used a custom-made polymethacrylate squared mask (with a centered squared hole) and a cooper TEM grid.

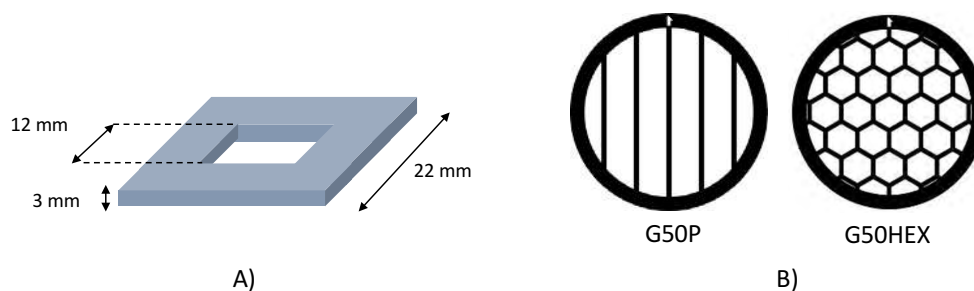


**Figure II-7.** Schematic representation of the used masks. **A)** Polymethacrylate squared mask with a centred squared hole. **B)** TEM grid used as a cooper mask G50P (with 50 mesh lines / inch, 85  $\mu\text{m}$  bar width and 416  $\mu\text{m}$  hole width) and G50HEX (with 50 mesh lines / inch, 500  $\mu\text{m}$  pitch, 70  $\mu\text{m}$  bar width and 430  $\mu\text{m}$  hole width).

The  $\mu\text{CP}$  technique consists on a stamp that was used to print on the surface of a modified substrate. The fabrication of the stamp consisted on a silicon rubber (PDMS) prepared by using an 8:1 ratio (v/v) of elastomer and curing agent (Sylgard 184 kit). After mixing, the mixture was degassed under vacuum and it was spread over a master stamp, Figure II-8, which was previously designed by GEMAT group and fabricated by the *Centro Nacional de Microelectrónica* (CNM, Spain).<sup>63,69</sup> Then, the extended PDMS mixture was cured over-night at 70°C to crosslink the dimethylsiloxane chains. To reduce contamination of the printed surface due to unreacted crosslinker or PDMS monomer/oligomers, the stamp was cleaned with ethanol for 5 min and 5 min in ethanol with the help of an ultrasonic bath, and finally, it was dried under a stream of nitrogen. Finally, the stamp was made hydrophilic by treatment with 50%  $\text{Ar}/\text{O}_2$  mixture plasma at 15 W for 10 min. Consequently, the surface could absorb hydrophilic substances such as fluorophores. After the immersion of the stamp in an alcoholic fluorescein-5-thiosemicarbazide (FTSC) solution (for 50 min), the FTSC were absorbed on the stamp and dried in a stream of nitrogen.



**Figure II-8.** Master stamp.<sup>63</sup>

Printing was achieved by placing the stamp onto the PFM modified surface and applying a little pressure for 15 min to enhance the contact between the stamp and the sample. The fluorescent

substrates were analysed by a fluorescent microscope AxioVs40 (Carl Zeiss Inc., Deutschland) with the 546, 470 and 365 nm filters.

### 2.2.7 Modified Surface Characterization.

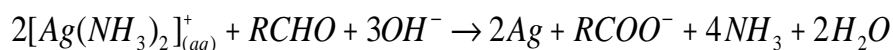
The modified surfaces were characterized through water contact angle (WCA; DSA100, Krüss), time-of-flight secondary ion mass spectrometry (TOF-SIMS), ultrahigh-resolution field emission scanning electron microscopy (UHRFESEM; NovaNanoSEM 230, FEI) with high voltage, optical microscope and 3D microscopy with dual confocal technology, Dual Core 3D Measuring Microscope, (DM2500 and DCM 3D, respectively, Leica, Wetzlar, Germany). To analyse the surface modification by WCA, samples were directly analysed after polymerization.

The TOF-SIMS analyses were performed using a TOF-SIMS IV (ION-TOF, Munster, Germany) operated at a pressure of  $5 \times 10^{-9}$  mbar. Samples were bombarded with a pulsed bismuth liquid metal ion source ( $\text{Bi}_3^{+2}$ ), at energy of 25 keV. The gun was operated with a 20 ns pulse width and 0.3 pA pulsed ion current for a dosage lower than  $5 \times 10^{11}$  ions /  $\text{cm}^2$ , well below the threshold level of  $1 \times 10^{13}$  ions/ $\text{cm}^2$  generally accepted for static SIMS conditions. Secondary ions were detected with a reflector time-of-flight analyser, a multichannel plate (MCPs), and a time-to-digital converter (TDC). Measurements were performed with a typical acquisition time of 10 s, at a TDC time resolution of 200 ps and 100 us cycle time. Charge neutralization was achieved with a low-energy (20 eV) electron flood gun. Secondary ion spectra were acquired from a randomly rastered surface areas of  $100 \mu\text{m} \times 100 \mu\text{m}$  within the sample's surface. Secondary ions were extracted with 2 kV voltages and postaccelerated to 10 keV kinetic energy just before hitting the detector. Mass spectral acquisition was performed within the ION-TOF Ion Spec software (version 4.1).

### 2.2.8 Silver Deposition.

In order to achieve the antimicrobial coating, the silver was reduced by a reductive sugar using the silver mirror reaction (Tollens' reagent),<sup>70</sup> Scheme II-1. This method consists of the complexation of the silver ions with ammonia and its subsequent reduction using a reductive sugar on a heated bath. By using an immobilized sugar, the diamminesilver (I) ions will be reduced to metallic silver resulting in a surface coating. The glucosamine solution was prepared by dissolving glucosamine hydrochloride in Milli-Q water at 1 M. Then, pH was adjusted to 7.4 with concentrated sodium hydroxide. The reaction between glucosamine and the modified surface was performed by incubating the modified samples in a glucosamine solution for 6 h. Tollens' reagent was prepared by adding 25  $\mu\text{L}$  of 15% ammonia to 1 mL of 0.1 M silver nitrate, observing the precipitation of the silver oxide. Then, another 25  $\mu\text{L}$  of 15% ammonia was added, and the complete dissolution of the precipitate was observed due to the complexation of the silver by ammonia. The modified samples with the attached glucosamine were introduced on a vial with 4 mL of Milli-Q water. Then, 1 mL of the Tollens' reagent was added and heated on a water bath at 90 °C for the desired time of reaction, 60 min. Silver was quantified using an inductive coupled plasma optical emission spectroscopy (ICP-OES; Optima 2100 DV, Perkin Elmer).

**Scheme II-1.** Silver Mirror Process.



### 2.2.9 Silver Release and Total Silver Amount.

The Ag ion release of the coated samples was measured with ICP–OES.<sup>71</sup> Different coated samples were immersed in 5 mL of tryptic soy broth (TSB) and in 5 mL of Milli–Q water at 37 °C. After the desired time, 4 mL of each solution was collected for analysis and replaced with 4 mL of fresh solution. The solutions were replenished and analysed each day for 20 days. For the anoxic silver release, experiments were carried out in an argon atmosphere and used degassed Milli–Q water and TSB media.

The total amount of silver onto the silver-coated samples was dissolved using nitric acid. After dissolving the silver layer, the solution was diluted with Milli–Q water and quantified with the ICP-OES (Optima 2100 DV, Perkin Elmer, Waltham, MA, USA).

### 2.2.10 Bacterial in vitro Assay.

Bacterial cultures were performed at the *Hospital Universitari de Bellvitge* in Barcelona using commercial *P. aeruginosa* (PAO1) and *S. aureus* subsp. *aureus* (ATCC<sup>®</sup> 29213) strains. An overnight bacterial culture was diluted with fresh TSB medium to obtain a bacterial density of 10<sup>6</sup> cfu / mL. PDMS samples (modified with silver and nonmodified) were placed at the bottom of the wells of a sterile 24-well plate, and 1 mL of the previously prepared bacterial suspension was added. The well plate with the samples was incubated at 37 °C without agitation for 24 h. After the incubation time, the supernatant of each well was aspirated and the samples were washed 7 times with Milli–Q water. Subsequently, samples were placed in a sterile 24-well plate and stained with the fluorescent Live/Dead BacLight Bacterial Viability Kit (Invitrogen), following the manufacturer's instructions. The 24-well plate was covered from light and incubated for 15 min. After incubation time, samples were washed with Milli–Q water and their fluorescence was observed on a confocal microscope; images of the double-labeled sections were acquired using a True Confocal Scanner Leica (TCS-SL) filter-free spectral confocal laser scanning microscope (Leica Microsystems, Mannheim, Germany) equipped with a 488 nm argon laser, 543 and 633 nm He/Ne lasers (*Serveis Científics i Tecnològics, Universitat de Barcelona*, Barcelona, Spain) using a 63x oil immersion objective (1.4 numerical aperture), image resolution of 1024 x 1024 pixels.

### 2.2.11 Animal Cell in vitro Assay.

In order to evaluate the cytotoxicity of the silver-coated samples, animal cell line experiments were performed using the *Cercopithecus aethiops* kidney fibroblast SV40 transformed (COS-7, ATCC<sup>™</sup> CRL-1651) type. Cells were grown in cell media (DMEM supplemented with 10% FBS, 1% glutamine, and 1% penicillin/streptomycin) and plated in 96-well plates at a cellular density of 1.2x10<sup>5</sup> cells/mL. After cells were plated, the medium was aspirated and substituted with a previously incubated medium

with silver samples for 1, 2, 3, and 6 days (0.5, 0.3, 0.2, and 0.1 ppm, respectively). In addition, 1.2 ppm of pure silver nitrate was added as positive control because it corresponds to the high concentration that can be achieved during the silver release. After 24 h, cell viability was assessed via MTS (CellTiter 96 AQueous One Solution Cell Proliferation Assay, Promega Corp., Madison, WI, USA) following the manufacturer's instructions. Briefly, cells were washed with PBS and incubated with a solution of the MTS reagent and complete media at 37 °C for 1 h. The absorbance was measured via a microplate reader (Spectramax M2, Molecular Devices, Sunnyvale, CA, USA) at the wavelength of 490 nm.

*Unless otherwise stated, all experimental data were done in triplicate and the average mean was represented with standard deviation represented as error bars.*

## 2.3 Results and Discussion

### 2.3.1 Grafting modification on nylon and PTFE plates

Initially, a few exploratory experiments were carried out with flat disposable membranes to analyse the behaviour of the plasma treatments in the previously studied grafting conditions by our group, GEMAT<sup>72</sup> and to evaluate the ability of perform bi-side modification.

In the first experiments, nylon membranes were used to evaluate the degree of grafting modification using pentafluorophenyl methacrylate (PFM) in the horizontal plasma reactor (HPR). Modified samples were further reacted with a hydrophobic molecule, such as decylamine. The degree of modification was assessed by changes in the hydrophilicity / hydrophobicity of the final samples using WCA measurements.

As shown in Figure II-9, plasma treatment resulted in membrane folding, which was probably caused by either the high temperature reached during the activation process.

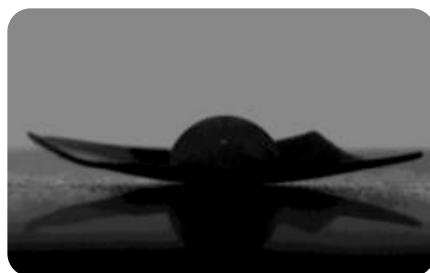


**Figure II-9.** Folded nylon membrane after the grafting treatment. The plasma power peak was set at 50 W for 10 min and the PFM monomer was fed for 10 min.

As it can be observed in Figure II-10, the blank sample, non-modified nylon, had a contact angle of 63°. The samples grafted with PFM and subsequently reacted with decylamine, showed a water contact angle of 118°; instead of 45° from the grafted nylon with PFM. The variation between the bare nylon and grafted PFM was not the expected, because PFM is a hydrophobic substance and an increase on the angle contact was expected, similar to the pp-PFM<sup>54</sup>. However, grafting treatments created active sites on the surface that react with the monomer in the vapour phase. If, after the reaction process, the PFM has reacted in a low density, several active sites may still be present and may further react when the sample was put in contact with the air or water, resulting in the formation of hydroxyl groups and other species on the surface that may increase the hydrophilicity of the surface. The grafting modification of the sample with decylamine showed an increased hydrophobicity on the surface, as it was expected due to the high hydrophobicity of the decylamine.

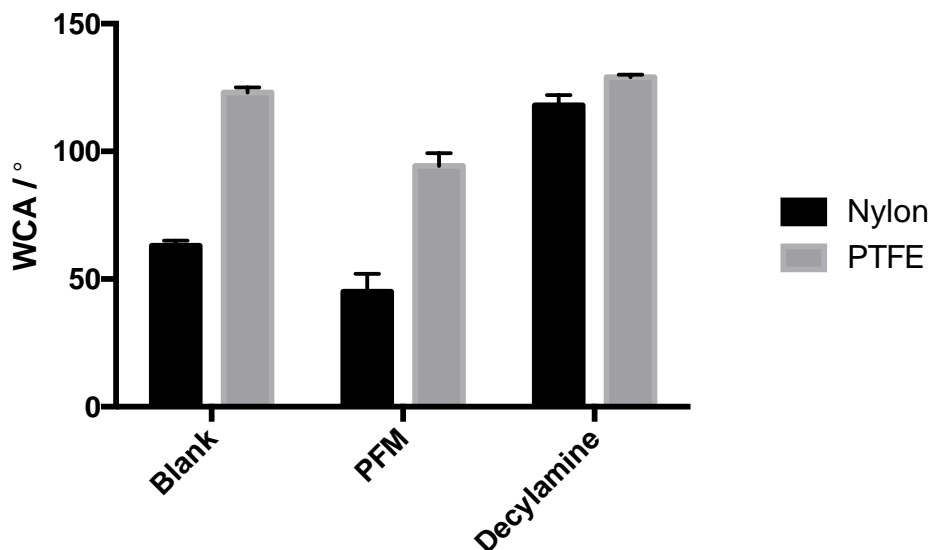


**Figure II-10.** Water contact angles (WCA) of modified samples. (Blank) non-modified surfaces, (PFM) modified surfaces with PFM, and (Decylamine) PFM + decylamine by plasma grafting technique. The plasma power peak was set at 50 W for 10 min and the PFM monomer was fed for 10 min. After that, samples were incubated in decylamine for 10 min.

Additionally, when the modification was carried out using PTFE membranes, samples showed a similar behaviour than in nylon. Initially, non-modified PTFE showed a WCA of 123°, while after grafting modification with PFM, a decrease in WCA to 94° was observed because of the non-reacted active sites, similarly as before when nylon was used. However, after the reaction with the decylamine, there was an increase in the WCA until 129°, indicating that decylamine chains reacted with the grafted PFM groups and therefore the hydrophobicity increased due to the decylamine chains nature and entanglement.

These results showed that plasma grafting is an interesting technique to modify the surface of different materials, such as nylon or even chemically stable materials, such as PTFE. The modification allowed the functionalization of the surface with grafted PFM and thus, the possibility to anchor different amine-bearing molecules showing different surface behaviour versus the raw material.

Due to the difficulty to modify chemical stable materials, the modification of PTFE was very promising and therefore, further experimentation was performed to evaluate the structuration and reactivity of the deposited coatings.

### 2.3.2 Microstructuration of grafted PTFE plates

In order to evaluate the ability of the plasma techniques to selectively modify the surfaces, it was interesting to explore the use of micro-contact printing techniques to selectively modify the surface and provide a fluorescent patterning.

The samples were modified using the grafting technique and followed by PFM incubation. After the PFM treatment, the samples were washed with ethanol. While the samples were treated, the stamp

was activated with oxygen and soaked with a FTSC solution. In Figure II-11, the fluorescent pattern “IQS CNM” can be observed, which persisted after some washing treatments with ethanol, although the fluorescence pattern was slightly blurred. This phenomenon might be caused by the reaction of the non-reacted FTSC with the remaining PFM active sites during the washing with ethanol.

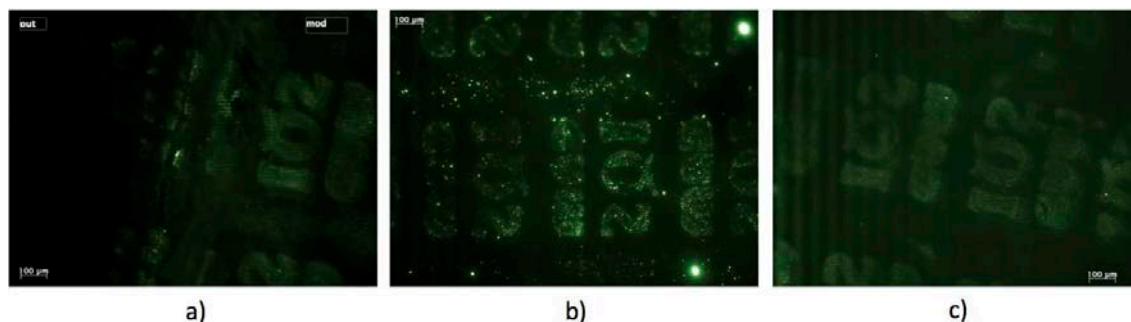


**Figure II-11.**  $\mu$ Structured samples using  $\mu$ contact printing technique. PTFE sample patterned with the  $\mu$ contact printing technique after treated by grafting method and reacted with PFM. **A)** Non-washed sample where the modified zone (right) and non-modified (left) can be observed. **B)** Non-washed sample. **C)** Washed sample. The plasma power peak was set at 50 W for 25 min followed by a 15 min of PFM treatment. After the PFM treatment, samples were washed with ethanol for 120 min.

The WCA and micro-structure results showed that the grafting method was an interesting treatment to modify different kinds of substrates, although it provided lower functionalization leading a structuration with lower definition of the pattern. In addition, the obtained reactive surfaces allowed micro-structuration using  $\mu$ -contact printing techniques, which increased the possibility to create structured patterns to, for example, avoid or increase cell adhesion.

As mentioned before, controlled surface modification on medical devices opened the possibility of designing new systems with improved features, such as improved biocompatibility, tailored tissue regeneration or antimicrobial activity. Thus, to provide antibacterial activity to the medical devices, silver was immobilized onto the modified surfaces.

### 2.3.3 Silver Deposition on grafted PTFE plates

Once the PFM was clearly deposited onto the surfaces of different materials using plasma grafting modification, and the grafted-PFM was reactive with amine-bearing molecules ( $\mu$ contact printing using FTSC solution), the next step consisted in the modification of the grafted-PFM to create antibacterial surfaces. Therefore, as mentioned before, a salt of metallic elements, such as silver, was used to provide antimicrobial activities to the materials.

Silver coating was obtained using a three-step procedure design, (Figure II-12): (1) surface modification with PFM to create a reactive area, (2) immobilization of a reductive molecule, such as glucose, and (3) silver salt reduction using the previous reductive surface.

Initially, material surface was modified with PFM to obtain a reactive coating capable to react with amine bearing molecules. After the plasma modification, a reductive amine-bearing molecule, such as

glucosamine, was reacted with the PFM. In this case, the amine group of glucosamine did not interfere in the reduction reaction, therefore it could be used to react with the PFM active group. Finally, a thin film of metallic silver was obtained using a complexed silver solution (Tollens' reagent).

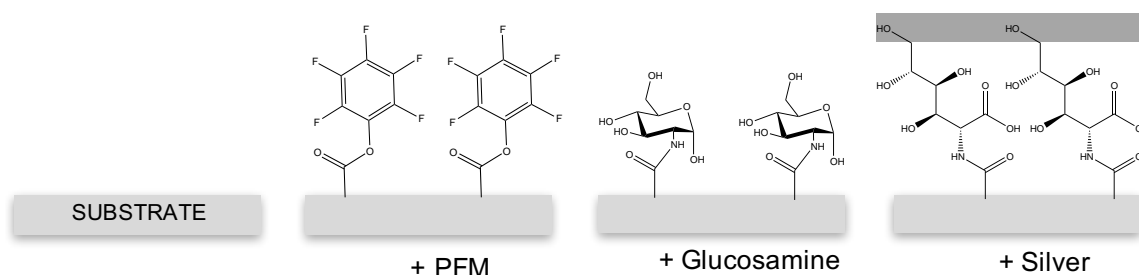


**Figure II-12.** Schematic representation of antibacterial coating. The developed antibacterial surface used a three-step synthesis strategy in combination with silver mirror reaction.

PTFE membranes were activated and then placed into a vial with PFM to react. Subsequently, samples were washed and reacted with glucosamine. After the immobilization with glucosamine, silver was reduced only on top of the surfaces.

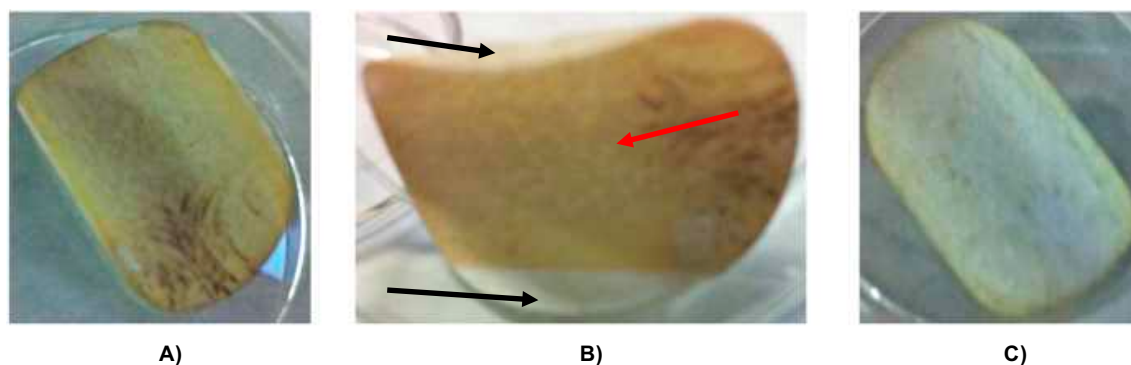


**Figure II-13.** PTFE sample coated with silver in a three-step process. Sample was, firstly, grafted with PFM using a square mask; secondly, sample was reacted with glucosamine; and finally, samples were incubated with Tollens' reagent: **A)** Silver coated (brown); **B)** Structured sample, silver coated (brown, red arrow) and non-modified area (white, black arrow); and **C)** Reverse non-modified surface (white). The plasma power peak was set at 50 W for 25 min with 15 min of PFM incubation. Samples were incubated with 3 mL of glucosamine 1 M for 5 h, and then washed with Milli-Q water. Finally, samples were incubated with Tollens' reagent (1 mL  $\text{AgNO}_3$  1 M + 2 x 25  $\mu\text{L}$   $\text{NH}_3$ , 15%) for 60 min at 90°C.

As it can be observed in Figure II-13, the immobilization of silver was accomplished showing a brown surface onto the surface of the PTFE membrane. In addition, the result of the macro-structuration using a mask can be observed in the samples, showing silver modified areas (brown) and non-modified areas. However, the soft colour intensity of the silver reduced on the surface indicated that the modification process produced low density of the reactive groups leading to a low silver quantity around  $0.3 \mu\text{g}/\text{mm}^2$ . These results showed that the modification on different materials was achieved, even in a chemically stable and rough material, such as PTFE, and it was possible to control the desired side and the macro-



structure of the surface. However, a low quantity of immobilized silver was achieved due to a low density of functional groups.

Previous results clearly indicated that although plasma grafting showed a great potentiality and great versatility, the low amount of reactive groups minimized the yield of the process and difficult the possibility to obtain a homogeneous film coating.<sup>73</sup>

Taking these results into account, it was interesting to move forward to use the plasma polymerization technique (PECVD) to create a homogeneous plasma polymerized (*pp*-) coating onto the surfaces. This technique allowed to obtain a thin film covalently attached to the material surface and it was possible to control the structure and reactivity of the resulted coating.

### 2.3.4 PECVD modification on PTFE plates

Plasma Enhance Chemical Vapour Deposition, technique produces a covalently attached polymeric coating on the surface, which is formed by the polymerization of the monomer. In comparison to grafting techniques, surfaces modified by PECVD present a higher density of PFM groups available to react with the desired target. Additionally, this technique does not require an intense process to activate the surface through an etching process.

PTFE foil samples were modified with plasma polymerized PFM (*pp*-PFM) to create a continuous and homogeneous reactive surface. The resulting surface was further reacted with a hydrophilic amine-bearing alcohol, such as ethanolamine. The ethanolamine reduced the hydrophobicity of the PTFE due to the reaction between the amine and the reactive group of the *p*-PFM resulting in a lower hydrophobic surface onto PTFE. In order to assess the control of PECVD on PTFE samples, half of the PTFE foil was protected in order to avoid plasma modification and the other half was left exposed to the modification treatment. Samples were then reacted with ethanolamine in an ultrasonic bath. After the treatment, the samples were removed and their water contact angle were measured. As it can be observed in Figure II-14, *pp*-PFM samples showed a WCA of 75° instead of the 89° of the bare PTFE. The reduction on the WCA indicated the change on the chemical nature of the surface, there was a new chemically structure on top of the surface, in this case, the value was around the expected (~80°) for the *pp*-PFM.<sup>54,74</sup>

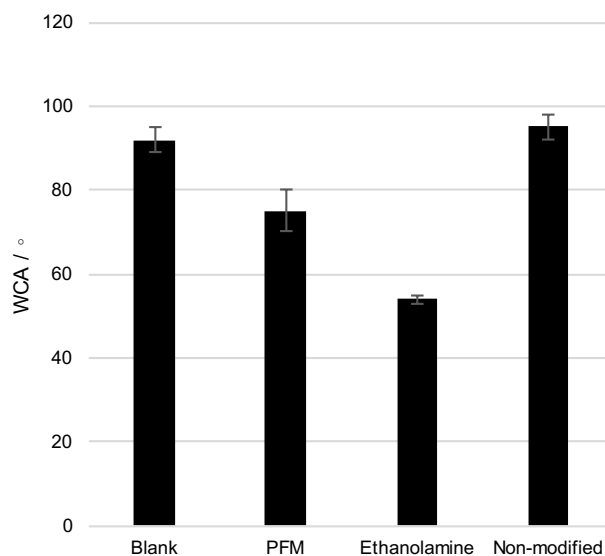


**Figure II-14.** WCA measurements of different studied samples. Non-modified PTFE samples, modified pp-PFM samples, modified pp-PFM samples and non-modified pp-PFM area, both reacted with ethanolamine 10% for 30 min. The plasma power peak was set at 15 W with a DC of 0.5 for 5 min with PFM. After the plasma, there was a 3 min of PFM flow.

After the reaction with ethanolamine, the coated surface presented a decrease in its water contact angle to 54° due to the loss of the hydrophobic fluorinated group and the attachment of the hydrophilic ethanolamine. As it was expected, after the treatment with ethanolamine, the non-modified area remained constant as the same as bare PTFE.

In addition, the wettability behaviour of the non-modified and modified PTFE sample can be observed in Figure II-15, where half of the sample was modified with pp-PFM and subsequently with ethanolamine, and the other half was kept unmodified. When placed in water, the part of the sample modified with ethanolamine (reduced hydrophobicity) sank into the water, whereas the unmodified part remained on the surface due to its higher hydrophobicity. These results showed the novelty of the modification process to control the modification area and to change the chemical composition of the material surface (even chemical stable material, such as PTFE) allowing different properties and behaviour. In this case, PTFE showed a reduction in the hydrophobic properties allowing the material to be wetted by water.

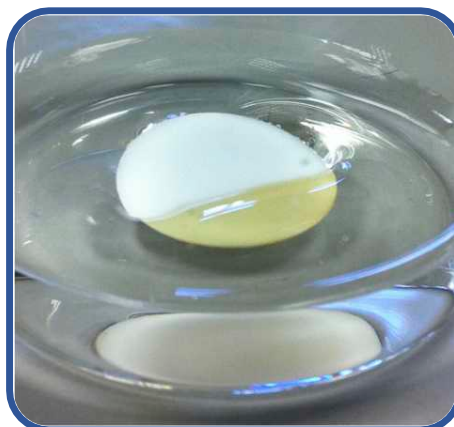


**Figure II-15.** Wettability behaviour of modified PTFE sample. PTFE was partially modified with PFM by PECVD and treated with ethanolamine (yellow) in Milli-Q water. The plasma power peak was set at 15 W with a DC of 0.5 with PFM for 3 min and After the plasma, there was a 3 min of PFM flow.

### 2.3.5 Silver Deposition on PTFE plates

As mentioned before, the key factor was to obtain a metallic silver surface covalently attached onto the materials surface with a homogeneous, stable, and with enough quantity of silver to present antibacterial properties due to the release of the silver ions.

After evaluating the viability to pp-PFM on the surfaces of the materials (even on PTFE), the next step consisted in the reduction of the silver onto the modified PTFE substrates. To evaluate the novelty selectivity of the treatment and the silver mirror process, half of the PTFE sample was covered and the sample was modified by PECVD with PFM. After the modification, the sample was reacted with glucosamine and washed with Milli-Q water. Subsequently, immobilized glucosamine was used to reduce silver on the surface of the sample using the silver mirror reagent.



**Figure II-16.** PTFE sample coated with metallic silver. Two areas can be differentiated, a non-modified one (left) and the coated with silver (right). The plasma power peak was set at 15 W with a DC of 0.5 with PFM for 3 min. After the plasma, there was a 3 min of PFM flow and then samples were incubated with 3 mL of glucosamine 1 M for 5 h, and then washed with Milli-Q water. Finally, samples were incubated with Tollens' reagent (1 mL  $\text{AgNO}_3$  1 M + 2 x 25  $\mu\text{L}$   $\text{NH}_3$ , 15%) for 60 min at 90°C.

In Figure II-16, two differentiated areas, the non-modified and the coated area with silver, can be observed. As it was expected, only the modified pp-PFM surface was coated with silver, while the non-modified remained unaltered. This result showed the ability of the plasma techniques to modify the materials surfaces and even to create a reactive layer able to develop further chemistry. In addition, the results showed the ability to control the structure of the modification areas. PECVD samples showed a homogeneous and continuous metallic silver coating instead of the dispersed and aged (brown) silver coating obtained using the grafting technique. The amount of silver was similar ( $0.37 \mu\text{g}/\text{mm}^2$ ), but the homogeneity of the coating indicates the possibility to control the silver amount by controlling the time and conditions of the silver mirror reaction.

The results suggest that, when a homogeneous and continuous coating is required, the former technique should be prioritized over grafting processes.

### 2.3.6 PECVD Modification and Structuration of PDMS Plates

In order to move forward the aim of the work, to obtain a controlled silver deposition on a material used in medical applications, such as silicone, it was necessary to further assess the feasibility of PECVD technique to immobilize PFM groups and obtain a homogeneous and stable silver coating onto PDMS substrates (material used to manufacture the tracheal stents and other medical devices).

Initially, as a first step to evaluate the modification, silicon wafer was used to control the PFM deposition. Films deposited from PFM showed a water contact angle higher than  $60^\circ$ . However, an extremely hydrophobic surface became an inconvenient for enhancing the interaction between the surface and water-soluble molecules. The WCA results showed the hydrophobicity of the PFM coating onto silicon wafer samples, which was  $83 \pm 1^\circ$ <sup>54,74</sup> instead of  $39 \pm 4^\circ$  from silicon wafer, indicating the correct deposition of the pp-PFM film onto the surface of the PDMS. These results showed chemical changes onto the PDMS surface and therefore, the next step consisted on the modification and characterization of modified samples to further assess the reactivity of the pp-PFM coating.

The interaction between the pp-PFM and the PDMS surface plays an important role regarding the nano-structuration of the surface. As it can be observed in Figure II-17, the PFM polymerized onto the PDMS surface created a homogeneous nanostructured PFM film with wrinkle- and fold-like structures (rippling surface) of about 100-200 nm caused by the interaction between the pp-PFM layer and the PDMS surface. Additionally, after incubation in aqueous solution (Milli-Q water), pp-PFM showed a non-swelling behaviour as a result of PFM chains reorientation causing nanometer protrusions<sup>75</sup> (about 50 nm) that lead to a nanostructured surface inside the previous nanostructured surface. The amine bearing biomolecules shall adopt this structuration after reacting with the pp-PFM-modified surface.

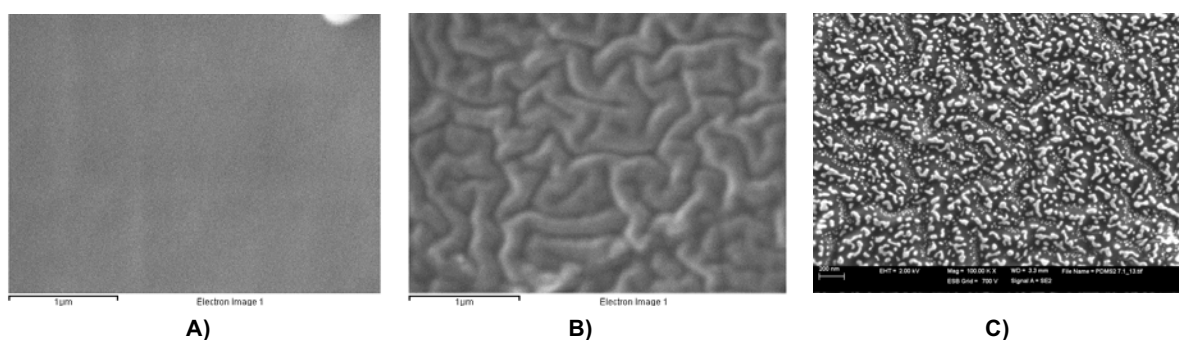


**Figure II-17.** SEM images of the PDMS samples. **A)** Non modified PDMS, **B)** Modified PDMS with PFM and **C)** Modified PDMS with PFM incubated with aqueous solution (Milli-Q water).

In order to assess the potential of micro-structuration of the PDMS surfaces, samples were modified with a grid onto their surface, resulting in modified and non-modified areas corresponding to the grid shape, as it can be observed in Figure II-18. Additionally, samples were incubated with AF488 resulting in fluorescent samples, where the fluorescent areas matched with the PFM modified areas. These results highlight the ability of the PECVD to easily modify PDMS samples or other materials and the capability to microstructure the surface as desired.

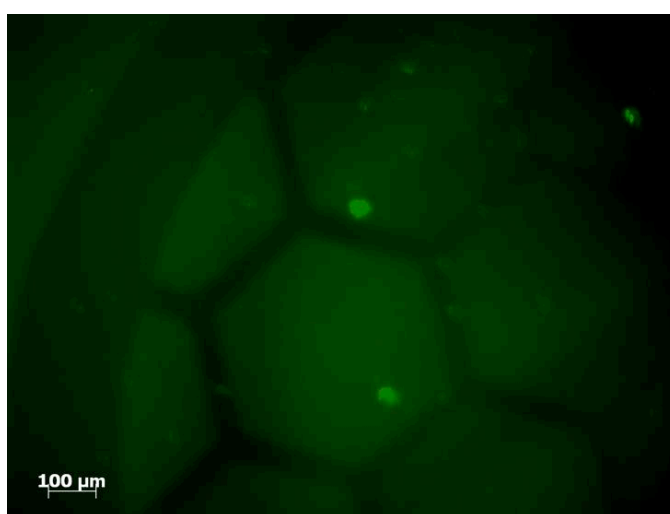


**Figure II-18.** Fluorescent micro-structured PFM coated PDMS.

In addition to the structuration ability using masks, this technology has a tremendous potential to be used to create selective modifications regarding to each side of samples. It should not be ignored that in the current days, where the medical implants are revolutionizing the medicine, there are a lot of medical implants that require direct contact with different tissues at the same time. Moreover, the capability of differential modification between the surfaces could be an interesting tool for increasing the personalization of the devices.

Considering previous results, that one side-modification of PDMS can be achieved with amine-bearing molecules using the reactive pp-PFM, for the next step it was interesting to evaluate the

possibility to modify different sides of the material. These results could provide a prove of concept methodology to create bi-side modifications onto the same material to allow different functionalities and behaviors.

As it can be observed in Figure II-19, the bi-side functionalization of the PFM structured surfaces achieved a high degree of selectively and specificity. It is possible to observe the first modification with the AF350 fluorophore and the second modification (on the opposite side) with the AF488 fluorophore. Additionally, it is important to remark that if the protective step was performed correctly, due to the transparency properties of the PDMS, it was possible to focus one side at a time and no contaminations of surfaces were observed.

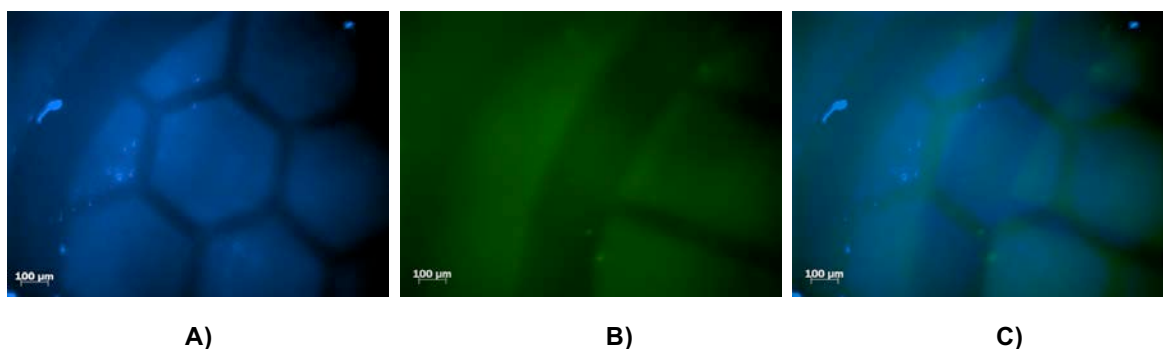


**Figure II-19.** Bi-side modification of PDMS samples. **A)** First side modification with AF350. **B)** Second side modification with AF488. **C)** Merge of both modifications.

As it can be observed, these modifications can be easily controlled and only the desired surface was modified. Regarding the micro-structuration, the technology allowed the possibility to create different shapes on the surface using masks. In this sense, the technology presented in this paper, showed the potential to create functionalized surfaces capable to be micro-structured with different functionalization regarding to each surface.

At this point, it is important to remark the ability of these new selectively modified surfaces to be functionalized in order to present biological activity. Due to the preferential reactivity of the PFM with amine-bearing molecules, surfaces coated with PFM could be functionalized with different biomolecules<sup>55</sup>, antibacterial agents like silver<sup>76</sup> or even nanoparticles.

### 2.3.7 Silver modification onto PDMS plates by PECVD

Once single and bi-side modification onto PDMS samples were achieved with promising results, the next step was to move forward to create antibacterial surface using silver. Therefore, after the deposition of pp-PFM onto PDMS plates, samples were incubated with glucosamine and the silver mirror reaction was performed to reduce metallic silver on top of the surfaces.

In Figure II-20, the corresponding WCA results, using silicon-wafers as controls, can be observed, showing changes on the WCA. After the reaction between the pentafluorophenyl groups with

glucosamine, WCA changed from  $83 \pm 1^\circ$  to  $51 \pm 1^\circ$ . Reduced silver by the coated glucosamine originated an interesting hydrophobic surface with a water contact angle of  $104 \pm 1^\circ$ . This hydrophobic surface of metallic silver could be attributed to the nanostructured silver coating (similar to the lotus leaves).<sup>77,78</sup> Some authors have previously discussed the hydrophobic and superhydrophobic behaviour of surfaces, and it seems to be clearly related to multivalued topography where air was trapped<sup>79</sup> beneath the liquid in the valleys.<sup>70,80–83</sup> In fact, this hydrophobic effect could maximize the antibacterial effect of silver by acting as an antifouling surface to reduce bacterial adhesion.

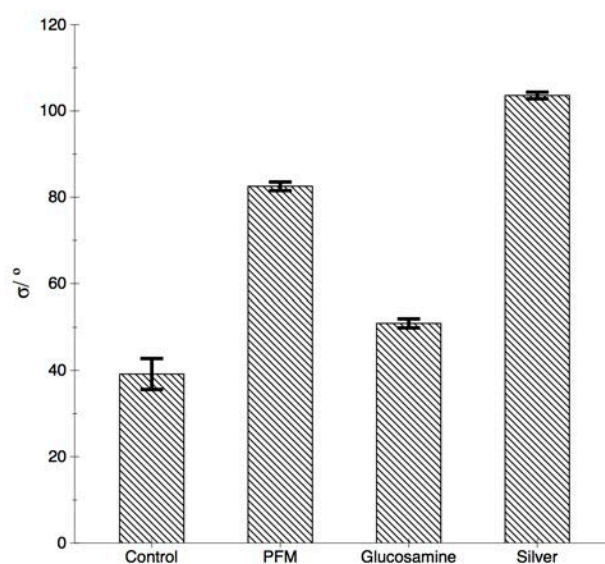


**Figure II-20.** WCA,  $\theta$  (deg), of silicon wafer samples. Samples were modified with different coatings on the surface, pp-PFM (PFM), pp-PFM + glucosamine (Glucosamine) and pp-PFM + glucosamine + silver (Silver).

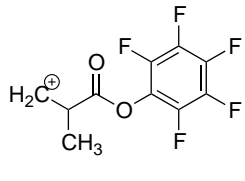
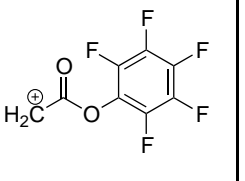
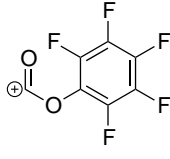
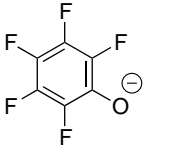
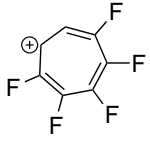
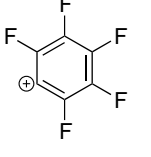
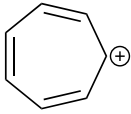
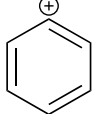
### 2.3.7.1.1 ToF-SIMS Analysis of Modified Surfaces

In order to demonstrate that surface modification onto PDMS was possible, the corresponding TOF-SIMS spectra, positive and negative ion, of PDMS samples with PFM, glucosamine, and silver coatings were studied (see the *Supporting Information*). The nonmodified PDMS samples showed the silicon mass fragment,  $m/z = 28$ , and additional PDMS typical peaks  $-SiCH_3^+$ ,  $CH_3SiO^-$ ,  $SiO_2^-$ ,  $SiC_3H_9^+$ ,  $CH_3SiO_2^-$  and  $Si_2OC_5H_{15}^+$  ( $m/z = 43, 59, 60, 73, 75$  and  $147$ ).<sup>84</sup> The PFM modified samples exhibit the typical methacrylate low mass fragments  $-C_2H_3^+$  and  $C_2H_5^+$  ( $m/z = 27$  and  $29$ ),<sup>85,86</sup> however, there was an interference between PDMS and PFM signals on the positive spectra. In these types of samples (PDMS based), the negative mass fragment ions could be more interesting in order to elucidate the fragments of the coating. In this case, the typical negative ion fragments related with the fluorinated ring consisted of  $-F^-$  and  $F_2H^-$  ( $m/z = 19$  and  $49$ ).

These fluorinated fragments confirmed the fluorinated ring in the polymeric structure, which was key for the further reactivity. Moreover, reassembling a series of different mass fragments (Table II-1) related with the fragmentation of the monomer confirmed the retention of the monomeric structure. In all spectra, there was a higher concentration of low-mass fragments. However, the presence of the

molecular ion ( $M$ ) could be detected at  $M+1$  ( $m/z = 253$ ). This effect of high concentration of low-mass fragments could be caused by a little etching or ablation process of the polymer, consequently with a coating reactivity decrease caused by plasma powers.<sup>87</sup>

**Table II-1.** Structure of Characteristic Peaks of pp-PFM. Possible Structure of the Secondary Ions for the Characteristic Peaks of the pp-PFM under Pulsed Plasma Conditions.

Structure	m/z	Structure	m/z
	253		225
	211		183
	181		167
	91		77

Additionally, an overlapping of the characteristic glucosamine peak can be observed ( $m/z = 72$  and  $180$ )<sup>88,89</sup> with the PDMS mass fragments when glucosamine sample (PDMS coated with PFM and incubated with glucosamine) was analysed. Finally, silver samples presented more simple spectra with the characteristic silver peaks  $-Ag^+$  ( $m/z = 107$  and  $109$ ).

At this point, what was really interesting was the possibility to observe the reactivity of the coatings by the variation on the fragments intensity.<sup>90,91</sup> There was an intensity variation between PFM characteristic peaks on the PFM-coated samples and glucosamine-coated samples. Initially, PFM samples presented a high intensity of  $m/z = 167$  and  $253$  (about 0.04 for both cases), but after incubation with glucosamine both intensities were reduced (about 75% and 50% for  $m/z = 167$  and  $253$ , respectively) as a consequence of the reaction between the ester and glucosamine.



### 2.3.7.1.2 Surface Structuration of Silver Coated PDMS Samples

Besides examining the physical and chemical properties of the plasma treated films, the surface morphology was also investigated using an optical microscope and a scanning electron microscope (SEM). In Figure II-21, a PDMS sample containing a thin film of metallic silver onto its surface is presented. As it can be observed, metallic silver was microstructured using a TEM grid to produce structured metallic silver surfaces onto flexible materials, such as PDMS. Additionally, the metallic silver was only located on the modified areas where the functionalization agent was immobilized. The controlled process and the structuration ability of the PECVD technique allowed the possibility to fabricate complex structures onto the surface without limitations.

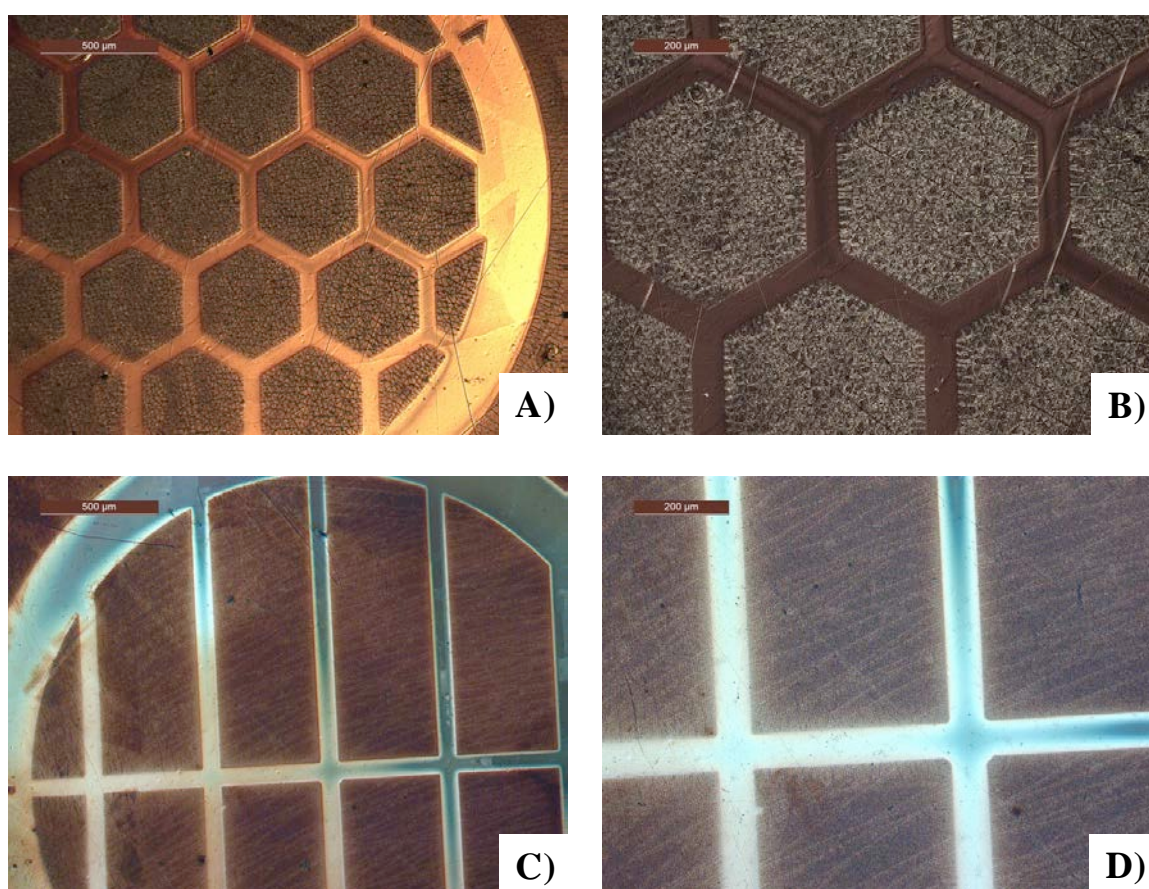


**Figure II-21.** Surface microscopy of structured silver surfaces. Optical microscopy of micro- and nanostructured silver coating of plasma polymerized PFM onto PDMS substrates for antibacterial applications.

In addition, significant differences in surface morphology were found between modified areas and nonmodified areas of PDMS samples. In Figure II-22 – A and B, the novel ability to structure the surface by PECVD can be clearly observed. This type of plasma modification technique allowed the possibility to fabricate homogeneous geometries with different chemical composition on the surface. In contrast to the surface homogeneity of the unmodified area, there was an increase of roughness on the areas that have been microstructured (Figure II-22 –A, B) attributed to the polymerization of the PFM onto PDMS surface. Furthermore, in Figure II-22 –C, D the nanostructuring of the silver coating resulted

in nanostructured branches and silver nanoparticles (about 70 - 150 nm) can be observed onto the high flexible PDMS surface.

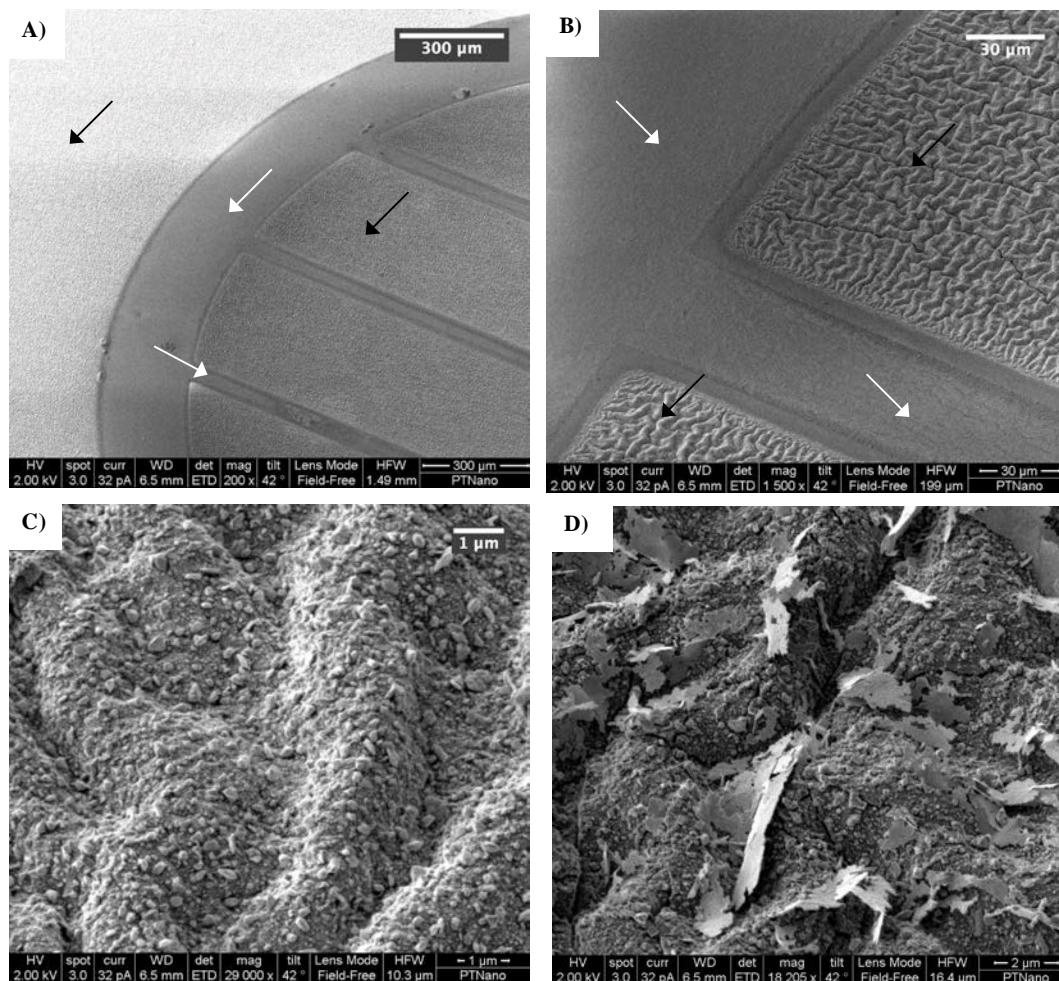


**Figure II-22.** Surface characterization of samples: SEM images of silver modified samples. **A)** modified sample with a G50P mask (Gilder Grids), **B)** magnified section of the grid structuration, **C)** nanostructuring of the modified area showing the multivalued roughness, and **D)** magnified of the nanostructuring of the modified area showing the fractal-like structures (modified area, black arrow; non-modified area, white arrow).

After the characterization of the surface morphology, modified samples were incubated for 2 h with different solvents (water, ethanol and hexane) in order to assess the behaviour of the nanostructure after immersion in solvents of different polarities. In Figure II-23, it can be observed that after the immersion of the samples with ethanol or hexane, the micro- and nano-structures did not change their size and shape (see Figure II-22 – 3, 4). This can be explained because ethanol and hexane did not interact with the silver nanoparticles and the silver coating. However, when samples were incubated with water there was an interesting change in the nanostructure, while the microstructure remains unaltered. As it can be observed in the water-incubated sample, the nanoparticles around 70-150 nm have disappeared and the remaining nanoparticles were around 20-40 nm. This can be explained by the digestive ripening<sup>92,93</sup> where (contrary to the Ostwald ripening<sup>94-96</sup> where small particles dissolve and diffuse to large nanoparticles) large nanoparticles broken apart and small nanoparticles increased



until a stable and uniform size was reached. As a result, water incubation resulted in a homogeneous distribution of small silver nanoparticles.

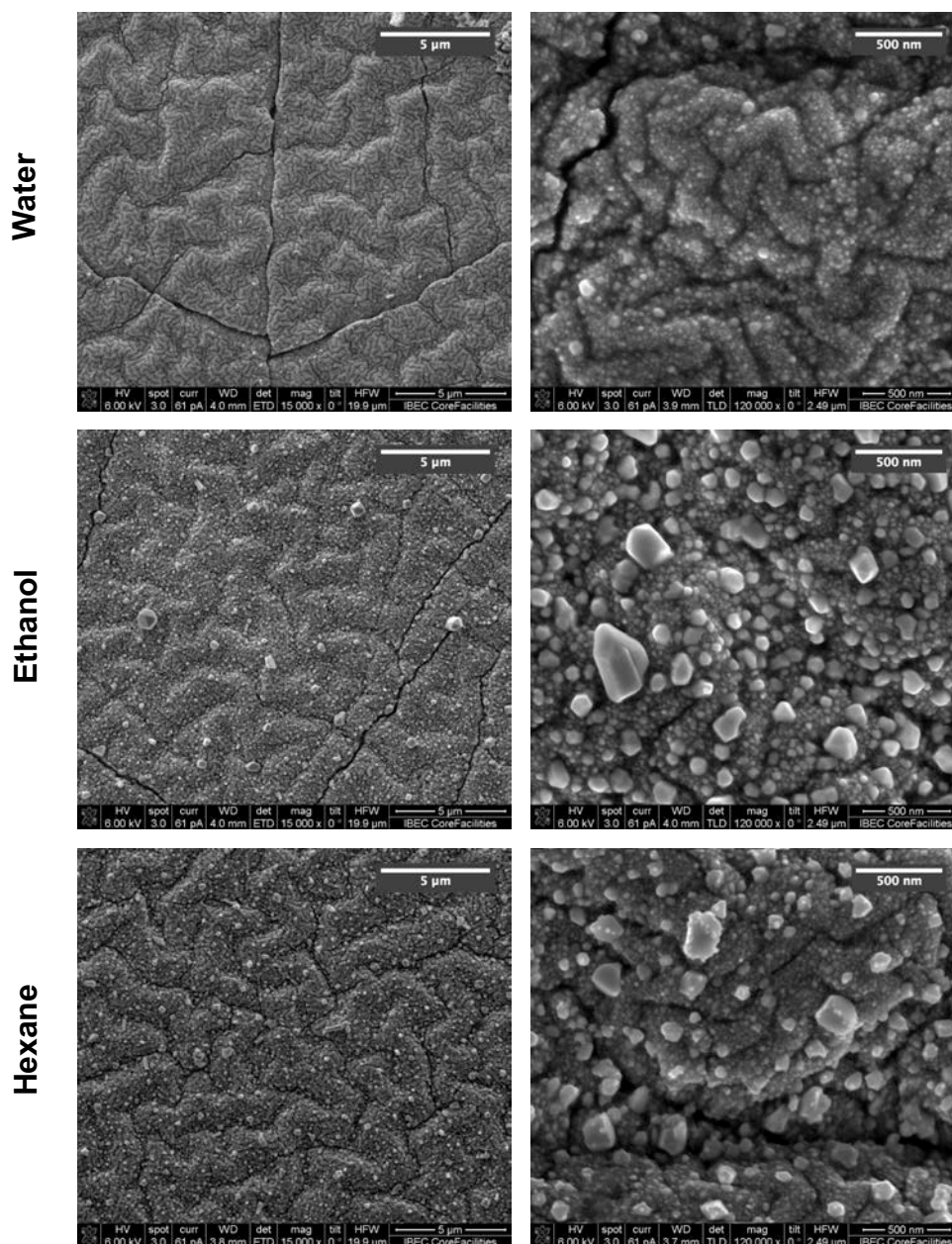


**Figure II-23.** Surface morphology of silver-coated PDMS samples after immersion with different liquids (water, ethanol, and hexane).

Considering that future devices will be in contact with different body liquids, such as mucus in the case of the trachea, the previously observed hydrophobic behaviour of the silver coated samples, was evaluate with mucus (mucine to simulate the mucus). In Figure II-24, when samples were treated with water, silver coated silicone samples showed an increase in the WCA higher to  $100^\circ$  in contrast with the  $75^\circ$  of the nonmodified silicone, similar to the previous results with silicon wafers, Figure II-20. In addition, silver coated samples showed a similar behaviour when treated with mucine, with an increase to  $100^\circ$  of the WCA. This increase in the hydrophobicity of the surfaces was very interesting to maximize

the antibacterial effect of silver coated samples by acting as an antifouling surface, reducing bacterial adhesion.

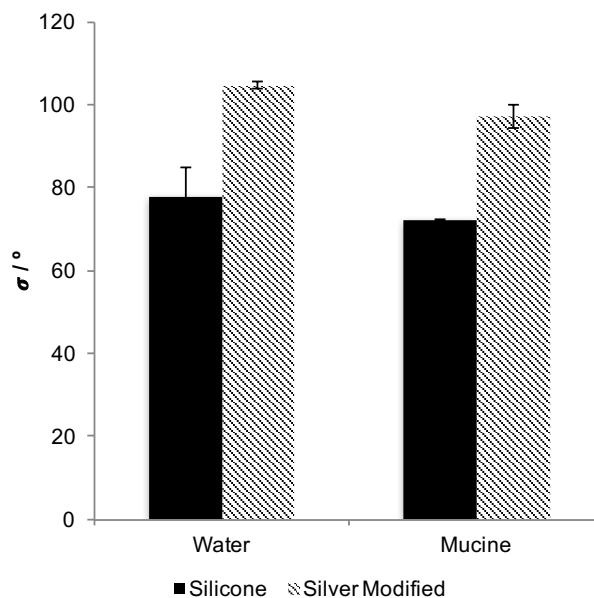
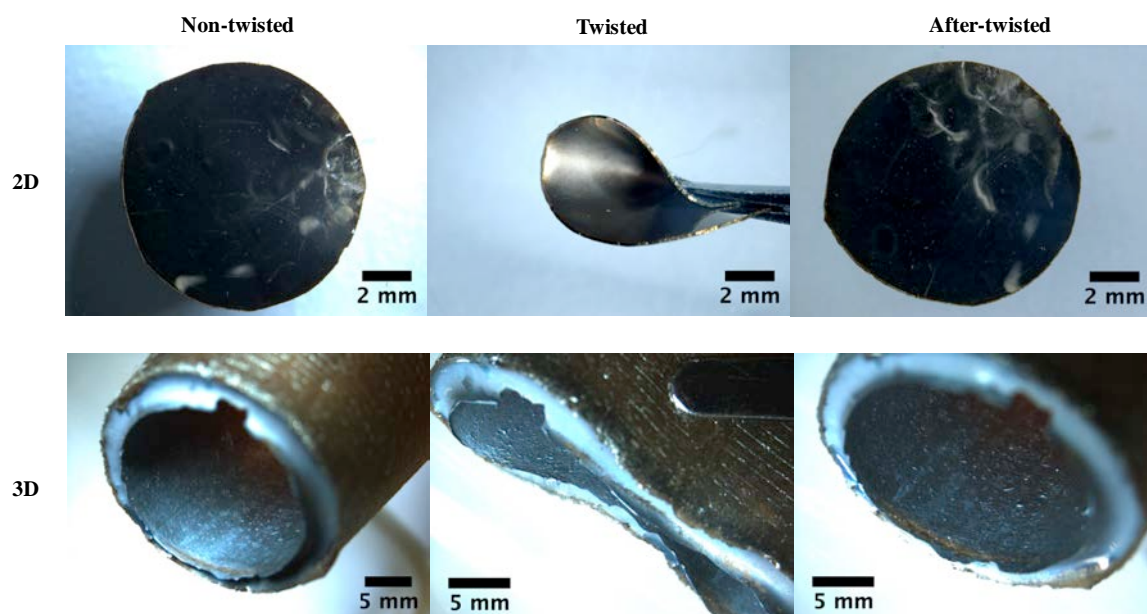


Figure II-24. WCA of silicone and silver modified silicone with water and mucine(10% p/v).

### 2.3.7.1.3 Behavior of Silver Coated 3D Structures

Additionally, silver coating was deposited onto a PDMS tube in order to demonstrate the method's novelty with complex shapes, such as 3D structures. As it can be observed in Figure II-25, the coating was perfectly adapted to 2D or 3D surface. In order to assess the flexibility of the coating, samples were twisted several times to observe the stability of the coating. These results showed that the coated tube could be easily twisted and non-delaminated after the implantation process because the thickness and flexibility of the coating allowed it to be adapted to the shape.



**Figure II-25.** Surface behaviour of 3D modified samples. Different PDMS-coated geometries before being twisted, during the twisting process, and finally, after being twisted.

#### 2.3.7.1.4 Silver Release of Coated PDMS Samples

The silver release of PDMS samples coated with silver (total amount of silver-coated samples, about  $0.45 \pm 0.15 \mu\text{g} / \text{mm}^2$ ) is illustrated in Figure II-26. Initially, there was a maximum release of  $\text{Ag}^+$  about 0.6 and 1.1 ppm (from TSB media and Milli-Q water, respectively) between the first 24 h of incubation. During the following 10 days of incubation, a concentration decay and a subsequent stabilization of silver ion release of about 0.1 ppm can be observed. As it is well-known, the antibacterial activity of silver is not attributed to a metallic element but to the silver ion ( $\text{Ag}^+$ ). Its activity mechanism is currently controversial, however it seems to be related to the complexation ability between silver ion and cysteine,<sup>21,97</sup> interaction with DNA,<sup>98,99</sup> cell disruption,<sup>36</sup> or inhibition of electron transport.<sup>100,101</sup>

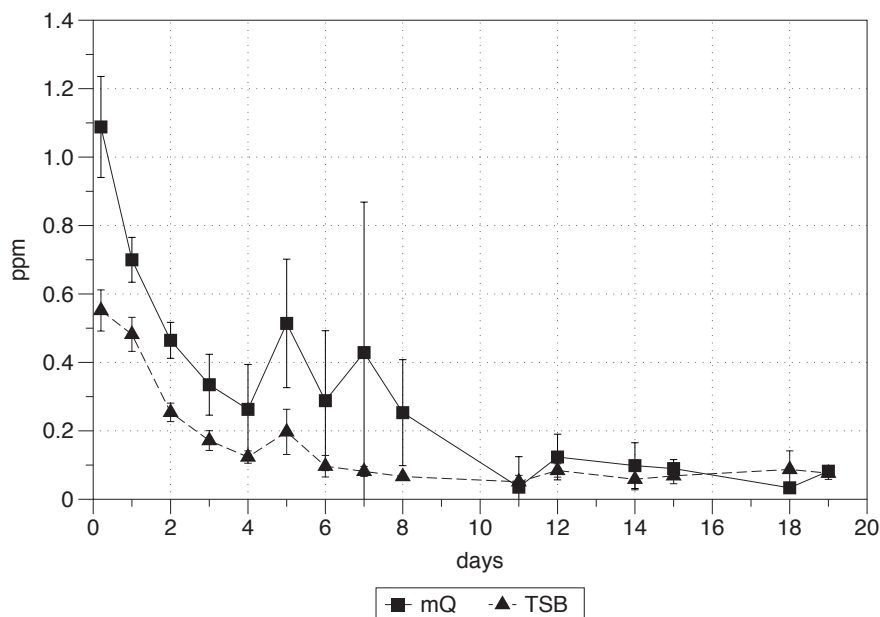


**Figure II-26.** Silver release of samples in different media, TSB and Milli-Q water in oxidic conditions.

In addition, in Figure II-26, different release profiles can be observed between water and TSB media related to the pH variation, 5.5 and 7.3 for water and TSB media, respectively. According to the thermodynamics of the silver oxidation, the amount of dissolved silver was directly proportional to the amount of dissolved oxygen and indirectly proportional to the pH.<sup>102</sup> Consequently, acidic pH increased silver release while basic pH decreased the silver release of silver ion. However, in the previous 24 h, even samples incubated with water and TSB media showed a burst of silver release that did not follow the kinetics of the oxidative reaction and was attributed to the release of the chemisorbed silver from the metallic silver surface.<sup>103</sup>

In order to further assess the release of the chemisorbed silver, in Figure II-27, samples incubated with oxidic and anoxic conditions can be observed. In comparison with the oxidative conditions, 1.1 and 0.6 ppm for water and TSB, respectively, in anoxic conditions there was a mildly release of silver, around 0.5 and 0.3 ppm for water and TSB, respectively. This silver release under anoxic conditions could not be attributed to the oxidative process as samples were incubated in an argon atmosphere and with absence of oxygen in the media, that was previously degassed with argon. These results proved that, at the beginning, both phenomena happened at the same time, the release of the chemisorbed silver ions from the metallic silver surface to the media that produced the initial burst release and the oxidative process.

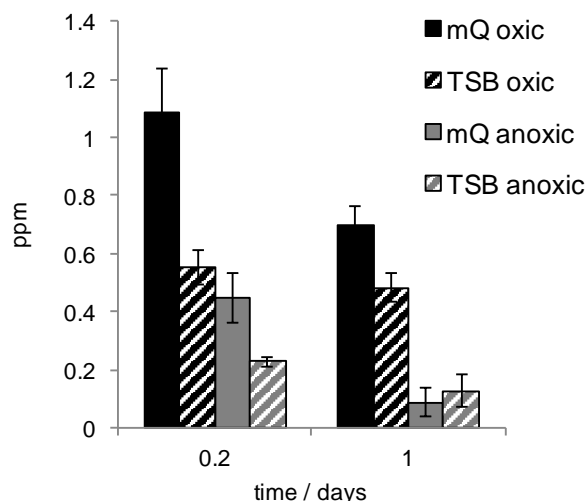


**Figure II-27.** Concentration of silver in solutions incubated with oxic and anoxic conditions for 5 h and 1 day.

At the beginning, Figure II-28, there was an initial burst of silver due to the release of the chemisorbed silver ions (fast and short process) and, at the same time, a homogeneous and stable release (slow and long process) due to the oxidative dissolution of the silver metal deposited on the surface.

The initial burst of silver was very promising due to its high concentration. This was because the reversible bacteria adhesion onto the medical implants occurred in the first hours after postimplantation.<sup>71</sup> High initial concentrations of silver ions in a short period of time could be a tremendous advantage to enhance the antibacterial activity once the device is implanted on the body. In addition, a continued release after this initial burst is desired in order to avoid the formation of the biofilm structures that takes place over a large time period.<sup>104</sup>

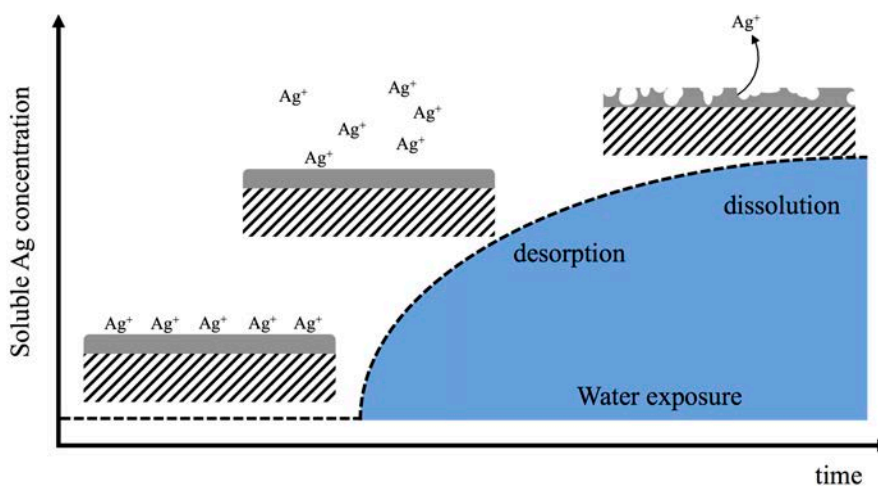


**Figure II-28.** Scheme of silver ion release. Initially, there is a desorption of the chemisorbed silver and an oxidative process, and at the end only the oxidative process takes place.<sup>103</sup>

At this point, it was important to compare the experimental silver ion concentrations released with the necessary silver concentrations for antibacterial activity. The initial concentrations, about 1.1 ppm for the water incubation and about 0.6 ppm for TSB, were clearly higher than the minimum concentration required for antimicrobial efficacy, 0.1 ppb<sup>71</sup>. In addition, even the basal release extended a long time, 0.1 ppm for Milli-Q water and TSB media, was higher than the minimum concentration. Moreover, these silver ion release levels were lower than the maximum toxic concentration for human cells, 10 ppm.<sup>105</sup>

#### **2.3.7.1.5 Bacteria Cultures onto Silver Coated Surfaces**

In order to test the antibacterial activity of the modified samples, PDMS were incubated using *S. aureus* and *P. aeruginosa* as Gram-positive and Gram-negative representatives, respectively. In Figure II-29A, the bacterial growth and biofilm structures can be clearly observed, especially on the nonmodified *P. aeruginosa* samples. However, the antibacterial effect of the silver ions onto the modified surfaces can be observed, causing a considerably decrease on bacteria viability, showing a 0% of bacterial survival. In Figure II-29B, an increase in the bacterial death caused by the silver coating can be observed. In addition, both strains had the same behaviour showing about 100% bacterial cell death in contrast to the 25% bacterial cell death in the control samples (PDMS).

Additionally, no extra bacterial adhesion on the modified surfaces could be observed as a consequence of the high antibacterial action of the silver ions and due to the hydrophobic surfaces caused by the nanostructures of the silver coating. In addition, after incubation of the nonmodified and modified samples with  $10^5$  cfu / mL (Figure II-29C) there was a complete reduction of bacteria viability, causing the death of all bacteria in the media.

Taking into account that post-implantation problem of bacterial colonization is localized on the device (not systemic) and requires the extraction of the stent and implantation of a new one, the goal of this work consisted on design an antibacterial device that is able to protect itself against bacteria colonization and increase the life-time of the device. In addition, the silver release in the surroundings, close to the surface of the modified samples, showed clear antibacterial properties avoiding the attachment of the bacteria and causing bacteria death.



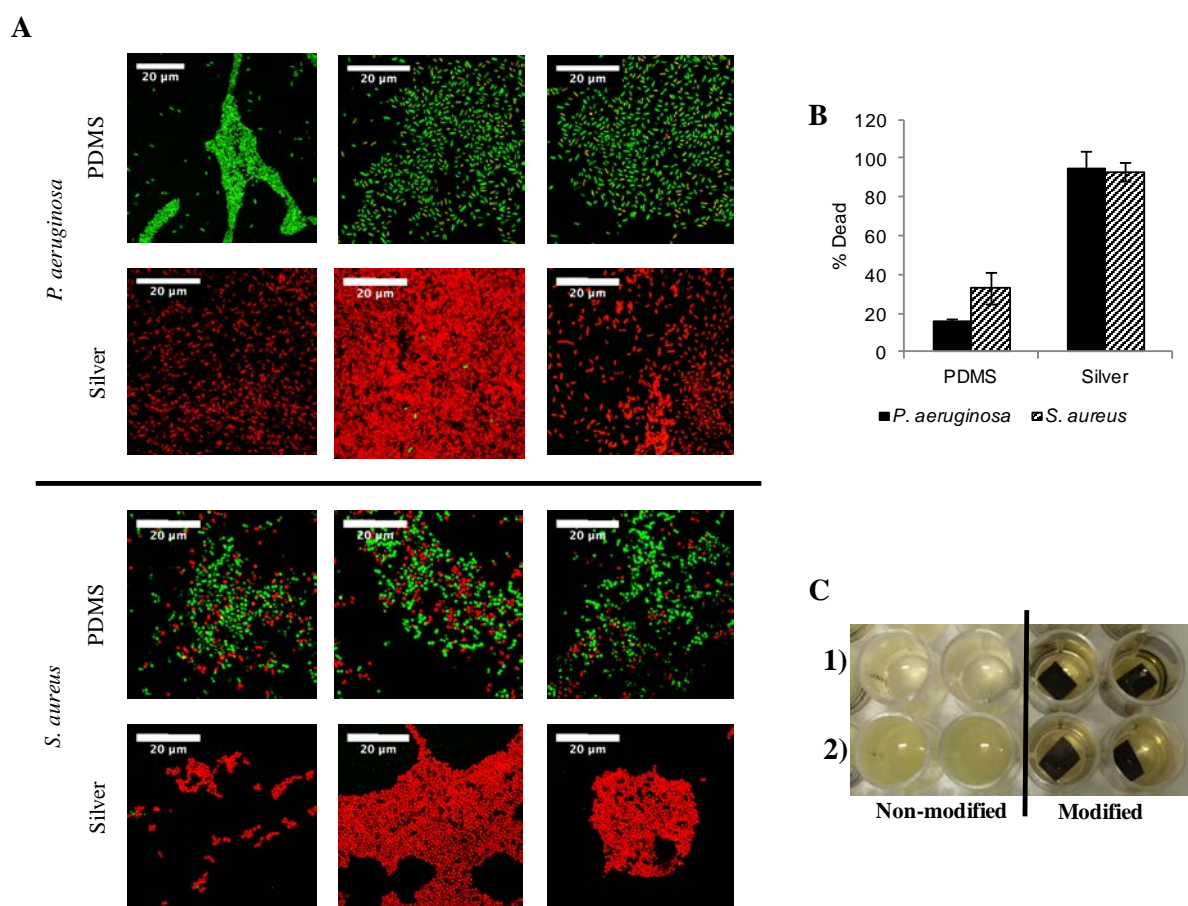


**Figure II-29.** Bacterial viability on coated and noncoated samples: **A**) bacterial cultures of different modified samples with silver stained with Live&Dead kit [Non-modified PDMS samples (PDMS) showing biofilm formation and silver-coated PDMS samples (silver); scale bar, 20  $\mu\text{m}$ ]; **B**) bacterial death comparison between different bacterial strains [results obtained analyzing previous images using imageJ software]; **C**) bacterial viability in the supernatant after being incubated with nonmodified and silver-coated samples with  $10^5$  cfu / ml. Row 1 is *S. aureus*, and row 2 is *P. aeruginosa*.

### 2.3.7.1.6 In Vitro Cytotoxicity of Silver Coated Samples

The *in vitro* cytotoxicity of the silver-coated surfaces was evaluated on COS-7 cells using MTS assay and silver nitrate as comparison. Cells were incubated with different silver releases with concentrations of silver ions around 0.5, 0.3, 0.2 and 0.1 ppm (obtained from cumulative release of samples incubated for 1, 2, 3 and 6 days, respectively). As shown in Figure II-30, no differences were observed for the released silver ions in the media in comparison with silver nitrate. Silver ions, in the range of the tested levels, showed no significant decrease in cellular viability. These results showed that the concentration of the silver ions released from the silver-coated samples were highly biocompatible for COS-7 cells.

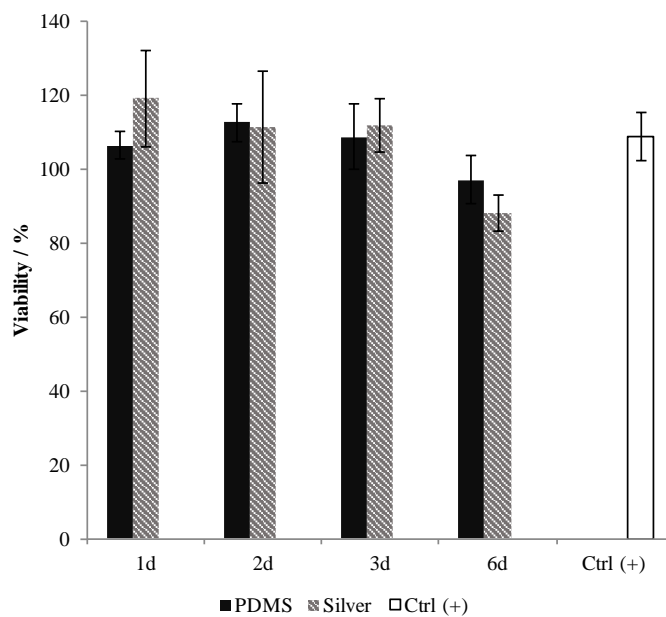


**Figure II-30.** Cell viability of silver modified samples on COS-7. Cells were incubated with media that was previously incubated with the nonmodified and modified samples for 1, 2, 3 and 6 days (0.5, 0.3, 0.2 and 0.1 ppm of silver ions, respectively). Cell viability (%) is expressed relatively to the untreated control cells.

## 2.4 Concluding Remarks

As it has been commented previously, in the current development of medical devices it is imperative to design and control the surfaces of the materials used. In this work, plasma treatments let to control the modification process and created selectively single or bi-side modified surfaces capable to covalently react with amine-bearing molecules. Additionally, different topologies on surfaces can be easily achieved with the ability to model the macroscopic and microscopic surface morphology and carries out chemical patterning. In addition, the process allowed to control the modification area and even the selectivity modification of each side of the material. Thus, medical devices could be selectively functionalized regarding to each side with different biological activities to interact with different tissues at the same time.

This work presents a novel methodology to create new structured surfaces capable to covalently immobilize nanostructured antibacterial agents, such as silver, showing hydrophobic surfaces to reduce biofilm formation and bacterial colonization. Additionally, this methodology has the advantage that it can be applied on different substrates and shapes allowing the possibility to microstructure the surface. Furthermore, the silver coating showed a highly antibacterial activity against Gram-positive and Gram-negative bacteria due to the silver ion release. Additionally, the hydrophobic behaviour related to the nanostructuring of the silver coating reduced bacteria adhesion and biofilm formation that contributed to a lower probability of postimplantation infections.

Finally, the initial rapid release of silver ion presented a remarkable antimicrobial activity within the first 24 h, followed by a lower sustained release for 20 days, which prolonged the biological activity of the device. The silver amounts achieved during the release showed no cytotoxic effect for COS-7 cells, but silver concentration was high enough to avoid *P. aeruginosa* and *S. aureus* adhesion. As a result, these functional surfaces could be promising candidates to develop implantable materials with antibacterial properties.

Once the development of a methodology to produce antibacterial surfaces onto the silicon-base materials, such as PDMS, has been achieved, the next step of this work will consist on the development of a surface platform for therapeutic drug delivery system. As previously described, the next unmet clinical need consists on the development of drug delivery surfaces to treat surrounding tissues of implanted devices, such as stenotic tissues. Therefore, considering the ability to selectively modify each side of the material, the next chapter will be focused on the development of silicon-based surfaces with a drug delivery system using nanoparticles capable of releasing antiproliferative drugs.

## 2.5 References

- (1) Davies, D. Understanding biofilm resistance to antibacterial agents. *Nat. Rev. Drug Discov.* **2003**, 2 (2), 114–122 DOI: 10.1038/nrd1008.
- (2) Nouraei, S. A. R.; Ma, E.; Patel, A.; Howard, D. J.; Sandhu, G. S. Estimating the population incidence of adult post-intubation laryngotracheal stenosis. *Clin. Otolaryngol.* **2007**, 32, 411–412 DOI: 10.1111/j.1749-4486.2007.01484.x.
- (3) Huang, C. J. Use of the silicone T-tube to treat tracheal stenosis or tracheal injury. *Ann. Thorac. Cardiovasc. Surg.* **2001**, 7 (4), 192–196.
- (4) Melkane, A. E.; Matar, N. E.; Haddad, A. C.; Nassar, M. N.; Almoutran, H. G.; Rohayem, Z.; Daher, M.; Chalouhy, G.; Dabar, G. Management of postintubation tracheal stenosis: Appropriate indications make outcome differences. *Respiration* **2010**, 79 (5), 395–401 DOI: 10.1159/000279225.
- (5) Hugo Marquette, C.; Mensier, E.; Copin, M. C.; Desmidt, A.; Freitag, L.; Witt, C.; Petyt, L.; Ramon, P. Experimental models of tracheobronchial stenoses: A useful tool for evaluating airway stents. *Ann. Thorac. Surg.* **1995**, 60 (3), 651–656 DOI: 10.1016/0003-4975(95)00460-3.
- (6) Hind, C. R.; Donnelly, R. J. Expandable metal stents for tracheal obstruction: permanent or temporary? A cautionary tale. *Thorax* **1992**, 47 (9), 757–758 DOI: 10.1136/thx.47.9.757.
- (7) Charokopos, N.; Foroulis, C. N.; Rouska, E.; Sileli, M. N.; Papadopoulos, N.; Papakonstantinou, C. The management of post-intubation tracheal stenoses with self-expandable stents: early and long-term results in 11 cases. *Eur. J. Cardio-Thoracic Surg.* **2011**, 40 (4), 919–924 DOI: 10.1016/j.ejcts.2010.12.042.
- (8) Martínez-Ballarín, J. I.; Díaz-Jiménez, J. P.; Castro, M. J.; Moya, J. a. Silicone stents in the management of benign tracheobronchial stenoses: Tolerance and early results in 63 patients. *Chest* **1996**, 109 (3), 626–629 DOI: 10.1378/chest.109.3.626.
- (9) Fernández Vaquero, M. A.; Bartolomé Cela, E.; Villegas Fernández, F. R. Revisión de las estenosis traqueales tras intubación: a propósito de un caso. *Med. Intensiva* **2009**, 33 (6), 301–305 DOI: 10.1016/S0210-5691(09)72199-0.
- (10) Semaan, R.; Yarmus, L. Rigid bronchoscopy and silicone stents in the management of central airway obstruction. *J. Thorac. Dis.* **2015**, 7, S352–S362 DOI: 10.3978/j.issn.2072-1439.2015.11.17.
- (11) Zakaluzny, S. Complications of tracheobronchial airway stents. *Otolaryngol. - Head Neck Surg.* **2003**, 128 (4), 478–488 DOI: 10.1016/S0194-5998(03)00002-0.
- (12) Liu, H. C.; Lee, K. S.; Huang, C. J.; Cheng, C. R.; Hsu, W. H.; Huang, M. H. Silicone T-tube for complex laryngotracheal problems. *Eur. J. Cardio-thoracic Surg.* **2002**, 21 (2), 326–330 DOI: 10.1016/S1010-7940(01)01098-3.
- (13) Harley, H. R. Laryngotracheal obstruction complicating tracheostomy or endotracheal intubation with assisted respiration. A critical review. *Thorax* **1971**, 26 (5), 493–533 DOI: 10.1136/thx.26.5.493.
- (14) Zannini, P.; Melloni, G.; Chiesa, G.; Carretta, A. Self-expanding stents in the treatment of tracheobronchial obstruction. *Chest* **1994**, 106 (1), 86–90 DOI: 10.1378/chest.106.1.86.
- (15) Mather, C. M.; Sinclair, R.; Gurr, P. Tracheal stents: the Montgomery T-tube. *Anesth. Analg.* **1993**, 77 (6), 1282–1284 DOI: 10.1213/00000539-199312000-00032.

- (16) Boston Medical Products. Tracheobronxane® Dumon™ Silicone Stent <http://www.bosmed.com/pulmonology/novatech-dumontm-tracheal-and-bronchial-stents.html> (accessed Jan 18, 2012).
- (17) Nouraei, S. A. R.; Petrou, M. A.; Randhawa, P. S.; Singh, A.; Howard, D. J.; Sandhu, G. S. Bacterial colonization of airway stents: a promoter of granulation tissue formation following laryngotracheal reconstruction. *Arch. Otolaryngol. Head Neck Surg.* **2006**, *132* (10), 1086–1090 DOI: 10.1001/archotol.132.10.1086.
- (18) Schmä, F.; Fegeler, W.; Terpe, H. J.; Hermann, W.; Stoll, W.; Becker, K. Bacteria and granulation tissue associated with Montgomery T-tubes. *Laryngoscope* **2003**, *113* (8), 1394–1400 DOI: 10.1097/00005537-200308000-00024.
- (19) Hench, L. L. Biomaterials: a forecast for the future. *Biomaterials* **1998**, *19* (16), 1419–1423 DOI: 10.1016/S0142-9612(98)00133-1.
- (20) Vasilev, K.; Sah, V.; Anselme, K.; Ndi, C.; Mateescu, M.; Dollmann, B.; Martinek, P.; Ys, H.; Ploux, L.; Griesser, H. J. Tunable antibacterial coatings that support mammalian cell growth. *Nano Lett.* **2010**, *10* (1), 202–207 DOI: 10.1021/nl903274q.
- (21) Chamakura, K.; Perez-Ballester, R.; Luo, Z.; Bashir, S.; Liu, J. Comparison of bactericidal activities of silver nanoparticles with common chemical disinfectants. *Colloids Surf., B* **2011**, *84* (1), 88–96 DOI: 10.1016/j.colsurfb.2010.12.020.
- (22) Raffi, M.; Mehrwan, S.; Bhatti, T. M.; Akhter, J. I.; Hameed, A.; Yawar, W.; Ul Hasan, M. M. Investigations into the antibacterial behavior of copper nanoparticles against *Escherichia coli*. *Ann. Microbiol.* **2010**, *60* (1), 75–80 DOI: 10.1007/s13213-010-0015-6.
- (23) Faúndez, G.; Troncoso, M.; Navarrete, P.; Figueroa, G. Antimicrobial activity of copper surfaces against suspensions of *Salmonella enterica* and *Campylobacter jejuni*. *BMC Microbiol.* **2004**, *4*, 19 DOI: 10.1186/1471-2180-4-19.
- (24) Lee, I.; Agarwal, R. K.; Lee, B. Y.; Fishman, N. O.; Umscheid, C. A. Systematic review and cost analysis comparing use of chlorhexidine with use of iodine for preoperative skin antisepsis to prevent surgical site infection. *Infect. Control Hosp. Epidemiol.* **2010**, *31* (12), 1219–1229 DOI: 10.1086/657134.
- (25) Shen, Y.; Stojicic, S.; Haapasalo, M. Antimicrobial efficacy of chlorhexidine against bacteria in biofilms at different stages of development. *J. Endod.* **2011**, *37* (5), 657–661 DOI: 10.1016/j.joen.2011.02.007.
- (26) Assar, N. H.; Hamuoda, H. M. Colloidal silver as a new antimicrobial agent. *Int. J. Microbiol. Res.* **2010**, *1* (1), 33–36.
- (27) Pratten, J.; Nazhat, S. N.; Blaker, J. J.; Boccaccini, A. R. In vitro attachment of *Staphylococcus epidermidis* to surgical sutures with and without Ag-containing bioactive glass coating. *J. Biomater. Appl.* **2004**, *19* (1), 47–57 DOI: 10.1177/0885328204043200.
- (28) Dai, T.; Huang, Y. Y.; Sharma, S. K.; Hashmi, J. T.; Kurup, D. B.; Hamblin, M. R. Topical antimicrobials for burn wound infections. *Recent Pat. Antiinfect. Drug Discov.* **2010**, *5* (2), 124–151 DOI: 10.2174/157489110791233522.
- (29) Ip, M.; Lui, S. L.; Poon, V. K. M.; Lung, I.; Burd, A. Antimicrobial activities of silver dressings: An in vitro comparison. *J. Med. Microbiol.* **2006**, *55* (Pt 1), 59–63 DOI: 10.1099/jmm.0.46124-0.
- (30) Atiyeh, B. S.; Costagliola, M.; Hayek, S. N.; Dibo, S. A. Effect of silver on burn wound infection control and healing: Review of the literature. *Burns* **2007**, *33* (2), 139–148 DOI: 10.1016/j.burns.2006.06.010.
- (31) Silverstein, P.; Heimbach, D.; Meites, H.; Latenser, B.; Mazingo, D.; Mullins, F.; Garner, W.;

- Turkowski, J.; Shupp, J.; Glat, P.; et al. An Open, Parallel, Randomized, Comparative, Multicenter Study to Evaluate the Cost-Effectiveness, Performance, Tolerance, and Safety of a Silver-Containing Soft Silicone Foam Dressing (Intervention) vs Silver Sulfadiazine Cream. *J. Burn Care Res.* **2011**, 32 (6), 617–626 DOI: 10.1097/BCR.0b013e318236fe31.
- (32) Del Nobile, M. A.; Cannarsi, M.; Altieri, C.; Sinigaglia, M.; Favia, P.; Iacoviello, G.; D'Agostino, R. Effect of Ag-containing Nano-composite Active Packaging System on Survival of *Alicyclobacillus acidoterrestris*. *J. Food Sci.* **2005**, 69 (2000), E379–E383 DOI: 10.1111/j.1365-2621.2004.tb09899.x.
- (33) Lo, S. F.; Hayter, M.; Chang, C. J.; Hu, W. Y.; Lee, L. L. A systematic review of silver-releasing dressings in the management of infected chronic wounds. *J. Clin. Nurs.* **2008**, 17 (15), 1973–1985 DOI: 10.1111/j.1365-2702.2007.02264.x.
- (34) Rupp, M. E.; Fitzgerald, T.; Marion, N.; Helget, V.; Puumala, S.; Anderson, J. R.; Fey, P. D. Effect of silver-coated urinary catheters: Efficacy, cost-effectiveness, and antimicrobial resistance. *Am. J. Infect. Control* **2004**, 32 (8), 445–450 DOI: 10.1016/j.ajic.2004.05.002.
- (35) Tobin, E. J.; Bambauer, R. Silver Coating of Dialysis Catheters to Reduce Bacterial Colonization and Infection. *Ther. Apher.* **2003**, 7 (6), 504–509 DOI: 10.1046/j.1526-0968.2003.00097.x.
- (36) Jung, W. K.; Koo, H. C.; Kim, K. W.; Shin, S.; Kim, S. H.; Park, Y. H. Antibacterial activity and mechanism of action of the silver ion in *Staphylococcus aureus* and *Escherichia coli*. *Appl. Environ. Microbiol.* **2008**, 74 (7), 2171–2178 DOI: 10.1128/AEM.02001-07.
- (37) Taglietti, A.; Arciola, C. R.; D'Agostino, A.; Dacarro, G.; Montanaro, L.; Campoccia, D.; Cucca, L.; Vercellino, M.; Poggi, A.; Pallavicini, P.; et al. Antibiofilm activity of a monolayer of silver nanoparticles anchored to an amino-silanized glass surface. *Biomaterials* **2014**, 35 (6), 1779–1788 DOI: 10.1016/j.biomaterials.2013.11.047.
- (38) Hamerli, P.; Weigel, T.; Groth, T.; Paul, D. Surface properties of and cell adhesion onto allylamine-plasma-coated polyethyleneterephthalat membranes. *Biomaterials* **2003**, 24 (22), 3989–3999 DOI: 10.1016/S0142-9612(03)00312-0.
- (39) Yang, J.; Bei, J.; Wang, S. Enhanced cell affinity of poly (D,L-lactide) by combining plasma treatment with collagen anchorage. *Biomaterials* **2002**, 23 (12), 2607–2614 DOI: 10.1016/S0142-9612(01)00400-8.
- (40) Duque, L.; Queralto, N.; Francesch, L.; Bumbu, G. G.; Borros, S.; Berger, R.; Förch, R. Reactions of plasma-polymerised pentafluorophenyl methacrylate with simple amines. *Plasma Process. Polym.* **2010**, 7 (11), 915–925 DOI: 10.1002/ppap.201000058.
- (41) Morent, R.; De Geyter, N.; Desmet, T.; Dubruel, P.; Leys, C. Plasma surface modification of biodegradable polymers: A review. *Plasma Process. Polym.* **2011**, 8 (3), 171–190 DOI: 10.1002/ppap.201000153.
- (42) Favia, P.; D'Agostino, R. Plasma treatments and plasma deposition of polymers for biomedical applications. *Surf. Coatings Technol.* **1998**, 98 (1–3), 1102–1106 DOI: 10.1016/S0257-8972(97)00285-5.
- (43) Hsu, S. H. S. H.; Chen, W. C. Improved cell adhesion by plasma-induced grafting of L-lactide onto polyurethane surface. *Biomaterials* **2000**, 21 (4), 359–367 DOI: 10.1016/S0142-9612(99)00191-X.
- (44) Dai, L.; StJohn, H. A. W.; Bi, J.; Zientek, P.; Chatelier, R. C.; Griesser, H. J. Biomedical coatings by the covalent immobilization of polysaccharides onto gas-plasma-activated polymer surfaces. *Surf. Interface Anal.* **2000**, 29 (1), 46–55 DOI: 10.1002/(SICI)1096-9918(200001)29:1<46::AID-SIA692>3.0.CO;2-6.
- (45) Vohrer, U.; Hegemann, D.; Oehr, C. XPS, AES, and AFM as tools for study of optimized plasma

- functionalization. *Anal. Bioanal. Chem.* **2003**, 375 (7), 929–934 DOI: 10.1007/s00216-003-1750-3.
- (46) Chu, P. K.; Chena, J. .; Wanga, L. P.; Huangb, N. Plasma-surface modification of biomaterials. *Mater. Sci. Eng. R Reports* **2002**, 36 (5–6), 143–206 DOI: 10.1016/S0927-796X(02)00004-9.
- (47) Siow, K. S.; Britcher, L.; Kumar, S.; Griesser, H. J. Plasma methods for the generation of chemically reactive surfaces for biomolecule immobilization and cell colonization - A review. *Plasma Process. Polym.* **2006**, 3 (6–7), 392–418 DOI: 10.1002/ppap.200600021.
- (48) Francesch, L.; Garreta, E.; Balcells, M.; Edelman, E. R.; Borrós, S. Fabrication of bioactive surfaces by plasma polymerization techniques using a novel acrylate-derived monomer. *Plasma Process. Polym.* **2005**, 2 (8), 605–611 DOI: 10.1002/ppap.200500042.
- (49) Alves, C. M.; Yang, Y.; Carnes, D. L.; Ong, J. L.; Sylvia, V. L.; Dean, D. D.; Agrawal, C. M.; Reis, R. L. Modulating bone cells response onto starch-based biomaterials by surface plasma treatment and protein adsorption. *Biomaterials* **2007**, 28 (2), 307–315 DOI: 10.1016/j.biomaterials.2006.09.010.
- (50) Prasad, G. R.; Daniels, S.; Cameron, D. C.; McNamara, B. P.; Tully, E.; O’Kennedy, R. PECVD of biocompatible coatings on 316L stainless steel. *Surf. Coatings Technol.* **2005**, 200 (1–4 SPEC. ISS.), 1031–1035 DOI: 10.1016/j.surfcoat.2005.02.009.
- (51) Nisol, B.; Poleunis, C.; Bertrand, P.; Reniers, F. Poly(ethylene glycol) films deposited by atmospheric pressure plasma liquid deposition and atmospheric pressure plasma-enhanced chemical vapour deposition: Process, chemical composition analysis and biocompatibility. *Plasma Process. Polym.* **2010**, 7 (8), 715–725 DOI: 10.1002/ppap.201000023.
- (52) Battiston, G. A.; Gerbasi, R.; Gregori, A.; Porchia, M.; Cattarin, S.; Rizzi, G. A. PECVD of amorphous TiO<sub>2</sub> thin films: effect of growth temperature and plasma gas composition. *Thin Solid Films* **2000**, 371 (1–2), 126–131 DOI: 10.1016/S0040-6090(00)00998-6.
- (53) Lewis, H. G. P.; Edell, D. J.; Gleason, K. K. Pulsed-PECVD films from hexamethylcyclotrisiloxane for use as insulating biomaterials. *Chem. Mater.* **2000**, 12 (11), 3488–3494 DOI: 10.1021/cm0003370.
- (54) Francesch, L.; Borros, S.; Knoll, W.; Förch, R. Surface reactivity of pulsed-plasma polymerized pentafluorophenyl methacrylate (PFM) toward amines and proteins in solution. *Langmuir* **2007**, 23 (7), 3927–3931 DOI: 10.1021/la062422d.
- (55) Duque, L.; Menges, B.; Borros, S.; Förch, R. Immobilization of biomolecules to plasma polymerized pentafluorophenyl methacrylate. *Biomacromolecules* **2010**, 11 (10), 2818–2823 DOI: 10.1021/bm100910q.
- (56) Harsch, A.; Calderon, J.; Timmons, R. B.; Gross, G. W. Pulsed plasma deposition of allylamine on polysiloxane: A stable surface for neuronal cell adhesion. *J. Neurosci. Methods* **2000**, 98 (2), 135–144 DOI: 10.1016/S0165-0270(00)00196-5.
- (57) De Bartolo, L.; Morelli, S.; Lopez, L. C.; Giorno, L.; Campana, C.; Salerno, S.; Rende, M.; Favia, P.; Detomaso, L.; Gristina, R.; et al. Biotransformation and liver-specific functions of human hepatocytes in culture on RGD-immobilized plasma-processed membranes. *Biomaterials* **2005**, 26 (21), 4432–4441 DOI: 10.1016/j.biomaterials.2004.11.009.
- (58) France, R. M.; Short, R. D.; Duval, E.; Jones, F. R.; Dawson, R. A.; MacNeil, S. Plasma Copolymerization of Allyl Alcohol/1,7-Octadiene: Surface Characterization and Attachment of Human Keratinocytes. *Chem. Mater.* **1998**, 10 (4), 1176–1183 DOI: 10.1021/cm970761+.
- (59) Horna, D.; Ramírez, J. C.; Cifuentes, A.; Bernad, A.; Borrós, S.; González, M. a. Efficient cell reprogramming using bioengineered surfaces. *Adv. Healthc. Mater.* **2012**, 1 (2), 177–182 DOI: 10.1002/adhm.201200017.

- (60) Langer, R.; Tirrell, D. a. Designing materials for biology and medicine. *Nature* **2004**, *428* (6982), 487–492 DOI: 10.1038/nature02388.
- (61) Förch, R.; Zhang, Z.; Knoll, W. Soft plasma treated surfaces: Tailoring of structure and properties for biomaterial applications. *Plasma Process. Polym.* **2005**, *2* (5), 351–372 DOI: 10.1002/ppap.200400083.
- (62) Yasuda, H. *Plasma Polymerization*; Academic Press: INC:NY, 1985.
- (63) Francesch de Castro, L. Surface modification of Polymers by plasma polymerization techniques for tissue engineering, Universitat Ramon Llull, 2008.
- (64) Arefi-Khonsari, F.; Tatoulian, M.; Bretagnol, F.; Bouloussa, O.; Rondelez, F. Processing of polymers by plasma technologies. *Surf. Coatings Technol.* **2005**, *200* (1–4), 14–20 DOI: 10.1016/j.surfcoat.2005.02.184.
- (65) Rossi, F.; Kylián, O.; Hasiwa, M. Decontamination of surfaces by low pressure plasma discharges. *Plasma Process. Polym.* **2006**, *3* (6–7), 431–442 DOI: 10.1002/ppap.200600011.
- (66) Belmonte, T.; Pintassilgo, C. D.; Czerwiec, T.; Henrion, G.; Hody, V.; Thiebaut, J. M.; Loureiro, J. Oxygen plasma surface interaction in treatments of polyolefines. *Surf. Coatings Technol.* **2005**, *200* (1–4), 26–30 DOI: 10.1016/j.surfcoat.2005.02.108.
- (67) Yasuda, H. *Luminous Chemical Vapor Deposition and Interface Engineering*; CRC, 2005; Vol. 122.
- (68) Cifuentes, A.; Borrós, S. Comparison of two different plasma surface-modification techniques for the covalent immobilization of protein monolayers. *Langmuir* **2013**, *29* (22), 6645–6651 DOI: 10.1021/la400597e.
- (69) Csucs, G.; Michel, R.; Lussi, J. W.; Textor, M.; Danuser, G. Microcontact printing of novel copolymers in combination with proteins for cell-biological applications. *Biomaterials* **2003**, *24* (10), 1713–1720 DOI: 10.1016/S0142-9612(02)00568-9.
- (70) Zhou, Y.; Li, M.; Su, B.; Lu, Q. Superhydrophobic surface created by the silver mirror reaction and its drag-reduction effect on water. *J. Mater. Chem.* **2009**, *19* (20), 3301–3306 DOI: 10.1039/b819251k.
- (71) Jamuna-Thevi, K.; Bakar, S. A.; Ibrahim, S.; Shahab, N.; Toff, M. R. M. Quantification of silver ion release, in vitro cytotoxicity and antibacterial properties of nanostructured Ag doped TiO<sub>2</sub> coatings on stainless steel deposited by RF magnetron sputtering. *Vacuum* **2011**, *86* (3), 235–241 DOI: 10.1016/j.vacuum.2011.06.011.
- (72) Cifuentes Rius, A. Comparació de la Polimerització Assistida per Plasma Front el Plasma-Grafting per a la Immobilització Superficial de Biomolècules, IQS, Universitat Ramon Llull, 2011.
- (73) Cifuentes Rius, A. Tailoring Carbon Nanotubes Properties for Gene Delivery Applications, Universitat Ramon Llull, 2013.
- (74) Cifuentes-Rius, A.; de Pablo, A.; Ramos-Pérez, V.; Borrós, S. Tailoring Carbon Nanotubes Surface for Gene Delivery Applications. *Plasma Process. Polym.* **2014**, *11* (7), 704–713 DOI: 10.1002/ppap.201300167.
- (75) Marí-Buyé, N.; O’Shaughnessy, S.; Colominas, C.; Semino, C. E.; Gleason, K. K.; Borrós, S. Functionalized, swellable hydrogel layers as a platform for cell studies. *Adv. Funct. Mater.* **2009**, *19* (8), 1276–1286 DOI: 10.1002/adfm.200801561.
- (76) Borrós, S.; Gilabert, J.; Martí, S.; Molina, M.; Montes, A.; Ramos, V.; Rosell, A. Process for



- Manufacturing a Customizable Medical Device and Device Obtained by Said Process. *WO 2016/023980* **2014**.
- (77) Lin, J.; Cai, Y.; Wang, X.; Ding, B.; Yu, J.; Wang, M. Fabrication of biomimetic superhydrophobic surfaces inspired by lotus leaf and silver ragwort leaf. *Nanoscale* **2011**, 3 (3), 1258–1262 DOI: 10.1039/c0nr00812e.
- (78) Guo, Z.; Liu, W. Formation mechanism of robust silver nanoparticle film with superhydrophobicity. *Appl. Phys. Lett.* **2010**, 97 (24), 243701 DOI: 10.1063/1.3525574.
- (79) Bartell, F. E.; Smith, J. T. Alteration of surface properties of gold and silver as indicated by contact angle measurements. *J. Phys. Chem.* **1953**, 57 (2), 165–172 DOI: 10.1021/j150503a008.
- (80) Marmur, A. From hydrophilic to superhydrophobic: Theoretical conditions for making high-contact-angle surfaces from low-contact-angle materials. *Langmuir* **2008**, 24 (14), 7573–7579 DOI: 10.1021/la800304r.
- (81) Roach, P.; Shirtcliffe, N. J.; Newton, M. I. Progress in superhydrophobic surface development. *Soft Matter* **2008**, 4 (2), 224–240 DOI: 10.1039/b712575p.
- (82) Guo, F.; Su, X.; Hou, G.; Li, P. Superhydrophobic silver surface with dendrites structure on steel substrate by a facile electroless galvanic deposition process. *Appl. Surf. Sci.* **2012**, 258 (11), 4906–4910 DOI: 10.1016/j.apsusc.2012.01.112.
- (83) Shen, L.; Ji, A.; Shen, J. Silver mirror reaction as an approach to construct superhydrophobic surfaces with high reflectivity. *Langmuir* **2008**, 24 (18), 9962–9965 DOI: 10.1021/la801774v.
- (84) Karen, A.; Man, N.; Shibamori, T.; Takahashi, K. TOF-SIMS characterization of industrial materials: From silicon wafer to polymer. *Appl. Surf. Sci.* **2003**, 203–204, 541–546 DOI: 10.1016/S0169-4332(02)00623-2.
- (85) Lub, J.; van Vroonhoven, F. C. B. M.; van Leyen, D.; Benninghoven, A. Time of flight static secondary negative ion mass spectra of poly(methylmethacrylate), poly(ethylmethacrylate), and poly(methylmethacrylate-co-ethylmethacrylate). Ion structures and quantification. *J. Polym. Sci., Part B: Polym. Phys.* **1989**, 27 (10), 2071–2080 DOI: 10.1002/polb.1989.090271011.
- (86) Huang, H. L.; Goh, S. H.; Lai, D. M. Y.; Huan, C. H. A. ToF-SIMS studies of poly(methyl methacrylate-co-methacrylic acid), poly(2,2,3,3,3-pentafluoropropyl methacrylate-co-4-vinylpyridine) and their blends. *Appl. Surf. Sci.* **2004**, 227 (1–4), 373–382 DOI: 10.1016/j.apsusc.2003.12.015.
- (87) Alexander, M. R.; Duc, T. M. The chemistry of deposits formed from acrylic acid plasmas. *J. Mater. Chem.* **1998**, 8 (4), 937–943 DOI: 10.1039/a708064f.
- (88) Kerwin, J. L.; Whitney, D. L.; Sheikh, A. Mass spectrometric profiling of glucosamine, glucosamine polymers and their catecholamine adducts. Model reactions and cuticular hydrolysates of *Toxorhynchites amboinensis* (Culicidae) pupae. *Insect Biochem. Mol. Biol.* **1999**, 29 (7), 599–607 DOI: 10.1016/S0965-1748(99)00037-5.
- (89) Pastorini, E.; Vecchiotti, S.; Colliva, C.; Persiani, S.; Rotini, R.; Roatti, G.; Zaccarelli, L.; Rovati, L. C.; Roda, A. Identification and quantification of glucosamine in rabbit cartilage and correlation with plasma levels by high performance liquid chromatography-electrospray ionization-tandem mass spectrometry. *Anal. Chim. Acta* **2011**, 695 (1–2), 77–83 DOI: 10.1016/j.aca.2011.04.003.
- (90) Vidal-Escales, E.; Borrós, S. New methodology to follow the evolution of squalene by-products during model compound vulcanization studies. *Talanta* **2004**, 62 (3), 539–547 DOI: 10.1016/j.talanta.2003.08.021.
- (91) Montero, L.; Baxamusa, S. H.; Borros, S.; Gleason, K. K. Thin hydrogel films with nanoconfined

- surface reactivity by photoinitiated chemical vapor deposition. *Chem. Mater.* **2009**, *21* (2), 399–403 DOI: 10.1021/cm802737m.
- (92) Lin, X.; Sorensen, C.; Klabunde, K. J. Digestive Ripening, Nanophase Segregation and Superlattice Formation in Gold Nanocrystal Colloids. *J. Nanopart. Res.* **2000**, *2* (2), 157–164 DOI: 10.1023/A:1010078521951.
- (93) Hwang, N.-M.; Jung, J.-S.; Lee, D.-K. Thermodynamics and Kinetics in the Synthesis of Monodisperse Nanoparticles. In *Thermodynamics - Fundamentals and Its Application in Science*; Morales-Rodriguez, R., Ed.; InTech, 2012; pp 371–388.
- (94) Gentry, S. T.; Kendra, S. F.; Bezpalko, M. W. Ostwald Ripening in Metallic Nanoparticles: Stochastic Kinetics. *J. Phys. Chem. C* **2011**, *115* (26), 12736–12741 DOI: 10.1021/jp2009786.
- (95) Liu, J.; Chai, P.; Tang, J.; Wen, H.; Shi, Y.; Xue, C. Electrochemical aging of silver nanoparticles and its effects on bio-chemical sensing properties. *Anal. Methods* **2012**, *4* (8), 2381–2387 DOI: 10.1039/c2ay05786g.
- (96) Zille, A.; Fernandes, M. M.; Francesko, A.; Tzanov, T.; Fernandes, M.; Oliveira, F. R.; Almeida, L.; Amorim, T.; Carneiro, N.; Esteves, M. F.; et al. Size and Aging Effects on Antimicrobial Efficiency of Silver Nanoparticles Coated on Polyamide Fabrics Activated by Atmospheric DBD Plasma. *ACS Appl. Mater. Interfaces* **2015**, *7* (25), 13731–13744 DOI: 10.1021/acsami.5b04340.
- (97) Taglietti, A.; Diaz Fernandez, Y. a; Amato, E.; Cucca, L.; Dacarro, G.; Grisoli, P.; Necchi, V.; Pallavicini, P.; Pasotti, L.; Patrini, M. Antibacterial activity of glutathione-coated silver nanoparticles against gram positive and gram negative bacteria. *Langmuir* **2012**, *28* (21), 8140–8148 DOI: 10.1021/la3003838.
- (98) Feng, Q. L.; Wu, J.; Chen, G. Q.; Cui, F. Z.; Kim, T. N.; Kim, J. O. A mechanistic study of the antibacterial effect of silver ions on *Escherichia coli* and *Staphylococcus aureus*. *J. Biomed. Mater. Res.* **2000**, *52* (4), 662–668 DOI: 10.1002/1097-4636(20001215)52:4<662::AID-JBM10>3.0.CO;2-3.
- (99) Shrivastava, S.; Bera, T.; Roy, A.; Singh, G.; Ramachandrarao, P.; Dash, D. Characterization of enhanced antibacterial effects of novel silver nanoparticles. *Nanotechnology* **2010**, *18* (22), 225103 DOI: 10.1088/0957-4484/18/22/225103.
- (100) Dallas, P.; Sharma, V. K.; Zboril, R. Silver polymeric nanocomposites as advanced antimicrobial agents: Classification, synthetic paths, applications, and perspectives. *Adv. Colloid Interface Sci.* **2011**, *166* (1–2), 119–135 DOI: 10.1016/j.cis.2011.05.008.
- (101) Alt, V.; Bechert, T.; Steinrücke, P.; Wagener, M.; Seidel, P.; Dingeldein, E.; Domann, E.; Schnettler, R. An in vitro assessment of the antibacterial properties and cytotoxicity of nanoparticulate silver bone cement. *Biomaterials* **2004**, *25* (18), 4383–4391 DOI: 10.1016/j.biomaterials.2003.10.078.
- (102) Liu, J.; Hurt, R. H. Ion release kinetics and particle persistence in aqueous nano-silver colloids. *Environ. Sci. Technol.* **2010**, *44* (6), 2169–2175 DOI: 10.1021/es9035557.
- (103) Dobias, J.; Bernier-Latmani, R. Silver release from silver nanoparticles in natural waters. *Environ. Sci. Technol.* **2013**, *47* (9), 4140–4146 DOI: 10.1021/es304023p.
- (104) Hetrick, E. M.; Schoenfisch, M. H. Reducing implant-related infections: active release strategies. *Chem. Soc. Rev.* **2006**, *35* (9), 780–789 DOI: 10.1039/b515219b.
- (105) Hardses, J.; Ahrens, H.; Gebert, C.; Streitbuenger, A.; Buerger, H.; Erren, M.; Gunsel, A.; Wedemeyer, C.; Saxler, G.; Winkelmann, W.; et al. Lack of toxicological side-effects in silver-coated megaprotheses in humans. *Biomaterials* **2007**, *28* (18), 2869–2875 DOI: 10.1016/j.biomaterials.2007.02.033.

*This page left blank intentionally*

**Chapter III. Drug Delivery System with  
Immobilized Nanoparticles**

*This page left blank intentionally*

### 3.1 Introduction

The previous chapter (Chapter II) showed a study of plasma surface modification (grafting and PECVD) capable of modifying the surface of different materials, such as silicone for medical applications, to fabricate reactive bioactive surfaces. These modified surfaces were designed to react specifically with amine-bearing molecules via the activated ester contained in the polymeric layer. In addition, the novelty and versatility of this technique allowed to selectively modify different surfaces of the same material with different reagents. This allows bi-side modification, which opens a wide range of modifications and coatings to provide different bioactivity to materials in order to interact with different tissues at the same time.

The combination of the modified surface with a modified silver mirror reagent resulted in a metallic silver coating on the surface of the materials. In addition, the silver coating was completely flexible, avoiding cracking, due to the nanometric thickness. Additionally, it was observed that the resulting metallic surface was formed by fusion of silver nanoparticles yielding a nano-structuration with interesting hydrophobic properties (similar to the lotus leave). Finally, the developed silver surface showed antibacterial and antifouling properties against gram-positive and gram-negative strains.

In this context, and considering the second main problem after stent implantation, which is the recurrence of the tracheobronchial stenosis and granulation tissue formation, this chapter aims to design a solution to treat biological tissues with abnormal growth, such as stenotic or granulation tissue using drugs.

As mentioned before, tracheal stenosis is defined by a gradual reduction of airway lumen caused by different conditions.<sup>1</sup> Stenosis carries different degrees of morbidity and even causes death by asphyxiation if it is not treated correctly.<sup>2</sup> Often, its diagnosis occurs in advanced stages in the form of severe acute respiratory insufficiency, which requires urgent treatment.<sup>3</sup>

Different benign and malignant conditions can cause tracheobronchial stenosis resulting in a respiratory distress with dyspnea, and if not treated early, can lead to asphyxia and death. The most common benign etiology is usually prolonged post-intubation and prolonged post-tracheotomy<sup>4,5</sup>, although there are other causes, such as idiopathic, infections, chemical aggressions (gastroesophageal reflux or toxic inhalation), radiotherapy or associated systemic diseases (i.e., Wegener). Despite the different causes, the most common mechanism seems to be an abnormal re-epithelialization with chronic inflammation and fibrosis of the epithelium-tracheal mucosa after an aggression, which conditions an increase of the thickness of the mucosa.<sup>6</sup>

Post-inflammatory tracheal stenosis is the most common non-malignant tracheal lesion and is usually caused by prolonged ischemia and concomitant infection causing tracheal wall necrosis. Repair of the damaged wall may result in abnormal formation of granulation tissue and stenotic scarring.<sup>7</sup> Regarding the malignant tracheal stenosis, it originates from primary tumors of the thorax (lungs, pleura and

esophagus) or from metastases. Different resective endoscopic procedures can be performed to recover the opening of the lumen, and once open, to implant a stent to prevent re-stenosis. Current stents only present mechanical expansion, obviating adaptability, biocompatibility, biofunctionality and stability. However, re-stenosis of post-inflammatory scars (50% of patients)<sup>8</sup>, as well as the growth of inflammatory granulation tissue, can be a life-threatening complication, if it is not treated properly. Both complications could be resolved by activating pharmacologically the stents with antiproliferative drugs, such as the drug-eluting stents used in cardiology<sup>9-11</sup>.

Mitomycin and paclitaxel (PCTXL) are antimitotic drugs that have been used in the treatment of a wide variety of tumours and stenotic tissue with effective results reducing the abnormal proliferation. The published results, mainly in dogs and in children, indicate that the topical use of mitomycin or paclitaxel reduce the tracheal stenotic tissue, avoids the occlusion of the stent, and the restenosis.<sup>12,13</sup> Thus, it is reasonable to propose a combination of local use of antiproliferative agents with stents to significantly reduce the stenotic tissue and the tissue growth (granulation tissue) around the stent,<sup>14,15</sup> resulting in tissue healing and reduced stent implantation time.<sup>16,17</sup> In addition, another action of antiproliferative drugs, beyond inflammation, would be focused at locally treating some type of tumours. For example, after various animal model assays,<sup>18</sup> various treatments based on coating stents with antiproliferative drugs, such as cisplatin, have been proposed to treat patients with tumors causing airway occlusion.

Some reports indicated a reduction in the tracheal stenosis when mitomycin was applied either topically or using a bioabsorbable stent.<sup>19-21</sup> However, there is a controversy in the literature regarding the beneficial activity of mitomycin. In this regard, the activity of mitomycin depends on the dose, and high doses of drug leads to toxic effects.<sup>22</sup> Previous results (in animal model) indicated that while with low doses of mitomycin (lower than 0.4 mg / mL) showed a reduction of stenotic tissue, higher doses of mitomycin (0.4 mg / mL and higher) did not prevent stenosis tissue. These results are especially relevant when mitomycin is used to treat laser wound, since a significant risk of acute airway obstruction was observed.<sup>23</sup> Some studies found necrotic ulcer, skin necrosis, and even tracheal stenosis when high doses of mitomycin were used (0.5 mg / mL) topically.<sup>12,24</sup> According to the literature, it seems that the activity of topical mitomycin is highly dose-dependent showing interesting results when low dose was used and tissue damage, if the correct dose was exceeded.

Similar results have been observed when topically paclitaxel was used in the trachea wall and even in the bile duct.<sup>25</sup> Local drug accumulation of paclitaxel could damage the tissue in contact, leading to epithelial denudation, moderate mucosal inflammation and fibrosis. However, these damages were expected and acceptable respectively to safety, considering the beneficial clinical therapeutic results.<sup>26,27</sup> Recent studies have demonstrated a reduction of tissue growth around the stent and a reduction of stenotic tissue, increasing patient's patency, when paclitaxel was used topically, with drug-eluting balloon or with exhale drug eluting stents.<sup>15,16,21,28,29</sup> Therefore, considering all the data around the use of paclitaxel to treat stenotic tissues, in the airway track and even in cardiology, paclitaxel

showed promising results to create drug eluting stents with a controlled time-release and doses to treat stenotic tissues and increase stent patency.

As mentioned before, the main problem and limitation of using antiproliferative drugs is the local concentration in the treatment area. Topically administered drugs showed high concentration, and due to the different histological differences of trachea wall compared to blood vessels, the accumulated drugs caused important damages in the tissues. In contrast, when this type of drugs were used in blood vessels, where blood flow produces a continuous lavage of drug, there was no overdose in the treatment area and no toxic or damaging effects on tissues were observed.<sup>28</sup>

In addition to dose-dependent toxic effects and poor therapeutic outcomes caused by the systemic distribution of PCTXL, the application of PCTXL is compromised due to its poor solubility in aqueous media. To overcome these disadvantages, various drug delivery systems, such as liposomes<sup>30</sup>, nanoparticles (NPs),<sup>31,32</sup> polymer drug conjugates<sup>33</sup> and micelles<sup>34</sup>, have been developed from different viewpoints. Among them, biodegradable polymeric NPs in the range of 70-300 nm, have been successfully utilized to encapsulate PCTXL, reducing PCTXL-associated side effects as well as better therapeutic benefits over commercial Taxol.<sup>35</sup>

Taking into account the previous described problems when using dose-dependent drugs with non-controlled delivery system, and considering the demonstrated feasibility of nanoparticles system to control the drug delivery, and the clinical benefits of low doses of paclitaxel to treat tracheal stenosis; a nanoparticle system capable to release paclitaxel in low doses in a controlled manner over time could show promising results to treat tracheal stenosis. However, most nanoparticles systems have been designed to be administered through oral<sup>36,37</sup> or intravenous<sup>38,39</sup> system and this application (tracheal stent) requires a surface-immobilized drug delivery system in order to treat only the affected surrounding tissues where stent is implanted. Then, the nanoparticles technology must be designed to be able to be immobilized onto the surface of the silicone-based materials.

In this case, the previous chapter (Chapter II) showed the modification of a surface to provide bi-side modifications and antibacterial properties. Considering that the system was designed to react with aminated-molecules, this creates a wide range of possibilities and applications. Therefore, this previously developed technology could be adapted to go beyond the previous results and design more complex surfaces with a drug delivery system to release PCTXL in a controlled manner on the desired tissues. To obtain a suitable drug delivery system, the polymer must be biodegradable, non-toxic and capable of entrapping PCTXL. Additionally, the polymer must be able to form nanoparticles and the system must be stable, present amine groups on the surface of the formed NPs and degrade in aqueous media.

To achieve this goal, this chapter seeks to combine the previously described surface modification technology, with an adaptation of previously developed intravenous polyester-PEG NPs technology (by our research group<sup>40</sup>) into an effective amine-bearing immobilized drug delivery nanoparticles system



for efficient delivery of active drug molecules. The resulting technology could be implemented in the surfaces of medical devices, such as tracheal stent, to avoid granulation and stenotic tissue.

## 3.2 Materials and Methods.

### 3.2.1 Materials.

Argon 5.0 and oxygen 5.0 were purchased from Abelló Linde S.A. (Barcelona, Spain). PFM was purchased from Apollo Scientific LTD (Stockport, UK). Acetone, acetic acid, methanol, tween-80, fluorescein diacetate (FDA), 1,8-octanediol (98%), D-(+)-Glucosamine hydrochloride (99%), ethidium bromide (EB), Phalloidin-TRITC, 4',6-diamidino-2-phenylindole (DAPI), Triton x-100, Phosphate-buffered saline (PBS), paraformaldehyde (PFA), 4-(2-hydroxyethyl)-1-piperazineethanesulfonic acid (HEPES), insulin human transferrin and sodium selenite (ITS), docetaxel and amphotericin B were purchased from Sigma-Aldrich (Madrid, Spain). PEG bis(amine) (Mw 2.000) were purchased from Sigma-Aldrich and Iris Biotech GMBH (Marktredwitz, Germany). Glutaric acid (99%) was obtained from Alfa Aesar (Haverhill, USA). Paclitaxel (PCTXL) was purchased from Yunnan Hande Bio-Tech CO, LTD, (Kunming, P.R. China). Ultrapure water (Milli-Q) was obtained using a Synergy UV<sup>®</sup> system from Merck Millipore (Billerica, MA, USA).

DMEM high Glucose with L-Glutamine, F12K, EMEM, fetal bovine serum (FBS), penicillin and streptomycin were purchased from Gibco Life Technologies (Grand Island, NY, USA). 3-[4, 5-dimethylthiazol-2-yl]-2, 5-diphenyltetrazolium bromide (MTT) was purchased from MBL, International Corporation (Woburn, MA, USA). Sylgard 184 kit was purchased from Ellsworth Adhesives (Madrid, Spain) and Si-wafers were purchased from Wafer World (West Palm Beach, FL, USA).

### 3.2.2 Preparation of substrates.

The Si-wafers and PDMS substrates were prepared as described in the previous chapter. Briefly, Sylgard kit (10:1) was spread using a paint applicator to obtain films of 500  $\mu\text{m}$  thickness and incubated overnight at 70°C. Then, films were cut in circular shapes of 21 and 10 mm. PDMS samples were washed with 5% SDS solution, rinsed with Milli-Q water, washed with 2% Hellmanex solution, rinsed again with Milli-Q water and finally with ethanol. Si-wafers were washed with the same protocol as PDMS samples. Finally, samples were dried in a stream of nitrogen and stored.

### 3.2.3 Surface modification by plasma techniques

The surface modifications carried out in this work were performed using a stainless steel vertical plasma reactor as it was described in the previous chapter using the SSVPR. Briefly, for plasma polymerization, vacuum was started until the base pressure of 0.001-0.003 mbar for was reached. Then, PFM was regulated through the needle valve and introduced to the reactor chamber in a vapour phase (heated at 75 °C) until 0.02-0.03 mbar. The continuous radio frequency power was fixed at 15 W (working power) and pulsed plasma polymerization duty cycle (DC) of 10/20 [ $\text{DC} = t_{\text{on}}/(t_{\text{on}}+t_{\text{off}})$ ]<sup>41</sup> was carried out for 3-10 min. Plasma discharge was then turned off, and the PFM vapour flow was kept constant for additional 15 min. After the polymerization process, plasma-polymerized PFM (pp-PFM) samples were carefully removed from the reaction chamber and stored until further use under argon

atmosphere. For plasma activation, a working power between 10-100 W was used and instead of PFM, oxygen gas was feed until a working pressure of 0.14 mbar for the desired experimental time (1-40 min) was reached.

After the treatment, the monomer or gas valves were closed, vacuum was cut off, and samples were removed from the reactor and stored under an argon atmosphere until further use.

### 3.2.4 Polymer Synthesis

A block co-polymer, constituted by a rigid and a flexible alternating blocks, was synthesized by the esterification of 1,8-octanediol with glutaric acid and subsequently with PEG bis amine.

#### 3.2.4.1.1 Microwave Polycondensation Polymer (PAm)

Briefly, 1,8-octanediol (5.48 g, 37.5 mmol) and glutaric acid (5.95 g, 45 mmol), molar ratio of 1:1.2, were reacted in a microwave reactor (Discovery CEM) at a power of 100 W for 60 min.<sup>40</sup> The reaction was performed under vacuum (100 mbar) with continuous stirring and cooling the system with compressed air to maintain the temperature constant at 120 °C. Once the pre-polymer or rigid block was generated (PreAm), it was subsequently reacted with PEG 2000 at a molar ratio of 1:1. The polycondensation was performed in the microwave reactor under the previously described conditions. The resulting polymer (PAm) was stored in a desiccator until used.

#### 3.2.4.1.2 Polymerization via acid chloride (PAmN)

Briefly, 1,8-octanediol (200 mg, 1.4 mmol) and glutaryl dichloride (0.21 mL, 1.6 mmol), molar ratio of 1:1.2, were reacted with continuous agitation at 70 °C for 30 min. Then, PEG 2000 in a molar ratio of 1:0.2 with 1,8-octanediol, was added and the polycondensation was performed at room temperature for 45 min. After the reaction, the polymer was washed three times with MilliQ-water to rinse the non-reacted PEG 2000. The resulting polymer (PAmN) was stored in a desiccator until used.

### 3.2.5 Nanoparticles Synthesis

Nanoparticles were obtained according to a modified nanoprecipitation method (or solvent displacement method)<sup>42</sup> using a KD Scientific syringe pump (Holliston, USA). Briefly, 20 mg of (PAm or PAmN) polymer were suspended in 1 mL of acetone. The solution was vortexed and collected in a 1 mL syringe (4.70 mm inner diameter) connected to a peek tube (1/16" OD x .010" ID) using a Luer Adapter 1/4-28 (IDEX Health & Science, Oak Harbor, USA) and placed in the syringe pump. The droplets were collected in a 20 mL of Milli-Q water with an agitation about 120 rpm at room temperature. The syringe pump was set with a continuous flow rate of 50 µl/min.

In order to encapsulate drugs, such as paclitaxel (PCTXL), 20 mg of polymer and the specified quantity of PCTXL were dissolved in acetone, a suitable organic solvent pharmacologically accepted regarding to toxicity. This organic phase was then added to a dispersing phase, in which the polymer is insoluble, using the syringe pump as described previously. The resulting nanoparticles (NPs) suspension was stirred at room temperature until complete evaporation of the organic solvent.

After nanoprecipitation and solvent evaporation, NPs were purified by centrifugation or tangential flow filtration (TFF). Briefly, the centrifugation processes (EBA 21, Hettich Centrifuge, Tuttlingen, Germany) was performed at 6000 g for 45 min with an ultra-centrifugal device (Amicon Ultra-15, Ultracel membrane with 100.000 MWCO, Millipore, USA). The supernatant containing the dissolved free drug was discarded and the pellet was suspended with Milli-Q water and the suspension was ready to use.

The TFF process was performed using a regenerated cellulose membrane (Pellicon<sup>®</sup> XL Cassette, Ultracel<sup>®</sup> 300 kDa, 0.005 m<sup>2</sup>, Millipore, USA) with a peristaltic pump. Briefly, a freshly precipitated NPs suspension was mixed the same volume of Milli-Q water. Then, after sonicating and washing the TFF cassette with Milli-Q water, the flow rate of the pump was adjusted to 30-50 mL/min to ensure optimal tangential flow filtration process (according to the manufacturer's instructions). The diluted NPs suspension was connected to the "feed" and "retention" tube, and the "permeated" tube (waste) was connected to a waste beaker. During the filtration process, Milli-Q water was added to the NPs suspension until the osmolality of the suspension was lower than 10 mOsm/kg (analysed with a Fiske<sup>®</sup> Micro-Osmometer, 210, Tecil S.A., Spain). When the filtration process was completed, the suspension was ready to use.

Finally, in order to determine the nanoparticles recovery, the filtrated NPs suspension was freeze-dried (Telstar, LyoAlfa 6, Terrassa, Spain) for 48 hours without lyoprotectant. The nanoparticles recovery was calculated using Equation III-1.

**Equation III-1.** *Nanoparticles Recovery.*

$$NPs\ recovery\ \left(\% \frac{w}{w}\right) = \frac{Mass\ of\ NPs\ recovered}{Mass\ of\ polymer\ and\ drug\ used\ in\ formulation} \times 100$$

### 3.2.6 Nanoparticles Characterization

#### 3.2.6.1.1 Determination of Nanoparticles Size, Polydispersity and Surface Charge and Morphology

The NPs size distributions and polydispersity were measured by Dynamic Light Scattering (DLS) (Zeta Sizer Nano Series, Malvern Instruments, UK) at 25 °C with a scattering angle of 90°. Briefly, just after centrifugation and resuspension of NPs, sample or a dilution about 1:10 with Milli-Q water was measured with the DLS. For each sample, the intensity-weighted mean value was recorded as the average of three measurements.

NPs were also characterized in terms of the zeta ( $\zeta$ ) potential. The analysis was performed in triplicate on DLS (Zeta Sizer Nano Series, Malvern Instruments, UK) with a Smoluchowsky constant  $F(K_a)$  of 1.5 to achieve zeta potential values from electrophoretic mobility. For each sample the mean zeta potential was recorded as the average of three measurements.

### 3.2.6.1.2 Drug Incorporation Efficiency and Immobilized Drug Quantification

Freeze-dried NPs loaded with PCTXL and dried PDMS samples with immobilized NPs loaded with PCTXL were dissolved in acetonitrile and the amount of entrapped drug was detected by Ultra Performance Liquid Chromatography (UPLC) (Waters ACQUITY UPLC H-Class). A reverse phase BEH C18 column (1.7  $\mu\text{m}$  2.1 x 50 mm) was used. The mobile phase consisted in a mixture (65:35 v/v) of mobile phase A (Milli-Q water, containing 0.1% of acetic acid) and mobile phase B (methanol, containing a 0.1% of acetic acid) and was delivered at a flow rate of 0.6 mL/min. A 1.0  $\mu\text{l}$  aliquot was injected into the UPLC system, and total analytical run time was 3 min. Paclitaxel and docetaxel as internal standard (I.S.) were quantified by UV detection ( $\lambda=227$  nm, Waters TUV detector). Drug incorporation efficiency expressed as drug content (D.C. %), encapsulation efficiency (E.E. %), and drug immobilization content were calculated by Equation III-2, Equation III-3 and Equation III-4, respectively.

**Equation III-2.** Drug Content (D.C. %).

$$\text{Drug Content} \left( \% \frac{w}{w} \right) = \frac{\text{Mass of drug in NPs}}{\text{Mass of NPs recovered}} \times 100$$

**Equation III-3.** Encapsulation Efficiency (E.E. %).

$$\text{Encapsulation Efficiency} (\%) = \frac{\text{Mass of drug in NPs}}{\text{Mass of drug used in formulation}} \times 100$$

**Equation III-4.** Drug immobilization content (D.I.C. ng/mm<sup>2</sup>).

$$\text{Drug Immobilization} \left( \frac{\text{ng}}{\text{mm}^2} \right) = \frac{\text{Mass of drug in sample (ng)}}{\text{Area of sample (mm}^2\text{)}}$$

### 3.2.6.1.3 In vitro Drug Release Analysis

*In vitro* drug release of PCTXL loaded NPs was performed using a modified dialysis-bag diffusion technique.<sup>43,44</sup> Briefly, a known amount of freeze-dried PCTXL-NPs (about 0.3 mg of PCTXL) was suspended in a dialysis bag (regenerated cellulose tubular membrane, Cellu SEP® T2, nominal MWCO 6000 – 8000, membrane filtration products, Inc, TX) containing 10 mL of PBS solution (0.1 M at pH 7.4 and 0.3% v/v of Tween-80). The bag with NPs suspension was placed in a 50 mL centrifuge tube (Fisher Scientific Company, Houston, TX) containing 30 mL of release medium (PBS solution and 0.3% v/v of Tween-80). The system was then shaken with an orbital shaking incubator (LM-450D, Yihder Co., Ltd) at 37°C, 200 rpm. Defined aliquots, such as 1 or 2 mL, of released medium was withdrawn and replaced with an equal volume of fresh medium to maintain the sink conditions. Then, the withdrawn aliquots

were lyophilized, suspended with acetonitrile and filtered through a 0.2  $\mu\text{m}$  syringe filter directly into UPLC vials and immediately capped. The total amount of PCTXL released in each time point was quantified using UPLC with a reverse phase BEH C18 column (1.7  $\mu\text{m}$  2.1 $\times$ 50 mm) coupled with a UV detector ( $\lambda=227$  nm, Waters TUV detector). The mobile phase consisted of a mixture of Milli-Q water/acetonitrile delivered at a flow rate of 0.5 mL/min. The percent drug release was calculated as percentage of the total encapsulated drug.

### **3.2.7 Nanoparticles Immobilization**

Nanoparticle immobilization was carried out using a suspension of nanoparticles between 20-100 mg/mL. The pH of the suspension was adjusted to 7.4 with concentrate sodium hydroxide. The immobilization reaction of nanoparticles was performed incubating pp-PFM PDMS samples in a NPs suspension for 6 h with an agitation of 140 rpm. After the incubation process, samples were washed exhaustively with Milli-Q water and dried with compressed air until further use.

In order to study the cell viability of different cell types, some samples were incubated with blocking agents, such as FBS or collagen, to react with the non-reacted PFM groups.

#### **3.2.7.1.1 FBS coating of silicones**

After NPs immobilization, NPs immobilized on PDMS samples were incubated with a FBS solution of 0.1 mg/mL to react with the remaining active points of the PFM coating.

#### **3.2.7.1.2 Collagen coating of silicones**

After NPs immobilization, NPs immobilized on PDMS samples were incubated with a collagen solution of 0.1 mg/mL to react with the remaining active points of the pp-PFM coating.

### **3.2.8 Determination of in vitro cytotoxicity of drug-loaded nanoparticles**

In order to evaluate the cytotoxicity of the drug loaded nanoparticles, animal cell line experiments were performed using Human Lung Normal Fibroblast (IMR-90, ATCC, CCL-186), Adenocarcinomic Human Lung Alveolar Basal Epithelial cells (A549, ATCC, CCL-185), Normal Human Dermal Fibroblasts (NHDFs, Promocell, C-12302) and non-stenotic and stenotic Primary Respiratory Human Fibroblast, cells extracted from a patient by surgical biopsy, (T-01MVV).

Human lung normal fibroblasts (IMR-90, ATCC<sup>®</sup> CCL-186<sup>™</sup>) were purchase from the American Type Culture Collection (ATCC, Manassas, VA, USA) and cultured in EMEM medium supplemented with 10% FBS and penicillin (100 U/ml) / streptomycin (100  $\mu\text{g}/\text{ml}$ ) solution according to the manufacturer's recommendations. Cells were maintained at 37°C in a humidified 5% CO<sub>2</sub> atmosphere.

Bronchial-alveolar epithelial human cells (A549, ATCC<sup>®</sup> CCL-185<sup>™</sup>) were purchased from the American Type Culture Collection (ATCC, Manassas, VA, USA) and cultured in F12K medium supplemented with 10% FBS and penicillin (100 U/ml) / streptomycin (100  $\mu\text{g}/\text{ml}$ ) solution according to

the manufacturer's recommendations. Cells were maintained at 37°C in a humidified 5% CO<sub>2</sub> atmosphere.

Normal Human Dermal Fibroblast (NHDFs), were purchased from Promocell (C-12302, Heidelberg, Germany) and cultured in DMEM medium supplemented with 10% FBS and penicillin (100 U/ml) / streptomycin (100 µg/ml) solution and 1% Glutamine, according to the manufacturer's recommendations. Cells were maintained at 37°C in a humidified 5% CO<sub>2</sub> atmosphere.

All human tissues were procured and managed in accordance with the Declaration of Helsinki, and the study was approved by the ethics committee of *Hospital Universitari de Bellvitge* (Hospitalet de Llobregat, Barcelona, Spain). Written informed consent was obtained from all subjects before recruitment.

Adult human tracheal fibroblasts (T-01MVV) were obtained from tracheal tissue from patients who underwent surgical procedure for the treatment of tracheal stenosis. The harvested tracheal tissue samples were maintained in DMEM high Glucose with L-Glutamine medium with HEPES and insulin human transferrin and sodium selenite (ITS) until processing. Then, samples were cut into small pieces, and placed into 6 well-plates (Nunc Thermo Scientific, Waltham, MA, USA) with growth medium; DMEM supplemented with 10% FBS, penicillin (100 U/ml)/streptomycin (100 µg/ml) solution and 25 µg/ml amphotericin B. Cells were cultured at 37 °C in a humidified atmosphere of 5% CO<sub>2</sub>. Spindle-like primary fibroblasts started to grow out from tissue samples on day 2 to 3. Outgrowth of fibroblasts took 1 to 2 weeks. Tissue samples were then removed by aspiration, and cells were allowed to reach confluence. Fibroblasts at confluence were expanded by trypsinization and passaged every 4 to 5 days at 1:4 ratio. Tracheal fibroblasts were identified by the typical spindle morphology and immunohistochemistry; vimentin and α-smooth muscle actin (α-SMA) positive, and factor VIII and surfactant C-negative staining. Cells between passages numbers 4 and 7 were used in this study.

#### **3.2.8.1.1 Cytotoxicity of Drug Loaded Nanoparticles**

IMR-90, A549, and extracted non-stenotic and stenotic T-01MVV cells were plated in 96-well plates at a cellular density of 1000 cells/well. After 24h, medium was aspirated and substituted with medium with various paclitaxel concentrations (10 nM, 14 nM and 20 nM) of free drug, 1% and 3% theoretical drug loaded nanoparticles. The experiment was designed as the following: one column of cells with non-encapsulated paclitaxel at the same range of concentrations (10-20 nM) was used as positive control; one column of cells without nanoparticles and without paclitaxel was used as negative control, and another column without cells was used as blank. Between 1 and 14 days, cell viability was assessed via MTT (Quick Cell Proliferation Assay Kit II, JM-K302-500) following the manufacturer's instructions and pictures were taken to follow the changes in the cell morphology. Briefly, cells were washed with PBS and incubated with a solution of the MTT reagent and complete media at 37 °C. The absorbance, which represented cell viability, was measured via microplate reader (Multiskan Ex, Thermo Scientific) at 450 nm with 650 nm of reference wavelength. Cells stained positively with MTT were considered

viable cells. Cell viability was calculated using Equation III-5 and expressed as percentage of viable cells compared to control cells.

**Equation III-5. Cell Viability.**

$$\text{Cell Viability (\%)} = \frac{\text{Abs}_{\cdot\text{sample}} - \text{Abs}_{\cdot\text{blank}}}{\text{Abs}_{\cdot\text{control}} - \text{Abs}_{\cdot\text{blank}}} \times 100$$

#### **3.2.8.1.2 Viability of Drug Loaded Nanoparticles Immobilized onto PDMS plates**

Cell culture dishes were washed with 4 mL PBS 1X and treated with 2 mL of trypsin for 3 min at 37 °C. Next, the activity of trypsin was inhibited by the addition of 8 mL of supplemented DMEM. Then, the cell suspension was centrifuged at 1000 rpm during 5 min and suspended with the appropriate volume of cell culture media to achieve the desired cell concentration.

Cells were seeded onto the silicones previously subjected to different treatments at a cell concentration of  $1.2 \times 10^5$  cells/mL for the silicones (45900 cells/silicone). As control, cells were seeded in well of the plate without silicone at a cell concentration of  $1.2 \times 10^5$  cells/mL for the 24-well plate wells (52312 cells/24-well plate). Cell densities were calculated taking into account the surface area difference between the silicones and the 24-well plate wells.

#### **3.2.8.1.3 Live & Dead Staining**

In order to evaluate the toxicity of cells cultured onto silicones, cells were treated simultaneously with fluorescein diacetate (FDA) and ethidium bromide (EB). FDA is used as viability probe that measures both enzymatic activity and membrane integrity. The first, leads to the hydrolysis of FDA by intracellular esterases yielding fluorescein, while the latter allows the intracellular retention of the fluorescent product. In contrast, EB is not permeable for living cells and it only stains dead cells or cells with a damaged cell membrane.

First, culture medium was removed from the well using a micropipette and cells were washed three times with PBS 1X. Next, cell cultures were covered with 100  $\mu$ l of staining solution, which contains FDA and EB in a concentration of 10  $\mu$ g/ml and 40  $\mu$ g/ml in PBS 1X respectively<sup>45-47</sup>. Cells were incubated with the staining solution during 5 min in the dark at room temperature. Then, the staining solution was removed and cell cultures were washed three times with PBS 1X. Finally, cell cultures were observed under fluorescence microscope (Axiovert 200M inverted microscope with coupled ApoTome system, Carl Zeiss AG, Germany).

#### **3.2.8.1.4 Dapi/Phalloidin Staining**

This staining method allows the simultaneous observation of the cell nuclei and cytoskeleton, as DAPI (4',6-diamidino-2-phenylindole) binds to the minor groove of double stranded DNA and phalloidin binds to the F-actin filaments of the cytoskeleton of cells. First, cell cultures were fixed with sterile 1% (w/v)



PFA for 30 min at 4 °C, then three washes of 10 min each with PBS 1X on an orbital shaker were performed. Next, in order to permeabilize the cell membrane, fixed cell cultures were incubated with a 0.1% (v/v) Triton x-100 in PBS 1X during 30 min at room temperature. Then, cells were incubated with Phalloidin-TRITC at a final concentration of 1 µg/ml in PBS 1X for 25 min in the dark. Next, a DAPI solution of 1µg/ml was added onto the previous solution and incubated for 5 min in the dark. Finally, three washes of 10 min each with PBS 1X on an orbital shaker were performed. Samples were observed under fluorescence microscope (Axiovert 200M inverted microscope with coupled ApoTome system, Carl Zeiss AG, Germany).

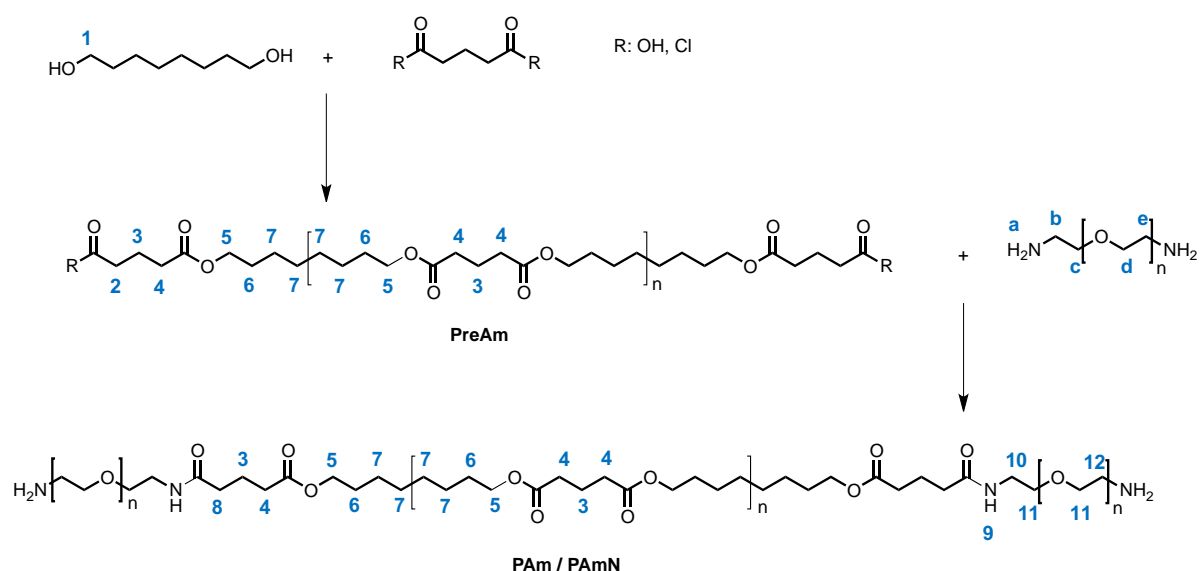
*Unless otherwise stated, all experimental data were done in triplicate and the average mean was represented with standard deviation represented as error bars.*

### 3.3 Results and Discussion

As mentioned before, in order to obtain an immobilized drug delivery system based on the previous developed surface technology, it was necessary to develop and characterize a degradable polymer. The structure of this polymer must present terminal amines in order to react with pp-PFM. Additionally, this polymer must be capable form nanoparticles and entrap hydrophobic drugs such as paclitaxel. Finally, the resulting drug delivery system should present a controlled antiproliferative activity against different types of cells such as fibroblast over time in order to avoid stenotic tissue, recurrence and reduce the toxic behaviour of high doses of paclitaxel.

#### 3.3.1 Synthesis and Characterization of Block Co-polymers PAmX

Polyester-PEG polymers, have been described as suitable polymers to be used for encapsulation of hydrophobic drugs, such as paclitaxel.<sup>42-44</sup> Previously in our group, a degradable polymer capable to create nanoparticles were synthesized.<sup>40</sup> The design of the polymer allowed to entrap hydrophobic drugs, such as paclitaxel in order to create a controlled drug-release platform. Therefore, an amphiphilic polymer was necessary to design to encapsulate hydrophobic drugs and disperse the nanoparticles or polymer-drug conjugates in aqueous media. The proposed co-polymer, presented a rigid block (polyester) suitable to encapsulate hydrophobic drugs and secondly, a flexible block (PEG), which consists of a hydrophilic molecule to stabilise the core in aqueous media. However, the resulting nanoparticles were not able to react with the previously developed pp-PFM surfaces because no amines were present in the structure of the initial polymer. Therefore, an PEG with an amino terminal group was selected in order to create nanoparticles with an amine corona capable to react with the reactive pp-PFM surfaces.



**Scheme III-1.** Synthesis of block co-polymer PAmX by polycondensation.

Block co-polymers PAmX formed by flexible (PEG bis amine 2000) and rigid blocks (1,8-octanediol and glutaric acid) were synthesized by polycondensation. The characterization of the obtained polymers was determined by using FTIR,  $^1\text{H-NMR}$  and GPC. In Figure III-1 can be observed the FTIR of PAm and PAmN polymer, which are consistent with the expected structure. A strong band at  $1732\text{-}1735\text{ cm}^{-1}$  can be observed corresponding to the C=O stretch of the ester. In addition, the absorption band at  $3200\text{-}3500\text{ cm}^{-1}$  can be attributed to the N-H stretch (for both polymers) and even some residual O-H stretch of non-reacted 1,8-octanediol (in the case of PAm). At  $2919\text{-}2850\text{ cm}^{-1}$ , the C-H stretch band of the polyester  $\text{CH}_2$  can be observed. In addition, some differences between both polymers (PAm and PAmN) can be observed such as the band between  $1180\text{-}1148\text{ cm}^{-1}$  corresponding to C-N stretch of aliphatic amines. These differences could be explained by the presence of residual non-reacted PEG bis amine. After the synthesis of each polymer, PAmN was washed gently with Milli-Q water, while the PAm was used without any workup or washing step which may result in the presence of unreacted PEG.

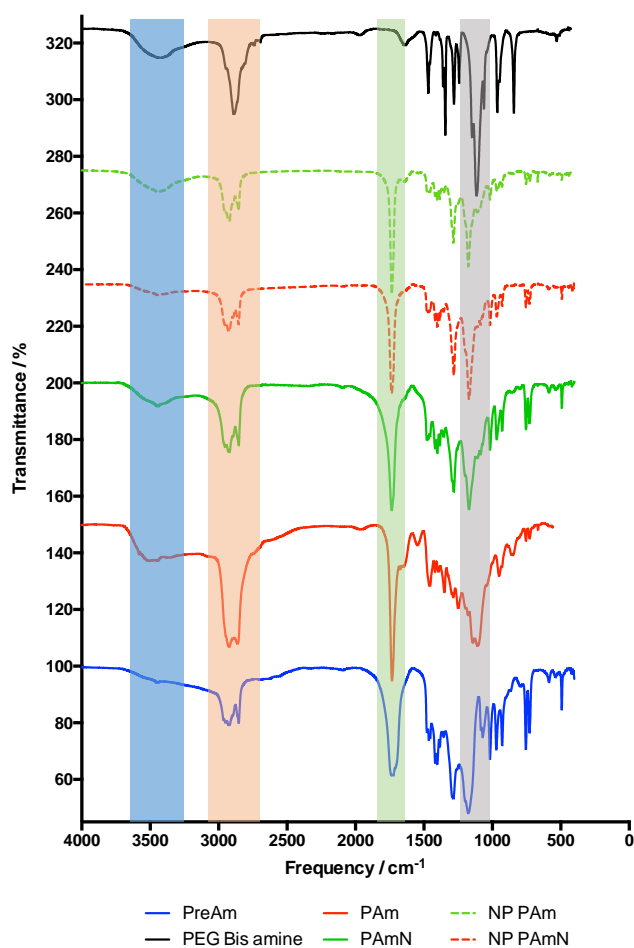


Figure III-1. FTIR spectra of the synthesized polymers.

Taking the IR spectrum results into account, the composition of the different polymers was confirmed by  $^1\text{H-NMR}$ . In Figure III-2 and Figure III-3, the  $^1\text{H-NMR}$  spectrum of the PAm and PAmN polymers can be observed, respectively. The large signals at 3.63 and 3.64 ppm (PAm and PAmN, respectively) were

assigned to the methylene groups of the PEG bis amine 2000 (signal 11). The multiplets at 4.05 and 4.06 ppm (PAm and PAmN, respectively), 1.60 and 1.61 ppm (PAm and PAmN, respectively) and 1.31 ppm corresponded to the  $-CH_2-$  protons of 1,8-octanediol (signal 5, 6 and 7, respectively). The multiplets at 2.35 and 2.36 ppm (PAm and PAmN, respectively) were assigned to the glutaric acid methylene protons in  $\alpha$  of the carbonyl group (signals 4 and 8); while the multiplet at 1.94 ppm (signal 3) was assigned to the glutaric acid methylene protons in  $\beta$  of the carbonyl group. Finally, as it can be observed in Figure III-4, the amine coupling was successfully accomplished. In the spectra, a shift from 2.87 ppm, corresponding to  $-CH_2-$  bonded to the amine of the PEG (signal b), to 3.45 ppm (signal 10) can be observed because of the pegylation.

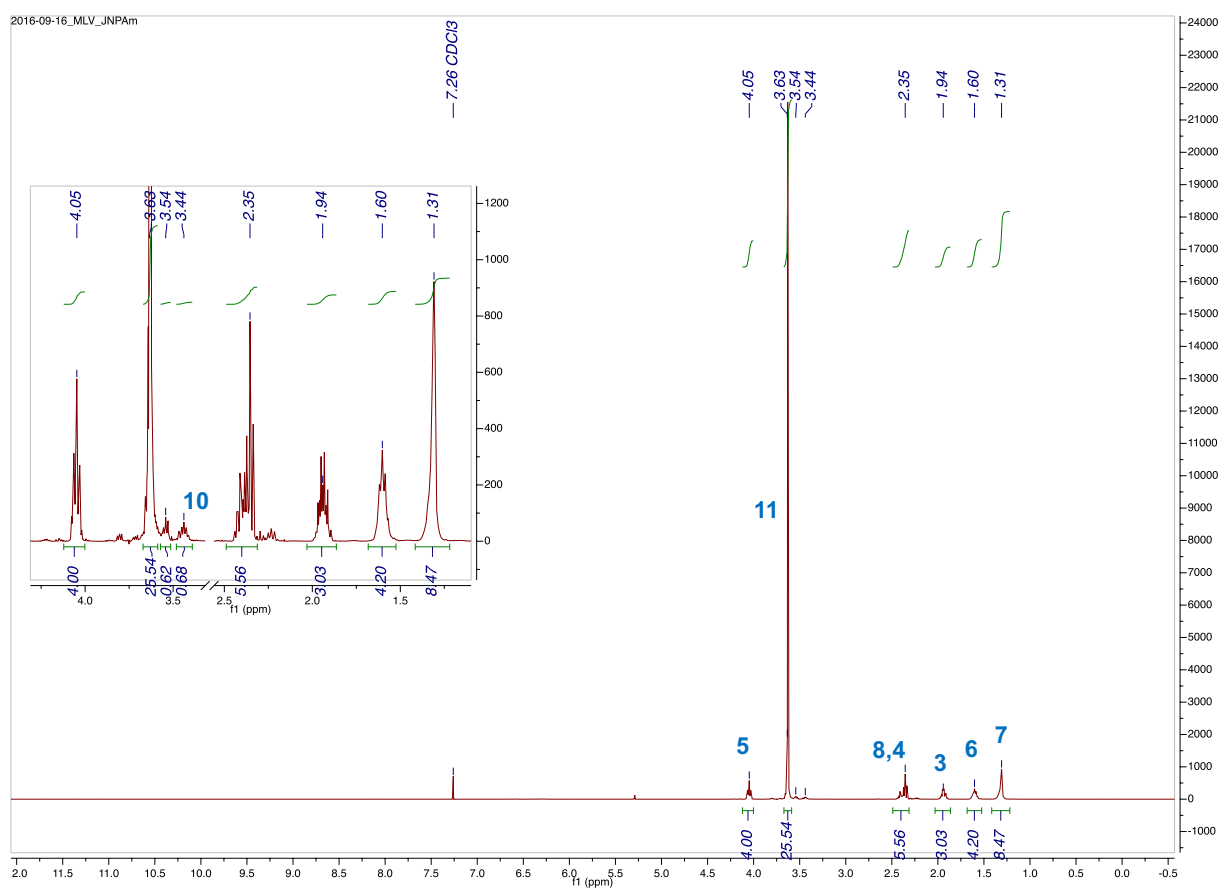


Figure III-2.  $^1\text{H-NMR}$  of the PAm polymer.

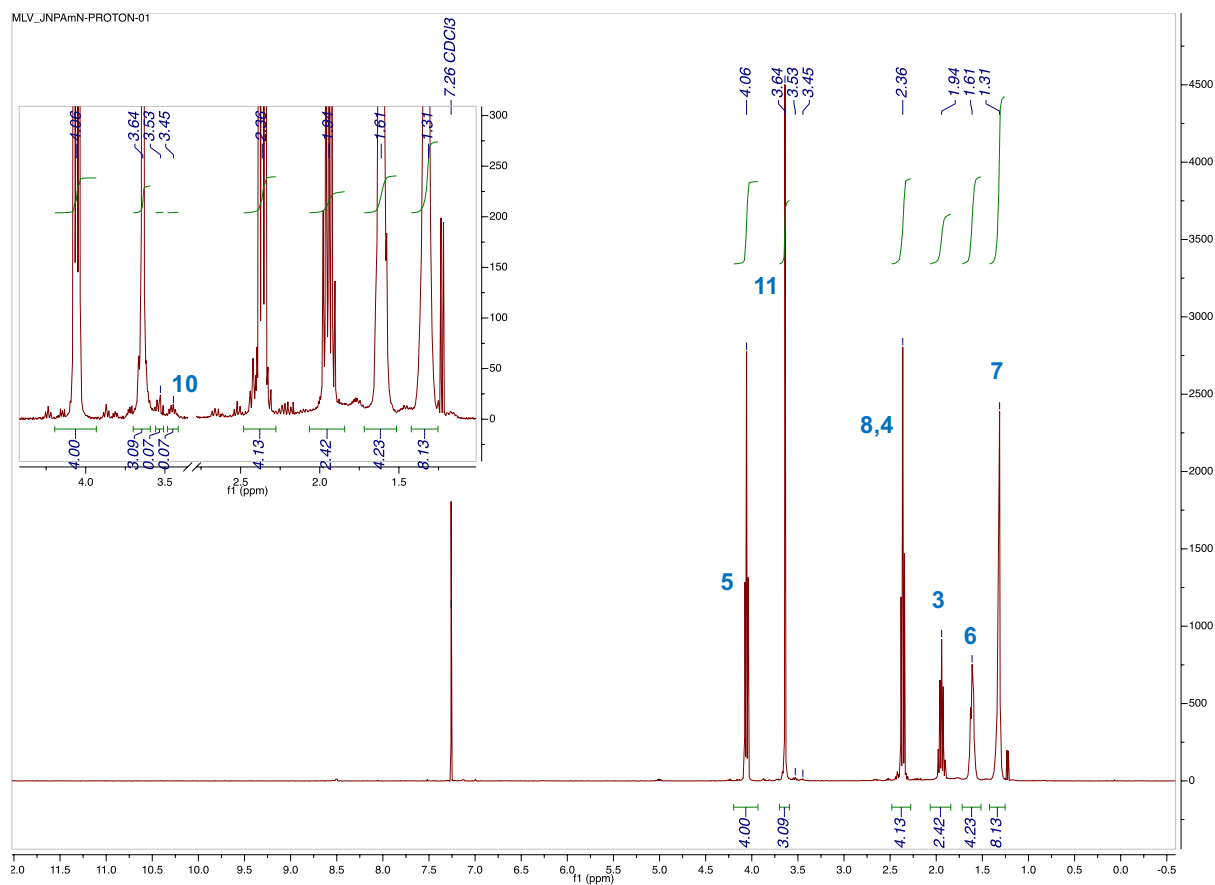


Figure III-3. <sup>1</sup>H-NMR of the PAmN polymer.

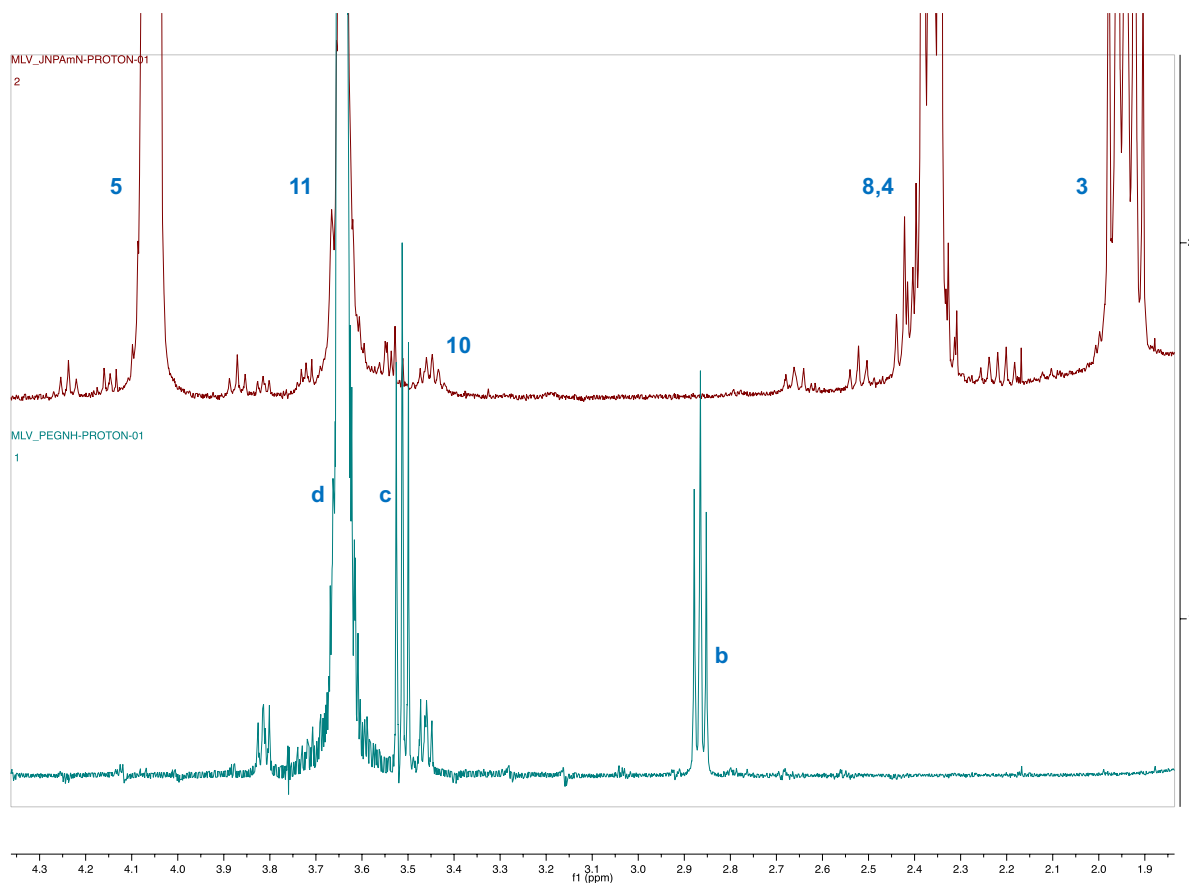


Figure III-4.  $^1\text{H-NMR}$  stack of PEG bis amine (green) and PAmN polymer (red).

In addition to the structure identification, the polymer was also characterized by GPC to evaluate the polymer chain distribution. In Figure III-5 and in Table III-1, the molecular weight distribution of the different polymers synthesized in this work, polyester-PEG bis amino (PAm and PAmN) can be observed. PAm polymer was obtained by a two-step synthesis in which, initially, there was a polycondensation of the alcohol and the acid (synthesis of the PreAm) and then, the addition of the PEG bis amino, to the residual acids of the polyester chains, was performed without any workup or washing step. PreAm showed a wide distribution with polydispersity ( $Q$ ) around 1.9. However, when, PEG bis amine was added, PAm polymer showed an increase in its molecular weight with similar wide distribution ( $Q = 2.0$ ). Regarding to PAmN polymer, after the polycondensation between the acid chloride and the di-alcohol (PreAmN), PEG bis amine was added with no workup or washing step. As it can be observed, in Figure III-5 and in Table III-1, PreAmN showed higher MW distribution than PreAm because of the polycondensation reaction which showed a higher rate of reaction than in the  $\mu\text{wave}$  synthesis.

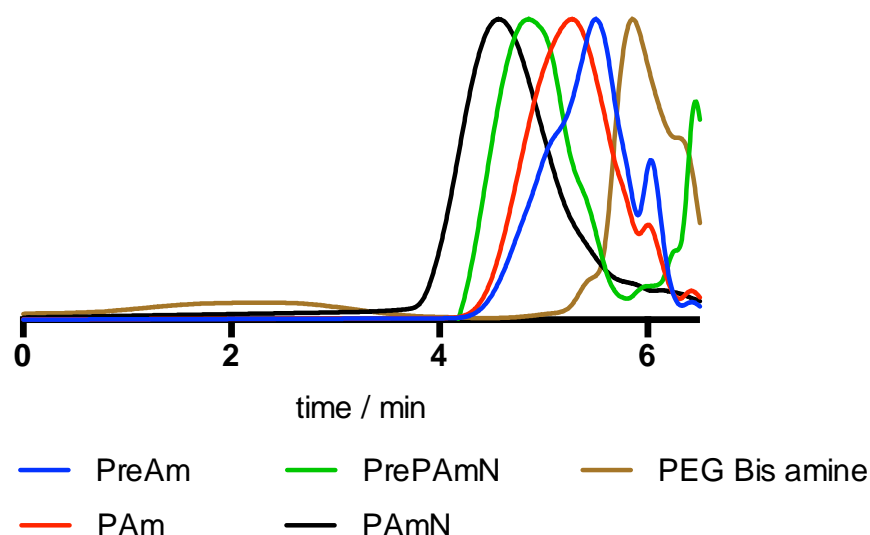
As expected, after the addition of the PEG bis amine, the resulting polymer, PAmN showed higher distribution than PreAmN (due to the polymer chain growth and the PEG addition) with a wide MW distribution ( $Q = 3.1$ ).

**Table III-1.** Characterization of different synthesized nanoparticles by GPC.

	PreAm	PAm	PreAmN	PAmN	PEG Bis amine
<b>Q</b>	1.90	2.00	1.70	3.10	1.50
<b>Mn</b>	2451	2992	5993	6517	548
<b>Mw</b>	4766	5846	10018	20306	847
<b>Mz</b>	13401	13715	12837	38499	1331
<b>Mp</b>	2122	3603	9609	18767	935

The comparison between PAm and PAmN polymers showed wide MW distributions with a difference in the size of the MW distribution. This difference can be explained due to the kinetics of the reactions and consequently due to the length of the rigid block. Analysing the rigid blocks of each polymer, the so-called pre-polymers, it can be observed that the reaction on the microwave (PreAm) resulted in polymer chains with a wider distribution and lower MW than PreAmN.

Additionally, it is important to highlight that PAmN polymer had a washing step with Milli-Q water after the synthesis to purify the polymer and remove the non-reacted chains. Considering the MW of PreAmN and the PAmN, it can be observed that the difference in the MW between them were almost two units of PreAmN. However, it was difficult to conclude the type of the chains that formed the resulting polymers (PAm and PAmN) because the calibration was performed using polystyrene standards. Therefore, it is possible to assume that the MW increase between PreAm and PAm could be caused by the addition of PEG one or two PEG chains, while PAmN could present two units of PreAmN and one or two units of PEG bis amine in its structure.

**Figure III-5.** GPC elution profiles of synthesized polymers. PEG Bis amine is used as reference.

### 3.3.2 Preparation and Characterization of Nanoparticles

As mentioned before, the drug loaded nanoparticles are nanocarriers of great interest to locally deliver antiproliferative drugs, such as paclitaxel (PCTXL) to treat the stenotic tissue of the trachea wall. In this work, PCTXL loaded nanoparticles were successfully synthesized and characterized through chain distribution, size, zeta potential, release profile and *in vitro* activity.

The GPC characterization of the synthesized nanoparticles, Figure III-6 and Table III-2, showed no obvious differences between the synthesized nanoparticles of each polymers. However, PAm polymer and its nanoparticles, NP\_PAm, showed a different distribution being the nanoparticles distribution more concentrated in polymer chains of high molecular weight.

On the one hand, as it was observed previously, PAm showed a lower MW than PAmN with a wide distribution. Because PAm was used as synthesized, without any washing steps to remove non-reacted PEG, polyester chains, diol or acid, the precipitation process acted as a purification process causing a high molecular polyester-PEG chains enrichment and eliminating the non-reacted PEG. At this point, these results are in line with the  $^1\text{H-NMR}$  (Figure III-2) where the signal ratio between signal 5 and 11, indicates an excess of non-reacted PEG for the PAm polymer. Considering these results, it is possible to expect that the yield of the process could be diminished due to the washing process.

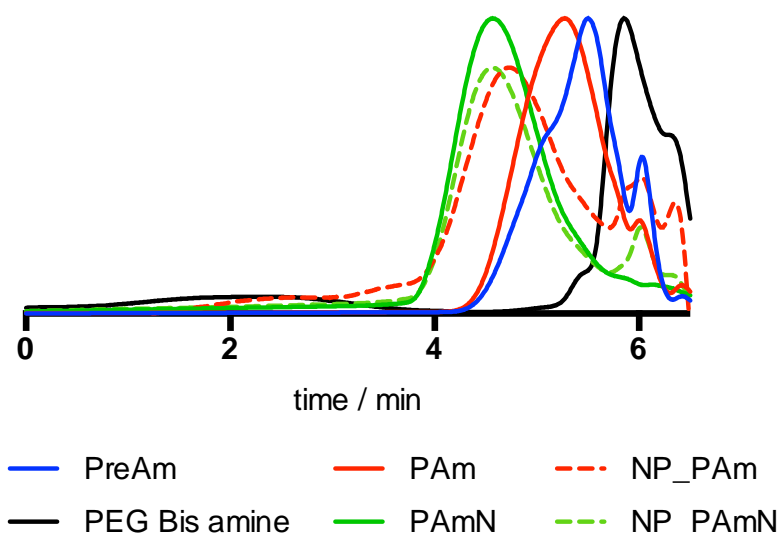


**Figure III-6.** GPC elution profiles of PAmX and its nanoparticles. Continuous lines indicate polymers and dashed lines indicate nanoparticles.

**Table III-2.** Characterization of different synthesized nanoparticles by GPC.

	NP_PAm	NP_PAmN
<b>Q</b>	3.00	2.50
<b>Mn</b>	6301	8601
<b>Mw</b>	19057	21185
<b>Mz</b>	46144	40176
<b>Mp</b>	13123	18767



On the other hand, PAmN and its nanoparticles showed the same MW distribution, indicating that during the washing step with water (same solvent used to synthesize the NPs), the non-pegylated chains and low MW chains were discarded, and only the polymer chains with a suitable hydrophilic/hydrophobic relation to form NPs were purified. These results are in concordance with the distribution changes of PAm and its NPs once the polymer was washed during the precipitation process. Additionally, it is possible to observe that both type of nanoparticles had similar MW distribution. Considering the width of each distribution, this slightly difference can be attributed to the differences between the length of the rigid block of each polymer and can probably be avoided.

These GPC results showed that the precipitation process worked as a washing step (when non-washed PAm polymer came in contact with the aqueous solution, the non-reacted PEG, alcohol and acid, were washed) and the nanoprecipitation process acted as a filter to only select high molecular weight of polyester-PEG chains with some specific hydrophobic/hydrophilic block relation to form the nanoparticles.

#### **3.3.2.1.1 Size Distribution and Zeta Potential**

The PCTXL loaded NPs were characterized using the dynamic light scattering technique to ensure the stability at different pHs. The pH of concentrated NPs was analysed after synthesized, showing a pH about 4.5-5. Then, to evaluate the stability of the NPs, a pH titration was performed between pH 4 to pH 7.4. Considering the previous mentioned application, the immobilization of NPs onto a pp-PFM surface of a medical device, the final pH of the titration curve was decided with a balance between non-protonated amines (negative zeta potential of the NPs) and a slightly basic pH to avoid hydrolysis of the reactive pp-PFM groups.

In Figure III-7, the Zeta Potential and Size Characterization of the different NPs formulations can be observed. Both families of polymer NPs (PAm NPs and PAmN NPs) showed the same behaviour regarding to the zeta potential. Initially, due to the free amines on the termini of the polymers, NPs showed a positive charge (about 30 mV) indicating the protonation of the amines and corroborating the previous results of the IR, <sup>1</sup>H-NMR and GPC. During the basification process, protonated amines were neutralized and the global net charge was reduced until the isoelectric point (IEP) was reached, around pH 5.5. At higher pH, nanoparticles started to show negative charge, which can be explained due to the deprotonation of terminal carboxylic acids of some polyester chains (non-pegylated) that, in combination with the pegylated-polyester chains, form the nanoparticles.

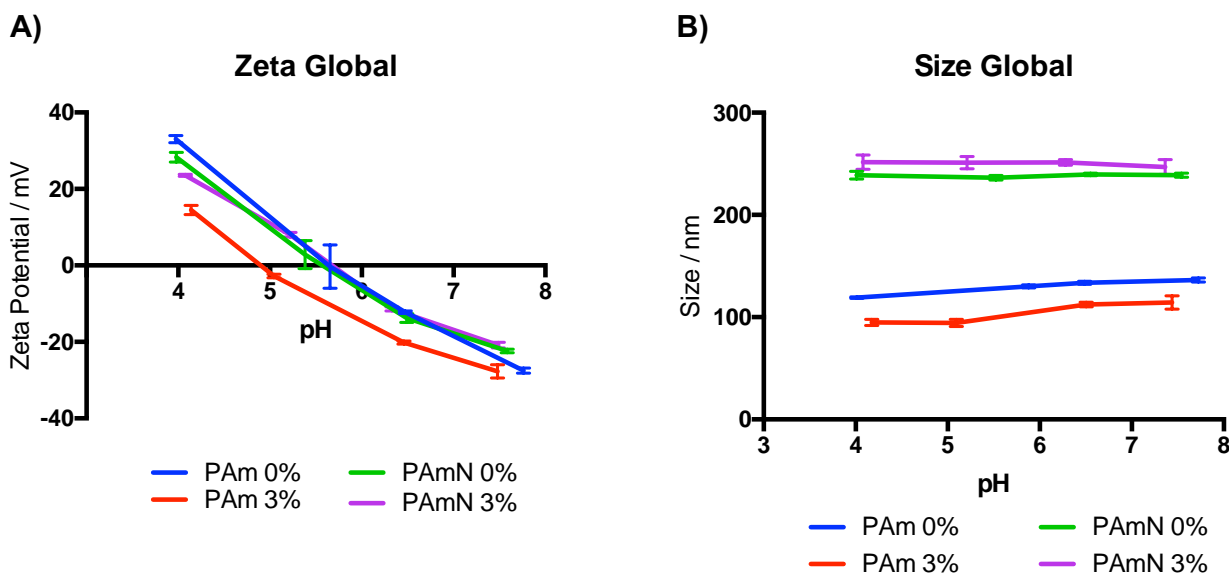


**Figure III-7.** Zeta potential and size characterization of the synthesized nanoparticles. **A)** Zeta Potential of nanoparticles with 0% (non-loaded PCTXL) and 3% of loaded PCTXL, and **B)** Size characterization of nanoparticles with 0% (non-loaded PCTXL), and 3% of loaded PCTXL. PAm and PAmN correspond to NPs synthesized with PAm and PAmN polymer, respectively.

Besides the zeta potential, the size characterization showed stable NPs in the range of analysed pHs. In this case, PAm NPs showed smaller size than PAmN, approximately 117 nm (130 nm for 0% PCTXL and 104 nm for 3% PCTXL) and 244 nm (238 nm for 0% PCTXL and 250 nm for 3% PCTXL) respectively. As mentioned before, the differences between samples can be attributed to the differences in the length of the chains of each polymer, because to the differences between the rigid block of each polymer. Nevertheless, both type of NPs, are in correlation with previous works, with expected values for this type of polyester-PEG NPs nanoprecipitated in water, about between 100-275 nm.<sup>40</sup>

Besides examining the surface characterization, the nanoprecipitation yield was studied. As it can be observed in Figure III-8, the NPs recovery (Equation III-1) showed similar values between polymers, 70% for the PAmN polymer vs 53% for PAm polymer. The higher yield of PAmN can be explained with the structure of the NPs and the purity of the polymers. As expected, the differences in the purity of each polymer and the washing step of the nanoprecipitation process are directly related with the NPs recovery, being the PAm polymer the one with lower NP recovery.

### 3.3.2.1.2 Drug incorporation Efficiency

Taking into account all this characterization, it is important to evaluate the yield of the encapsulation process to assess the capability of this system to entrap drugs in its core. Besides the NPs recovery, the Encapsulation Efficiency (EE) for both polymers showed similar behaviour with EE values of 57% and 63% for PAm and PAmN polymers, respectively. This result indicates that the composition of the NPs, more specifically the composition of the core of the NPs, were similar in both types of NPs families, with the polyester part of the chains entrapping the paclitaxel in the core of the NPs, protecting itself and the drug from the water. These results are consistent with previous results in the literature, where

pegylated NPs and polyester base NPs showed a 70% of PCTXL EE.<sup>31,40,48</sup> In addition, Figure III-8 shows the measured Drug Content (DC) of different polymer samples, which was 3.4% and 2.6% (for PAm and PAmN, respectively) with no statistical differences between polymers. Also, the CV% around 10% (13%) seems appropriated for this type of systems. These results encourage to choose this system as method to encapsulate hydrophobic drugs, such as PCTXL.

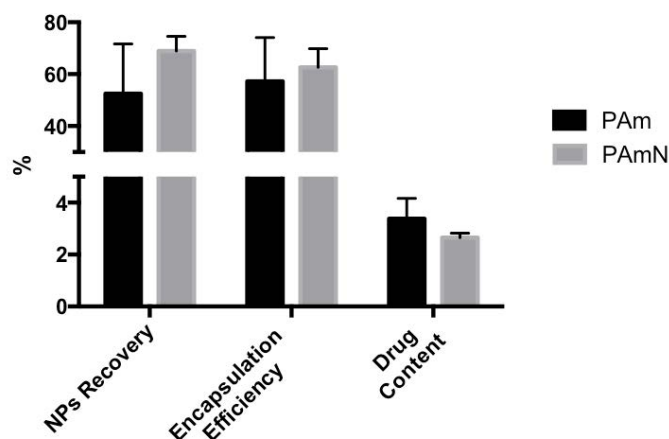


**Figure III-8.** NPs Characterization showing NPs Recovery (%) and Encapsulation Efficiency (%) of different polymers. The comparison has been performed with theoretical 3% loaded NPs.

Based on the previous results and considering that both polymers had the same chemical composition, it can be assumed that their ability to form NPs was the same. In addition, formed NPs present the same capacity to encapsulate hydrophobic drugs, such as PCTXL, and the similar ratios of EE of both polymers. Therefore, both synthesized polymers were used indistinctively. However, for the scalability it should be considered that the acid chloride route was more controllable, resulting in the increased reproducibility and reaction yields. Additionally, this reaction allows fabrication of larger batches of polymer. These characteristics are highly sought for pharmaceutical development of this type of technologies.

### 3.3.2.1.3 *In vitro Drug Release from Loaded Nanoparticles*

To evaluate the potential of the synthesized polyester-PEG NPs with amide bond, the *in vitro* release profile was performed and it was compared with the release profile of a previous studied polyester-PEG NPs using the P polymer, a polyester-PEG (polyethylene glycol MW 1.500 Da) with only ester bonds in its structure.<sup>40</sup>

In Figure III-9, the release profile of different PCTXL loaded NPs can be observed, showing an interesting first-order release with an initial release about 20% of PCTXL at day 1 and with a 90% of drug release at 10 and 14 days for P polymer and PAmX polymer, respectively. Both polymers have similar behaviour with the new synthesized polymer PAmX showing slower release kinetics. Since NPs are prepared by the same synthesis process and with similar reagents, diol, di-acid and PEG, the difference in PCTXL percentage release can be explained as follows. Both NPs were synthesized using

polymers with the same hydrophobic block (rigid block) formed by the polycondensation of the 1,8-octanediol and glutaric acid. However, the pegylation of the polyester chains had a slight difference. For the P polymer, the coupling between the polyester and the PEG were performed yielding an ester bond while PAmX uses an amide bond. This difference in pegylation could cause a more controlled release for the PAmX NPs. While the ester bonds are easily hydrolysed, the amide bond are less susceptible because the carbonyl carbon of the amide bond is less electrophilic and the aminated moiety is a poor leaving group. Therefore, during the hydrolysis process, the amide group showed a lower degradation process than the P polymer with ester bonds in all its structure. Considering that the resulting polymer has two types of bonds, amide and ester, the amide bond hydrolysis delayed the initial degradation while the ester bond showed similar behaviour than pure polyester-PEG polymer with only ester bonds in its structure. This confirms the importance of the amide bond because, can delay the release profile and therefore, changing the nature of the chain bonds it is possible to control de release profile.

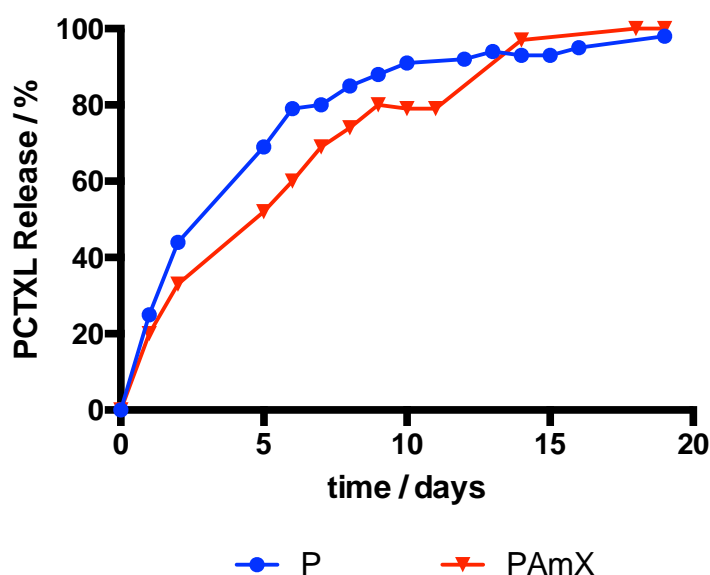


**Figure III-9.** In vitro release kinetics of PCTXL loaded nanoparticles at 3% w/w theoretical drug content. **P** indicates previous studied polymer with only ester bonds in its structure (hydroxyl terminal polyester-PEG chains); **PAmX** consists on ester and amide bonds in its structure (amine terminal polyester-PEG bis amine chains).

Moreover, the initial burst absence and the almost nearly linear behaviour indicates the absence of adsorbed PCTXL on NPs surface. Considering the previous results, the developed polymer, PAmX, showed an interesting PCTXL release behaviour, similar to previous developed PEG-polyester nanoparticles<sup>40</sup>. Just by changing the bond types, the addition of amide bonds in the structure of the polymers, allows the system to control the release profile creating a controlled release over time, about 14 days.

The developed NPs showed a more controlled PCTXL and better results against other pegylated systems, such as poly lactide-co-glycolide, poly(trimethylene carbonate) and poly  $\epsilon$ -caprolactone, with

a PCTXL release over 50% in the first hours and the total cargo released in 2-4 days.<sup>31-33,35,49</sup> The amide-pegylated NPs (PAmX) allows a controlled sustainable release of PCTXL over 14 days, which could increase the efficacy of clinical therapy.

### 3.3.3 Nanoparticles Immobilization

Despite the characterization of the NPs release profile, it was necessary to study the immobilization capacity of the synthesized amine bearing nanoparticles. As seen before, the formulated polyester-PEG bis amine nanoparticles showed free amines on the surfaces which can interact with the reactive surface of pp-PFM. However, direct formulation of the NPs showed a pH around 4 with positive zeta potential indicating the protonation of the amines. To obtain the coupling between the nanoparticles with the surface, the pH of the NPs solution should be adjusted to ensure the non-protonation to the amines. As seen before, when the pH was adjusted from 4 to 7.4, the zeta potential of the surface nanoparticles was shifted from positive (protonated free amines) to negative (non-protonated free amines) (Figure III-10), indicating that the free amines of the nanoparticles were available to react with the pentafluorophenyl groups of the pp-PFM on the surface of the samples or devices.

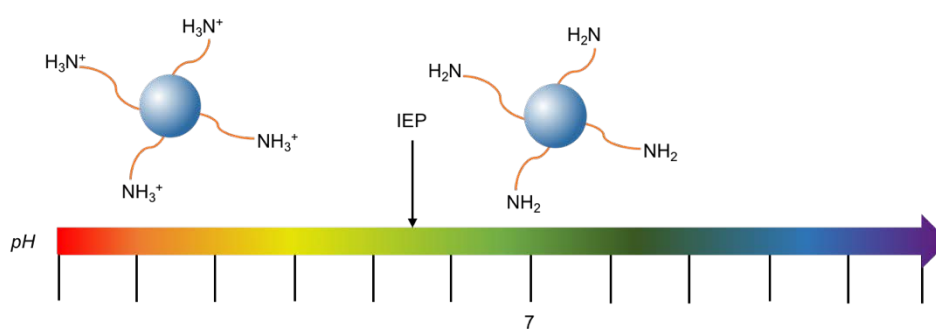


**Figure III-10.** Scheme of the amine bearing nanoparticles behaviour under different pH conditions.

After adjusting the pH of the nanoparticles suspension to 7.4 (negative zeta potential of the suspension), no changes in the NPs size were observed. Different pp-PFM samples (silicon wafer and PDMS plates) were incubated with the adjusted suspension of NPs during 6 h. This time of incubation was chosen taking into account the kinetics of a reaction involving an immobilized reagent (on the surface) and the release profile of the NPs, considering that at 1 day there was about 20% of released PCTXL.

In order to further assess the nanoparticles immobilization, covalently attached drug-loaded NPs were quantified. Despite the difficulty to quantify the NPs attached on the surface, an indirect quantification using PCTXL was performed. Samples were incubated with acetonitrile to dissolve the nanoparticles and extract the PCTXL. As it can be observed in Figure III-11, the quantification of the PCTXL indicates that about 0.5 and 0.4 ng/mm<sup>2</sup> of PCTXL were immobilized for silicon and PDMS samples, respectively with no statistical difference. These results indicate the novelty of the system to obtain a bioactive coating on the surface of the materials (or device) capable of releasing hydrophobic drugs, such as paclitaxel, in a controlled manner. In this case, and taking into account the release profile of the

synthesized nanoparticles, this system should create a coating onto the surfaces of the materials and devices capable to release the treatment (paclitaxel or other hydrophobic drugs) to the surrounding tissues during 20 days, having its maximum release point between day 3 and 5, about 50% of released PCTXL.

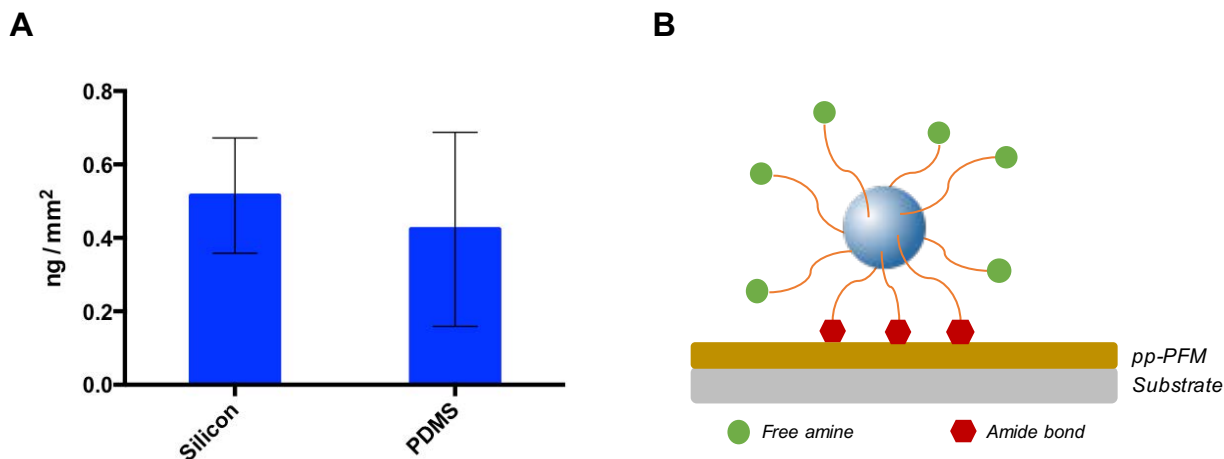


**Figure III-11.** Immobilization of PCTXL loaded nanoparticles at 3% w/w theoretical drug content. **A)** Quantification of the immobilized PCTXL on different substrates, silicon wafers and PDMS plates. Data normalized by area of each sample, ng/mm<sup>2</sup>. **B)** Representation of the immobilized amine-bearing PCTXL drug loaded nanoparticles onto pp-PFM substrate.

### 3.3.4 In vitro Assessment of Developed Nanoparticles

#### 3.3.4.1.1 In vitro Antiproliferative Efficiency of Suspended NPs

In order to further assess the behaviour of the designed system, synthesized nanoparticles were evaluated in *in vitro* cell cultures to determine the biocompatibility and activity of the drug release system.

First, it was necessary to evaluate the behaviour of the suspended NPs with different cells lines located in the implantation area of a tracheal device. In this case, the cell viability of epithelial cells (A549), Human Lung Fibroblast cells (IMR-90) and *ex vivo* samples (Primary Respiratory Human Fibroblast cells (T-01 MVV) with synthesized NPs were analysed. Cells were incubated with drug-free NPs and with 3% PCTXL loaded NPs at 10, 14 and 20 nM PCTXL concentrations. This range of concentrations was selected because it corresponds to plasma levels of the drug achievable in humans with clinically relevant intracellular concentrations.<sup>26,27,50,51</sup>

In Figure III-12, the *in vitro* assay of anti-proliferative effect of paclitaxel-loaded nanoparticles with different human cell lines can be observed. It can be observed that in A549 cell line, free drug loaded nanoparticles showed no obvious cytotoxicity indicating the biocompatibility of the synthesized polymers. However, when cells were treated with loaded nanoparticles (with a total concentration of PCTXL about 14 nM at 100% drug release) there was a rapid decrease in cell viability, indicating that A549 cells were very sensitive to PCTXL treatment. In addition, after some time point (between day 4

and 6) it can be observed a gradual recovery in cell viability attributed to the immortality behaviour of the cell line.

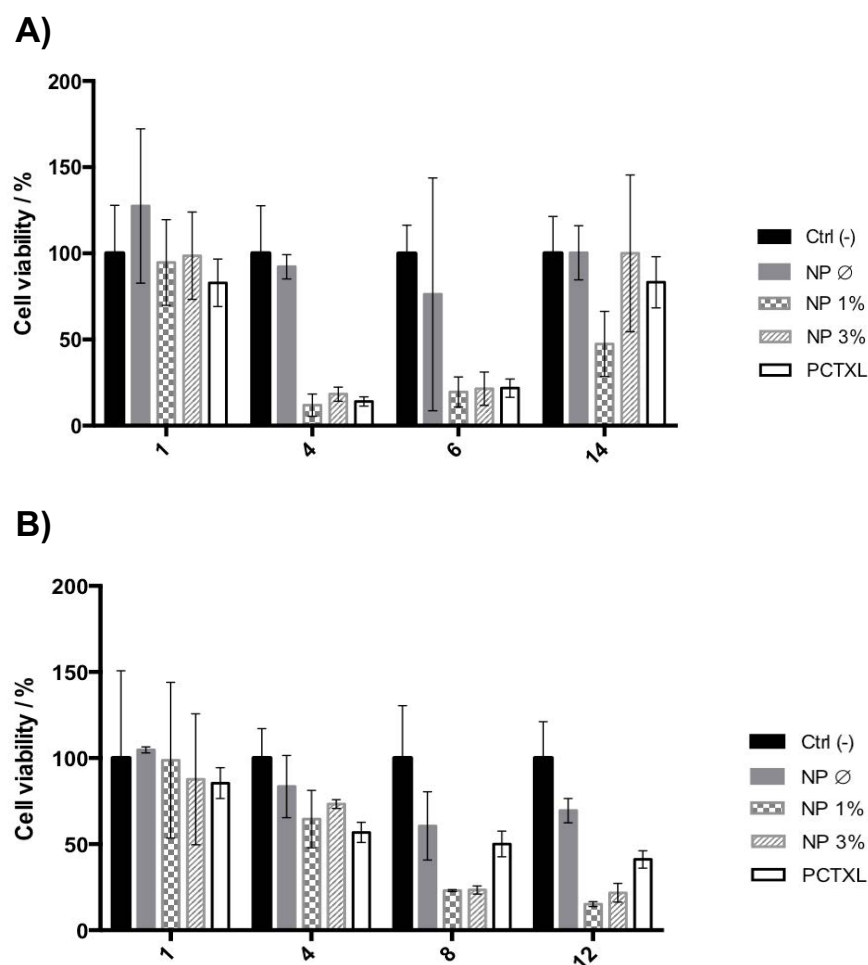


**Figure III-12.** Cell viability of different in vitro cell lines with synthesized NPs (total concentration of PCTXL about 14 nM at 100% drug release). **A)** viability of A549 cells and **B)** viability of IMR-90 cells. Samples incubated with PCTXL NPs at 10 nM and 20 nM, exhibited similar results. All plots are normalized to untreated cell.

Regarding the Human Normal Lung Fibroblast (IMR-90) cell line, free drug loaded nanoparticles show a slight decrease in cell viability but the effect is more dramatic with paclitaxel loaded nanoparticles with similar behaviour to pure paclitaxel. The same profile was observed when *ex vivo* fibroblasts (non-stenotic and stenotic) were treated with nanoparticles, (Figure III-13). In all cases, drug free nanoparticles showed no obvious cytotoxicity confirming the biocompatibility of the synthesized nanoparticles polymer.

In addition, when cells are treated with both, PCTXL NPs and pure PCTXL, a clear inhibitory effect can be observed, Figure III-12 and Figure III-13. However, both drug loaded nanoparticles (1% and 3%) with a total amount of drug above 14 nM (100% drug release), showed a decrease in cell viability (about 80% for both, 1% and 3% respectively, in case of IMR-90; and 70% and 80% for 1% and 3% respectively, in case of *ex vivo* stenotic fibroblast) being a slightly more drastic with the *ex vivo* non-

stenotic fibroblasts. Moreover, during the treatment, a progressive reduction in cell viability was observed. This controlled reduction can be explained by taking into account the results of released PCTXL from NPs, about 93-97% at 14 days, with an accumulation of paclitaxel on the media until a total drug concentration about 14 nM. Additionally, comparing drug loaded nanoparticles treatment with pure paclitaxel a similar behaviour can be observed, but it can be appreciated that drug-loaded nanoparticles improves cytotoxicity effect increasing in some cases the cell decreasing viability caused by the effect of the paclitaxel in the media.

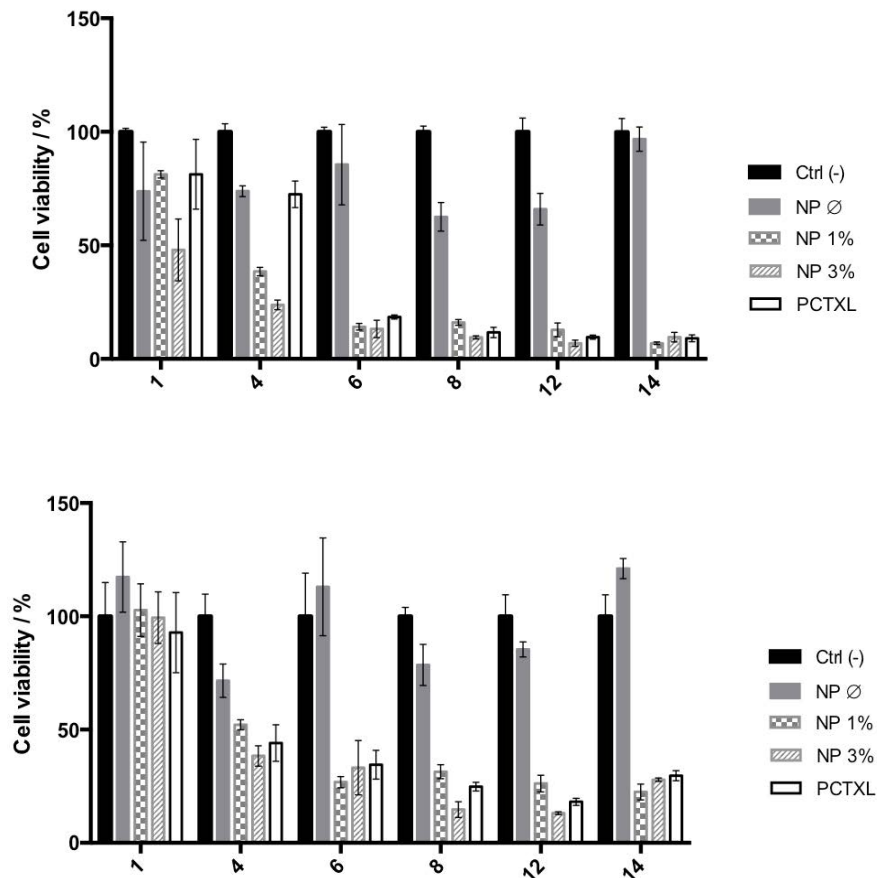


**Figure III-13.** Cell viability of different ex vivo cell lines with synthesized NPs (total concentration of PCTXL about 14 nM at 100% drug release). **A)** viability of T-01 MVV cells (healthy area, away from stenotic tissue) and **B)** viability of T-01 MVV stenotic cells. Samples incubated with PCTXL NPs at 10 nM and 20 nM, exhibited similar results. All plots are normalized to untreated cell.

Finally, it may be concluded that in all cases, despite the specific effect of paclitaxel in each type of cell, PCTXL loaded NPs showed a controlled release of paclitaxel causing a significant decrease in cell viability, in a similar behavior of pure paclitaxel. Additionally, the behavior and cell viability of non-loaded nanoparticles confirmed the biocompatibility of the polymeric material. PCTXL-loaded NPs (3%) at 10 and 20 nM showed similar effects on all types of tested cells (IMR-90, A549 and non-stenotic and stenotic T-01 MVV) than 3% PCTXL-NPs at 14 nM, indicating that the developed drug-loaded nanoparticles did not decrease the PCTXL activity and that the cytotoxicity against the evaluated cells was time dependent.



### 3.3.4.1.2 In vitro Antiproliferative Efficiency of Immobilized NPs

Taking into account the idea of a manufactured medical grade silicone device, first of all, it was necessary to evaluate the cell viability onto PDMS samples. In Figure III-14, the cell viability of human fibroblasts onto PDMS samples during 15 days can be observed. Initially, PDMS (non-treated) showed a cell viability around 30% and a slight increase until 70% at 15 days, indicating a low biocompatibility. This low cell viability was probably caused by the hydrophobicity and the surface chemistry (methylene groups) of the PDMS samples causing a low protein and cell adhesion. In order to overcome this problem, PDMS samples were treated with oxygen plasma in order to increase the surface free energy and increase the adhesion.<sup>52</sup> In this case, treated PDMS samples showed a high cell viability during all time points of the treatment (until 15 days), caused by the surface modification with oxygen, increasing the wettability and the adhesion of molecules. In addition, it can be observed that this increase in biocompatibility was constant during the time of experimentation indicating the robustness of the treatment.

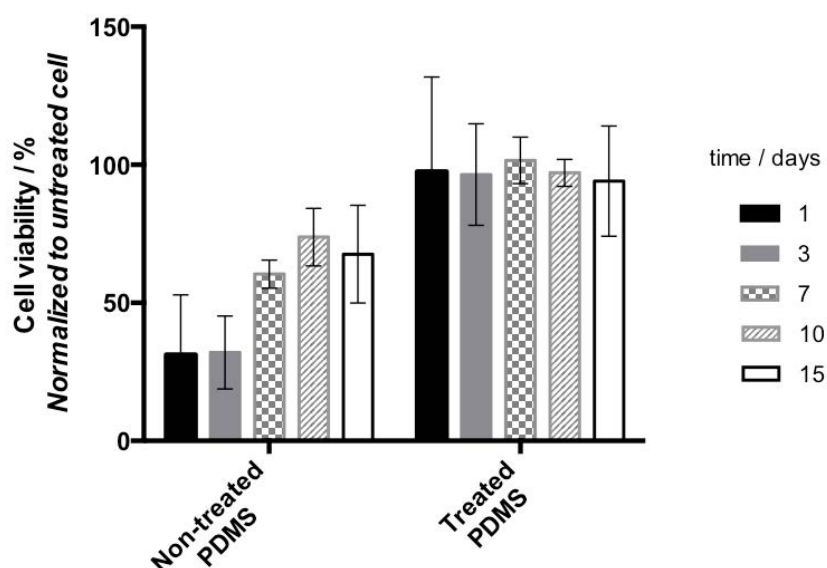


**Figure III-14.** Cell viability of human fibroblast with non-treated and treated PDMS with O<sub>2</sub> plasma. Normalized to untreated cell.

After the activation treatment of the PDMS to create a biocompatible PDMS surface, synthesized NPs were immobilized onto a pp-PFM surfaces. During this process, amine groups of the aminated NPs covalently reacted with the pentafluorophenyl groups of the pp-PFM PDMS surfaces. Samples with immobilized NPs were incubated with normal human dermal fibroblasts (NHDFs) in order to evaluate the biocompatibility of the non-drug loaded NPs and the cell viability of the drug loaded NPs. Initially, after NPs immobilization, samples were incubated with FBS in order to block the remaining reactive sites of pp-PFM. After the blocking treatment, different modified samples (oxygen activated PDMS, pp-PFM PDMS, non-drug loaded NPs onto pp-PFM PDMS and 3% drug loaded NPs onto pp-PFM PDMS) were incubated with NHDFs during 10 days. In Figure III-15-A, the Live&Dead<sup>®</sup> staining of the NHDFs over different samples can be observed. As expected with previous results, oxygen

activated samples acted as the control treatment, and showed a biocompatibility surface for normal human dermal fibroblasts. However, when cells were previously incubated with FBS to block the pp-PFM, there was a decrease in cell viability indicating some cytotoxicity of the surface. In this case, due to the toxic nature of the pentafluorophenol group, the possible remaining non-reacted pentafluorophenyl groups in the polymer surface could lead to the release of this toxic group in the media during the cell incubation.<sup>53</sup> In addition, the cells incubated with these samples were not homogeneously distributed, showing a cluster behaviour caused by the hydrophobicity of the surface and the toxicity effect of the non-reacted polymer. Nevertheless, non-drug loaded NPs samples showed better biocompatibility, but cells showed the same cluster behaviour. In this case, the non-drug loaded nanoparticles showed no obvious toxicity and the viability was only affected by the polymer surface such as with the pp-PFM samples. Finally, when cells were incubated with immobilized drug-loaded NPs on the surface, no viability was observed, all cells were dead as a result of the antiproliferative activity of the released paclitaxel.

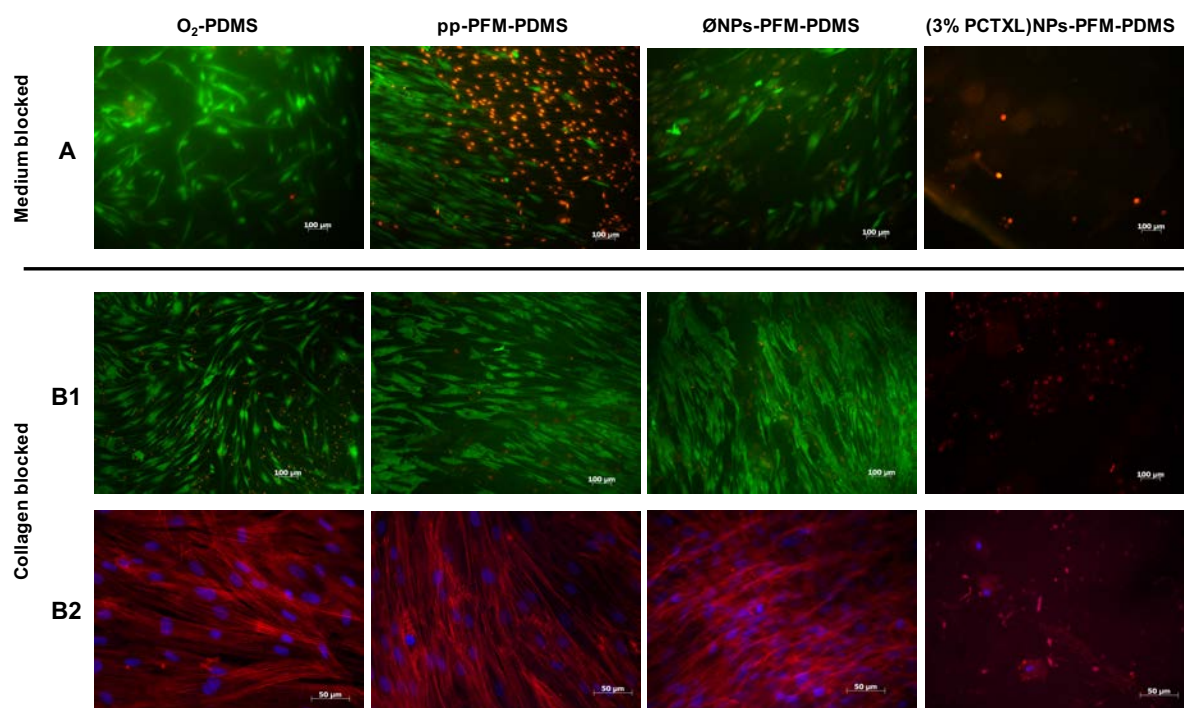


**Figure III-15.** Cell viability of Normal Human Dermal Fibroblasts (NHDFs) on coated and noncoated samples: **A)** cell cultures of different modified samples with drug loaded and non-drug loaded NPs, blocked with medium, and stained with Live&Dead kit (scale bar, 100 µm); **B1)** cell cultures of different modified samples with drug loaded and non-drug loaded NPs, blocked with collagen, and stained with Live&Dead kit (scale bar, 100 µm); **B2)** dapi/phalloidin staining on B1 collagen blocked samples (scale bar, 50 µm).

In order to further assess the influence of the blocking treatment to avoid the release of the pentafluorophenol groups from the pp-PFM, a collagen coating was used after NPs immobilization. Collagen was selected because it is the major component of the extracellular matrix and has been widely used in tissue engineering and biomedical applications. Collagen fibrils were incubated with NPs immobilized surfaces to react with the active sites of pp-PFM and increase the biocompatibility of the

designed surfaces. As it can be observed in Figure III-15-B1 and B2, the use of collagen instead of the FBS coating increase tremendously the biocompatibility of the surfaces (pp-PFM and non-drug loaded NPs surfaces) causing the NHDFs cells to show their characteristic morphology (elongate cells), such as in the FBS coating but in this case, there was no cluster observed and the samples were homogeneously coated with cells. On the contrary, when cells were incubated with drug-loaded NPs, all cells were dead, as expected due to the paclitaxel activity.

These results indicate the capacity of the PDMS samples with immobilized drug-loaded NPs to release paclitaxel on the media avoiding the proliferation of the cells. These surfaces can be used on different medical devices to treat abnormal proliferative tissue, such as stenotic or cancerous tissues. In addition, it has been observed that the blocking step of the remaining active sites of the pp-PFM are a key point to evaluate in order to avoid the toxicity of the pentafluorophenol group and increase the biocompatibility of the samples.

### 3.4 Concluding Remarks

This chapter presents a proof of concept of bioactive surfaces to be used in medical applications with biodegradable polymeric nanoparticles capable to entrap hydrophobic to deliver drugs in a controlled manner.

First of all, the synthesis of a biodegradable block co-polymer has been performed through different synthetic methods. This pegylated polyester showed two clear differentiated zones, a rigid block (hydrophobic) and flexible block (hydrophilic). The hydrophobic block (polyester) was designed to interact with hydrophobic drugs and to constitute the core of a nanoparticles. Due to the hydrophilic behaviour of the PEG (flexible block), the nanoparticles were stable in water and could interact or administrated on aqueous media and body fluids. The synthesized polymer was designed to show a terminal amine in order to express this amine moiety on the surface once the nanoparticles were formed. Due to this moiety, the nanoparticles could be used with click chemistry to functionalize different elements such as surfaces, drugs or carriers.

Synthesized polymer was used to form biodegradable nanoparticles with a size about 117 nm for PAm and 244 nm for PAmN, respectively, similarly to other polymeric pegylated nanoparticles described in the literature. Due to the terminal amine of the polymer chain of NPs, the nanoparticles were pH sensitive, and its surface potential (zeta potential) could be adjusted by changing the pH of the solution (protonation or non-protonation of the terminal amine). In addition, the nanoparticles were able to encapsulate hydrophobic drugs, such as paclitaxel, with a drug content until 3% and showing an interesting nanoparticles recovery (50-70%) and encapsulation efficiency (60-70%). Additionally, these nanoparticles showed a controlled drug release on the first days, about 60% at day 6, with a total drug release at day 15. Moreover, the chemistry bonds of the polyester-peg polymer could be used to modify the hydrolysis kinetics and the drug release profile. The drug loaded nanoparticles were reacted with the reactive sites of the pp-PFM and after the reaction, the NPs were covalently attached to the modified surface of PDMS.

In addition, NPs and immobilized NPs were tested *in vitro* with different cell lines to evaluate the biocompatibility of the synthesized materials and the activity of the drug delivery system. In this case, the designed drug delivery system showed an effective antiproliferative activity, with a reduction of 80% of the stenotic tissue in 12 days and the nanoparticles polymer showed no obvious cytotoxicity with the treated cells. However, it has been observed that the pp-PFM coating could show some toxic activity, if it is not blocked. Collagen coating showed interesting results by blocking the surface of the remaining active sites of pp-PFM and creating a biocompatible surface to increase cell adhesion.

The results in this chapter and the obtained surfaces showed different technologies that combined could improve the behaviour of current medical devices. The developed surfaces were able to entrap hydrophobic drugs, such as paclitaxel, and the controlled drug release profile could be used to treat a desired pathology, such as abnormal proliferation, locally and avoiding burst releases.

The combination of the previous results in Chapter II, the development of antibacterial surface covalently attached to the surface of silicone (most used stents and other medical devices are manufactured by medical silicone) with the results in this chapter, demonstrated the possibility to design selectively bi-side bioactive surfaces onto medical devices. Additionally, some experiments with microstructures and cylinders, have demonstrated the novelty of this technology to be transferred to more complex structures such as 3D designed anatomical devices. Despite this technology is still in prove of concept, it showed promising results with a wide range of possible medical applications.

As described in the Introduction (Chapter I), considering the proposed requirements to avoid pots-implantation problems such as bacterial colonization, stenotic tissue and migration, the next step should be the development of an anatomical adapted stent to increase the adaptability. Therefore, the following chapter will be focused on the design of personalized stents by use customizable and versatile manufacturing techniques such as 3D printing.

### 3.5 References

- (1) Zias, N.; Chroneou, A.; Tabbá, M. K.; Gonzalez, A. V.; Gray, A. W.; Lamb, C. R.; Riker, D. R.; Beamis, J. F. Post tracheostomy and post intubation tracheal stenosis: report of 31 cases and review of the literature. *BMC Pulm. Med.* **2008**, *8*, 18 DOI: 10.1186/1471-2466-8-18.
- (2) Saji, H.; Furukawa, K.; Tsutsui, H.; Tsuboi, M.; Ichinose, S.; Usuda, J.; Ohira, T.; Ikeda, N. Outcomes of airway stenting for advanced lung cancer with central airway obstruction. *Interact. Cardiovasc. Thorac. Surg.* **2010**, *11* (4), 425–428 DOI: 10.1510/icvts.2010.238196.
- (3) Martínez-Ballarín, J. I.; Díaz-Jiménez, J. P.; Castro, M. J.; Moya, J. a. Silicone stents in the management of benign tracheobronchial stenoses: Tolerance and early results in 63 patients. *Chest* **1996**, *109* (3), 626–629 DOI: 10.1378/chest.109.3.626.
- (4) Galluccio, G.; Lucantoni, G.; Battistoni, P.; Paone, G.; Batzella, S.; Lucifora, V.; Iacono, R. Dello. Interventional endoscopy in the management of benign tracheal stenoses: definitive treatment at long-term follow-up. *Eur. J. Cardio-thoracic Surg.* **2009**, *35* (3), 429–433 DOI: 10.1016/j.ejcts.2008.10.041.
- (5) Lorenz, R. R. Adult laryngotracheal stenosis: etiology and surgical management. *Curr. Opin. Otolaryngol. Head Neck Surg.* **2003**, *11* (6), 467–472 DOI: 10.1097/00020840-200312000-00011.
- (6) Zagalo, C.; Santiago, N.; Grande, N. R.; Martins dos Santos, J.; Brito, J.; Aguas, A. P. Morphology of trachea in benign human tracheal stenosis: a clinicopathological study of 20 patients undergoing surgery. *Surg. Radiol. Anat.* **2002**, *24* (3–4), 160–168 DOI: 10.1007/s00276-002-0031-8.
- (7) Huang, C. J. Use of the silicone T-tube to treat tracheal stenosis or tracheal injury. *Ann. Thorac. Cardiovasc. Surg.* **2001**, *7* (4), 192–196.
- (8) Maldonado, F.; Loiselle, A.; Depew, Z. S.; Edell, E. S.; Ekbohm, D. C.; Malinchoc, M.; Hagen, C. E.; Alon, E.; Kasperbauer, J. L. Idiopathic subglottic stenosis: An evolving therapeutic algorithm. *Laryngoscope* **2014**, *124* (2), 498–503 DOI: 10.1002/lary.24287.
- (9) Rensing, B. J.; Vos, J.; Smits, P. C.; Foley, D. P.; Van Den Brand, M. J. B. M.; Van Der Giessen, W. J.; De Feijter, P. J.; Serruys, P. W. Coronary restenosis elimination with a sirolimus eluting stent: First European human experience with 6-month angiographic and intravascular ultrasonic follow-up. *Eur. Heart J.* **2001**, *22* (22), 2125–2130 DOI: 10.1053/euhj.2001.2892.
- (10) Sousa, J. E.; Costa, M. A.; Abizaid, A. C.; Rensing, B. J.; Abizaid, A. S.; Tanajura, L. F.; Kozuma, K.; Langenhove, G. Van; Sousa, A. G. M. R.; Falotico, R.; et al. Clinical Investigation and Reports Sustained Suppression of Neointimal Proliferation by Sirolimus-Eluting Stents One-Year Angiographic and Intravascular Ultrasound Follow-Up. *Circulation* **2001**, *104*, 2007–2012 DOI: 10.1161/hc4201.098056.
- (11) Vogt, F.; Stein, A.; Rettemeier, G.; Krott, N.; Hoffmann, R.; Dahl, J. Vom; Bosserhoff, A. K.; Michaeli, W.; Hanrath, P.; Weber, C.; et al. Long-term assessment of a novel biodegradable paclitaxel-eluting coronary polylactide stent. *Eur. Heart J.* **2004**, *25* (15), 1330–1340 DOI: 10.1016/j.ehj.2004.06.010.
- (12) Iñiguez-Cuadra, R.; San Martín Prieto, J.; Iñiguez-Cuadra, M.; Zúñiga Erranz, S.; Jofré Pavez, D.; González Bombardiere, S.; Guilemany Toste, J. M.; Iñiguez-Sasso, R. Effect of mitomycin in the surgical treatment of tracheal stenosis. *Arch. Otolaryngol. Head Neck Surg.* **2008**, *134* (7), 709–714 DOI: 10.1001/archotol.134.7.709.
- (13) Warner, D.; Brietzke, S. E. Mitomycin C and airway surgery: How well does it work? *Otolaryngol. - Head Neck Surg.* **2008**, *138* (6), 700–709 DOI: 10.1016/j.otohns.2008.02.011.

- (14) Choong, C. K.; Haddad, F. J.; Gee, E. Y.; Cooper, J. D. Feasibility and safety of airway bypass stent placement and influence of topical mitomycin C on stent patency. *J. Thorac. Cardiovasc. Surg.* **2005**, *129* (3), 632–638 DOI: 10.1016/j.jtcvs.2004.07.062.
- (15) Cardoso, P. F. G.; Snell, G. I.; Hopkins, P.; Sybrecht, G. W.; Stamatis, G.; Ng, A. W.; Eng, P. Clinical application of airway bypass with paclitaxel-eluting stents: Early results. *J. Thorac. Cardiovasc. Surg.* **2007**, *134* (4), 974–981 DOI: 10.1016/j.jtcvs.2007.05.040.
- (16) Choong, C. K.; Phan, L.; Massetti, P.; Haddad, F. J.; Martinez, C.; Roschak, E.; Cooper, J. D. Prolongation of patency of airway bypass stents with use of drug-eluting stents. *J. Thorac. Cardiovasc. Surg.* **2006**, *131* (1), 60–64 DOI: 10.1016/j.jtcvs.2005.07.057.
- (17) Zhu, G. H.; Ng, A. H. C.; Venkatraman, S. S.; Boey, F. Y. C.; Wee, A. L. Y.; Trasti, S. L.; Yee Lim, L. H. A novel bioabsorbable drug-eluting tracheal stent. *Laryngoscope* **2011**, *121* (10), 2234–2239 DOI: 10.1002/lary.22175.
- (18) Chao, Y. K.; Liu, K. S.; Wang, Y. C.; Huang, Y. L.; Liu, S. J. Biodegradable cisplatin-eluting tracheal stent for malignant airway obstruction: In vivo and in vitro studies. *Chest* **2013**, *144* (1), 193–199 DOI: 10.1378/chest.12-2282.
- (19) Eliashar, R.; Eliachar, I.; Esclamado, R.; Gramlich, T.; Strome, M. Can topical mitomycin prevent laryngotracheal stenosis? *Laryngoscope* **1999**, *109* (10), 1594–1600 DOI: 10.1097/00005537-199910000-00009.
- (20) Ward, R. F.; April, M. M. Mitomycin-C in the treatment of tracheal cicatrix after tracheal reconstruction. *Int. J. Pediatr. Otorhinolaryngol.* **1998**, *44* (3), 221–226 DOI: 10.1016/S0165-5876(98)00061-5.
- (21) Choong, C. K.; Cardoso, P. F. G.; Sybrecht, G. W.; Cooper, J. D. Airway Bypass Treatment of Severe Homogeneous Emphysema: Taking Advantage of Collateral Ventilation. *Thorac. Surg. Clin.* **2009**, *19* (2), 239–245 DOI: 10.1016/j.thorsurg.2009.04.003.
- (22) Rubinfeld, R. S.; Pfister, R. R.; Stein, R. M.; Foster, C. S.; Martin, N. F.; Stoleru, S.; Talley, A. R.; Speaker, M. G. Serious complications of topical mitomycin-C after pterygium surgery. *Ophthalmology* **1992**, *99* (11), 1647–1654 DOI: 10.1016/S0161-6420(92)31749-X.
- (23) Roh, J.-L.; Lee, Y.-W.; Park, C. II. Can mitomycin C really prevent airway stenosis? *Laryngoscope* **2006**, *116* (3), 440–445 DOI: 10.1097/01.mlg.0000199403.21409.90.
- (24) Porter, G. T.; Gadre, S. A.; Calhoun, K. H. The effects of intradermal and topical mitomycin C on wound healing. *Otolaryngol. - Head Neck Surg.* **2006**, *135* (1), 56–60 DOI: 10.1016/j.otohns.2006.02.024.
- (25) Lee, D. K.; Kim, H. S.; Kim, K. S.; Lee, W. J.; Kim, H. K.; Won, Y. H.; Byun, Y. R.; Kim, M. Y.; Baik, S. K.; Kwon, S. O. The effect on porcine bile duct of a metallic stent covered with a paclitaxel-incorporated membrane. *Gastrointest. Endosc.* **2005**, *61* (2), 296–301 DOI: 10.1016/S0016-5107(04)02570-2.
- (26) Merchan, J. R.; Jayaram, D. R.; Supko, J. G.; He, X.; Bublely, G. J.; Sukhatme, V. P. Increased endothelial uptake of paclitaxel as a potential mechanism for its antiangiogenic effects: potentiation by Cox-2 inhibition. *Int. J. cancer* **2005**, *113* (3), 490–498 DOI: 10.1002/ijc.20595.
- (27) Weaver, B. A. How Taxol/paclitaxel kills cancer cells. *Mol. Biol. Cell* **2014**, *25* (18), 2677–2681 DOI: 10.1091/mbc.E14-04-0916.
- (28) Serrano, C.; Lostalé, F.; Rodríguez-Panadero, F.; Blas, I. de; Laborda, A.; de Gregorio, M. A. Tracheal Self-Expandable Metallic Stents: A Comparative Study of Three Different Stents in a Rabbit Model. *Arch. Bronconeumol.* **2015**, *52* (3), 123–130 DOI: 10.1016/j.arbres.2015.04.012.
- (29) Greer, M.; Fuehner, T.; Warnecke, G.; Noack, H.; Heilmann, T.; Haverich, A.; Welte, T.; Gottlieb,

- J. Paclitaxel-coated balloons in refractory nonanastomotic airway stenosis following lung transplantation. *Am. J. Transplant.* **2014**, *14* (10), 2400–2405 DOI: 10.1111/ajt.12845.
- (30) Harmon, A. M.; Lash, M. H.; Sparks, S. M.; Uhrich, K. E. Preferential cellular uptake of amphiphilic macromolecule-lipid complexes with enhanced stability and biocompatibility. *J. Control. Release* **2011**, *153* (3), 233–239 DOI: 10.1016/j.jconrel.2011.04.004.
- (31) Danhier, F.; Lecouturier, N.; Vroman, B.; Jérôme, C.; Marchand-Brynaert, J.; Feron, O.; Préat, V. Paclitaxel-loaded PEGylated PLGA-based nanoparticles: In vitro and in vivo evaluation. *J. Control. Release* **2009**, *133* (1), 11–17 DOI: 10.1016/j.jconrel.2008.09.086.
- (32) Xin, H.; Chen, L.; Gu, J.; Ren, X.; Wei, Z.; Luo, J.; Chen, Y.; Jiang, X.; Sha, X.; Fang, X. Enhanced anti-glioblastoma efficacy by PTX-loaded PEGylated poly( $\epsilon$ -caprolactone) nanoparticles: In vitro and in vivo evaluation. *Int. J. Pharm.* **2010**, *402* (1–2), 238–247 DOI: 10.1016/j.ijpharm.2010.10.005.
- (33) Yu, Y.; Zou, J.; Yu, L.; Ji, W.; Li, Y.; Law, W.; Cheng, C. Functional Polylactide-*g*-Paclitaxel-Poly(ethylene glycol) by Azide-Alkyne Click Chemistry. *Macromolecules* **2011**, *44* (12), 4793–4800 DOI: 10.1021/ma2005102.
- (34) Tao, Y.; Liu, R.; Chen, M.; Yang, C.; Liu, X. Cross-linked micelles of graftlike block copolymer bearing biodegradable  $\epsilon$ -caprolactone branches: A novel delivery carrier for paclitaxel. *J. Mater. Chem.* **2012**, *22*, 373–380 DOI: 10.1039/c1jm13950a.
- (35) Jiang, X.; Xin, H.; Sha, X.; Gu, J.; Jiang, Y.; Law, K.; Chen, Y.; Chen, L.; Wang, X.; Fang, X. PEGylated poly(trimethylene carbonate) nanoparticles loaded with paclitaxel for the treatment of advanced glioma: In vitro and in vivo evaluation. *Int. J. Pharm.* **2011**, *420* (2), 385–394 DOI: 10.1016/j.ijpharm.2011.08.052.
- (36) Saremi, S.; Atyabi, F.; Akhlaghi, S. P.; Ostad, S. N.; Dinarvand, R. Thiolated chitosan nanoparticles for enhancing oral absorption of docetaxel: Preparation, in vitro and ex vivo evaluation. *Int. J. Nanomedicine* **2011**, *6*, 119–128 DOI: 10.2147/IJN.S15500.
- (37) Minimol, P. F.; Paul, W.; Sharma, C. P. PEGylated starch acetate nanoparticles and its potential use for oral insulin delivery. *Carbohydr. Polym.* **2013**, *95* (1), 1–8 DOI: 10.1016/j.carbpol.2013.02.021.
- (38) Lashof-Sullivan, M. M.; Shoffstall, E.; Atkins, K. T.; Keane, N.; Bir, C.; VandeVord, P.; Lavik, E. B. Intravenously administered nanoparticles increase survival following blast trauma. *Proc. Natl. Acad. Sci. U. S. A.* **2014**, *111* (28), 10293–10298 DOI: 10.1073/pnas.1406979111.
- (39) Williams, J.; Lansdown, R.; Sweitzer, R.; Romanowski, M.; LaBell, R.; Ramaswami, R.; Unger, E. Nanoparticle drug delivery system for intravenous delivery of topoisomerase inhibitors. *J. Control. Release* **2003**, *91* (1–2), 167–172 DOI: 10.1016/S0168-3659(03)00241-4.
- (40) Di Mauro, P. P.; Borrós, S. Development of High Drug Loaded and Customizing Novel Nanoparticles for Modulated and Controlled Release of Paclitaxel. *Pharm. Res.* **2014**, *31* (10), 3461–3477 DOI: 10.1007/s11095-014-1434-z.
- (41) Förch, R.; Zhang, Z.; Knoll, W. Soft plasma treated surfaces: Tailoring of structure and properties for biomaterial applications. *Plasma Process. Polym.* **2005**, *2* (5), 351–372 DOI: 10.1002/ppap.200400083.
- (42) Fessi, H.; Puisieux, F.; Devissaguet, J. P.; Ammoury, N.; Benita, S. Nanocapsule formation by interfacial polymer deposition following solvent displacement. *Int. J. Pharm.* **1989**, *55* (1), R1–R4 DOI: 10.1016/0378-5173(89)90281-0.
- (43) Kim, S. Y.; Shin, I. G.; Lee, Y. M.; Cho, C. S.; Sung, Y. K. Methoxy poly(ethylene glycol) and  $\epsilon$ -caprolactone amphiphilic block copolymeric micelle containing indomethacin. *J. Control. Release* **1998**, *51* (1), 13–22 DOI: 10.1016/S0168-3659(97)00124-7.



- (44) Averineni, R. K.; Shavi, G. V; Gurram, A. K.; Deshpande, P. B.; Arumugam, K.; Maliyakkal, N.; Meka, S. R.; Nayanabhirama, U. PLGA 50:50 nanoparticles of paclitaxel: Development, in vitro anti-tumor activity in BT-549 cells and in vivo evaluation. *Bull. Mater. Sci.* **2012**, *35* (3), 319–326 DOI: 10.1007/s12034-012-0313-7.
- (45) Hong, Y.; Song, H.; Gong, Y.; Mao, Z.; Gao, C.; Shen, J. Covalently crosslinked chitosan hydrogel: Properties of in vitro degradation and chondrocyte encapsulation. *Acta Biomater.* **2007**, *3* (1), 23–31 DOI: 10.1016/j.actbio.2006.06.007.
- (46) Schulze-Tanzil, G.; Lemke, M.; Meier, C.; Ertel, W.; Kohl, B.; Huang, Z.; Muschik, M.; Markart, M.; Hoyer, M.; Arens, S. Characterization of Human Anulus Fibrosus&ndash; and Nucleus Pulposus&ndash;Derived Cells During Monolayer Expansion and in Hydrogel Cultures. *Bone Tissue Regen. Insights* **2014**, *5*, 15 DOI: 10.4137/BTRI.S13604.
- (47) Yagi, T.; Hardin, J. a.; Valenzuela, Y. M.; Miyoshi, H.; Gores, G. J.; Nyberg, S. L. Caspase inhibition reduces apoptotic death of cryopreserved porcine hepatocytes. *Hepatology* **2001**, *33* (6), 1432–1440 DOI: 10.1053/jhep.2001.24560.
- (48) Gaucher, G.; Marchessault, R. H.; Leroux, J. C. Polyester-based micelles and nanoparticles for the parenteral delivery of taxanes. *J. Control. Release* **2010**, *143* (1), 2–12 DOI: 10.1016/j.jconrel.2009.11.012.
- (49) Hu, Q.; Gu, G.; Liu, Z.; Jiang, M.; Kang, T.; Miao, D.; Tu, Y.; Pang, Z.; Song, Q.; Yao, L.; et al. F3 peptide-functionalized PEG-PLA nanoparticles co-administrated with tLyp-1 peptide for anti-glioma drug delivery. *Biomaterials* **2013**, *34* (4), 1135–1145 DOI: 10.1016/j.biomaterials.2012.10.048.
- (50) Zasadil, L. M.; Andersen, K. A.; Yeum, D.; Rocque, G. B.; Wilke, L. G.; Tevaarwerk, A. J.; Raines, R. T.; Burkard, M. E.; Weaver, B. A. Cytotoxicity of Paclitaxel in Breast Cancer Is due to Chromosome Missegregation on Multipolar Spindles. *Sci. Transl. Med.* **2014**, *6* (229), 229ra43–229ra43 DOI: 10.1126/scitranslmed.3007965.
- (51) Li, J.; Tang, J.; Li, Y.; Yu, J.; Zhang, B.; Yu, C. Pharmacokinetic profile of paclitaxel in the plasma, lung, and diaphragm following intravenous or intrapleural administration in rats. *Thorac. Cancer* **2015**, *6* (1), 43–48 DOI: 10.1111/1759-7714.12139.
- (52) Hauser, J.; Zietlow, J.; Köller, M.; Esenwein, S. A.; Halfmann, H.; Awakowicz, P.; Steinau, H. U. Enhanced cell adhesion to silicone implant material through plasma surface modification. *J. Mater. Sci. Mater. Med.* **2009**, *20* (12), 2541–2548 DOI: 10.1007/s10856-009-3826-x.
- (53) He, L.; Szameit, K.; Zhao, H.; Hahn, U.; Theato, P. Postpolymerization modification using less cytotoxic activated ester polymers for the synthesis of biological active polymers. *Biomacromolecules* **2014**, *15* (8), 3197–3205 DOI: 10.1021/bm500902t.

## **Chapter IV. Design of a 3D Printed Tracheal Device**

*This page left blank intentionally*

## 4.1 Introduction

The previous chapters (Chapter II and III) show the development of a technology capable of modifying the surfaces of different materials and furnish them with different activities. Initially, different applications require of an antibacterial surface to avoid bacterial colonization and biofilm. In this context, considering the antibacterial requirements of different medical devices, such as a tracheal stent, a flexible antibacterial coating was developed using metallic silver. This coating presents the ability to be applied onto different substrates, controlling the surface geometry and structure and additionally, showing an antifouling behaviour thus increasing the antibacterial effect. Furthermore, the developed technology was adapted to create a coating capable of releasing antiproliferative agents and acting as a drug release platform. The developed technology consists of a drug delivery system, using biodegradable nanoparticles loaded with PCTXL, covalently immobilized onto the surface of the material. The system allows a local controlled release of PCTXL during 14 days with drug doses lower than reported toxic concentrations for human cells. The developed platform releases effective doses against tested cells (IMR-90, A549 and human trachea extracted cells) which indicate that the platform can be a potential system to avoid the granulation tissue formation and eliminate the stenotic tissue.

As mentioned before, there are different therapeutic approaches to treat airway stenosis, such as electrocautery, tracheal resection and reconstruction and a transoral endoscopic positioning of an endoluminal tracheal stent (stenting).<sup>1</sup> Stents were engineered to be minimally-invasive procedure aimed to restore airway patency and for acute relief of dyspnea. It is mostly indicated in patients suffering from trachea stenosis untreatable by open-neck tracheal resection and anastomosis or tracheoplastic procedures or when surgery has already failed and it is not repeatable.<sup>2-4</sup>

Current stents are concentrically silicone cylinders (tube-like geometries) with several dimensions to find some fit to the patient made of metallic wire, silicone or a mixture of both materials, and each device has advantages and disadvantages depending on the material and design.<sup>5</sup> However, these designs do not take into account the patient anatomical features, such as pitch in between tracheal ring, angulations, non-circular section (D-shape) and diameter changes causing low adaptability and disadvantages.<sup>6-8</sup> This means that stents may migrate from their original position back and forward through the trachea causing pain and formation of granulation tissue due to the mechanical stress and rubbing.<sup>9,10</sup> As a result, several unwanted effects have been described, including perforation, malposition, esophageal impingement, granulation tissue formation and hemorrhage.<sup>11-14</sup> Additionally, stent migration, especially in proximal lesions near the vocal cords, can acutely threaten the cords and the ability to speak.

Previous report performed market analysis to evaluate the adaptability requirements of tracheal stents. The main missing characteristics consist on simple placing and removal of the stent, and the customization of the product. In fact, the common opinion of physicians is that personalized devices may avoid stent migration because of the correct fitting, and consequently the reduction or elimination of associated problems.<sup>4</sup> In this case, it is clear that if the stent is designed considering the patient's

anatomy, one of the most difficult choice for physicians (to choose the proper diameter and length) will disappear because the device shall exactly reproduce the patients anatomy and thus, the performance of the stent would be improved avoiding migration.

Although customization of stents or implants, is an expensive and time-consuming process<sup>15</sup>, the demand for customized designs for biomedical applications is very high<sup>16</sup>. However, the number of implanted tracheal stents is relatively low, about 160,000 cases per year in developed regions, when compared with other implants.<sup>17,18</sup> This suggests that to be economically competitive, the new stents must be produced using small batches.<sup>4</sup> Moreover, hospitals spend great amounts of resources and time acquiring standardized implants and/or prosthetics that are not suitable for all patients, and many of them become unusable products that must be discarded after their expiration date.<sup>19</sup> Therefore, a solution can be to manufacture personalized prosthesis, tracheal stents, using a CT scan of the patient in combination with the additive manufacturing (AM) technologies.<sup>20,21</sup>

Therefore, in order to design a workflow to manufacture personalized devices, the development process for anatomically personalized medical devices presents multiple steps, as shown in Figure IV-1. Initially, anatomical data from the patient must be obtained, usually through a Computerised Axial Tomography (CAT) or Magnetic Resonance Imaging (MRI). Both systems are medical imaging systems that provide a series of image, which corresponds to slices of the internal and external tissues.<sup>21</sup> Typically, the output format of the CAT consists on a digital imaging and communication in medicine (DICOM) file that contains the linear attenuation coefficient of the patient's body material at each scanned point. Each point represents a volume in the space and are defined as voxels. In order to obtain a precise anatomical model, high quality medical data is imperative and this relies on the thickness of the slice (defined by the radiologists with a maximum about 0.8 mm on both directions on the plane normal to the CAT and 0.5 mm for the axial direction) and the size of the pixel.

Secondly, after the data acquisition, DICOM files are transferred into a visualization software, where data is treated and analysed, region of interest (ROI) is set and anatomical structures are selected using the threshold of the linear attenuation coefficient of each voxel.<sup>6</sup> After this process, an STL file (set of triangles with associated vector) is generated with a 3D reconstruction of the selected object/tissue. Then, the STL file requires an optimization to avoid holes, intersecting triangles, bad contours, noise shells and overlapping triangles.

At this point, it is possible to characterize the object (analysing the dimensions) and perform different CAD operations to design and remodel the 3D reconstructed object and even design devices or prosthesis, to be inserted or adapted to this anatomical geometry. Once the object is designed and optimized, the generated STL file is segmented into a set of layers than can be interpreted by an AM printer and manufactured.

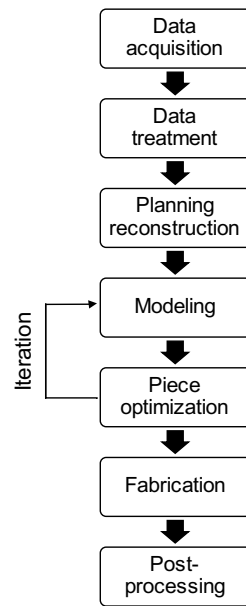


**Figure IV-1.** Workflow to manufacture anatomical personalized medical device.

After the manufacturing process, samples require a post-processing step to finish the fabricated piece. In this case, surfaces treatments, such as polish, paint, varnish or other coatings, smooth contours and other pieces assembling are typical finishing processes.

Additive manufacturing, known as 3D printing, is a process of joining materials to create objects from three-dimensional (3D) data, usually layer by layer. As mentioned, the principle of AM consists on taking the information from a computer-aided design (CAD) and then, the CAD model is virtually segmented in different cross-section (layers), which are jointly manufactured by an AM printer, creating the final object.<sup>22</sup>

Since the first development of AM in the 80's, various AM machines have been developed (Figure IV-2), stereolithography (SL), fused deposition modelling (FDM), selective laser sintering, (SLS) selective laser melting (SLM), laminated engineered net shaping (LENS), electron beam melting (EBM), 3D printing or inkjet (3DP), direct metal deposition (DMD), laser metal deposition (LMD) and laminated object manufacturing (LOM). This versatility of printers and technology allows the use of a wide range of materials, covering from metals<sup>23,24</sup>, and plastics<sup>25-27</sup> to ceramics<sup>28,29</sup> and even biological<sup>30,31</sup>. The interesting advantages of AM is that these new technologies are revolutionizing the current manufacturing systems and the business models because they provide a cost-effective and time-efficient way to produce low-volume, customized products with complicated geometries, advanced material properties and functionalities, reduce, or eliminate, the assembling parts and minimize the waste materials.<sup>32,33</sup>

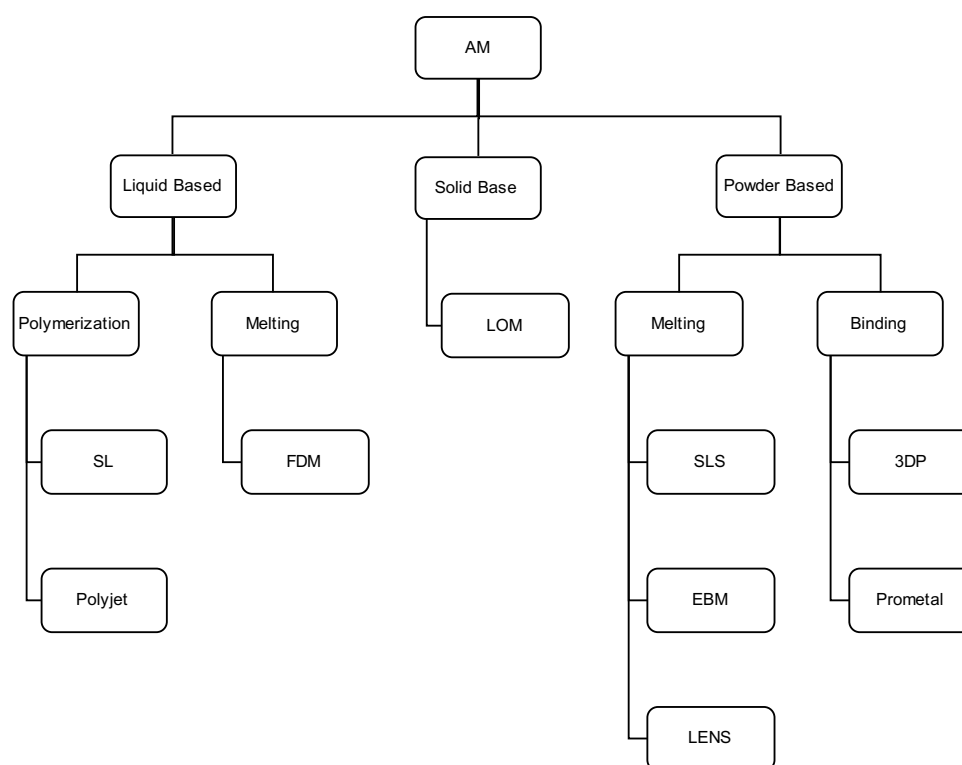


**Figure IV-2.** AM classification technologies according to the raw material.

However, despite the wide range of techniques and materials used in AM, there are some limitations due to the lack of biocompatible polymers approved for medical use and capable to be printed with AM technologies.<sup>34</sup> More specifically, polydimethylsiloxane (PDMS) elastomer has been widely used as biomaterial to manufacture prosthesis and medical devices, micro-fluidic channels,<sup>35,36</sup> stretchable cell substrates<sup>37</sup>, spiders nets<sup>38</sup> and even bionic organs such as ears<sup>39</sup>. PDMS shows great biocompatibility<sup>40</sup>, optical transparency and high oxygen permeability<sup>41</sup> properties and considering the ease of fabrication by spin-coating or moulding, makes it a suitable material for biomedical applications, such as medical device fabrication. However, the low viscosity of the liquid pre-polymer and its low reticulation kinetics, limits its use in more advanced fabrication approaches, such as 3D printing. Additionally, the relatively long gelation time allow the material to flow once deposited making to loss the print fidelity.<sup>26</sup> Therefore, despite some promising advances in additive manufacturing have led to new methods to 3D-print hydrogels or PDMS, such as syringe-based extrusion or freeform reversible embedding of suspended hydrogels (FRESH)<sup>42</sup>, the scalability and regulatory framework requires time and more research and optimization. Therefore, it is possible to mix the conventional manufacturing system with the most advanced personalized fabrication, such as 3D printing. It is possible to use AM to manufacture personalized and customized moulds, using CT data and then, use the fabricated moulds in a classical injection moulding process.

To sum up, considering that current stents (normalized geometries and dimensions) are causing problems of migration, pain and granulation tissue because of their low adaptability, this work aims to develop a fabrication protocol for producing personalized tracheal stents, using a CT scan with the

patient information, with 3D printing technologies (AM). Considering that the most widely used tracheal stents are the silicone-based, and the difficulty to 3D print PDMS elastomer, a combination of advanced and classical manufacturing systems will be used. Patient's information will be used to generate the 3D model and design the most suitable stent to perfectly fits in the trachea lumen and then the AM technology will be used to manufacture a mould, which will be subsequently filled with silicone as traditional injection process. Despite the final device will be manufactured with medical grade silicone, this work uses PDMS as proof of concept in order to evaluate the behaviour and the techniques required to achieve anatomical silicone based medical devices.



## 4.2 Materials and Methods

### 4.2.1 Materials

Argon 5.0 and oxygen 5.0 were purchased from Abelló Linde S.A. (Barcelona, Spain). PFM was purchased from Apollo Scientific LTD (Stockport, UK). D-(+)-Glucosamine hydrochloride, sodium dodecyl sulphate (SDS), Hellmanex, and silver nitrate were purchased from Sigma-Aldrich (Madrid, Spain), ethanol was purchased from Scharlab (Barcelona, Spain) and a Sylgard 184 kit was purchased from Ellsworth Adhesives (Madrid, Spain). Ultrapure water (Milli-Q) was obtained using a Synergy UV<sup>®</sup> system from Merck Millipore (Billerica, MA, USA).

### 4.2.2 3D model generation

#### 4.2.2.1.1 Data acquisition

The scanner used to examine thorax and the trachea was a Toshiba Aquilion One characterized by a 320-row detector that enables ultra-fast scanning of organs in one rotation, resulting in multiplanar and 3D images demonstrating perfect continuity along the Z-axis, without motion and distortion image. Airway imaging was accomplished using a central airway protocol, which includes thin-cut helical images of the neck and chest in expiration and inspiration phase of respiration<sup>43</sup> using no contrast material (slice thickness, 0.5 mm; interval, 0.5 mm; pitch, 1.388:1; pixel spacing, 0.69/0.69; kilovolt peak, 100 mA). The output was a DICOM file with a 616 (512 x 512) bitmap images.

#### 4.2.2.1.2 Software

The generated DICOM file from the CT scan were imported to two visualization software, 3D Slicer (<https://www.slicer.org>) and the MIMICS Innovation Suite<sup>®</sup> (Materialise, Belgium, <http://www.materialise.com/en/medical/mimics-innovation-suite>).

3D Slicer is a free, cross-operating system, open source software platform for medical image informatics, image processing, and three-dimensional visualization. Built over two decades on the basis of experiences at the Massachusetts Institute of Technology and Surgical Planning Laboratory and through support from the National Institutes of Health and a worldwide developer community, Slicer brings processing tools to physicians, researchers, and the general public.<sup>44–46</sup>

Mimics Innovation Suite<sup>®</sup> is a commercial medical image processing and analysis software. Built over the experience for more than 25 years, Mimics<sup>®</sup> is the most advanced segmentation toolbox for patient specific-device design or medical image-based research and development. Mimics<sup>®</sup> provide both basic functionality and an additional Pulmonology module to process the airways in lung CT scans. Additionally, Mimics Innovation Suite<sup>®</sup> present the design and meshing software (3-matic<sup>®</sup>) capable to treat, modify and create surfaces with CAD capacities.<sup>47,48</sup>

### 4.2.3 3D Printer

In this work, two type of printers have been used, an FDM Fortus 400mc<sup>®</sup> and the Insight<sup>®</sup> software (Stratasys<sup>®</sup>, MN, US) and a stereolithography printer, Stalactite Series 102 (Stalactite, Barcelona, Spain) with the Stalactite Workshop software, Figure IV-3. The FDM printer used a polycarbonate as a printing material and a “SR-100<sup>TM</sup>” as a printing-support material (acrylic copolymer) both acquired from the manufacturer. The support material was gently removed following the manufacturer’s instructions, using a high alkaline solution with a pH up to 12.6-13 at 70-85 °C until material dissolution.

For the Stalactite printer, an acrylate base resin “standard” was used with a visible photo-crosslinker provided by the manufacturer. The printing process was performed following the manufacturer’s instructions for the selected material.

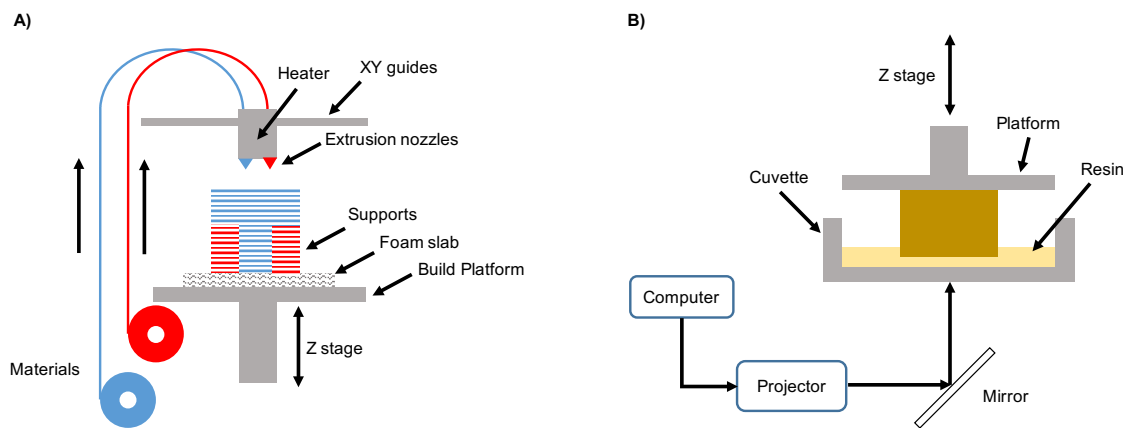


Figure IV-3. Scheme of different 3D printers used in this work. **A)** FDM printer and **B)** Stereolithography printer.

### 4.2.4 Prosthesis un moulding

After the mould fabrication, it was washed gently with Milli-Q water and ethanol. After the washing treatment, the mould received a visible light bath between 15-60 min to ensure the curing process of the resin. After this process, the mould was washed again with water and ethanol and dried under compressed air. Then, a PDMS kit (10:1) was injected inside using the injections holes designed to allow the silicone to fill the mould. PDMS filled with silicone was introduced in the oven between 73 °-110 ° for 180-10 min respectively.

Once the curing process of the PDMS was completed, the mould was cooled at room temperature and the silicone prosthesis was un moulded by cracking the mould. The resulting silicone prosthesis was washed with Milli-Q water and ethanol and dried with compressed air.

#### 4.2.1 Surface modification and Silver Deposition.

The surface modifications carried out in this work was carried as described in previous work.<sup>49,50</sup> Briefly, before introduction of the substrate, the chamber was cleaned in continuous wave O<sub>2</sub>/Ar (1:1) plasma for approximately 1 h at a power of 150 W. Samples were placed at the centre of an aluminium

plate and vacuum was started until the base pressure of 0.001-0.003 mbar was reached. Then, PFM was regulated through the needle valve and introduced to the reactor chamber in a vapour phase (heated at 75 °C) until 0.02-0.03 mbar. The continuous radio frequency power was fixed at 15 W (working power) and pulsed plasma polymerization duty cycle (DC) of 10/20 [ $DC = t_{on}/(t_{on}+t_{off})$ ]<sup>51</sup> was carried out for 3-10 min. Plasma discharge was then turned off, and the PFM vapour flow rinsed was kept constant for additional 15 min. After the polymerization process, plasma-polymerized PFM (pp-PFM) samples were carefully removed from the reaction chamber and stored until further use under argon atmosphere.

For the silver deposition, silver was reduced by a reductive sugar using the silver mirror reaction (Tollens' reagent)<sup>52</sup>. The glucosamine solution was prepared by dissolving glucosamine hydrochloride in Milli-Q water at 1 M. Then, pH was adjusted to 7.4 with concentrated sodium hydroxide. The reaction between glucosamine and the modified surface was performed by incubating the modified sample in a glucosamine solution for 6 h. Tollens' reagent was prepared by adding 25  $\mu$ L of 15% ammonia to 1 mL of 0.1 M silver nitrate, observing the precipitation of the silver oxide. Then, another 25  $\mu$ L of 15% ammonia was added, and the complete dissolution of the precipitate was observed due to the complexation of the silver by ammonia. The modified sample with the attached glucosamine were introduced on a vial with 4 mL of Milli-Q water. Then, 1 mL of the Tollens' reagent was added and heated on a Milli-Q water bath at 90 °C for the desired time of reaction, 60 min.

## 4.3 Results

As mentioned before, in order to obtain a 3D model ready to manufacture, extracted data from the patients must be imported to visualization and sketch (CAD) software to analyse, modify and re-design the device. For this work, 3D Slicer and Mimics<sup>®</sup> software have been used.

### 4.3.1 Data Extraction and Analysis

#### 4.3.1.1.1 Data import

Thorax data of the patient scanned using the CT was imported in both 3D Slicer and Mimics<sup>®</sup> software. Once data was imported, software interpreted the CT images and produced a visualization of the scanned structures. For 3D Slicer, data was imported using the *Welcome to Slicer* module with the *Load DICOM Data* command, and for the Mimics<sup>®</sup>, the import command was the *New project wizard*, located under the *File* menu.

**Table IV-1.** Commands for Data import into 3D Slicer and Mimics<sup>®</sup>.

ROI	Command
3D Slicer	Welcome to Slicer / Load DICOM
Mimics <sup>®</sup>	File / New project wizard

As it can be observed in Figure IV-4, once files were loaded in both software, it was possible to find three or four different views, corresponding to axial, coronal and sagittal planes of the thorax. The fourth view corresponded to the 3D reconstruction of the selected area. Additionally, there were different scroll-bars for each view to move the plane along the different slices that form the scanned area. It is interesting to observe the difference threshold values of the soft tissues in grey (organs and tissues) versus the hard tissues in white (bones) because of higher radiation absorption in hard tissues. This was useful because tissues could be easily differentiated and the tissue selections through different masks could have better resolution.

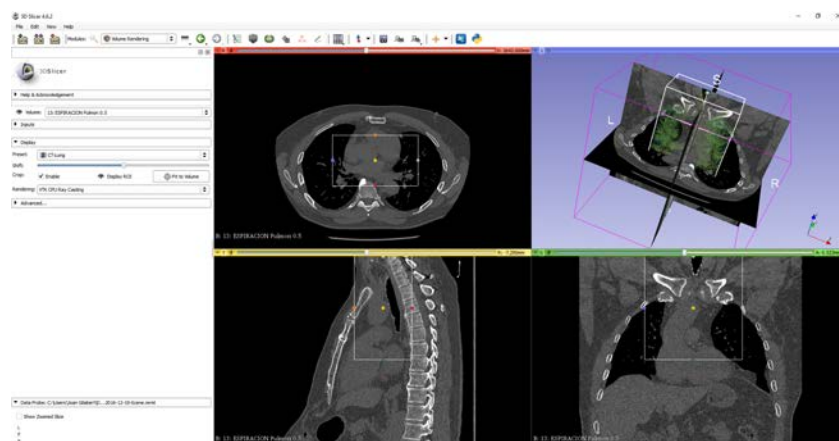
#### 4.3.1.1.2 Region of Interest (ROI)

After data loading, it was necessary to define a region of interest (ROI) to design the working area. Therefore, a cubical ROI with the length, width, and a height that covers the area of the airway to study. This cubic ROI represented the tracheal airway from the neck to the bronchial ramification, discarding the lungs to minimize calculations and visualization.

**Table IV-2.** Commands of selected ROI for 3D Slicer and Mimics®.

ROI	Command
3D Slicer	Volume Rendering / Crop Volume
Mimics®	File or Image / Crop Project or Segmentation Crop mask

A)



B)

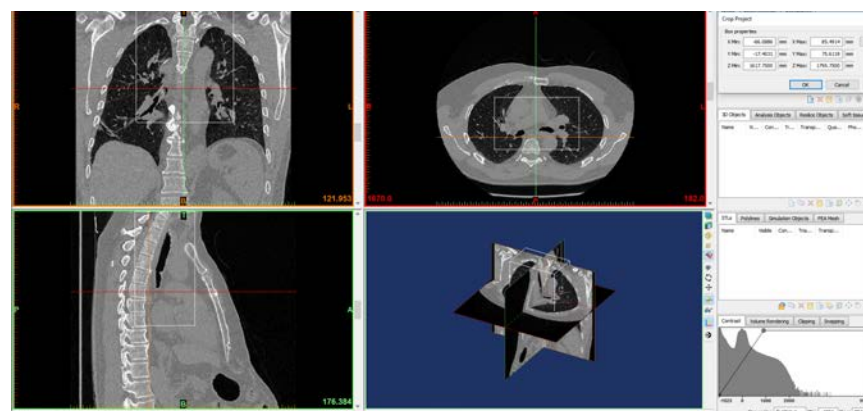


**Figure IV-4.** Different views of axial, coronal and sagittal planes of thorax after file imported. ROI was selected according with the dimensions of the airway. **A)** 3D Slicer view and **B)** Mimics®.

#### 4.3.1.1.3 Thresholding and Assessment of Tracheal Tissue

After ROI definition, the area was cropped and it was necessary to start the segmentation to generate a 3D volumetric images of the patient’s trachea. To do so, different layers or masks for each tissue were created using a manual, semi-automatic or automatic method. For manual segmentation, it is necessary to perform the entire structure delineation slice by slice. Considering that the defined ROI can contain more than 300 slices and the complexity of the structure, manual segmentation can be very time-consuming and impractical. Semi-automatic segmentation, Table IV-3, consists on a defined threshold

range, normally between -990 HU to -50 (or -120 HU), for the trachea<sup>47</sup>, that selects all pixels in that range. However, the results are not accurate and there was a lot of noise. However, some software, such as Mimics<sup>®</sup>, besides of the previously detailed options to create masks, have other algorithms that solves the reproducibility and the time-consuming problems. A “Dynamic region growing” is an algorithm that segments a region based on the connectivity of grey scale in a certain range, and the “Deep airways segmentation” module segmented the trachea based on two seed points in the axial view. The first point was the starting point of the trachea and the second point was defined several slices down, to define the trachea direction. During the pre-processing, it was possible to select different levels of leakage detection. Higher leakage detection levels showed a 3D reconstruction with lower leakages but the 3D structure has fewer branches. On the contrary, lower leakage detection level could lead more detected branches, even parts of the lungs but it is possible that the algorithm starts calculating inside the lungs, which is very time-consuming and the results could not provide additional information.

**Table IV-3.** Commands to create new masks for segmentation under 3D Slicer and Mimics<sup>®</sup>.

<b>Masks</b>	<b>Module</b>	<b>Command</b>
<b>3D Slicer</b>	Threshold	Editor / ThresholdEffect
<b>Mimics<sup>®</sup></b>	Threshold	Segmentation / Thresholding
	Dynamic Region Growth	Segmentation / Dynamic Region Growing
	Segmentation Airway	Pulmonary / Segment Airway

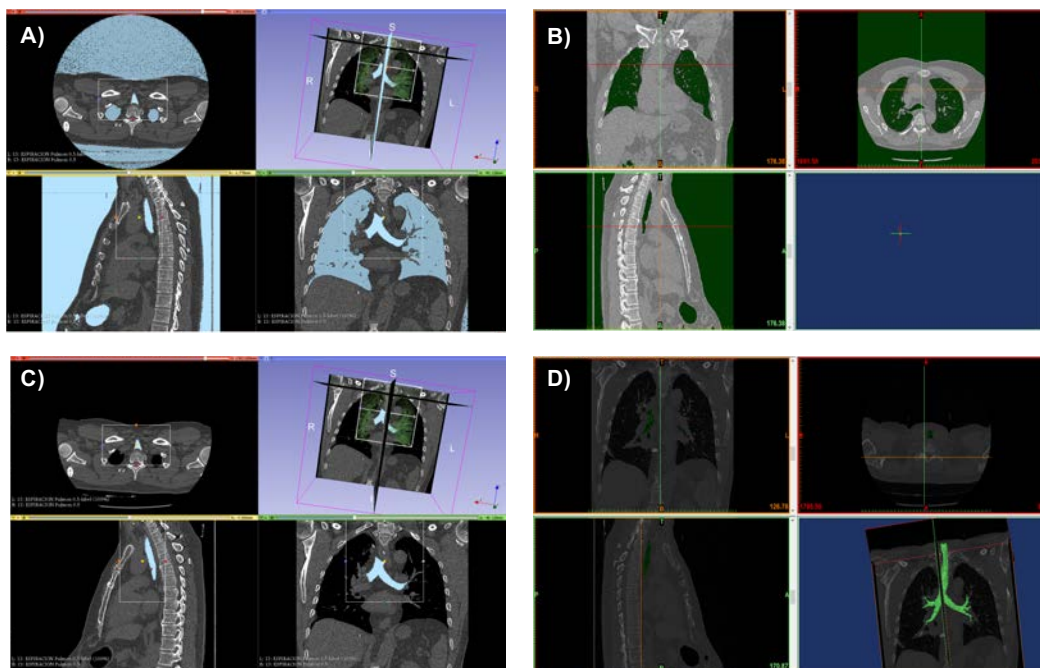


**Figure IV-5.** Visualization of different mask selection with threshold and 3D reconstruction. **A)** 3D Slicer mask (blue) definition between -1,050 to -200 HU and **B)** Mimics® mask (green) definition between -1024 to -600 HU. Final mask after manually edited the selected pixels in **C)** 3D Slicer (blue) and **D)** Mimics® (green).

As it can be observed in Figure IV-5, the manual threshold works in both cases by just adjusting the correct threshold range, by trial and error (despite the previously defined values), but not only the desired area (airway) was selected. Instead, as mentioned before, other tissues, such as lungs and air cavities were selected. Therefore, a manual process to edit each mask, slice by slice, was necessary to correct the erroneously selected pixels. There are some commands that can perform manual operations or semi-automatic operations. Manual commands, Table IV-4, work as a paintbrush or eraser to add or remove pixels, while the semi-automatic commands work by removing or adding pixels at the border of all islands of the currently selected layer mask. This hand-made pixels' edition increased the quality of the masks, however it was very time-consuming and due to the definition of the bronchial ramification, and the pixels' size, the decision to select or un-select some pixels was very subjective causing very low reproducibility.

**Table IV-4.** Selection of most used commands to edit mask pixels under 3D Slicer and Mimics®.

Masks	Command Effect	Function
<b>3D Slicer</b>	Paint	Add pixels' layer
	Erase	Remove pixels' layer
	Erode	Add pixels at border of islands
	Dilate	Remove pixels at border of islands
<b>Mimics®</b>	Cavity Fill	Fills internal gaps of the selected mask
	Edit mask	Add or remove pixels' layer

Besides preparing the masks by the manual threshold method, semi-automatic modules, such as the Dynamic Region Growth (DRG) and the Segmentation airway module (Segmentation Airway, SA) of Mimics® was used to create masks. In both cases, it was necessary to indicate a seed point or a start point in the inside of the trachea. For the DRG, the seed point set a base point with a value of greyscale, and then with a deviation range (defined by the user), the algorithm started to compare the grey values of the neighbouring pixels that obeyed the defined parameters. It was possible to provide additional seed points to increase the threshold range of the selected pixels. The combination of the seed point and the additional points created a minimum and a maximum range of greyscale values that act as a threshold. As a result, this command created a new mask that completely selected the airway with the lungs and the air cavities un-selected. However, in Figure IV-6, the generated mask with some pixels unidentified can be observed, showing that the obtained mask was not perfectly defined. Therefore, despite the high quality of the generated masks, a manual edition with the previously commented limitations was necessary. In contrast, the Segment Airway module (SA) is a command that semi-automatically segments the airway track using a comparison between the contrast of the airway regions and the airway wall. If a decrease in the contrast was detected, this indicated that there was a leakage. In such regions, the segmentation leaked into the pulmonary parenchyma and subsequently, lung tissue was erroneously selected as airway. However, low values of leakage found and selected higher numbers of airway branches. As it can be observed, SA gave a mask with higher definition of the airway track than DRG and in addition, a higher number of bronchial branches was observed, while in DRG it was very difficult to obtain due to the manual process required.



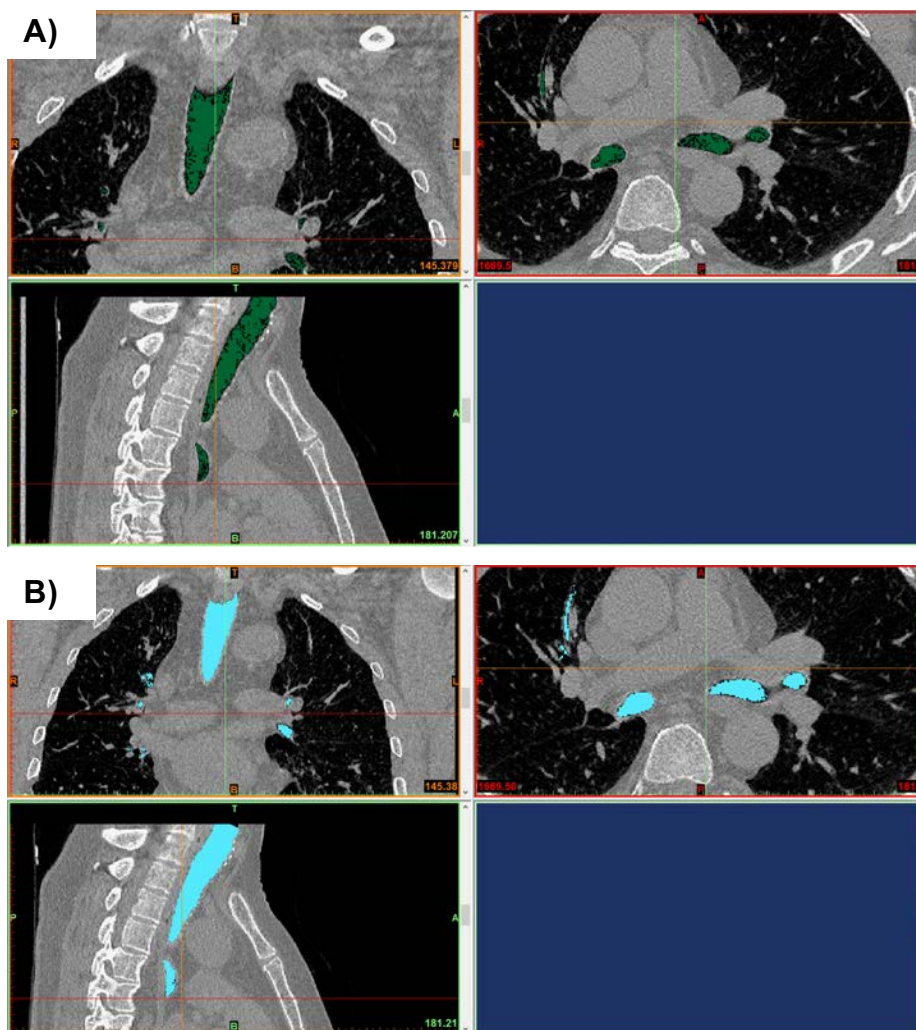


**Figure IV-6.** Overview of the generated mask by different methods. **A)** Dynamic Region Growth (DRG) and **B)** Segment Airway (SA).

After the segmentation and mask generation, it was possible to generate a 3D model with the information of the selected points in the mask. During the 3D model generator, it was possible to define several parameters to create the 3D object, such as the label from which the information is extracted, the matrix and triangle reduction, and the smoothing.

**Table IV-5.** Selection of the most used commands to edit mask pixels under 3D Slicer and Mimics®.

Masks	Command Effect
3D Slicer	Model Maker
Mimics®	Calculate 3D from mask

These parameters were used to create the 3D model by means of triangulation of the segmented area. It is important to highlight that the number of triangles determines the quality of the reconstruction, higher number of triangles resulted in a higher quality 3D model. However, a greater number of triangles required greater requirements of memory and calculations. In this context, the matrix reduction can be very useful because allows grouping of voxels to calculate triangles resulting in reduced calculation times, but also reducing the quality of the final reconstruction. Additionally, rough surfaces can be smoothed using the “smooth” function, which works as a noise filter. This filter function increases the finished quality of the 3D object, but greater number of iterations of smoothing factor could turn 3D object into a sphere-like object. Normally, small number of iterations are recommended, specially with a high smooth factor.

In Figure IV-7, the results of the 3D object generation can be observed. The 3D model generated using the masks obtained by the threshold method showed no bronchial branches. Only the left and right bronchus, with only few millimetres of the intermediate trunk and the upper lobe of the right bronchus were observed. Despite the good quality and definition of the object, this low ramification was expected because the mask did not contain the ramification information due to the difficulty to manually select the airway track. However, the 3D object generated by the DRG mask showed a high number of ramifications because the semi-automatic algorithm was able to identify differences in the threshold values. But despite this high number of branches, the airway track was not well defined, with great number of holes and noise because it requires several additional seed points to obtain all the threshold ranges that presents the airway. Nevertheless, it was important to take into account that great number of seed points in order to obtain a wide range of thresholds could lead to additional tissues selection, such as the lungs. Finally, the SA module showed more reliable results. The resulting objects showed more defined airway track and additionally more ramification branches (depending on the leakage factor). This semi-automatic algorithm compares the contrast between the airway and the airway wall and was developed and optimized to segment the airway track. Therefore, the resulting masks showed higher definition and results than the other methods. However, as mentioned before, high number of leakage detection could difficult the mask selection (with large calculations time) and a 3D object with high amount of structures.

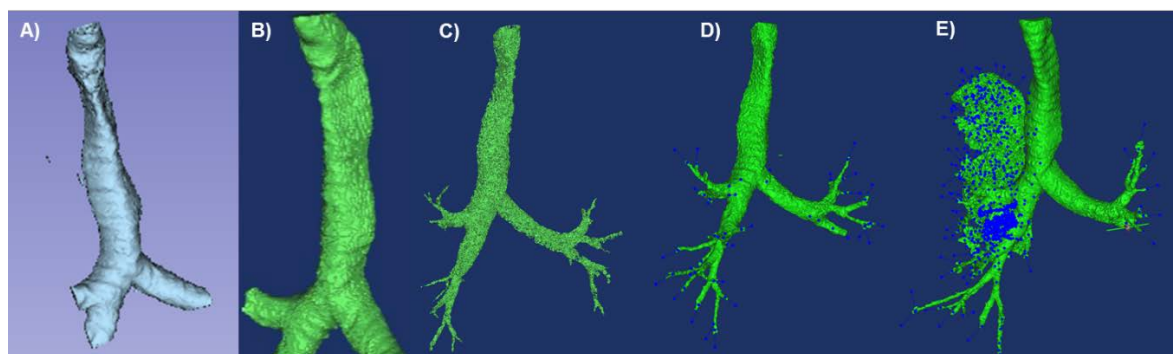


**Figure IV-7.** 3D reconstruction of masks obtained by different methods. **A)** 3D reconstruction of generated mask by threshold method in 3D-Slicer. **B)** 3D reconstruction of generated mask by threshold method in Mimics®. **C)** 3D reconstruction of generated mask by the Dynamic Region Growth with values of threshold about -1,024 HU to -960 HU. **D)** 3D reconstruction of the mask generated by the Segmentation airway module with 75% of strong leakage detection. **E)** 3D reconstruction of the mask generated by the Segmentation airway module with 0% of strong leakage detection.

Additionally, the matrix reduction and the smoothing tool was evaluated to compare the different results. In Figure IV-8, different parameters used to generate the 3D models can be observed. When 3D model generation was used with low quality, the obtained object showed no homogeneous surface with low definition. Low quality only showed a matrix reduction with a ratio 6:3, causing great number of grouped triangles, which was translated into to low definition of the surfaces. However, when the matrix reduction is reduced (from 6:3 to 1:1), the definition of the object surface increased (medium, high and optimal quality). In addition, when the smooth factor was used, the rough surfaces were smoothed reducing the noise (high quality). But, as expected, differences between low and high values of smooth factor, lead to noised or polished surfaces. Comparison between high and optimal quality, lower matrix reduction should result in an increase of the surface definition. However, the smooth factor was reduced too, causing lower polish effect. Thus, the resulting object showed good definition of the branches and the airway track, but very noised surface.

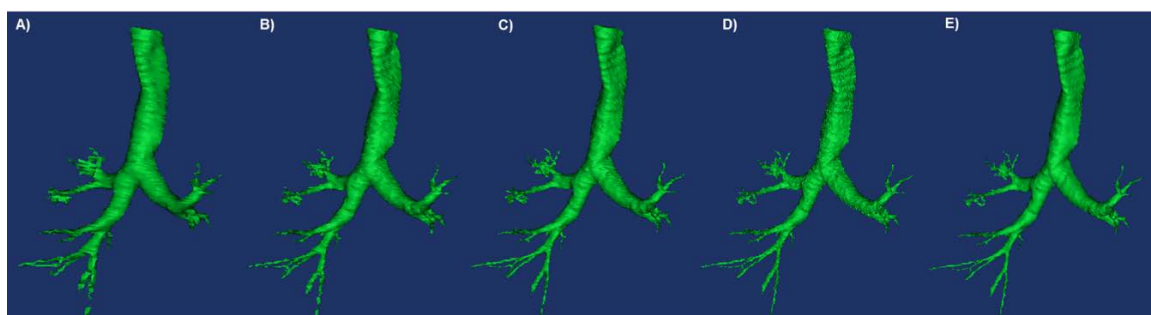


**Figure IV-8.** Different 3D models generated from the same segmentation using Segment Airway module. **A)** model generated with “Low” quality (6:2, matrix reduction); **B)** generated with “Medium” quality (3:2 matrix reduction); **C)** generated with “High” quality (2, iteration; 0.5, smooth factor; 2:1, matrix reduction and no triangle reduction); **D)** generated with “Optimal” quality (2, iteration; 0.3, smooth factor; 1:1, matrix reduction and triangle reduction); and **E)** model generated by “Custom” quality (3, iteration; 0.7, smooth factor; 1:1, matrix reduction and triangle reduction).

As observed in the previous results, the final 3D model generation requires some parameters that must be defined by the user. Therefore, in order to obtain an optimal 3D model, it is necessary to edit some of the parameters. In this case, Mimics<sup>®</sup> software recommends the use of the optimal conditions, however due to the pixelation and noise in the surface of the generated object, it was necessary to use customized conditions with the same parameters than optimal quality, but increasing the smooth factor to obtain a more smooth and polished surface.

Despite both software allowed to segmented the patients' information to extract a mask of the desired structure and generate a 3D model, Mimics<sup>®</sup> presents additional robust modules, such as advanced manual editing commands or DRG and SA, which results in better mask qualities. Additionally, the 3D module generation show additional parameters and calculations modules that result in better 3D objects. However, in this case, price and simplicity could tip the balance to the free-software (3D-Slicer).

After the 3D model generation, the obtained structure was exported as a STL. This allowed to perform CAD/CAE operations with the structure to design a suitable tracheal stent to reduce migration and avoid granulation tissue. Once the STL file was imported into a CAD software, modifications such as deletion or addition of certain features and dimensions sizing was performed to redesign the stent. Additionally, considering the previous discussion about the difficulty to print silicone with AM, the redesigned STL file was used to create an injection mould to be filled with silicone and obtain a silicone airway.

#### **4.3.2 Treatment and modelling of the STL file**

After the data segmentation and 3D model creation, the resulting object was imported into a CAD software. In this work 3-matic<sup>®</sup> (Mimics Innovation Suite<sup>®</sup>) was used. This software has a specific module specially developed to treat meshes facilitating the treatment and modelling.

To import an STL file to 3-matic<sup>®</sup>, can be easily drag to the software interface or through File / Import Part. Then, a fix module is used to analyse the quality of the imported triangles. The module analyses inverted triangles, bad edges, shells, overlapping and intersecting triangles. When the previous generated STL was imported (in Custom quality), errors about the last three parameters were found. The module fixed and eliminated the errors, but in some cases (shells and overlapping triangles), the module required a manual interaction because the automatic algorithm was not able to solve the problem due to the complexity of the triangles. However, in Figure IV-9-A, it can be observed that the problematic errors were triangles of regions with complex geometries, located where the mask lost its definition.

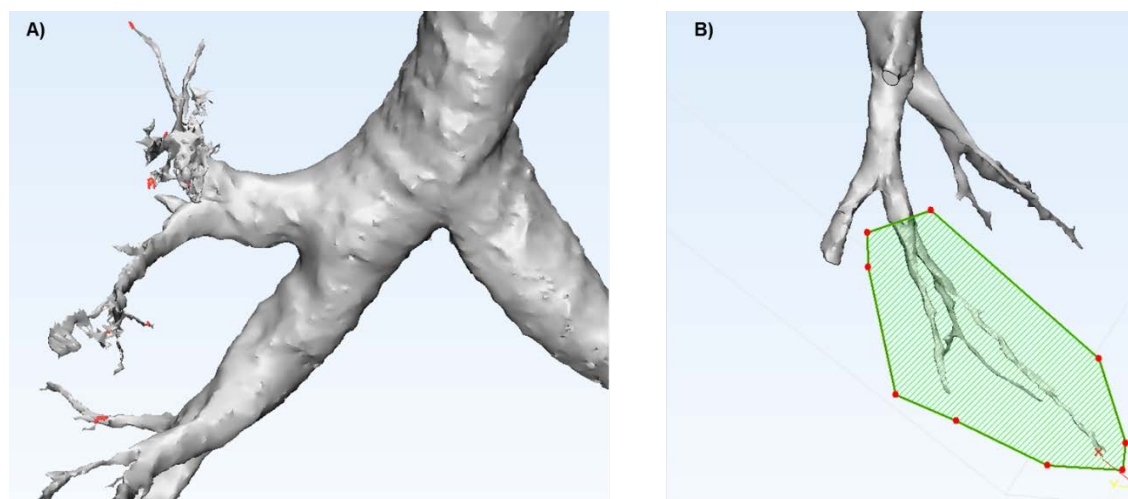


**Figure IV-9.** Overview of the branched airway. **A)** Selected errors (overlapped triangles, in red) by the fix module. **B)** Cut process of the noised branches.

For the current work, with the trachea, right primary bronchus, left primary bronchus and few millimetres of right upper lobe and intermediate trunk was sufficient to design a silicone tracheal stent as a proof of concept. Therefore, the noised ramified branches of the airway track were deleted, Table IV-6, because no additional information was provided and consequently, the overlapped triangles errors were eliminated. Thus, the resulting mesh were cleaned and fixed and the model was simplified.

**Table IV-6.** Most used commands to crop the STL file in 3-matic®.

Masks	Command
3-matic®	Finish / Trim or Design / Create Datum Plane and Design / Cut

Once the model is analysed and cleaned, the structure required additional operations to redesign the stent. As commented before, stent consists on a concentric cylindrical tube to allow the air pass, but the current 3D object it was only a triangle mesh. Therefore, the next step consisted in generating an offset of the current mesh to create a hollow structure. The 3-matic® software has a command to generate an inside, outside or both directions offset to the mesh. Considering that stents were anchored on the trachea by applying mechanical pressure, they required to be oversized normally, about a greater oversizing of 10% to 20% than the maximal tracheal diameter to avoid stent migration.<sup>53,54</sup> These values range is chosen to avoid radial stress on the tracheal tissue and therefore reduce in-stent restenosis.<sup>55,56</sup> In Figure IV-10, a 1.5 mm outside offset can be observed, corresponding to an oversize of 19% to a tracheal diameter of 16 mm.

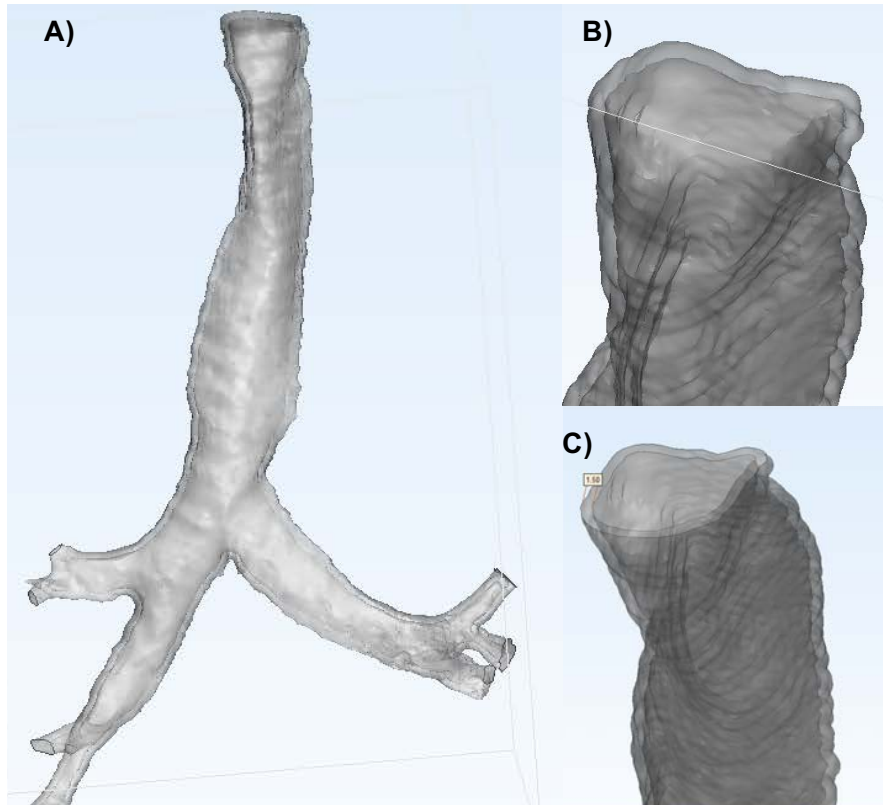


**Figure IV-10.** Oversized trachea with 1.5 mm offset. For a 16 mm tracheal diameter this offset increase in a 19% the final diameter of the stent. **A)** General overview of the resulting oversized trachea model with 2 surfaces. **B)** Zoom of the top region of the trachea model with the 2 surfaces. **C)** Cut of the top region of the trachea to observe the 2 meshes with an oversize of 1.5 mm.

After the model was trimmed and the desired offset, between 10-20%, was applied, the model was ready to export as STL file in order to print. However, due to the different applied operations, the *Fix Module* was used to analyze the object. Then, the new 3D object was exported as STL file from the File menu.

#### 4.3.3 3D Printing of extracted model

Once the model was analyzed, edited and exported to STL, it was imported into the Insight<sup>®</sup> software from Stratasys<sup>®</sup> to print using the FDM Fortus 400mc<sup>®</sup> and to Stalactite Workshop to print using the stereolithography printer Stalactite. First, the model was imported into the FDM software with the back surface of the trachea lying down to the printing cuvette. Then, because the inside of the trachea model was empty and the low planarity of the trachea surface, it was necessary to fill the trachea with support material and create a support base in order to avoid errors during the printing process. After around 5h of printing process, the trachea object was printed in PC with SR-100<sup>™</sup> acting as a support material. This type of support was selected because it can be eliminated using a hot sodium hydroxide solution. In Figure IV-11, the printed trachea model (in white) can be observed in the printing cuvette after the printing process was finished. Additionally, the support material (in brown) used to fill the cavity of the airway track can be observed. After the printing process, the resulting object was incubated in a heated sodium hydroxide solution to remove the support material and then, the trachea model was washed



with Milli-Q water and rinsed with ethanol. The resulting printed trachea model showed rigid properties because it was printed in polycarbonate and all the anatomical detail of the patient. However, due to the FDM technology, the use of support material to fill all the empty cavities could be a drawback because could difficult the printing of an injection mold with all the necessary cavities to inject the silicone.

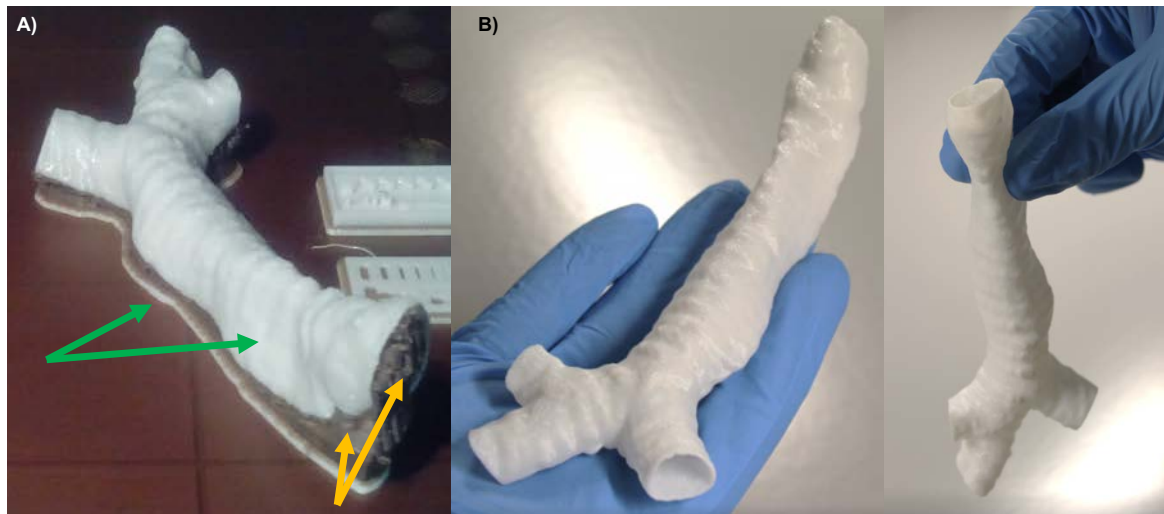


**Figure IV-11.** 3D-printed trachea model using FDM technology (Fortus 400mc®). **A)** 3D-printed model in the printing cuvette of the printer with the support material, and **B)** resulting 3D model without the support material. Green arrow (printing material, polycarbonate) and yellow arrow (support material, SR-100™).

Therefore, a stereolithography printer (Stalactite 102) was used to print the trachea. This technology was selected because as its name reflects, the objects were built from top to bottom. In this case, the light source was a commercial video projector that irradiates, with a defined pattern, to a mirror which is under a photocurable liquid resin. The platform was moved upwards when each layer was photopolymerized. The printer resolution was at Z axis, layer thickness, from 100 to 25  $\mu\text{m}$ , and at XY axis, construction area, from 100 to 50  $\mu\text{m}$ . The printing speed was approximately 30 mm/h at 100  $\mu\text{m}$  resolution, at Z axis.

Once the STL file was loaded into the printer software, the object was located on the building area of the printer. Then, the object was rotated to ensure a correct centre of mass because the object was printed vertically. Considering that some parts of the trachea required supports, the trachea was located over a resin base to anchor the vertical supports and facilitate the cutting of the object from the printing platform. In Figure IV-12, the positioning of the trachea model with the supports on the printing platform can be observed. After the set-up, the slicing was performed to transform the printing object into a series of slices. Then, the printer started to project each layer onto the liquid resin in contact with the printing platform. After each layer, the platform moved upward and the next layer was printed. At the end, of the printing process, the object, with the corresponding supports, was obtained hanging from the printing platform. The printed object was cut from the platform and the supports were removed. In almost all cases, after the washing treatment with water and ethanol, the printed object showed sticky properties

as a consequence of non-photocured resin. Therefore, the object was placed under a cabin with visible light to photocure the non-photopolymerized resin and eliminate the sticky properties.

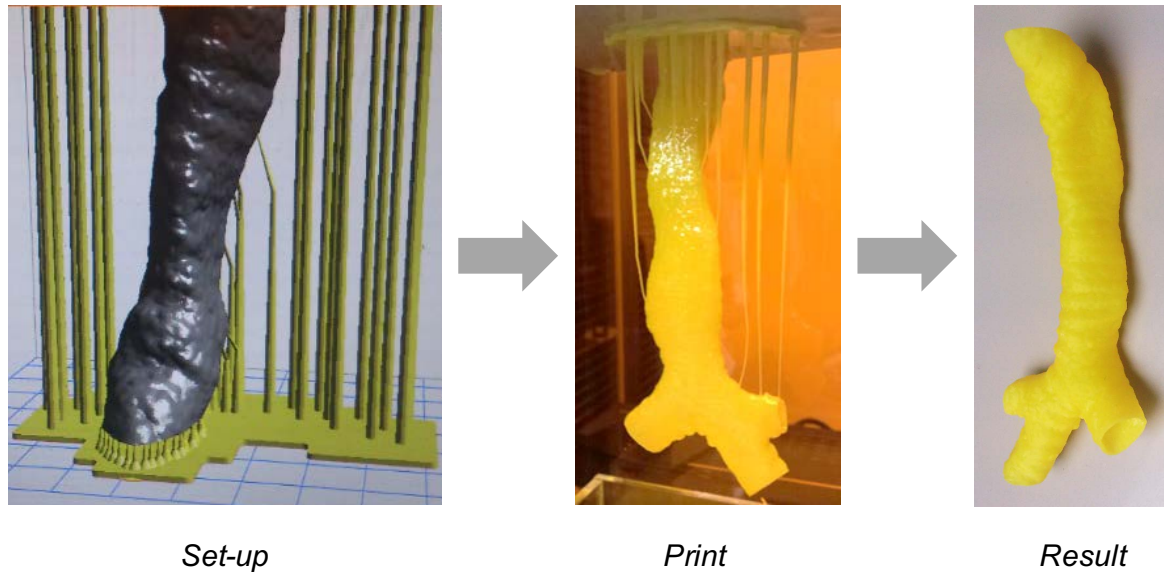


**Figure IV-12.** Printing process of the trachea model using the Stalactite printer. During the set-up, the model was placed in the printing platform and the base and supports were designed. After the set up and the slicing process, the trachea and the supports were printed layer by layer. Finally, after cutting the trachea model from the supports, the object was washed with Milli-Q water and ethanol and photocured under visible light if necessary.

The previous results showed the great feasibility of 3D printing technology to print sophisticated geometries, such as anatomical geometries extracted from patients. Additionally, both technologies used in this work were able to use previously edited STLs' created from a patient scanner. However, due to the printing process technology, stereolithography showed better results than FDM because of the printing orientation and the use of liquid material.

#### 4.3.4 Mould design of anatomical silicone tracheal stent

As mentioned before, this work pretends to develop a process to obtain anatomical medical devices combining revolutionary new technologies (AM) with classical manufacturing techniques, such as molds. Therefore, in order to move forward to achieve the aim of this work, it was necessary to develop an anatomical mold capable to be injected with silicone.

Therefore, the first step consisted in the importation of the previous STL file and the triangles mesh was analyzed and fixed with 3-matic<sup>®</sup>. Then, a 1.5 mm offset was generated to create the cavity of the mold where the silicone will be injected. In order to minimize the complexity of the mold, the bronchus and their ramifications were deleted from the trachea airway, just to select the trachea segment. Then, a rectangular hexahedron, Figure IV-13, was created using the command *Create Mold Shape* under the *Tooling* module. In this case, the hexahedron was adjusted to the trachea in order to minimize the use of material. Then, it was necessary to create the mould cavity from the trachea airway. To do so, a



*Boolean Subtraction* operation was performed from the *Design* menu and selecting the tracheal airway as subtraction entity.

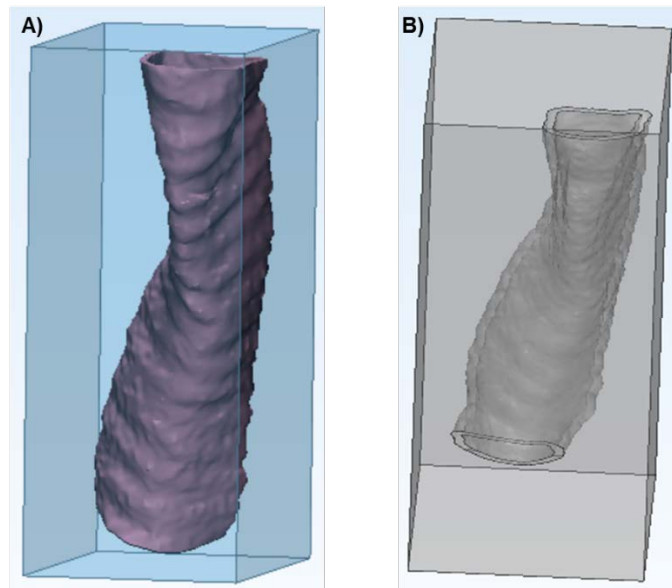


**Figure IV-13.** Mould cavity creation from the trachea airway. **A)** Creation of a rectangular hexahedron over the edited trachea and **B)** Resulting mould cavity with subtracted trachea airway.

Once the mold cavity with the anatomical geometry of the trachea airway was performed, it was necessary to create the injection channels to facilitate the silicone injection. Initially, due to the low viscosity of the PDMS, top channels should be sufficient to fill the mold with silicone by gravity. However, additional channels were designed to increase the filling process, avoid empty spaces and facilitate air release and oxygen diffusion. Channels were designed by drawing lines in the mold using different drawn plans. Firstly, using the *Sketch* menu, new planes were created (*New Sketch*) to anchor the channels. Secondly, the *Create Line* command allowed to draw channels on the desired location between the external surface of the mold box and the external surface of the trachea, using the previous created planes. Diameters (1 mm) were provided using the *Create Runner* command, and finally, a *Boolean Subtraction* operation between the mold box and the created channels was performed to open the channels. In Figure IV-14, the resulting mold can be observed with different channels to inject silicone and to allow air to be released during the injection process in order to avoid empty spaces.

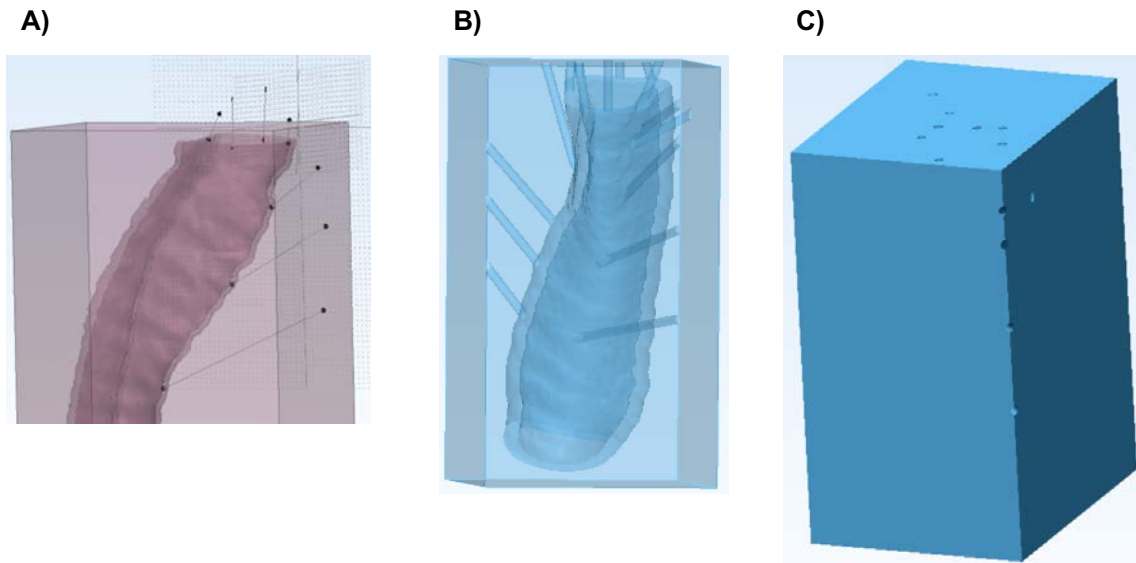


**Figure IV-14.** Injection mould with different channels for injection and air release. **A)** Sketch of different channels created in the mould, **B)** Channels generation over the mould with 1 mm of diameter, and **C)** external mould overview to observe the entries of each channel.

Finally, after the channels creation the mould was almost ready to be printed. However, as mentioned previously, the aim of this fabrication was to inject silicone and then unmount the silicone stent by breaking the mould. Therefore, to facilitate the stent cutting and to reduce material and weight, the mould was emptied using the previous commented *Hollow* command (*Design* menu) leaving a wall thickness of 1 mm. In Figure IV-15, the final design of the mould with the channels and the emptied box can be observed. The top of the trachea design was anchored to the top layer of the mould box, using injections channels, to avoid the use of supports.

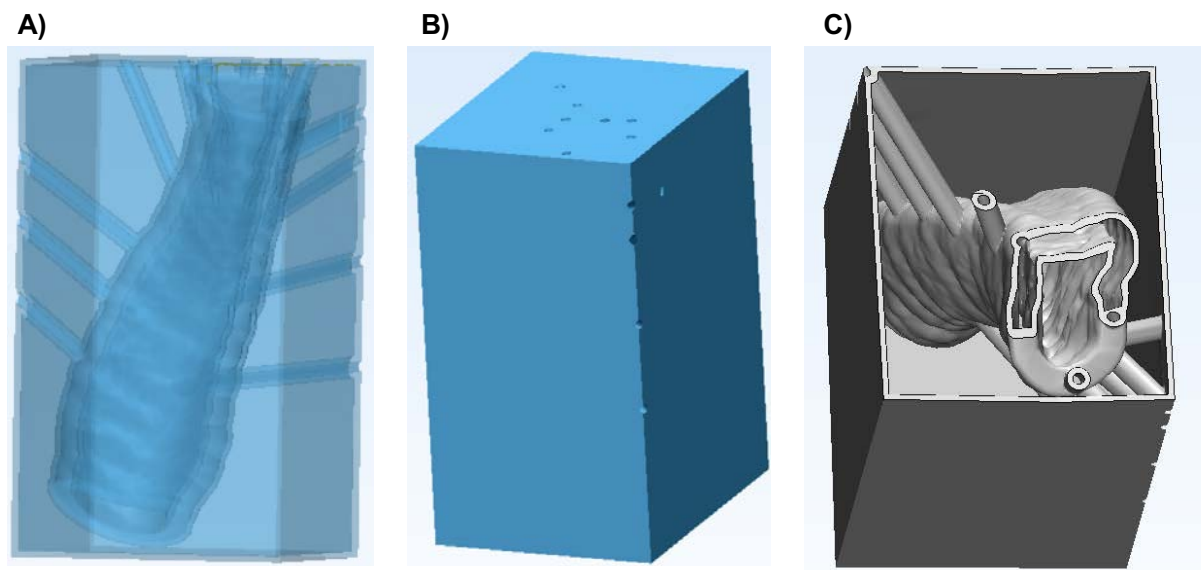


**Figure IV-15.** Final design of the tracheal stent mould to inject silicone. **A)** Internal mould overview of the trachea, channels and wall thickness, and **B)** external mould overview with the channels entries. **C)** Overview of the internal parts of the designed mould.

#### 4.3.5 3D Printing of Designed Mould and PDMS injection

Once the mold was designed, the next step was to use the 3D printing technology to manufacture the personalized mold. Considering the design of the mold, the FDM technology will manufacture the box of the mold completely solid using high quantities of support material. Additionally, channels and the trachea reservoir for the silicone would be printed using support material, which would be difficult to wash and to empty the mold. Therefore, the mold was printed using the stereolithography to avoid the requirement of supports and to reduce the material because the non-reacted liquid resin will fall to the cuvette, leading the mold box empty of liquid.

The trachea mold was printed similarly to the previous trachea model using stereolithography and with the top part of the mold box anchored to the printing platform to avoid the use of additional supports. In Figure IV-16, the printing process of the mould with a stereolithography can be observed. The mold was anchored to the printing platform because the channels were additionally used to anchor the internal part of the mold to avoid additional supports.

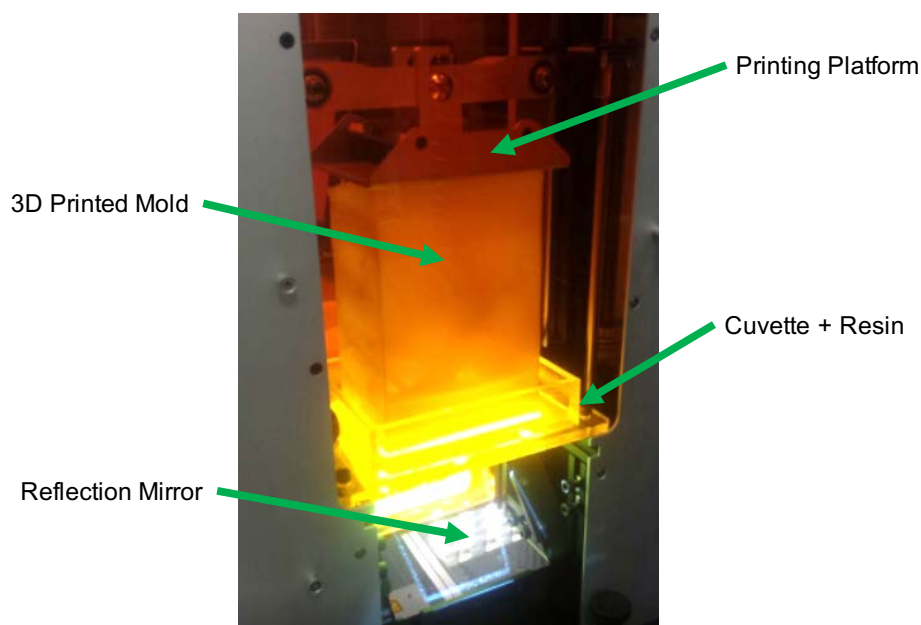


Figure IV-16. Image of the mold's printing process with a stereolithography printer.

After the mould's printing, it was washed with Milli-Q water and ethanol to remove non-cured resin. After the washing treatment, the mould was still sticky because the resin was not completely cured. Therefore, the mould was placed under visible light for 30-60 min to finish the curation process. Then, after the resin was completely cured, the PDMS kit was prepared and injected using 1-2 mL syringe through the injections channels. To facilitate the injection a new mould with additional channels on the top were designed and printed. The mould with the PDMS silicone was incubated at 75 °C for 3 h and after PDMS curation, the tracheal stent was released by breaking the mould. In some designs, with no additional channels for air release, the curation process was not performed homogeneously and the silicone of the most distal part from the top, remained liquid. This can be explained because of the

aeration process inside the mould. The PDMS silicone requires oxygen to cure effectively. Therefore, if the mould has not a good aeration process, the curation process cannot be performed. However, it was important to take into account that a high number of air channels could difficult the injection and the curation process because silicone can be leaked through those channels. In Figure IV-17, the resulting 3D tracheal stents can be observed. The obtained tracheal stents were easily cutted from the mould, which was easily broken. The silicone trachea was completely flexible, homogeneous, transparent. However, some air bubbles due to the non-continuous injection process were observed. The air bubbles could be solved using a vacuum line during the injection and the use of an automated high pressure syringe could increase the injection speed, reduce the air bubbles and facilitate the silicone to completely fill the mould. In addition, when the wall thickness was small, about 0.5-1 mm offset, some printing and injection problems occurred. Printing problems could be solved by adjusting the printing parameters, such as printing speed and XY and Z resolution. Lower printing speed showed more defined results because the resin was completely cured and the layer was better defined. Regarding to the injection problems with lower wall thickness, normal syringe was not able to apply enough pressure to facilitate the silicone to flow over all the geometry in order to fill all the mould. In this case, the use of an automated injection syringe with an injection connection on the mould could increase the silicone injection and the result of the silicone object.



**Figure IV-17.** Anatomical silicone stents manufactured using 3D printing technology in combination with mould fabrication.

#### **4.3.6 Silver deposition onto 3D anatomical stent**

Finally, after manufacturing of a patient's anatomically stent, the next step consisted in the addition of the antibacterial properties. Considering that no changes in the chemical composition of the material was performed, the 3D stent was made of silicone (PDMS), the previous developed antibacterial coatings were easily applied. Anatomically stent was placed in the PECVD reactor and the same plasma conditions and post-process (reductive sugar immobilization and metallic silver reduction) was performed. In Figure IV-18, the resulting antibacterial anatomically stent with antibacterial properties can be observed. Despite the modification could be performed selectively on the desired surface side of the stent, the coating was deposited all over the surface of the material to avoid internal and external stent colonization. The most obvious colonization is formed on the internal side of the stent where the

mucus and the body fluids are flowing, however, the external side of the stent (in contact with the trachea wall) could present some holes between the trachea rings and the surface of the stent (even in an anatomically designed stent because it is oversized) which are interesting anchor sites for bacteria to colonize and grow.



**Figure IV-18.** Patient's anatomical stent with antibacterial properties

The resulting stent, showed and homogeneous metallic silver coating on the surface with flexible properties and completely adapted to the complex geometries of the manufactured stent. These results showed the novelty of the previous developed surface modifications indicating that the developed coating can be applied on different geometries, not only on flat plates (2D) but in 3D structures such as cylindrical and anatomical tubes.

This resulting 3D manufactured stent using patient's information with antibacterial properties is a proof of concept of the next generation of medical devices. These devices combine bioactivities, functionalities and device-tissue interaction that increase the biocompatibility and the biofunctionality avoiding post-implantation problems, such as stenotic tissue, granuloma, migration, pain, colonization and tissue rejection.

## 4.4 Concluding Remarks

The described methodology showed the ability of the current available visualizers' software to interpret DICOM images and extract different masks of the desired tissues. Additionally, different selection methods can be used, being the semi-automatic the most interesting because is faster, more reliable and provides a higher degree of detail than the manual methods.

Moreover, once the tissue was selected, the pixels were easily transformed into triangles using the 3D conversion commands, resulting in a 3D construction of the object. In addition, the use of specific software, such as 3-matic<sup>®</sup>, allowed to treat the triangles, fixing segmentation problems such as inverted triangles, bad edges, shells, overlapping and intersecting triangles. Furthermore, the software provides sketch's modules that allowed to design parts of the 3D object, even with the possibility to re-design the 3D object. Additionally, this work showed the ability of the CAD design to easily create injections moulds for the anatomical objects. Finally, the CAD object was exported to a 3D printers format, STL.

Besides the CAD design, this work used two types of additive manufacturing technologies to fabricate the designed anatomical object. In this case, the trachea airway was manufactured using FDM and stereolithography technology, being the latter more interesting because of the reduction of the support material. This effect was more important for the mould printing in which the FDM was required to fill almost all the mould with support material. However, the stereolithography resulted in a mould free of support material.

The obtained 3D printed object was manufactured using PDMS to demonstrate the feasibility of the technology and workflow. Despite PDMS cannot be implanted in humans, it acted as a control to evaluate the manufacturing proceedings. Additionally, PDMS kit showed low viscosity and could be injected easily into the manufactured mould, however, the viscosity of medical silicone is higher than PDMS and cannot be injected easily. Therefore, in future developments, the silicone injection process must be redefined to be adapted to medical silicone properties.

Considering that a future final prosthesis should be implanted, the prosthesis must be sterilized. Therefore, this work obtained a silicone-based prosthesis, however, the future medical grade silicone prosthesis can be easily sterilized using typical sterilization processes, such as oxygen plasma, an autoclave or even ethylene oxide.

As previously commented, the medical community requires new personalized solutions to avoid low adaptability causing migration problems, high acute pain and granulation tissue formation. The previous results showed the high potential of this technology to create new anatomical silicone stents. The previous workflow demonstrate the high potential of this methodology to extract, customize, design and manufacture personalized medical devices, such as anatomical models<sup>57</sup>, implants<sup>58</sup> or even surgical instruments<sup>59</sup>.

Finally, resulting anatomically 3D manufactured stent with antibacterial properties were easily modified with the previously developed antibacterial coating showing and homogeneous metallic silver coating covalently attached to the surface of the stent. The coating was completely flexible and adapted to the stent geometries avoiding cracking and delamination.

These results are completely in combination with the previous chapters in this work. As observed in the previous chapter, flat plates and even cylinders can be easily modified to provide antibacterial properties to avoid bacteria colonization and biofilm formation. In addition, an adapted version of the previously developed coating has been used in combination with degradable nanoparticles capable to entrap hydrophobic drugs, to release antiproliferative drugs, such as paclitaxel. Both chapters used the plasma deposition process, which showed high versatility to modify complex structures, and therefore, the 3D printed structures developed in this chapter could easily incorporate the previously developed properties, i.e. antibacterial and drug delivery features.

## 4.5 References

- (1) Walser, E. M. Stent placement for tracheobronchial disease. *Eur. J. Radiol.* **2005**, 55 (3), 321–330 DOI: 10.1016/j.ejrad.2005.03.005.
- (2) Bacon, J. L.; Patterson, C. M.; Madden, B. P. Indications and interventional options for non-resectable tracheal stenosis. *J. Thorac. Dis.* **2014**, 6 (3), 258–270 DOI: 10.3978/j.issn.2072-1439.2013.11.08.
- (3) Wassermann, K.; Mathen, F.; Eckel, H. E. Concurrent glottic and tracheal stenoses: Restoration of airway continuity in end-stage malignant disease. *Ann. Otol. Rhinol. Laryngol.* **2001**, 110 (4), 349–355.
- (4) Fiorentino, A.; Marena, G.; Ceretti, E.; Piazza, C.; Hendrichs, N. Challenges in design and production of customized tracheal stents. In *High Value Manufacturing: Advanced Research in Virtual and Rapid Prototyping*; CRC Press, 2013; pp 597–602.
- (5) Saito, Y.; Imamura, H. Airway Stenting. *Surg. Today* **2005**, 35 (4), 265–270 DOI: 10.1007/s00595-004-2942-y.
- (6) Ugarte, D.; Izaguirre, A.; Rosell, A. Personalised Trachea Stent Designer: A Knowledge Feature. *Procedia CIRP* **2012**, 3 (1), 597–601 DOI: 10.1016/j.procir.2012.07.102.
- (7) MacKenzie, C. F.; McAslan, T. C.; Shin, B.; Schellinger, D.; Helrich, M. The shape of the human adult trachea. *Anesthesiology* **1978**, 49 (1), 48–50.
- (8) Mehta, S.; Myat, H. M. The cross-sectional shape and circumference of the human trachea. *Ann. R. Coll. Surg. Engl.* **1984**, 66 (5), 356–358.
- (9) Pérez del Palomar, A.; Trabelsi, O.; Mena, A.; López-Villalobos, J. L.; Ginel, A.; Doblaré, M. Patient-specific models of human trachea to predict mechanical consequences of endoprosthesis implantation. *Philos. Trans. A. Math. Phys. Eng. Sci.* **2010**, 368 (1921), 2881–2896 DOI: 10.1098/rsta.2010.0092.
- (10) Stone, P. H.; Coskun, A. U.; Kinlay, S.; Clark, M. E.; Sonka, M.; Wahle, A.; Ilegbusi, O. J.; Yeghiazarians, Y.; Popma, J. J.; Orav, J.; et al. Effect of endothelial shear stress on the progression of coronary artery disease, vascular remodeling, and in-stent restenosis in humans: in vivo 6-month follow-up study. *Circulation* **2003**, 108 (4), 438–444 DOI: 10.1161/01.CIR.0000080882.35274.AD.
- (11) Petersen, B. D.; Uchida, B. T.; Barton, R. E.; Keller, F. S.; Rösch, J. Gianturco-Rösch Z Stents in Tracheobronchial Stenoses. *J. Vasc. Interv. Radiol.* **1995**, 6 (6), 925–931 DOI: 10.1016/S1051-0443(95)71214-3.
- (12) Lee, P.; Kupeli, E.; Mehta, A. C. Airway Stents. *Clin. Chest Med.* **2010**, 31 (1), 141–150 DOI: 10.1016/j.ccm.2009.08.002.
- (13) Ko, P.-J.; Liu, C.-Y.; Wu, Y.-C.; Chao, Y.-K.; Hsieh, M.-J.; Wu, C.-Y.; Wang, C.-J.; Liu, Y.-H.; Liu, H.-P. Granulation formation following tracheal stenosis stenting: Influence of stent position. *Laryngoscope* **2009**, 119 (12), 2331–2336 DOI: 10.1002/lary.20615.
- (14) Hramiec, J. E.; Haasler, G. B. Tracheal wire stent complications in malacia: Implications of position and design. *Ann. Thorac. Surg.* **1997**, 63 (1), 209–213 DOI: 10.1016/S0003-4975(96)00925-3.
- (15) Smith, J. A.; Seyfarth, A. Patient-adaptable biomedical devices: Benefits and barriers for granting patients more control. In *BIODEVICES 2008 - Proceedings of the 1st International Conference on Biomedical Electronics and Devices*; 2008; Vol. 1, pp 245–248.



- (16) Jun, Y. Morphological analysis of the human knee joint for creating custom-made implant models. *Int. J. Adv. Manuf. Technol.* **2011**, 52 (9–12), 841–853 DOI: 10.1007/s00170-010-2785-1.
- (17) Gompelmann, D.; Eberhardt, R.; Schuhmann, M.; Heussel, C. P.; Herth, F. J. F. Self-expanding Y stents in the treatment of central airway stenosis: a retrospective analysis. *Ther. Adv. Respir. Dis.* **2013**, 7 (5), 255–263 DOI: 10.1177/1753465813489766.
- (18) Saji, H.; Furukawa, K.; Tsutsui, H.; Tsuboi, M.; Ichinose, S.; Usuda, J.; Ohira, T.; Ikeda, N. Outcomes of airway stenting for advanced lung cancer with central airway obstruction. *Interact. Cardiovasc. Thorac. Surg.* **2010**, 11 (4), 425–428 DOI: 10.1510/icvts.2010.238196.
- (19) Melgoza, E. L.; Vallicrosa, G.; Serenó, L.; Ciurana, J.; Rodríguez, C. a. Rapid tooling using 3D printing system for manufacturing of customized tracheal stent. *Rapid Prototyp. J.* **2013**, 20 (1), 2–12 DOI: 10.1108/RPJ-01-2012-0003.
- (20) Singare, S.; Liu, Y.; Li, D.; Lu, B.; Wang, J.; He, S. Individually prefabricated prosthesis for maxilla reconstruction. *J. Prosthodont.* **2008**, 17 (2), 135–140 DOI: 10.1111/j.1532-849X.2007.00266.x.
- (21) Sun, J.; Xi, J.; Chen, X.; Xiong, Y. A CAD/CAM system for fabrication of facial prostheses. *Rapid Prototyp. J.* **2011**, 17 (4), 253–261 DOI: 10.1108/13552541111138379.
- (22) Rengier, F.; Mehndiratta, A.; Von Tengg-Kobligk, H.; Zechmann, C. M.; Unterhinninghofen, R.; Kauczor, H. U.; Giesel, F. L. 3D printing based on imaging data: Review of medical applications. *Int. J. Comput. Assist. Radiol. Surg.* **2010**, 5 (4), 335–341 DOI: 10.1007/s11548-010-0476-x.
- (23) Ryan, G. E.; Pandit, A. S.; Apatsidis, D. P. Porous titanium scaffolds fabricated using a rapid prototyping and powder metallurgy technique. *Biomaterials* **2008**, 29 (27), 3625–3635 DOI: 10.1016/j.biomaterials.2008.05.032.
- (24) Wiria, F. E.; Shyan, J. Y. M.; Lim, P. N.; Wen, F. G. C.; Yeo, J. F.; Cao, T. Printing of Titanium implant prototype. *Mater. Des.* **2010**, 31 (SUPPL. 1), S101–S105 DOI: 10.1016/j.matdes.2009.12.050.
- (25) Zopf, D. A.; Hollister, S. J.; Nelson, M. E.; Ohye, R. G.; Green, G. E. Bioresorbable Airway Splint Created with a Three-Dimensional Printer. *N. Engl. J. Med.* **2013**, 368 (21), 2043–2045 DOI: 10.1056/NEJMc1206319.
- (26) Hinton, T. J.; Hudson, A.; Pusch, K.; Lee, A.; Feinberg, A. W. 3D Printing PDMS Elastomer in a Hydrophilic Support Bath via Freeform Reversible Embedding. *ACS Biomater. Sci. Eng.* **2016**, acsbiomaterials.6b00170 DOI: 10.1021/acsbiomaterials.6b00170.
- (27) Serra, T.; Planell, J. A.; Navarro, M. High-resolution PLA-based composite scaffolds via 3-D printing technology. *Acta Biomater.* **2013**, 9 (3), 5521–5530 DOI: 10.1016/j.actbio.2012.10.041.
- (28) Seitz, H.; Rieder, W.; Irsen, S.; Leukers, B.; Tille, C. Three-dimensional printing of porous ceramic scaffolds for bone tissue engineering. *J. Biomed. Mater. Res. - Part B Appl. Biomater.* **2005**, 74 (2), 782–788 DOI: 10.1002/jbm.b.30291.
- (29) Wu, C.; Fan, W.; Zhou, Y.; Luo, Y.; Gelinsky, M.; Chang, J.; Xiao, Y. 3D-printing of highly uniform CaSiO<sub>3</sub> ceramic scaffolds: preparation, characterization and in vivo osteogenesis. *J. Mater. Chem.* **2012**, 22 (24), 12288–12295 DOI: 10.1039/c2jm30566f.
- (30) Hong, S.; Sycks, D.; Chan, H. F.; Lin, S.; Lopez, G. P.; Guilak, F.; Leong, K. W.; Zhao, X. 3D Printing of Highly Stretchable and Tough Hydrogels into Complex, Cellularized Structures. *Adv. Mater.* **2015**, n/a--n/a DOI: 10.1002/adma.201501099.
- (31) Schuurman, W.; Khristov, V.; Pot, M. W.; van Weeren, P. R.; Dhert, W. J. a; Malda, J. Bioprinting of hybrid tissue constructs with tailorable mechanical properties. *Biofabrication* **2011**, 3 (2),

- 21001 DOI: 10.1088/1758-5082/3/2/021001.
- (32) Huang, Y.; Leu, M. C.; Mazumder, J.; Donmez, A. Additive Manufacturing: Current State, Future Potential, Gaps and Needs, and Recommendations. *J. Manuf. Sci. Eng.* **2015**, *137* (1), 14001 DOI: 10.1115/1.4028725.
- (33) Wong, K. V.; Hernandez, A. A Review of Additive Manufacturing. *ISRN Mech. Eng.* **2012**, *2012*, 1–10 DOI: 10.5402/2012/208760.
- (34) Melchels, F. P. W.; Domingos, M. A. N.; Klein, T. J.; Malda, J.; Bartolo, P. J.; Huttmacher, D. W. Additive manufacturing of tissues and organs. *Prog. Polym. Sci.* **2012**, *37* (8), 1079–1104 DOI: 10.1016/j.progpolymsci.2011.11.007.
- (35) Kolesky, D. B.; Homan, K. A.; Skylar-Scott, M. A.; Lewis, J. A. Three-dimensional bioprinting of thick vascularized tissues. *Proc. Natl. Acad. Sci. U. S. A.* **2016**, *113* (12), 3179–3184 DOI: 10.1073/pnas.1521342113.
- (36) Kolesky, D. B.; Truby, R. L.; Gladman, A. S.; Busbee, T. A.; Homan, K. A.; Lewis, J. A. 3D bioprinting of vascularized, heterogeneous cell-laden tissue constructs. *Adv. Mater.* **2014**, *26* (19), 3124–3130 DOI: 10.1002/adma.201305506.
- (37) Wipff, P. J.; Majd, H.; Acharya, C.; Buscemi, L.; Meister, J. J.; Hinz, B. The covalent attachment of adhesion molecules to silicone membranes for cell stretching applications. *Biomaterials* **2009**, *30* (9), 1781–1789 DOI: 10.1016/j.biomaterials.2008.12.022.
- (38) Qin, Z.; Compton, B. G.; Lewis, J. A.; Buehler, M. J. Structural optimization of 3D-printed synthetic spider webs for high strength. *Nat. Commun.* **2015**, *6* (May), 8038 DOI: 10.1038/ncomms8038.
- (39) Mannoor, M. S.; Jiang, Z.; James, T.; Kong, Y. L.; Malatesta, K. A.; Soboyejo, W. O.; Verma, N.; Gracias, D. H.; McAlpine, M. C. 3D printed bionic ears. *Nano Lett.* **2013**, *13* (6), 2634–2639 DOI: 10.1021/nl4007744.
- (40) Bélanger, M. C.; Marois, Y. Hemocompatibility, biocompatibility, inflammatory and in vivo studies of primary reference materials low-density polyethylene and polydimethylsiloxane: A review. *J. Biomed. Mater. Res.* **2001**, *58* (5), 467–477 DOI: 10.1002/jbm.1043.
- (41) Camci-Unal, G.; Alemdar, N.; Annabi, N.; Khademhosseini, A. Oxygen-releasing biomaterials for tissue engineering. *Polym. Int.* **2013**, *62* (6), 843–848 DOI: 10.1002/pi.4502.
- (42) Hinton, T. J.; Jallerat, Q.; Palchesko, R. N.; Park, J. H.; Grodzicki, M. S.; Shue, H.; Ramadan, M. H.; Hudson, A. R.; Feinberg, A. W. Three-dimensional printing of complex biological structures by freeform reversible embedding of suspended hydrogels. *Sci. Adv.* **2015**, *1* (October), 1–10 DOI: 10.1126/sciadv.1500758.
- (43) Bankier, A. a; O'Donnell, C. R.; Boiselle, P. M. Quality Initiatives Respiratory Instructions for CT Examinations of the Lungs: A Hands-on Guide. *RadioGraphics* **2008**, *28* (4), 919–931 DOI: 10.1148/rg.284085035.
- (44) Cheng, G. Z.; Estepar, R. S. J.; Folch, E.; Onieva, J.; Gangadharan, S.; Majid, A. Three-dimensional printing and 3D slicer powerful tools in understanding and treating structural lung disease. *Chest* **2016**, *149* (5), 1136–1142 DOI: 10.1016/j.chest.2016.03.001.
- (45) Egger, J.; Kapur, T.; Nimsky, C.; Kikinis, R. Pituitary Adenoma Volumetry with 3D Slicer. *PLoS One* **2012**, *7* (12), 1–7 DOI: 10.1371/journal.pone.0051788.
- (46) Fedorov, A.; Beichel, R.; Kalphaty-Cramer, J.; Finet, J.; Fillion-Robbin, J.-C.; Pujol, S.; Bauer, C.; Jennings, D.; Fennessy, F.; Sonka, M.; et al. 3D slicers as an image computing platform for thw quantitative imaging network. *Magn. Reson. Imaging* **2012**, *30* (9), 1323–1341 DOI: 10.1016/j.mri.2012.05.001.3D.

- (47) Reynisson, P. J.; Scali, M.; Smistad, E.; Hofstad, E. F.; Leira, H. O.; Lindseth, F.; Nagelhus Hernes, T. A.; Amundsen, T.; Sorger, H.; Langø, T. Airway Segmentation and Centerline Extraction from Thoracic CT - Comparison of a New Method to State of the Art Commercialized Methods. *PLoS One* **2015**, *10* (12), e0144282 DOI: 10.1371/journal.pone.0144282.
- (48) Magne, P. Virtual prototyping of adhesively restored, endodontically treated molars. *J. Prosthet. Dent.* **2010**, *103* (6), 343–351 DOI: 10.1016/S0022-3913(10)60074-1.
- (49) Duque, L.; Menges, B.; Borros, S.; Förch, R. Immobilization of biomolecules to plasma polymerized pentafluorophenyl methacrylate. *Biomacromolecules* **2010**, *11* (10), 2818–2823 DOI: 10.1021/bm100910q.
- (50) Duque, L.; Queralto, N.; Francesch, L.; Bumbu, G. G.; Borros, S.; Berger, R.; Förch, R. Reactions of plasma-polymerised pentafluorophenyl methacrylate with simple amines. *Plasma Process. Polym.* **2010**, *7* (11), 915–925 DOI: 10.1002/ppap.201000058.
- (51) Förch, R.; Zhang, Z.; Knoll, W. Soft plasma treated surfaces: Tailoring of structure and properties for biomaterial applications. *Plasma Process. Polym.* **2005**, *2* (5), 351–372 DOI: 10.1002/ppap.200400083.
- (52) Zhou, Y.; Li, M.; Su, B.; Lu, Q. Superhydrophobic surface created by the silver mirror reaction and its drag-reduction effect on water. *J. Mater. Chem.* **2009**, *19* (20), 3301–3306 DOI: 10.1039/b819251k.
- (53) Semaan, R.; Yarmus, L. Rigid bronchoscopy and silicone stents in the management of central airway obstruction. *J. Thorac. Dis.* **2015**, *7*, S352–S362 DOI: 10.3978/j.issn.2072-1439.2015.11.17.
- (54) Bojrab, M. J.; Waldron, D. R.; James P., T. *Current Techniques in Small Animal Surgery*, 5th ed.; Teton NewMedia, 2014.
- (55) Chen, H. Y.; Hermiller, J.; Sinha, A. K.; Sturek, M.; Zhu, L.; Kassab, G. S. Effects of stent sizing on endothelial and vessel wall stress: potential mechanisms for in-stent restenosis. *J. Appl. Physiol.* **2009**, *106* (5), 1686–1691 DOI: 10.1152/jappphysiol.91519.2008.
- (56) Ratnovsky, A.; Regev, N.; Wald, S.; Kramer, M.; Naftali, S. Mechanical properties of different airway stents. *Med. Eng. Phys.* **2015**, *37* (4), 408–415 DOI: 10.1016/j.medengphy.2015.02.008.
- (57) Salmi, M.; Paloheimo, K. S.; Tuomi, J.; Wolff, J.; Mäkitie, A. Accuracy of medical models made by additive manufacturing (rapid manufacturing). *J. Cranio-Maxillofacial Surg.* **2013**, *41* (7), 603–609 DOI: 10.1016/j.jcms.2012.11.041.
- (58) Singare, S.; Yaxiong, L.; Dichen, L.; Bingheng, L.; Sanhu, H.; Gang, L. Fabrication of customised maxillo-facial prosthesis using computer-aided design and rapid prototyping techniques. *Rapid Prototyp. J.* **2006**, *12* (4), 206–213 DOI: 10.1108/13552540610682714.
- (59) Kondor, S.; Grant, G.; Liacouras, P.; Schmid, J. R.; Parsons, M.; Rastogi, V. K.; Smith, L. S.; Macy, B.; Sabart, B.; Macedonia, C. On Demand Additive Manufacturing of a Basic Surgical Kit. *J. Med. Device.* **2013**, *7* (September 2013), 030916–1 DOI: 10.1115/1.4024490.

## **Chapter V. Conclusions**

*This page left blank intentionally*

## Conclusions

A proof of concept of a bioactive material (silicone-based) with antibacterial properties capable to avoid bacterial colonization and biofilm formation was developed. In addition, the plasma treatments were adapted to create a controlled drug delivery platform onto the surface of the materials in order to avoid stenotic tissue and recurrence and reduce the formation of the granulation tissue. Finally, an anatomically personalized tracheal stent was developed using additive manufacturing technology to increase the implant adaptability and avoid migration and pain.

- Surface modification has been performed on different materials, such as nylon, PTFE and PDMS, and it was possible to selectively attach different molecules to each surface (bi-side modification), adding different properties or activities depending on the materials sides. Additionally, surfaces have been micro-structured using  $\mu$ Contact Printing techniques or micro-structured masks.
- Glucosamine has been covalently attached to the surface through the reactive PFM group. Silver deposition was achieved through a three-step reaction using PFM, glucosamine and the silver's mirror reaction by both methods, plasma grafting and PECVD.
- PECVD method allowed the deposition a homogeneous thin film with higher amount of silver when compared to grafting methods. In addition, PECVD allowed different topologies on surfaces with the ability to model the macroscopic and microscopic surface morphology and carries out chemical patterning. The obtained silver coating, formed by the fusion of silver nanoparticles, resulted in a homogeneous micro- and nanostructured surface with hydrophobic properties.
- Silver-coated surfaces were tested *in vitro* with bacterial cultures and presented antibacterial properties against *Pseudomonas aeruginosa* and *Staphylococcus aureus* avoiding biofilm formation. Furthermore, the hydrophobic silver coated surfaces showed lower bacterial adhesion on the surface of the developed materials (antifouling behaviour) when compared with the non-modified samples.
- The *in vitro* release demonstrated the release of silver ions from the surface to the media, showing an initial rapid release within the first 24 h, followed by a lower sustained release over 20 days. The achieved silver amounts during the release showed no cytotoxic effect *in vitro* using COS-7 cells.
- A block co-polymer (PAmX) with amines at both ends of the polymer chains was successfully synthesized via microwave or acid catalysis polycondensation to fabricate paclitaxel (PCTXL) loaded nanoparticles population with low polydispersity via nanoprecipitation.

- Paclitaxel loaded nanoparticles showed drug content of approximately 3% of paclitaxel with encapsulation efficiencies about 60%, resulting in similar values of other pegylated nanoparticles and polyester base NPs.
- *In vitro* release experiments have demonstrated that NPs release PCTXL with an approximately first-order profile and without initial burst. The comparison between the synthesized nanoparticles (with amide bonds in its structure) and polyester-peg nanoparticles (previously developed in our group with just ester bonds), showed that amide bonds had slower release because of the stability of the amide bond.
- For the *in vitro* cells experiments, biocompatibility and *in vitro* antiproliferative activity against epithelial cells (A549), Human Lung Fibroblast cells (IMR-90) and *ex vivo* samples (Primary Respiratory Human Fibroblast cells (T-01 MVV) and human fibroblasts cell lines, have been assessed. The drug-loaded nanoparticles caused a reduction of 80% in cell proliferation within 12-14 days of incubation similar to pure paclitaxel. Additionally, when pp-PFM was not blocked properly, cellular cytotoxicity was observed.
- A mould with an anatomical design (extracted from patients' scan) was designed with injection channels to allow oxygen diffusion and therefore, the curing of the PDMS. An anatomical silicone 3D printed trachea was obtained by injecting silicone (PDMS) onto the printed mould. The result was a transparent, homogeneous and flexible silicone trachea with 100% anatomical geometries.
  - The obtained anatomical 3D tracheal stent was coated with the previous developed antibacterial coating technology allowing a homogeneous antibacterial silver coating onto the surface of the manufactured object.